

Alma Mater Studiorum – Università di Bologna

DOTTORATO DI RICERCA IN
MECCANICA E SCIENZE AVANZATE DELL'INGEGNERIA

Ciclo 35

Settore Concorsuale: 09/A2 – MECCANICA APPLICATA ALLE MACCHINE

Settore Scientifico Disciplinare: ING-IND/13 – MECCANICA APPLICATA ALLE MACCHINE

MARS DELIVERY SERVICE

DEVELOPMENT OF THE ELECTRO-MECHANICAL SYSTEMS OF THE
SAMPLE FETCH ROVER FOR THE MARS SAMPLE RETURN CAMPAIGN

Presentata da: Paolo Ridolfi

Coordinatore Dottorato

Lorenzo Donati

Supervisore

Marco Carricato

Esame finale anno 2023

Great things are achieved by embracing great dangers.

Herodotus

ABSTRACT

This thesis describes the development of the Sample Fetch Rover (SFR), studied for Mars Sample Return (MSR), an international campaign carried out in cooperation between the National Aeronautics and Space Administration (NASA) and the European Space Agency (ESA). The focus of this document is the design of the electro-mechanical systems of the rover, in particular its locomotion and sample acquisition systems.

After placing this work into the general context of robotic planetary exploration and summarising the state of the art for what concerns Mars rovers, the architecture of the Mars Sample Return Campaign is presented. This work began with the iteration of several concepts in response to an evolving lander interface. Following that, a complete overview of the current SFR architecture is provided, touching upon all the main subsystems of the spacecraft. For each area, it is discussed what are the design drivers, the chosen solutions and whether they use heritage technology (in particular from the ExoMars Rover) or new developments. This research focuses on two topics of particular interest, due to their relevance for the mission and the novelty of their design: locomotion and sample acquisition, which are discussed in depth.

The early SFR locomotion concepts are summarised, covering the initial trade-offs and discarded designs for higher traverse performance. Once a consolidated architecture was reached, the locomotion subsystem was developed further, defining the details of the suspension, actuators, deployment mechanisms and wheels. This technology is presented here in detail, including some key analysis and test results that support the design and demonstrate how it responds to the mission requirements.

Another major electro-mechanical system developed as part of this work is the one dedicated to sample tube acquisition. The concept of operations of this machinery was defined to be robust against the unknown conditions that characterise the mission. The design process led to a highly automated robotic system which is described here in its main components: vision system, robotic arm and tube storage.

ACKNOWLEDGEMENTS

I would like to express the deepest gratitude to my supervisor, Professor Marco Carricato for his technical guidance, encouragement and advice, without which this work would not have been possible. I am also greatly indebted to the department managers and project managers at Airbus who supported this initiative over the years. Furthermore, I would like to thank my colleagues and my customers at the European Space Agency, who have always shown enthusiasm for this study and willingness to help me along this path.

The Mars Sample Return (MSR) campaign is a cooperation between the National Aeronautics and Space Administration (NASA) and the European Space Agency (ESA). The Sample Fetch Rover (SFR) was studied by Airbus Defence and Space Ltd., UK for ESA in the context of this campaign. The work presented in this document was carried out between 2018 and 2022 and brought the project from its Preliminary Requirements Review (PRR) to Preliminary Design Review (PDR).

A particular acknowledgement is due to the engineers of the SFR Team at Airbus for giving me the opportunity to lead the development of these systems and learn from their unparalleled expertise in building such unique spacecraft. Without their mastery, the SFR project, let alone this PhD, would have never existed. I am honoured to have been part of this team and proud of having contributed to the realisation of this craft.

Some of the technology described herein was developed by the contractors and partners in the large industrial consortium led by Airbus. Wherever possible, this is indicated in the text where the relevant technology is discussed. With reference to major electromechanical systems, particularly relevant to this research, it shall be noted that the SFR locomotion mechanism, named Fetch Actuator System for Traverse (FAST) was developed by MacDonald, Dettwiler and Associates Ltd., Canada. The SFR wheels were provided by NASA Glenn Research Center, USA. The SFR Arm and Gripper Subsystem (AGS) was developed by Leonardo S.p.A., Italy.

Part of this research was carried out at the Jet Propulsion Laboratory, California Institute of Technology, under a contract with NASA (80NM0018D0004).

Where figures, charts and tables are reported from external sources, credit is given to the originating organisations in their caption. Items that do not have a credit statement have been produced by the author as part of this research.

TABLE OF CONTENTS

1 Introduction	1
2 Robotic exploration of the Solar System	5
2.1 Brief history of the exploration of the Solar System	5
2.1.1 The Founding Era	6
2.1.2 The Grand Tour and the Stagnant Era.....	6
2.1.3 Present day.....	7
2.2 Reasons to explore	8
2.2.1 Scientific return.....	8
2.2.2 Technological return	9
2.2.3 International cooperation.....	9
2.2.4 Inspiration for the public.....	10
2.2.5 Transcendence of human limits	11
2.3 Destinations of interplanetary probes.....	11
2.3.1 The Sun	11
2.3.2 The inner planets	14
2.3.3 The outer planets.....	23
2.3.4 The minor bodies.....	32
2.3.5 The boundaries of the Solar System	35
3 Mars	39
3.1 History of the exploration of Mars.....	39
3.1.1 Early days and pioneering missions	39
3.1.2 Modern exploration of Mars.....	42
3.2 Scientific interest	47
3.2.1 Planetary formation and geology.....	47
3.2.2 Climate and habitability	47
3.2.3 Exobiology	48
3.3 The Martian environment.....	48
3.3.1 Gravity	48
3.3.2 Atmosphere.....	49
3.3.3 Temperatures.....	51
3.3.4 Regolith and dust.....	53
3.3.5 Seasons.....	55
3.3.6 Radiation	56
4 Mars rovers	59
4.1 Mobility on planetary surfaces.....	59
4.1.1 Wheeled locomotion.....	60
4.1.2 Tracked locomotion.....	61
4.1.3 Legged or walking locomotion	61
4.1.4 Unconventional locomotion strategies	62
4.2 Locomotion of wheeled planetary rovers.....	63
4.2.1 Rocker arm suspension.....	63
4.2.2 Rocker bogie suspension.....	64
4.2.3 Triple bogie suspension	66
4.2.4 Number and types of wheels.....	66
4.2.5 Actuators	68

4.3 Rover designs operated on Mars.....	70
4.3.1 Microrovers.....	70
4.3.2 Medium solar rovers	71
4.3.3 Large nuclear rovers	71
4.4 ExoMars Rover design	72
4.4.1 Spacecraft architecture	72
4.4.2 Mission profile	74
4.4.3 Locomotion	75
4.4.4 Actuator Drive Electronics.....	77
4.4.5 Guidance, Navigation and Control	77
4.4.6 On-Board Computer	79
4.4.7 Telecommunications	80
4.4.8 Scientific instruments	81
4.4.9 Structure.....	82
4.4.10 Thermal control.....	84
4.4.11 Electrical power system	85
4.4.12 Planetary protection.....	86
5 Mars Sample Return.....	89
5.1 History of Mars Sample Return.....	90
5.2 International MSR architecture	94
5.2.1 Sample caching	95
5.2.2 Sample retrieval	98
5.2.3 Sample return.....	100
5.2.4 Planetary protection.....	102
6 Overview of the Sample Fetch Rover	105
6.1 Early concepts and trade-offs.....	106
6.1.1 Lander interface	109
6.2 Spacecraft architecture	111
6.3 Mission profile	113
6.4 Locomotion	114
6.5 Actuator Control Electronics.....	114
6.6 Guidance, Navigation and Control	116
6.7 Integrated avionics	117
6.8 Telecommunications	119
6.9 Sample tube acquisition.....	119
6.10 Structure	120
6.11 Top deck mechanisms.....	120
6.12 Thermal control.....	121
6.13 Electrical power system	123
6.14 Planetary protection.....	124
7 Development of the SFR systems: locomotion.....	127
7.1 Trade-offs and early developments	128
7.1.1 Number of wheels	128
7.1.2 Actuator technology	130
7.1.3 Other critical technologies.....	132
7.1.4 The Gullwing design: peak locomotion performance.....	133
7.2 Design of the locomotion mechanisms	143
7.2.1 Rocker arm suspension.....	144

7.2.2 Actuators	152
7.2.3 Deployment.....	157
7.2.4 Wheels	160
7.3 Traverse analysis	165
7.3.1 Terramechanical simulations	165
7.3.2 Surface Operations Engineering Tool	169
7.3.3 Other analyses.....	171
7.4 Traverse testing.....	172
8 Development of the SFR systems: sample acquisition	177
8.1 RAS architecture	178
8.1.1 Design drivers	179
8.2 Tube fetching operations.....	182
8.2.1 Tube approach	182
8.2.2 Tube detection	183
8.2.3 Tube grasping.....	185
8.2.4 Tube stowing	186
8.3 Vision system.....	188
8.3.1 Cameras	189
8.3.2 Vision-Based Detection Software.....	190
8.4 Arm and Gripper Subsystem	190
8.4.1 Arm design.....	191
8.4.2 Gripper design.....	196
8.5 Tube storage	200
8.6 Fetching analysis.....	202
8.6.1 RSTA Acquisition and Fetching Timeline	202
8.6.2 Grasping error budget	205
8.6.3 Mechanical models of the arm.....	207
9 Conclusion.....	209
10 References	213

LIST OF FIGURES

Figure 2-1 – 1991 “Space Exploration” stamps	8
Figure 2-2 – American astronaut Thomas Stafford and Soviet cosmonaut Aleksey Leonov meet in the passage connecting the Apollo and Soyuz spacecraft (credit: Johnson Space Center / NASA)	10
Figure 2-3 – Artist’s impression of Solar Orbiter (credit: ESA / ATG Medialab / NASA)	13
Figure 2-4 – The view from Parker Solar Probe flying through the solar corona (credit: NASA / Johns Hopkins APL / Naval Research Laboratory)	14
Figure 2-5 – Artist’s impression of BepiColombo at Mercury (credit: ESA / ATG Medialab / NASA / JPL-Caltech).....	16
Figure 2-6 – The surface of Venus imaged by the Venera 13 lander’s front camera (credit: Russian Academy of Sciences / T. Stryk).....	17
Figure 2-7 – The night side of Venus in infrared light, imaged by the Akatsuki spacecraft (credit: JAXA/ ISAS / DARTS / D. Bouic).....	18
Figure 2-8 – A replica of the Lunokhod rover (credit: B. Borisov / RIA Novosti)	20
Figure 2-9 – Astronaut James Irwin with the Lunar Roving Vehicle and Mount Hadley in the background during Apollo 15 (credit: NASA / David Scott).....	21
Figure 2-10 – Solar System’s habitable zone (credit: NASA / JPL-Caltech / T. Pyle)	22
Figure 2-11 – Comparison between Mars and the Atacama Desert (credit: NASA / A. Airo, TU Berlin).....	23
Figure 2-12 – Vortices in Jupiter’s North North Temperate Belt imaged by NASA’s Juno spacecraft at low altitude (credit: NASA / JPL-Caltech / K. M. Gill).....	24
Figure 2-13 – A composite view of Europa obtained by images from the Galileo probe (credit: NASA / JPL-Caltech / SETI Institute)	25
Figure 2-14 – View of Saturn transiting in front of the Sun from the Cassini orbiter (credit: NASA / JPL-Caltech / Space Science Institute)	26
Figure 2-15 – Saturn’s moon Daphnis raising a trail of waves in the ring material imaged by Cassini (credit: NASA / JPL-Caltech / Space Science Institute)	27
Figure 2-16 – Water plumes rising from Enceladus imaged by Cassini (credit: NASA / JPL-Caltech / Space Science Institute).....	27
Figure 2-17 – Titan’s surface from the Huygens probe (credit: ESA / NASA / JPL-Caltech / University of Arizona).....	28
Figure 2-18 – Uranus from Voyager 2 (credit: NASA / JPL-Caltech)	29
Figure 2-19 – The architecture of the Voyager spacecraft, including main scientific instruments (credit: NASA / JPL-Caltech).....	30
Figure 2-20 – Neptune from Voyager 2 (credit: NASA / JPL-Caltech).....	31
Figure 2-21 – A mosaic view of Triton obtained by Voyager 2 imagery (credit: NASA / JPL-Caltech).....	32

Figure 2-22 – Comet 67P Churyumov–Gerasimenko showing significant outgassing activity imaged by the Rosetta orbiter (credit: ESA / Rosetta / NavCam).....	34
Figure 2-23 – View of Pluto under a low illumination angle by New Horizons (credit: NASA / JHUAPL / SwRI).....	35
Figure 2-24 – Diagram of the heliosphere and large-scale structures around the Solar System (credit: ESA / L. B. Jaffel / M. Kornmesser / L. L. Christensen)	36
Figure 3-1 – A JPL engineer colouring by hand the transmission strips of the first television image from Mariner 4 (credit: NASA / JPL-Caltech)	40
Figure 3-2 – Panorama of the Martian surface from Viking 2 (credit: NASA / JPL-Caltech)	41
Figure 3-3 – Winter frost around Viking 2 (credit: NASA / JPL-Caltech).....	42
Figure 3-4 – Visual summary of all the missions in the history of Mars exploration, categorised as flybys, orbiters, landers and rovers, updated as of July 2020 (credit: ESA)	43
Figure 3-5 – NASA’s Sojourner rover imaged by the Pathfinder lander (credit: NASA / JPL-Caltech)	44
Figure 3-6 – Opportunity’s path (from top to bottom) on Mars with the City of Bologna for scale (credit: NASA / JPL-Caltech)	45
Figure 3-7 – Curiosity panorama in front of Mont Mercou (credit: NASA / JPL-Caltech / MSSS)	46
Figure 3-8 – Ingenuity hovering 5 m above the ground, seen from Perseverance (credit: NASA / JPL-Caltech / ASU).....	46
Figure 3-9 – Mars-weight prototype of the ExoMars Rover in the Mars Yard facility (credit: Airbus).....	49
Figure 3-10 – Composite views of Spirit’s top deck before (left) and after (right) a cleaning event (credit: NASA / JPL-Caltech / Cornell)	50
Figure 3-11 – Temperature ranges at Gale Crater by NASA’s Curiosity rover, with temperatures in Los Angeles at equivalent seasonal points (credit: NASA / JPL-Caltech / CAB)	52
Figure 3-12 – Examples of occurrence of different regolith types on Mars (credit: G. Kruse)	53
Figure 3-13 – View from Opportunity’s Hazcams on Purgatory Dune (credit: NASA / JPL-Caltech)	54
Figure 3-14 – A regional dust storm imaged by NASA’s Mars Reconnaissance Orbiter (MRO) in 2007 (credit: NASA / JPL-Caltech / MSSS).....	55
Figure 3-15 – Mars imaged by NASA’s Mars Global Surveyor in June (left) and July (right) 2001 (credit: NASA / JPL-Caltech / MSSS)	56
Figure 3-16 – Examples of radiation doses for different scenarios (credit: NASA).....	57

Figure 4-1 – Spare wheel of NASA’s Apollo LRV (credit: Smithsonian National Air and Space Museum / E. Long).....	60
Figure 4-2 – Schematic of the track drive system and suspension of a 1950s tank (credit: allworldwars.com).....	61
Figure 4-3 – Testing of a walking robot prototype aimed at exploring Martian and Lunar caves (credit: NASA / JPL-Caltech).....	62
Figure 4-4 – Rocker arm suspension for a four-wheeled rover: (a) general layout, (b) with differential arm, (c) forces on level ground (credit: G. Genta).....	64
Figure 4-5 – Rocker bogie suspension for a six-wheeled rover: (a) general layout, (b) forces on level ground, (c) – (e) overcoming a step (credit: G. Genta).....	65
Figure 4-6 – Rocker bogie suspension for an eight-wheeled rover (credit: G. Genta)	65
Figure 4-7 – Triple bogie suspension: (a) general layout, (b) forces on level ground (credit: G. Genta)	66
Figure 4-8 – Comparison between Curiosity, Perseverance and ExoMars wheels (not to scale) with approximate contact patches on firm soil.....	67
Figure 4-9 – A prototype of the ExoMars Rover performing a point turn (credit: Airbus). 68	
Figure 4-10 – Rover prototype climbing a large obstacle thanks to active front bogies (credit: B. Ghotbi)	69
Figure 4-11 – Overview of the ExoMars Rover with some key features (Credit: ESA / ATG Medialab)	73
Figure 4-12 – ExoMars Rover entry, descent and landing sequence (credit: ESA).....	74
Figure 4-13 – ExoMars Structural and Thermal Model (STM) during vibration testing (credit: Airbus)	75
Figure 4-14 – ExoMars wheel climbing a large obstacle (credit: Airbus).....	76
Figure 4-15 – BEMA actuator types and locations (credit: MDA)	76
Figure 4-16 – Visualisation of the ExoMars GNC system planning a path and identifying hazardous terrain (credit: BBC)	78
Figure 4-17 – ExoMars Rover On-Board Computer (credit: RUAG Space).....	79
Figure 4-18 – ExoMars Analytical Laboratory Drawer and detail of the Sample Preparation and Distribution System (credit: ESA).....	81
Figure 4-19 – The ExoMars Rover body structure during construction (credit: RUAG Space)	83
Figure 4-20 – ExoMars Rover ALD loop heat pipes layout (top) and test rig (bottom) (credit: IberEspacio).....	84
Figure 4-21 – ExoMars Rover solar array assembly partially deployed (credit: Airbus)	85
Figure 4-22 – ExoMars Rover battery assembly (left) and unit cell (right) (credit: SAFT). 86	
Figure 4-23 – ExoMars Rover under test in the Airbus Bio-Clean Facility (credit: BBC).....	88
Figure 5-1 – Mission architecture for a 1984 Viking-based Mars Sample Return (credit: Martin Marietta).....	90

Figure 5-2 – Mobile MAV concept for Mars Sample Return (credit: NASA / JPL-Caltech)...	91
Figure 5-3 – Exploded view of the joint NASA / ESA Mars2018 mission (credit: NASA).....	92
Figure 5-4 – Sample collecting and handling systems on board Perseverance (credit: NASA / JPL-Caltech)	93
Figure 5-5 – Mars Sample Return campaign overview (credit: ESA / K. Oldenburg).....	95
Figure 5-6 – Cross section of an RSTA mounted in the coring bit (top), one of the flight RSTAs before integration into Perseverance (middle) and an X-ray of a sealed RSTA after a drilling test (bottom) (credit: NASA / JPL-Caltech).....	96
Figure 5-7 – Satellite view of the western rim of Jezero Crater with the potential routes for Perseverance and SFR (credit: NASA / JPL-Caltech).....	97
Figure 5-8 – Artist’s impression of the Sample Retrieval Lander on Mars (credit: NASA / JPL-Caltech)	98
Figure 5-9 – Artist’s impression of the Sample Fetch Rover on Mars	99
Figure 5-10 – Semi-transparent view of the MAV with key components (credit: NASA / MSFC).....	100
Figure 5-11 – ERO over a regular-sized basketball field (left) and broken down into main elements (right) (credit: Airbus).....	101
Figure 5-12 – EEV cross section (top) and impact testing (bottom) (credit: NASA / LRC)	102
Figure 6-1 – Sample Fetch Rover mission patch	105
Figure 6-2 – Evolution of the SFR baseline during its early phases, to scale.....	107
Figure 6-3 – Artist’s impression of SFR on Mars	108
Figure 6-4 – Evolution of SRL architecture and SFR deployment concept (credit: NASA / JPL-Caltech)	110
Figure 6-5 – Cross section of the SRL entry capsule (credit: NASA / JPL-Caltech)	111
Figure 6-6 – SFR overview with major external components	112
Figure 6-7 – Location of one ACE on SFR (left) and design of the unit (right) (credit: Sener)	115
Figure 6-8 – Visualisation of a path following sequence with AGL update	117
Figure 6-9 – Sample Fetch Rover IABS (credit: Beyond Gravity).....	117
Figure 6-10 – SFR top deck mechanisms stowed (left) and deployed (right).....	120
Figure 6-11 – Example of PCMC under test in a thermal chamber (credit: J. Stetina).....	122
Figure 7-1 – Stowed (top left) and deployed (bottom right) SFR Gullwing design	133
Figure 7-2 – Gullwing deployment kinematics with four-bar linkages	134
Figure 7-3 – Gullwing pivot assembly	134
Figure 7-4 – Cross section of the Gullwing pivot.....	135

Figure 7-5 – Possible differential layout on the rover underbelly.....	136
Figure 7-6 – Example of fractured terrain imaged by NASA’s Curiosity rover (credit: NASA / JPL-Caltech).....	137
Figure 7-7 – Obstacle climbing forces on wheels of different sizes.....	138
Figure 7-8 – Obstacle climbing forces with annotated geometry	139
Figure 7-9 – Plot of the function $f(\alpha)$	140
Figure 7-10 – Torques on a bogie for front and rear wheel climbing.....	141
Figure 7-11 – Scarab rover undergoing testing at NASA’s Glenn Research Center (credit: NASA / GRC / N. S. Kilkenny).....	142
Figure 7-12 – FAST overview (rear left wheel in the foreground)	144
Figure 7-13 – Kinematics of the FAST differential in presence of an obstacle: rear view (top left), right view (top right), orthogonal view of the rear face (bottom)	145
Figure 7-14 – Golombek’s CFA curves and in-situ measurements (credit: M. Golombek)	147
Figure 7-15 – Process to size obstacle climbing ability and ground clearance	148
Figure 7-16 – CAD visualisation of a diagonal slope case.....	149
Figure 7-17 – SFR critical stability angle as a function of heading angle.....	150
Figure 7-18 – Operating principle of a Frangibolt SMA actuator (credit: EBAD)	151
Figure 7-19 – Rear view of SFR with main locomotion components.....	152
Figure 7-20 – Automotive tie rods, similar to the FAST differential.....	152
Figure 7-21 – Torque / speed requirements and performance curves at -60°C for FAST and BEMA actuators	153
Figure 7-22 – FAST breadboard actuator (credit: Maxon Motors).....	156
Figure 7-23 – ExoMars BEMA flight actuator (credit: MDA).....	157
Figure 7-24 – FAST stowed and deployed, side views (left) and front views (right) with salient dimensions in mm	158
Figure 7-25 – FAST separation planes.....	159
Figure 7-26 – Visualisation of the FAST first motion and deployment.....	159
Figure 7-27 – SFR wheel and its constituent parts (credit: NASA / GRC)	161
Figure 7-28 – Phase transitions of nickel-titanium alloy.....	162
Figure 7-29 – Main steps in the construction of the Apollo wire mesh tyre (credit: D. Freidman)	163
Figure 7-30 – Process of interlacing springs to create a spring tyre (credit: NASA / Goodyear)	163
Figure 7-31 – Wheel prototype during life testing (credit: NASA / JPL-Caltech / GRC).....	164
Figure 7-32 – Visualisation of the terramechanical simulation solving an obstacle climbing case (credit: MDA).....	166

Figure 7-33 – Perseverance at “Rochette” sampling site (credit: NASA / JPL-Caltech).....	167
Figure 7-34 – Curiosity at “Namib dune” (credit: NASA / JPL-Caltech).....	168
Figure 7-35 – Information flow in SOET and associated analyses.....	170
Figure 7-36 – Drawbar pull as a function of slip ratio on ES-4 for a prototype SFR wheel	173
Figure 7-37 – Drawbar pull as a function of slip ratio on ES-2 for a prototype SFR wheel	173
Figure 7-38 – Design of the SFR locomotion breadboard (credit: MDA)	174
Figure 7-39 – Snapshots of the breadboard locomotion testing (credit: MDA / Beyond Gravity).....	176
Figure 8-1 – Tubes lying on terrain with rocks and crevasses (credit: NASA / JPL-Caltech)	180
Figure 8-2 – Tube pickup area in front of the rover (red circles)	181
Figure 8-3 – Tube pickup area with viewing cones from the NavCam.....	181
Figure 8-4 – Results of AGL-D performance simulation (credit: M. Dinsdale)	183
Figure 8-5 – NavCam (left) and RDC on the arm’s wrist (right) (credit: Neptec / Leonardo)	189
Figure 8-6 – Front face of the rover with RAS hardware annotated.....	191
Figure 8-7 – AGS in a tube pickup pose.....	191
Figure 8-8 – Extended robotic arm with key dimensions in mm	192
Figure 8-9 – Breadboard testing with the DELIAN arm in the Mars Yard.....	194
Figure 8-10 – Force torque sensor on board NASA’s Perseverance rover (credit: ATI)	195
Figure 8-11 – Body grip and head grip areas on the tube (credit for tube image: NASA / JPL- Caltech)	196
Figure 8-12 – Design of the SFR breadboard gripper (credit: AVS).....	197
Figure 8-13 – SFR breadboard gripper during testing (credit: AVS).....	198
Figure 8-14 – Maxon DC motor cross section (left) and stator magnetic circuit (right) (credit: Maxon Motors).....	199
Figure 8-15 – RRB prototype with superimposed tube volume (credit: Leonardo).....	200
Figure 8-16 – RSTA Storage Assembly	201
Figure 8-17 – Representation of the tube engagement geometry (credit for tube image: NASA / JPL-Caltech).....	201
Figure 8-18 – Grasping a tube in a depression using a wide opening (left) and a narrow opening (right).....	204
Figure 8-19 – Lateral error budget for tube grasping (credit for tube image: NASA / JPL- Caltech)	206

Figure 8-20 – Longitudinal error budget for tube grasping (credit for tube image: NASA / JPL-Caltech).....207

Figure 8-21 – FEM analysis of arm deflection under Martian gravity (credit: Leonardo).208

Figure 9-1 – SFR integrated breadboard field tests210

LIST OF TABLES

Table 3-1 – Composition of the Martian atmosphere measured by NASA’s Curiosity rover	50
Table 3-2 – Characteristics of Martian regolith types and corresponding ES simulants	53
Table 4-1 – Key features of NASA’s Sojourner rover	70
Table 4-2 – Key features of NASA’s MER rovers.....	71
Table 4-3 – Key features of NASA’s Curiosity rover.....	72
Table 4-4 – Key features of ESA’s ExoMars Rover	73
Table 5-1 – Summary of key MSR elements and their functions.....	94
Table 6-1 – Key features of the Sample Fetch Rover	112
Table 6-2 – Sample Fetch Rover mass budget.....	113
Table 7-1 – Trade-off on the number of wheels	128
Table 7-2 – Trade-off on actuator technology.....	130
Table 7-3 – Trade-off on the steering architecture	131
Table 7-4 – Main organisations and their roles in the development of the SFR locomotion	143
Table 7-5 – Sizing torque and speed requirements for FAST and BEMA actuators	153
Table 7-6 – Comparison between FAST and BEMA actuator architecture.....	154
Table 7-7 – Obstacle performance on different substrates predicted by the terramechanical model	169
Table 7-8 – Resistive torque contributors and uncertainty factors	172
Table 7-9 – Obstacle performance of the SFR locomotion breadboard on different substrates and slopes	175
Table 8-1 – Main organisations and their roles in the development of the RAS.....	179
Table 8-2 – Operational sequence for tube detection.....	184
Table 8-3 – Operational sequence for tube grasping.....	186
Table 8-4 – Operational sequence for tube stowing.....	188
Table 8-5 – Key features of the NavCam and RDC	189
Table 8-6 – AGS actuators specifications.....	193

LIST OF ABBREVIATIONS AND ACRONYMS

Acronym	Meaning	Acronym	Meaning
Acronym	Meaning	DHMR	Dry Heat Microbial Reduction
ACA	Adaptive Caching Assembly	DMM	Design Maturity Margin
AGL	Absolute Global Localisation	DOE	Department Of Energy
AGL-D	Absolute Global Localisation – Depot	DOF	Degree Of Freedom
AGL-T	Absolute Global Localisation – Traverse	DRV	Drive
AGS	Arm and Gripper Subsystem	DSN	Deep Space Network
AMS	Acquisition Management Software	ECSS	European Cooperation for Space Standardisation
AOCS	Attitude and Orbit Control System	EDL	Entry, Descent and Landing
AU	Astronomical Unit	EEC	Earth Entry Capsule
AutoNav	Autonomous Navigation	EEV	Earth Entry Vehicle
BDC	Brushed Direct Current	ERO	Earth Return Orbiter
BLDC	BrushLess Direct Current	ERV	Earth Return Vehicle
CAD	Computer-Aided Design	ES	Engineering Soil
CAN	Controller Area Network	ESA	European Space Agency
CBE	Current Best Estimate	FAST	Fetch Actuator System for Traverse
CFA	Cumulative Fractional Area	FEM	Finite Element Method
CLUPI	CLose-UP Imager	GNC	Guidance, Navigation and Control
COG	Centre Of Gravity	HD	Harmonic Drive
COSPAR	COMmittee on SPACe Research	HDRM	Hold-Down and Release Mechanism
DC	Direct Current	HEPA	High-Efficiency Particulate Air
DEM	Digital Elevation Model	HiRISE	High-Resolution Imaging Science Experiment
DEMAS	DEployable MAsT Subsystem	IABS	Integrated Avionics Box Subsystem
DEP	Deployment		

Acronym	Meaning	Acronym	Meaning
IMU	Inertial Measurement Unit	OBC	On-Board Computer
JPL	Jet Propulsion Laboratory	OS	Orbiting Sample
ISEM	Infrared Spectrometer for Exo-Mars	PanCam	Panoramic Camera
ISS	International Space Station	PCDE	Power Conditioning and Distribution Electronics
JAXA	Japan Aerospace eXploration Agency	PDR	Preliminary Design Review
JUICE	JUpiter ICy moon Explorer	PG	Planetary Gearbox
LCL	Latching Current Limiter	RAS	RSTA Acquisition System
LocCam	Localisation Camera	RDC	RSTA Detection Camera
LRV	Lunar Roving Vehicle	RGA	RSTA and Glove Assembly
Ma_MISS	Mars Multispectral Imager for Subsurface Studies	RHU	Radioisotope Heater Unit
MAV	Mars Ascent Vehicle	RLS	Raman Laser Spectrometer
MAX-C	Mars Astrobiology Explorer-Cacher	RRB	RSTA Re-grip Bracket
MDA	MacDonald, Dettwiler and Associates	RSA	RSTA Storage Assembly
MER	Mars Exploration Rover	RSS	Root Sum Squared
MFEX	Microrover Flight EXperiment	RSTA	Returnable Sample Tube Assembly
MLI	Multi-Layer Insulation	RTG	Radioisotope Thermoelectric Generator
MOMA	Mars Organic Molecule Analyser	SAM	Sample Analysis at Mars
MRN	Mars Relay Network	SDRAM	Synchronous Dynamic Random Access Memory
MRO	Mars Reconnaissance Orbiter	SFR	Sample Fetch Rover
MSR	Mars Sample Return	SMA	Shape-Memory Alloy
MSL	Mars Science Laboratory	SOET	Surface Operations Engineering Tool
NASA	National Aeronautics and Space Administration	SOLAS	SOLar Array Subsystem
NavCam	Navigation Camera	SRL	Sample Retrieval Lander
		SRF	Sample Receiving Facility

Acronym	Meaning	Acronym	Meaning
SPDS	Sample Preparation and Distribution System	TRL	Technology Readiness Level
STA	Sample Transfer Arm	UHF	Ultra-High Frequency
STM	Structural and Thermal Model	VBDS	Vision-Based Detection Software
STR	Steer	WISDOM	Water Ice Subsurface Deposits Observation on Mars
SUV	Sport Utility Vehicle	WTA	Wheel and Tyre Assembly
TPS	Thermal Protection System		

1 INTRODUCTION

The quest to return pristine material from Mars, advocated by scientists since the 1970s, studied by engineers since the 1980s and finally embraced by space agencies in the 2010s, evolved into a vast international cooperation based on three subsequent missions. A first caching mission would collect the samples and deposit them on the surface. A second retrieval mission would recover them and launch them into Mars orbit, while a third return mission would intercept them in orbit and travel back to Earth. The retrieval mission needed a highly capable vehicle to locate and acquire the samples before launch into Mars orbit. Between 2018 and 2022, an international group of engineers took on the task of answering this need. The outcome of that study is the Sample Fetch Rover (SFR), subject of this work.

Mars Sample Return (MSR) is a complex campaign carried out by the American and European space agencies and hailed as one of the most daring endeavours in the history of robotic spaceflight. It is an interplanetary choreography of multiple missions, carried out by numerous spacecraft interfacing with each other, some of which are already in flight while others are yet to be built.

The SFR capability was engineered to match the ambitious objectives, the uncertain mission profile and the pioneering intent of this undertaking. The result is a rather unique spacecraft: the first logistic vehicle for the surface of Mars, tasked with locating and retrieving its designated payload in time for launch into Mars orbit. SFR is a high-performance, compact solar-powered rover, characterised by advanced operational autonomy. Conceived as a multi-mission machine, flexible with respect to the scenario that it would face on Mars, it embodies the knowledge acquired on the ExoMars Rover and other predecessors, combined with innovative technologies and unconventional solutions.

However, by the time this document will be published, the Mars Sample Return Campaign will have changed. Bold enterprises like these unavoidably carry an amount of risk, and some of it can materialise well before the mission has even lifted off the ground. At the end of the period of this PhD research, SFR was met with a combination of adversities threatening its implementation. Significant challenges had arisen in accommodating the rover on an over-encumbered lander, when the deteriorating political situation in Europe left another

rover, ExoMars, in need of a lander, due to the loss of Russian partnership. Budgetary pressure and difficulties in developing new landing systems for both rovers in a short timespan left SFR stranded on Earth before its design could be finalised. The rover project was cancelled and MSR moved on with alternative, more basic architectures.

In front of the possibility of losing the technology developed so far, the know-how and the history of the SFR project, this document becomes the vessel of that knowledge. It attempts to capture what SFR was like when it was cancelled and how it came to be like that. These pages describe the thought process, the challenges and the innovations that shaped this peculiar spacecraft. They also provide context to the mission and the campaign, their environments and the motivations behind them, in view of the wider quest of the exploration of the Solar System.

It must be acknowledged that it is not possible to exhaustively describe the design of the spacecraft, let alone the campaign and its history, in a single volume of reasonable size. This work focuses on the major electro-mechanical systems of the rover, aiming to provide an understanding of their architecture, the design drivers, and the key technologies, as well as briefly describe the design, analysis and – in some cases – test process that they followed. The technical discussion is mostly centred on the topics of surface mobility and robotic systems, as they play a key role in the SFR mission and they contain novel solutions that are worth capturing in more detail.

Chapter 2 offers a brief overview of the main locations in our Solar System, the reasons why humans yearn to explore them and how they do that. Chapter 3 discusses in more depth the planet Mars and its characteristics. These chapters aim to provide the context to this research in terms of global exploration efforts into the Solar System and Mars in particular. Both chapters are meant to be read by anyone who is interested in space exploration, without the need of an engineering background.

Chapter 4 describes the technology presently available to explore Mars through mobile surface platforms, laying out what can be considered the “state of the art” for Mars rovers. This chapter includes an overview of the ExoMars Rover, which is the direct predecessor of SFR and established much of the technology that will be reused in this project. Chapters 5 and 6 introduce the topics of research that are the centre of this work: Mars Sample Return and the architecture of the Sample Fetch Rover. These three chapters are aimed at those with a general grasp of spacecraft engineering or similar engineering of complex systems, but they are, for the most part, easily readable by anyone with an interest in the field.

Chapters 7 and 8 treat in detail two specific areas of the SFR design: locomotion and sample acquisition. While the general objective is to provide a comprehensive picture of the system, these are two topics of particular interest in this research and are discussed to a greater depth. These chapters are best appreciated by the readers with experience in mechanical engineering, robotics or space systems.

As already noted, it would be impractical to provide an in-depth description of the spacecraft in these pages. While still preliminary, the SFR design is already far too intricate to be covered in a single document. The primary aim of this thesis remains to deliver a broad view of the system architecture, capturing the major challenges, the key solutions to them and transmit the design intent to anyone who might have an interest – or a use – for this technology. Probably, the same SFR design would not apply directly to future missions, but the knowledge on how to achieve the correct design would.

SFR is a highly capable and autonomous transportation system for an unprepared planetary surface. It is likely that someday, somewhere in the Solar System, someone will have a need for this machinery. Those engineers might face similar challenges to those that were overcome during this project. This document is written first and foremost for them.

2 ROBOTIC EXPLORATION OF THE SOLAR SYSTEM

The surface of the Earth is the shore of the cosmic ocean. From it we have learned most of what we know. Recently, we have waded a little out to sea, enough to dampen our toes or, at most, wet our ankles. The water seems inviting. The ocean calls. Some part of our being knows this is where we came from. We long to return.

Carl Sagan, Cosmos

As background to the work carried out in this PhD, this chapter offers a high-level summary of the exploration of the Solar System by humans and human-made probes up to the present day. The following pages describe the history of such endeavours and the motivations behind them, as well as some salient features of the places that these missions are visiting, which make these worlds worth travelling to.

2.1 Brief history of the exploration of the Solar System

On January 2nd 1959, just over a year after putting the first human-made object into orbit, the Soviet Union launched its Luna 1 mission. Despite missing the Moon, it became the first spacecraft to leave Earth orbit and thus can be considered the beginning of the exploration of the Solar System [1]. From that day, vessels have flown across our planetary system and beyond, carrying both machines and humans aboard.

Before describing the targets of exploration in the Solar System and the reasons to reach them, a general overview of the history of planetary exploration is provided below. For sake of brevity, the observation of Planet Earth from orbit is not included in this summary, being an equally rich field on its own. For the purposes of this thesis, planetary exploration begins where the Earth's gravitational sphere of influence ends. Crewed spaceflight is also not covered, being an even more complex enterprise and outside the scope of this work.

2.1.1 The Founding Era

In the days when the first ships were breaking free from our planet's gravity and flying beyond Earth orbit, a lot of the attention was obviously focused on the nearest available object: the Moon. However, attempts to reach Mars and Venus started happening remarkably soon. The first ones took place as early as 1960, although many of those attempts failed. Even the first successful lunar mission, the American Pioneer 4 in 1959, came after a considerable streak of failures: four American and four Soviet Lunar probes were all lost in rapid sequence. There have been years, like 1958 and 1960, when every single interplanetary probe exploded on the launchpad. Today such a high failure rate would be considered outrageous by the politicians financing space programmes, but in those pioneering times, characterised by a different mind-set, the acceptance of failure enabled incredibly rapid progress.

On December 14th 1962 the American probe Mariner 2 performed a successful flyby of Venus, marking the first planetary encounter by human-made spacecraft beyond the Moon. Less than three years later, on July 15th 1965, Mariner 4 achieved the same manoeuvre at Mars. At that time, the two key players in spaceflight, and especially in the exploration of the Solar System, were the United States of America and the Soviet Union. Each superpower used these achievements to prove its own superiority. The technology to explore space is, in fact, the same that is used to launch nuclear warheads and operate surveillance satellites. However, this inoffensive proxy of the military competition proved incredibly fortunate for the advancement in science and technology of all humankind. At the peak of the Cold War, the Golden Age of spaceflight was blooming.

The Soviet Union was lagging slightly behind in interplanetary travel, but leading in the exploration of the Moon, where it achieved the first soft landing on February 3rd 1966 with the Luna 9 probe. Exploration of the Moon dominated the remainder of the '60s and good part of the '70s, with a fleet of robotic and crewed spacecraft sent to our natural satellite. As elaborated by J. N. Nielsen in his paper 'Bound in Shallows: Space Exploration and Institutional Drift' [2], this time can be considered the "Founding Era" of space exploration, i.e., the period when public and private enterprises had clear, long-term goals for exploration and the means to achieve them, thus progress was swift and compelling. This age culminated in the Apollo moon landings, which, despite not being discussed as part of this work, are a key milestone in the advancement of humankind. To this day, we look back on these achievements as some of our highest moments as a civilisation.

2.1.2 The Grand Tour and the Stagnant Era

Despite the strong focus on Earth's moon, during the '70s the launch of probes to Venus and Mars continued at a steady pace. Orbiters and landers were delivered successfully to both planets, which, compared to previous flyby missions, greatly increased the scientific return by providing continuous observations and in-situ analysis. The first flyby of Mercury was performed by the American probe Mariner 10. Other notable events during this time are the launches of spacecraft further out into the Solar System, where distances quickly grow to light-hours¹, and so increase flight times and technological challenges. NASA's nuclear-powered probes Pioneer 10 and 11 were the first to perform flybys of Jupiter and Saturn.

¹ The distance covered in one hour by light in vacuum, approximately equal to one billion kilometres.

NASA engineers had noted that an alignment of Jupiter, Saturn, Uranus and Neptune occurring in the late 70's would enable a single spacecraft to visit all four planets by exploiting gravity assists². Such alignment occurs once every 175 years. This trajectory was named "The Grand Tour" and work commenced on a new mission to accomplish it. However, during that decade, the major spacefaring nations began to show a decreasing interest in space exploration missions, especially those that would not be completed during the term of office of their leaders. The Grand Tour faced budgetary cuts and was reduced to two cheaper, Mariner-derived spacecraft designed to work only for four years: as far as Saturn. The twin probes were named Voyager 1 and 2.

Engineers at the Jet Propulsion Laboratory (JPL) proved harder to distract from their original goals and did not put a single element in the design that would prevent the spacecraft from achieving the Grand Tour mission objectives. Voyager 1 and 2 were launched in the summer of 1977 and, by the time they were en route to the Outer Solar System, it was clear that they would not be followed by other ships in the near future. The rate of launches to other planets significantly slowed down in the '80s and still hasn't recovered, leading to an era of stagnation.

Largely untouched by these events, the Voyagers went on to explore Uranus and Neptune. Having completed successfully the reconnaissance of the Solar System and outlived most of their investors, they report discoveries from interstellar space to this date.

2.1.3 Present day

While today's rate of launches to low Earth orbit is increasing faster than ever, the exploration of the Solar System has yet to recover its original pace. Despite recent positive signs, it is still unclear if it ever will. This stagnation did not prevent enormously successful missions to distant planets like Cassini-Huygens and New Horizons, it just meant that they became very rare.

New trends emerged in spaceflight in recent times, with one planet in particular getting increasing attention, differently from all others. That planet is Mars, and this activity is due to scientific interest around its similarity to Earth, as well as the relatively contained travel time and mission cost, which fits the current exploratory appetite of major space agencies. A new type of spacecraft became particularly successful on Mars since NASA demonstrated its potential in 1997: rovers.

Rovers are mobile surface platforms that can make observations in multiple locations on a planetary body. On Mars, they commonly take the form of wheeled vehicles and, more recently, airborne rotorcraft. Their capability to explore a vast area compared to stationary landers made them the most desirable asset for the study of several celestial bodies. The history of Mars rovers and their achievements is discussed in detail in Chapter 3 of this document.

The last decade brought positive signals for the exploration of the Solar System, with several missions under advanced development or in flight for Mercury, Mars, the Sun, the moons of

² A gravity assist is a manoeuvre in which a spacecraft flies in close proximity of a massive object and exploits its gravitational pull to alter its course. This can achieve a considerable change in trajectory without using any propellant.

Jupiter and Saturn, a planned robotic and human return to the Moon and even another probe well on its way to interstellar space. Whether we are on the verge of a “Space Renaissance”, as sometimes described, remains to be seen. One difference with the past is that this time spaceflight it is not the venture of two antagonistic nations, but dozens of them, often in a coordinated group effort. The central project of this research rides on this wave of renewed interest, consisting in a decade-long, multi-mission, multi-agency endeavour to deepen our understanding of Mars.

2.2 Reasons to explore



Figure 2-1 – 1991 “Space Exploration” stamps

Figure 2-1 shows the “Space Exploration” set of stamps, issued by the United States Postal Service in 1991 to celebrate the reconnaissance of all the Solar System’s planets by American robotic probes. The last stamp depicts Pluto as a grey orb, with the caption “not yet explored”, since at that time Pluto was still considered a major planet. Curiously, that stamp became the symbol of the imperfect completion of the endeavour and ended up getting affixed to the New Horizons spacecraft, which carried it all the way to Pluto itself.

There are multiple reasons that push humans to explore the universe besides completing stamp collections; some key ones are listed below and analysed in the following paragraphs:

1. Scientific return
2. Technological return
3. International cooperation
4. Inspiration for the public
5. Transcendence of human limits

2.2.1 Scientific return

All space exploration missions have a set of major objectives that are scientific in nature and aim at expanding human knowledge about particular locations or phenomena. These are the main features on the basis of which space programmes are proposed and scrutinised by space agencies around the world. There are obviously many missions that have more practical, non-exploratory purposes, like communication, positioning or military services, but those are not the subject of this work.

Some of the high-level reasons to explore our Solar System are to understand how planets form and evolve, what dynamics produced the variety of worlds that we observe and what phenomena are currently shaping these bodies. For example, our understanding of atmospheres and climates, despite decades of research, is still shallow. This is mostly due to the complexity and chaos embedded in these systems, which can be more easily confronted

thanks to additional data points on different worlds. Even the functioning of the Sun, which is the main governor of these intricate systems, is yet to be fully modelled and understood. Geology (both of the Earth and of other planets) is another field where our knowledge is still blatantly incomplete, generally because of the impossibility to probe directly the depths of a planet and the reliance on indirect measurements or extrapolation of what happens on the surface.

Numerous other and more specific questions are asked by the scientists who focus on the study of the worlds of our Solar System, as summarised in Section 2.3. Nonetheless, there is one overarching subject that appears to be pressing for many explorers: life. Particularly, how life emerges and evolves on a planet, if that is possible elsewhere than Earth and how common it is. Moreover, they question whether any of these locations could be able to sustain human life one day. These are millennia-old questions that seem to have always troubled our species and for which we have previously turned to myth, religion and philosophy: where do we come from? Are we alone in the cosmos? What does the future hold for us? Today, technology is available to directly probe the Universe for hints on these questions.

2.2.2 Technological return

Technological return is often presented as one of the prominent contributions from spaceflight to human progress. For sake of clarity, it should be noted that two types of technological return can be identified in this case: direct and indirect. The direct returns are those strictly linked to the mission's purpose. For example, the launch of a constellation of positioning satellites enables space-borne positioning as a technology. On the other hand, the subject of this study are the mission with more exploratory intent, which typically generate indirect technological returns. These are technologies that are developed for the mission's purposes but then find other uses in different contexts on Earth. Notable examples can be found in the plethora of technical advancements brought by the Apollo programme: from microelectronics to medical imaging, water purification or thermal insulation.

However, this analysis is neglecting an even more direct technological return of venturing beyond our atmosphere: spaceflight itself is a technology, and one that will most likely be crucial to humankind in the future. Curiously, it is the only technology whose development is justified through the achievements of its by-products rather than its own, often because of fear of incomprehension by the general public. This argument is at risk of becoming counterproductive in the long run, pushing towards increasingly whimsical justifications instead of educating the public that learning to fly is the first reason for which flight should be practised.

2.2.3 International cooperation

Non-military space programmes provide attractive opportunities for cooperation between different countries or international institutions because, while scientific discoveries and technological advancements are not reduced when shared, development costs are. The campaign subject of this PhD is a clear example of collaboration between two major space agencies: NASA and ESA. Splitting the large investments involved in high-profile exploration missions makes them more palatable to finance officers, but it also brings complex diplomacy and, unfortunately, more likely schedule slips. Despite its challenges, it is only thanks to extensive cooperation between multiple agencies across the world that there has been continuous human presence in space since 2000 on the International Space Station (ISS).

Space exploration thus acts as a catalyst that encourages nations to work together peacefully and trust each other enough to share sensitive technologies. In some cases, these collaborations can be used to broadcast strong political messages. This was the case for the Apollo-Soyuz mission, performed jointly by the United States and the Soviet Union in 1975 to seal the end of the hostilities of the Cold War. For this mission, the two iconic capsules were modified to perform a rendezvous and docking manoeuvre, connecting their pressurised compartments to allow crewmembers from both nations to meet in orbit.



Figure 2-2 – American astronaut Thomas Stafford and Soviet cosmonaut Aleksey Leonov meet in the passage connecting the Apollo and Soyuz spacecraft (credit: Johnson Space Center / NASA)

2.2.4 Inspiration for the public

Among the secondary effects of space exploration missions, it is worth noting their influence on society and the wider public. A variety of positive stimuli are reflected into the social fabric of the nations and the communities that undertake spaceflight. Their resonance can be significant, depending on the effectiveness of the communication from their institutions.

The benefits include: inspiring the young to pursue scientific and technical education or career paths, attracting capable scientists, engineers and administrators to the aerospace field and motivating them to work for the progress of humankind. Furthermore, flying into space offers new perspectives on our planet and teaches us the importance of respecting it. Lastly, but perhaps most importantly, ambitious, long-term space programmes provide a shared purpose to the people committing to them, a central project that societies need to avoid drift and stagnation.

In general, these effects are only as good as the communication from the relevant institutions, particularly the space agencies and the governments that fund them. It is of great importance that the outreach in this field is well curated and aims at creating a connection with the wider public and not just with the enthusiasts already interested in the field.

2.2.5 Transcendence of human limits

The exploration of space and any other uncharted region or field of knowledge is also the response to a primal curiosity and desire for understanding coded into the more ancient parts of our brain. Such instincts are common among intelligent animals and at their most pronounced in humans. They are arguably some of the traits that have brought our species so far and made it such a successful animal despite not having many obvious biological advantages on other primates. The genus *Homo* includes, in fact, the only nomadic primates ever known to exist, who have survived through drastic climate change and global catastrophes thanks to their drive to expand their horizons.

Among the descendants of these pioneers, softened by the comforts of sedentary life, there are still those who understand this call. The need to explore and overcome our limits is the push to advance humankind towards becoming a more capable, prosperous and knowledgeable civilisation. Considering its prime importance, the simple argument of expanding the boundaries of our species should be the first and irrefutable argument for space exploration. Unfortunately, the policymakers controlling public investments are typically not as responsive to the thrill of exploration.

Even if slowed down by the hurdles of modern society, space exploration continues to advance our civilisation towards new worlds and new discoveries. The proof of its deep significance for us humans is that, when we look back on our collective history, we count these endeavours among our proudest achievements as a species.

2.3 Destinations of interplanetary probes

Having briefly discussed the reasons that bring humans and machines to leave the Earth for other celestial bodies, the next pages will describe the destinations of these journeys. This section lists the main regions of the Solar System to which humans have sent spacecraft. For each one, a brief explanation of the associated exploratory interest is provided, together with hints of what kind of spacecraft are flown there and how. This is by no means intended to be an exhaustive overview of the characteristics of these destinations and the concerning scientific research, but rather an indication of the human-made objects that have reached them, their goals and the engineering solutions adopted to achieve them.

2.3.1 The Sun

The central star in our planetary system, named Sol, is a 5-billion-year-old, yellow-white dwarf star. Identified as class G2 according to the Harvard spectral classification [3], it is an ordinary, but not exceedingly common type of star. The star accounts for 99.9% of the planetary system's mass. All the remaining objects, even those that we call worlds and strive so hard to explore, are nothing but debris scattered in the void, leftover from the star's formation. The Sun governs not only the gravitation, but also the radiation, magnetic and particle environment of all the objects in its sphere of influence. All the planets formed with the Sun and all will end with the Sun, either through incineration or freezing. The Sun controls their temperature, their atmosphere, their weather, and most of the phenomena that occur on their surfaces, including life.

For its key role in the planetary system, and also for being the only star that we can really observe up close, the Sun has been object of scientific investigation since long before space-flight was invented. These studies are aimed at improving our understanding of its working

principles, from the core to the corona, and our predictions on its behaviour. This applies to short-timescale phenomena, like flares and coronal mass ejections, which pose a threat to our technology, and also to medium-timescale phenomena, like the 11-year solar cycle and its drifts, which affect Earth's climate and the radiation environment for spacecraft and astronauts. The human lifespan (and that of human civilisation, for that matter) is too short to observe long-timescale phenomena in the evolution of a star, so for those we have to turn to other stars in different stages of their lives and extrapolate their behaviour.

The Sun is one of the few celestial objects on which we have a quite good view from our planetary home, so spacecraft to study the Sun are often placed into Earth orbit or in solar orbit in proximity of the Earth. Some of them, however, do need to get up close to achieve their objectives: sometimes close enough to fly through the scorching solar atmosphere. Among these daring missions, two recent examples are worth dwelling on: ESA's Solar Orbiter and NASA's Parker Solar Probe.

2.3.1.1 Solar Orbiter

Solar Orbiter has the objective of studying how the inner heliosphere³ works, how the Sun's internal dynamo regulates its magnetic field and aims to perform the first close-up observations of its polar regions. The spacecraft, launched in 2020, is using a series of flybys of Earth and Venus to modify its orbit. At its closest approach, it is expected to reach 0.28 AU⁴ (42 million km) from the Sun and achieve an orbital inclination of more than 33° with respect to the ecliptic plane⁵ [4]. Solar Orbiter carries both remote-sensing instruments to observe the Sun, and in-situ instruments to measure the solar wind around the spacecraft.

The probe is protected by a multi-layer titanium heat shield on its sun-facing side, designed to withstand more than 500°C on its surface whilst maintaining the internals of the spacecraft at room temperature. On the shield are peepholes with shutters that allow remote-sensing instruments to perform brief observations of the Sun.

All on-board hardware must be kept in the shield's shadow at all times whilst in proximity of the Sun or it would rapidly overheat. This is an exception of the solar panels, which obviously have to receive sunlight. Even those, however, are unable to withstand the full power of the solar radiation without damage, and are maintained tilted away from the direct line of sight to reduce flux density on their surface.

³ The heliosphere is the region surrounding the Sun that is filled with the solar magnetic field and the particles of the solar wind.

⁴ AU, Astronomical Unit, a measure of length equal to the average Sun-Earth distance, approx. 1.5×10^{11} m.

⁵ The ecliptic plane is the plane on which the orbits of all planets are located.

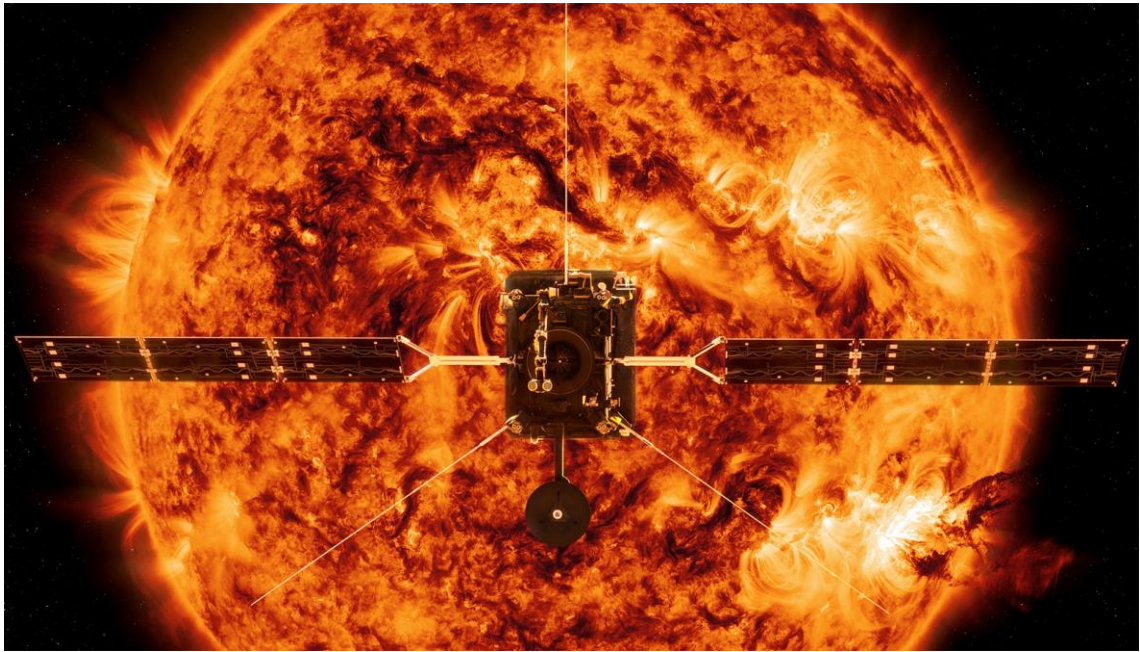


Figure 2-3 – Artist's impression of Solar Orbiter (credit: ESA / ATG Medialab / NASA)

2.3.1.2 Parker Solar Probe

The Parker Solar Probe, launched in 2018, has scientific objectives that complement the mid-range observations made by Solar Orbiter with in-situ measurements in the close proximity of the Sun. The mission aims at studying the dynamics of the solar corona and the solar wind, the behaviour of the plasma and magnetic fields in that environment and the mechanisms that accelerate and transport energetic particles from there outwards into the Solar System. To do so, the spacecraft will get to a daring 0.05 AU (6.9 million km) from the Sun's surface, or less than 10 solar radii.

The probe keeps tightening its approaches to the Sun through repeated flybys of Venus and will eventually reach, at perihelion⁶, the speed of 690 000 km/h, or 0.06% of the speed of light, making it by far the fastest object ever flown by humankind. During its close approaches, the spacecraft is fully immersed in the star's outer atmosphere, the corona, which is composed by plasma heated to more than a million degrees Celsius and will be sampled by the instruments on board. It is relevant to note that, even if the corona is extremely hot, it is also very rarefied, close to a vacuum, so the heat exchange to the craft is minimum and radiation remains the main mode of heat transfer.

To protect itself from the radiated heat, Parker Solar Probe is equipped with engineering solutions that are similar to those of Solar Orbiter, but brought to the extreme. They include a super-heated carbon-carbon composite shield designed to operate at 1400°C and water-cooled solar arrays that are retracted during close encounters with the sun. The heatshield is monolithic, as no optical instrument could survive staring at the Sun from that distance. The sun-pointing attitude has to be perfectly maintained or the probe would be vaporized.

⁶ The perihelion is the point in an object's orbit around the Sun where it is closest to the central star. It is opposed to the aphelion, which is the point at which the object is furthest from the Sun.

When flying through the corona, the plasma enveloping the craft precludes any communication with Earth and a shower of charged particles obfuscates its star trackers⁷. The Attitude and Orbit Control System (AOCS) must then resort to more rudimentary strategies like limb sensors, i.e., toughened sensors that, when illuminated, trigger an immediate response to correct the spacecraft angle [5]. Figure 2-4 shows a striking view of the solar corona from the Parker Solar Probe, with the Milky Way and Venus (bright spot on the right) visible behind the shower of energetic particles.

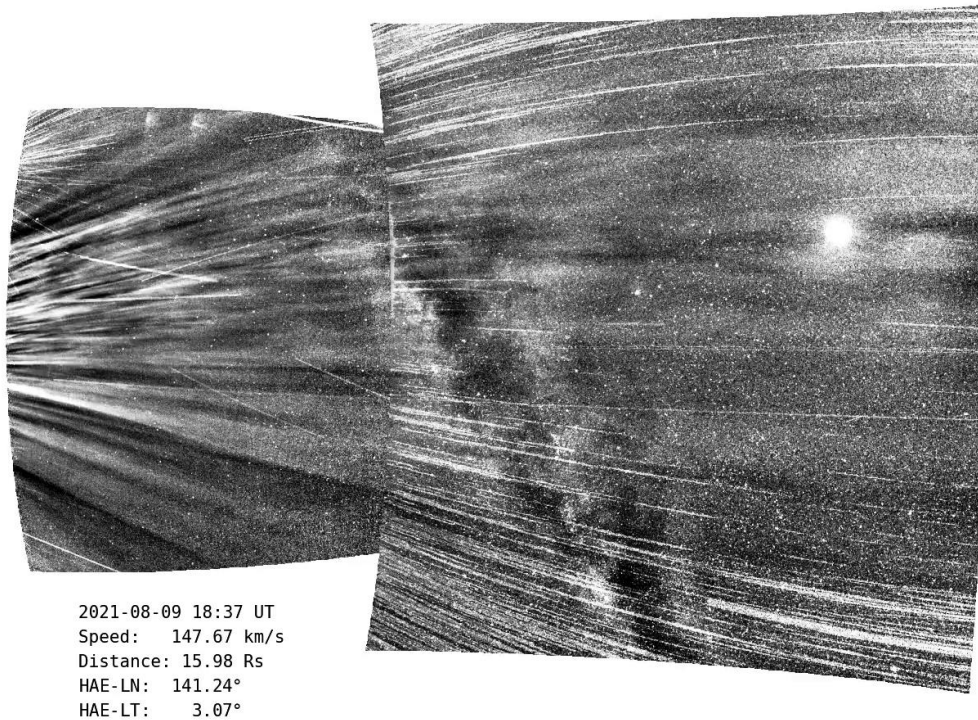


Figure 2-4 – The view from Parker Solar Probe flying through the solar corona (credit: NASA / Johns Hopkins APL / Naval Research Laboratory)

The probes described above surely account for the most daring manoeuvres that we have ever performed in proximity of our star, but they are only one part of the large family of missions that study the Sun. One last thing to note on these missions to the Sun or the inner Solar System is that they typically use a long series planetary flybys, also called “gravity assists”. Getting to these regions is, in fact, very costly in terms of propellant, which is counter-intuitive, as they are relatively close to the Earth. This is due to the fact that the Earth moves in its own orbit at an unforgiving 100 000 km/h, and the spacecraft that aim at getting close to the Sun need to considerably reduce that velocity to set a course towards the inner system.

2.3.2 The inner planets

The inner planets of the Solar System, or rocky planets, are the four worlds closer to Sol: Mercury, Venus, Earth and Mars. They are separated from the outer planets by the Asteroid

⁷ A star tracker is an imaging device that establishes a spacecraft’s attitude by recognition of known star patterns.

Belt, and they are broadly similar in the fact that they are primarily composed by silicate rocks and metals.

2.3.2.1 Mercury

The closest planet to our star is, unsurprisingly, a world of extremes. It is not only exceptionally hot during the day (up to 430°C), but also very cold at night (down to -180°C). The difference is due to the absence of an atmosphere, but also to the fact that the length of a day on Mercury (58 Earth days), is comparable to that of a year (88 Earth days), meaning that the illumination changes very slowly. As a consequence, enormous thermal gradients can arise on its surface, with variations of hundreds of degrees Celsius over distances of mere metres.

Without an atmosphere, the surface of the planet is exposed to hard vacuum, bathed in solar radiation and energetic particles. Gases and volatiles are actually produced on the surface by sublimation and venting from the lithosphere⁸, but they are constantly blown away by solar wind and radiation pressure, and they escape the planet's weak gravity (38% of Earth's). As a result, the whole planet is accompanied by a tail of volatiles (prominently sodium) flowing outwards into the Solar System, similarly to a comet. Even if much less dense than a comet's tail, it can be detected in Earth-based imagery and sampled by spacecraft in the proximity of the planet [6].

This extreme environment makes Mercury a difficult place for known biology and technology. The planet's geology is still not well understood, given contradictory hints provided by the heavily cratered surface, which suggest no recent geological activity, and the weak but evident global magnetic field, which suggest a dynamo effect in an active, molten core. Only three missions have braved the challenges of travelling to the innermost planet in the history of spaceflight, the last of which is still in transit at the time of writing:

- NASA Mariner 10, launched in 1973, which performed three flybys of the planet.
- NASA MESSENGER, launched in 2004, which orbited the planet from 2011 to 2015.
- ESA / JAXA⁹ BepiColombo, launched in 2018 and currently en route through a series of gravity assists, due to enter in orbit around Mercury at the end of 2025 (Figure 2-5).

Spacecraft flying to Mercury, in particular those that spend extended time in its proximity, face the same kind of challenges as the Sun orbiters described in Section 2.3.1, even if to a less extreme degree. It is worth noting that these probes have to protect themselves not only from the Sun, but also from the planet itself, which, at more than 400°C on its day side, glows brightly in near infrared and occupies a much larger portion of the sky. This radiation, even if less intense than that of the Sun, can still slowly overheat and kill exposed spacecraft, which have to resort once more to shielding, cooling and careful attitude management.

No landers have ever been sent to the surface of Mercury also because, with our current technology, they would be rather short lived: on the night side, in the freezing cold and without solar power, they would run out of energy in the attempt to keep themselves warm,

⁸ The lithosphere is the solid layer around a rocky planet, usually comprising an outer crust and a certain portion of inner layers, until the point at which they become fluid.

⁹ Japan Aerospace eXploration Agency

while on the day side, surrounded by the incandescent surface, they would stand little chance of rejecting the heat and avoiding meltdown.



Figure 2-5 – Artist's impression of BepiColombo at Mercury (credit: ESA / ATG Medialab / NASA / JPL-Caltech)

2.3.2.2 Venus

Due to its proximity to Earth, Venus was the first planet to be reached by robotic spacecraft. While being relatively easy to reach, this world proved much harder to explore. Contrary to the tropical paradise imagined by the ancient astronomers, Venus turned out to be a vision of hell: a 470°C desert enveloped by corrosive gases, at 93 times the pressure of Earth's atmosphere. The cause of these temperatures, even higher than Mercury's, is a runaway greenhouse effect in the thick, carbon dioxide atmosphere.

Venus is almost identical to Earth in dimensions and mass and it demonstrates that maintaining a stable habitable environment is not just a matter of size and composition. Its surface is always cloaked in thick clouds, which can be penetrated only by radar. It is now known to be rich in granite-like rocks that require abundant water to form. It is possible that the planet hosted liquid water on its surface for up to billions of years, compared to the few hundreds of millions for Mars. On Earth, that timespan has been amply sufficient to spawn life.

The scientific interest around Venus is centred on improving our understanding of the evolution of Earth-like worlds, but there are many other phenomena yet to be explained. Geological activity on this planet is not fully understood: it lacks plate tectonics¹⁰ or a global magnetic field, however, the dating of the surface through impact craters shows that it is no older than 700 million years. This suggests that Venus' surface was completely reshaped by

¹⁰ On Earth, plate tectonics is a process in which sections of the planet's outer crust glide over the mantle – the rocky inner layer above the core – allowing heat to escape through volcanism.

a worldwide volcanic event in its recent geologic past, but exactly what happened is still up for debate [7]. The atmosphere rotates 60 times faster than the surface, a phenomenon known as super-rotation, while the planet rotates slower on its own axis than around the Sun, i.e. one day on Venus is longer than a year (respectively, 243 Earth days and 224 Earth days). The planet also spins in the opposite direction as the typical one in our Solar System, i.e. the sun rises in a westerly direction. Most of these phenomena are not yet understood. A recent controversial discovery of phosphine (a potential biosignature) in the atmosphere has reignited astrobiological interest [8], but the findings are still unconfirmed.

Unfortunately, the extreme atmospheric conditions described above make it quite difficult to satisfy our curiosity. The Soviet Union was an undisputed leader in the early exploration of Venus, and the only nation to have operated landers on its surface to this day. These landers, part of the Venera programme, resembled more the design of a submarine than that of a spacecraft. They were based on a pressurised hull containing the instrumentation, which was as reinforced and thermally insulated as possible. Phase-change materials were included, to exploit latent heat to maintain a tolerable temperature for longer. Despite the extreme engineering effort, the Venera landers were designed to operate mere minutes before overheating. The most long-lived of them, Venera 13, transmitted data for 127 minutes. Figure 2-6 shows one of the most famous panoramic pictures of the surface of Venus (there are not many to choose from: only 6 have been taken in all history). Shot by Venera 13, it is the first colour image of Venus, relayed back to Earth in 1982.

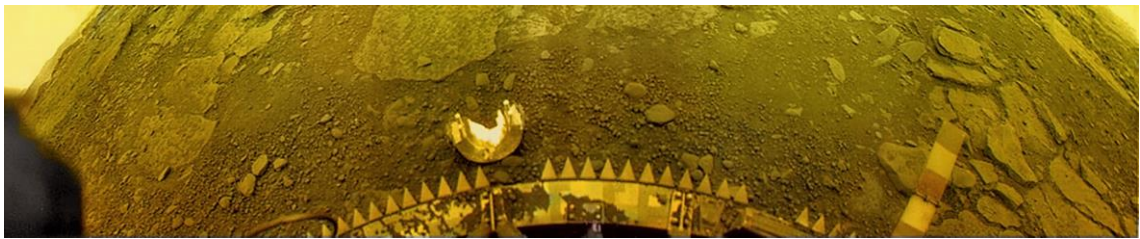


Figure 2-6 – The surface of Venus imaged by the Venera 13 lander’s front camera (credit: Russian Academy of Sciences / T. Stryk)

There have been several missions to Venus since the first landings, more commonly in the form of orbiters, which, provided the right instruments, can perform observations without having to face the hellish environment on the surface. In addition, the planet is often used for gravity assist by spacecraft on their way to other destinations in the Solar System, allowing for opportunistic science to be performed during these brief flybys. Today, only one spacecraft remains in orbit around Venus, that is the Japanese Akatsuki (あかつき, “Dawn”) probe. The mission was initially considered doomed when its main engine malfunctioned during its encounter with Venus in 2010 and failed to insert it into orbit. The spacecraft then spent 5 years orbiting around the Sun and, through a series of carefully planned trajectory correction manoeuvres, it reencountered Venus in 2015 and was able to achieve a stable orbit. Despite the long detour, all instruments were still in good health and most of the original science objectives were restored [9]. Akatsuki is still doing science to this date and transmitting spectacular images thanks to its infrared instruments, which exploit the glow of the fiery planet to map currents in its atmosphere. One of these pictures can be seen in Figure 2-7.



Figure 2-7 – The night side of Venus in infrared light, imaged by the Akatsuki spacecraft (credit: JAXA/ ISAS / DARTS / D. Bouic)

The geological, climatic and astrobiological interest around Venus is driving a positive trend for future missions, with at least three currently planned to launch before the 2030s. Other flybys are happening for gravity assist manoeuvres, like those of BepiColombo, mentioned in Section 2.3.2.1. A notable flyby is that of the ESA's mission JUICE (JUperiter ICy moon Explorer), planned to launch in 2023 and to encounter Venus on its long series of gravity assists to the Jupiter system. The spacecraft will carry an instrument able to detect phosphine with thousands of times better sensitivity than current observations, which might resolve the current disputes on the discovery.

2.3.2.3 Earth and Moon

As discussed in Section 2.1, the observation of planet Earth from space is not included in this summary, as it would be too vast a subject to be treated in these pages. As a matter of fact, in recent times, the majority of the space business was concentrated into Earth orbit, with scientific missions to study our planet, astronomical observatories, military and commercial satellites providing services like surveillance, mapping, navigation, communication, etc. Today, the launch rate to Earth orbit is increasing faster than ever and it will likely continue to do so. To maintain the emphasis on the exploration of the Solar System, we will not dwell on the thousands of satellites currently orbiting the Earth, but instead focus on the nearest planetary body: the Moon.

Earth's natural satellite attracted a lot of attention during the early days of space exploration because of its proximity and ease of access, becoming a well-suited target for the demonstration of technological superiority during the Cold War. During the '60s, the Moon was being visited by a growing swarm of robotic probes, with an average launch rate of nearly one Lunar mission every two months. These efforts culminated in the crewed Apollo Moon landings during the late '60s early '70s and then suddenly died out. Human spaceflight

retreated to low Earth orbit and the frequency of robotic missions to the Moon dropped to one or two every decade. This abrupt abandonment can be attributed to the political evolution of the Cold War, which directly influenced space exploration budgets, as well as the fact that the Moon did not prove as interesting as the early pioneers fantasised.

In reality, the scientific interest towards the Moon never decreased during the Apollo programme, but it was drowned out by the political drumbeat and never quite became the priority. It is true that the Moon is a “dead rock”, composed of the same stuff of Earth’s mantle, exposed to hard vacuum and baked by radiation, nonetheless, it is also a pristine fossil from Earth’s formation, with an active role in maintaining our planet habitable to this day. Only during the last of the Apollo flights, a professional geologist, Harrison Schmitt, was sent to the Lunar surface, a choice that greatly enhanced the scientific return of the mission. Schmitt’s trained eye was able to select the most relevant material and he stuffed the command module of Apollo 17 with more than 110 kg of Lunar samples, which were returned to Earth and still yield valuable science to this day.

In the long run, the Moon’s relevance for the geology, formation and evolution of our planet has driven a progressive return to our natural satellite, with the frequency of robotic missions visibly picking up since the early 2000s. This is in concomitance with renewed interest for human exploration, led by NASA’s Artemis programme. In addition to direct scientific interest, the Moon is acquiring strategic importance for other scientific, technological and exploratory endeavours. With its proximity, low gravity and vacuum environment, the Moon can be a suitable location for astronomical observatories, logistical bases and even mining or propellant production facilities to support expeditions outwards into the Solar System. Particular attention is being drawn by the polar regions, where water ice is still present and the low illumination angle offers important advantages for power generation and thermal control.

With regards to the technology required to fly to our moon, orbital probes do not require radically different solutions from those operating around the Earth, at exception of an increase in communication power and radiation shielding, being outside of our protective magnetosphere. Truth to be told, the Earth – Moon system (plus some near-Earth asteroids) is the only place where standard human technology is somewhat suited for spaceflight applications. Like our biological bodies, our technology evolved in Earth’s environment, in a warm, dense atmosphere, a 1 g¹¹ gravity field and a benign radiation environment. For how irritating it might be, the engineering mind is biased by millennia of solving problems that fully resided inside the Earth environment. The change of setting that comes with spaceflight is at the basis of most of the hardships of interplanetary travel. Nonetheless, our spacecraft in orbit around the Moon find a reasonable average temperature, plentiful solar energy, and a low communication delay.

These considerations apply to satellites that fly on controlled orbits or trajectories, however, as soon as a spacecraft lands on the surface, it is the Moon that controls the environment, which makes it far less benign. The average temperature is still approximately -20°C, but distributed over an unforgiving diurnal cycle of 29 days, with typical peaks of +125°C and lows of -170°C [10]. It is no coincidence that all Apollo missions landed at local dawn

¹¹ 1 g (one gee) is a non-SI measure of gravitational acceleration. 1 g is equivalent to the gravitational acceleration on the surface of the Earth, approximately 9.81 m/s².

and left the Moon before the midday sun could overheat the flight systems and kill the crew [11]. Naturally, the same cycle applies to solar power, which dies out at the time when energy is most needed to survive the cold of the night. Among other challenges, spacecraft on the surface of the Moon also have to face the omnipresent dust, which can cause issues like contamination, obscuration, abrasion and clogging for machinery and for humans, as observed during the Apollo programme [12].

This is particularly true for mobile surface platforms, or rovers, which constantly interact with the regolith¹². The first spacecraft of this kind was, in fact, operated on the Moon in 1970: the Soviet Lunokhod 1, shown in Figure 2-8.

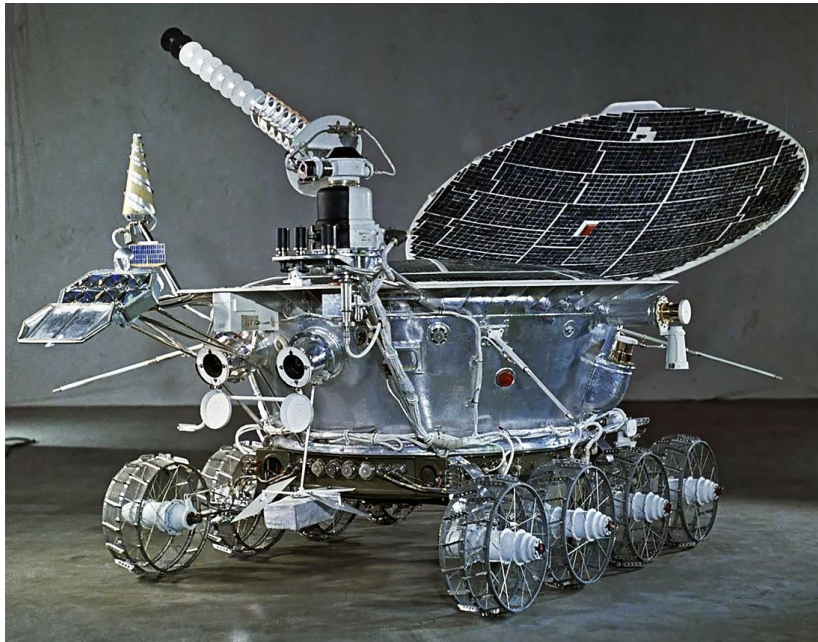


Figure 2-8 – A replica of the Lunokhod rover (credit: B. Borisov / RIA Novosti)

The Lunokhod is a particularly fitting example of the challenges of adapting terrestrial technology to space environment, in fact, instead of developing components able to work in the absence of an atmosphere, Soviet engineers decided to bring an atmosphere with them: the Lunokhod body was a large pressurised vessel and all sensitive components (electronics, cameras, motors...) were maintained at a pressure of 1 atmosphere. It was an aggressive solution and it came with a significant mass penalty, but it worked, and it made the Soviet Union the first nation to operate a mobile vehicle on another planetary body.

The rover had a “lid” covered with solar cells that opened during the Lunar day to generate power and expose a radiator on the top surface of the pressurised body. At sunset the lid would close to shroud the radiator and reduce the heat leak. During the cold Lunar night, the Lunokhod was kept warm by a polonium-210 Radioisotope Heater Unit (RHU). Eight metallic wheels propelled the vehicle, with independent drive actuators but no steering actuators: turning was achieved through skid-steering¹³. In the end, it was its pressurised design that doomed both Lunokhod 1 (which lost pressure and ceased to operate) and

¹² The regolith is the unconsolidated layer of loose rock and dust covering the bedrock on a planetary surface.

¹³ Skid-steering is a manoeuvre that commands wheels (or tracks) on different sides of the vehicle with different velocities to achieve a change in the heading.

Lunokhod 2 (which overheated because of dust on its radiator), but not before demonstrating the power of mobile exploration vehicles and setting some hard-to-beat records. Lunokhod 2 held the record for off-Earth roving distance (39 km) until July 27, 2014, when it was exceeded by NASA's Opportunity rover on Mars.

Among the numerous spacecraft operated on the Moon, another example is worth mentioning for its relevance to this research project: the Apollo Lunar Roving Vehicle (LRV), shown in Figure 2-9. Both Lunokhod and LRV were not autonomous vehicles but were piloted by humans, however, while the Lunokhod was teleoperated from Earth, the Apollo "Moon Buggy" was designed to be driven by astronauts on board and transport them during their Extra-Vehicular Activity (EVA) on the surface of the Moon. The rover was not meant to survive the night or recharge its battery, which allowed a rather simple design. It was nonetheless required to provide very high mobility performance to be advantageous to human explorers. The LRV was designed for a top speed of 13 km/h, but achieved approximately 18 km/h when driven by Eugene Cernan and Harrison Schmitt during Apollo 17. Such velocity is two orders of magnitude greater than that of the most modern robotic rovers.

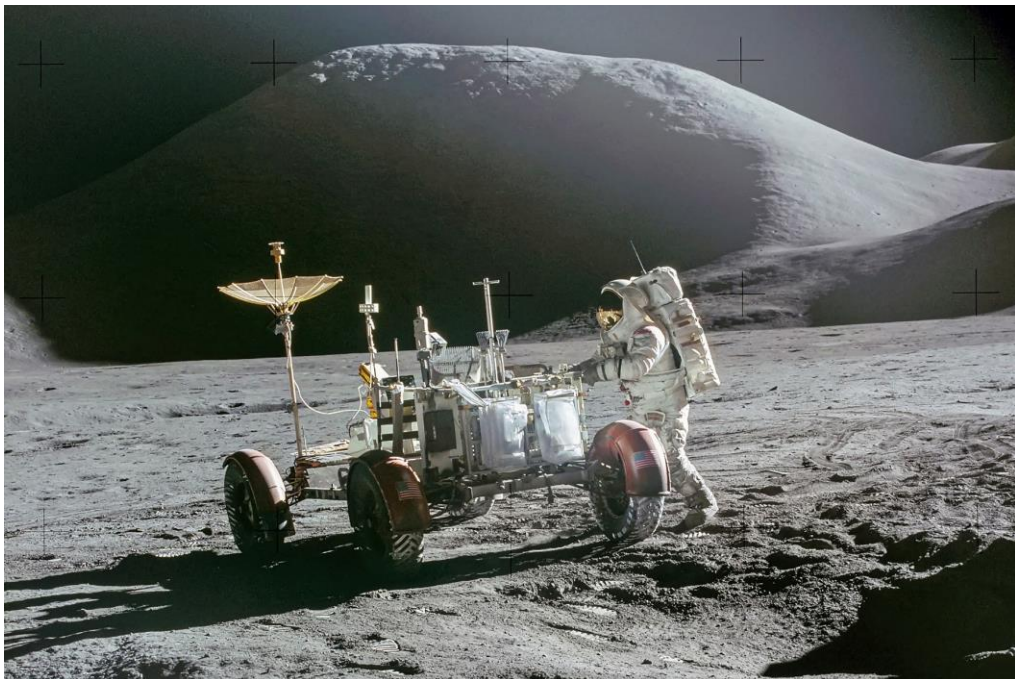


Figure 2-9 – Astronaut James Irwin with the Lunar Roving Vehicle and Mount Hadley in the background during Apollo 15 (credit: NASA / David Scott)

The feature of the Lunar Roving Vehicle that is of particular importance for this project resides in its wheels. The LRV's wire-mesh tyres were developed in cooperation between NASA and Goodyear to behave similarly to terrestrial off-road tyres. The resulting compliant tyre provided excellent traction and obstacle-envelopment capability, enabling the vehicle to output its well-known mobility performance. The same technology, more than half a century later, is being adapted to be used on the Sample Fetch Rover. The spring-mesh tyres, discussed in detail in Chapter 7, are the legacy of the ingenious design that carried Apollo astronauts on the surface of the Moon.

2.3.2.4 Mars

Due to its central role in this study, the exploration of Mars and the probes that pursued it are analysed in more detail in Chapter 3. In the tone of this simple summary, just one

consideration is offered here to introduce the interest behind travelling to our colder planetary neighbour. It can be drawn by observing Figure 2-10, which depicts in green the habitable zone of our planetary system and the orbits of the four inner planets.

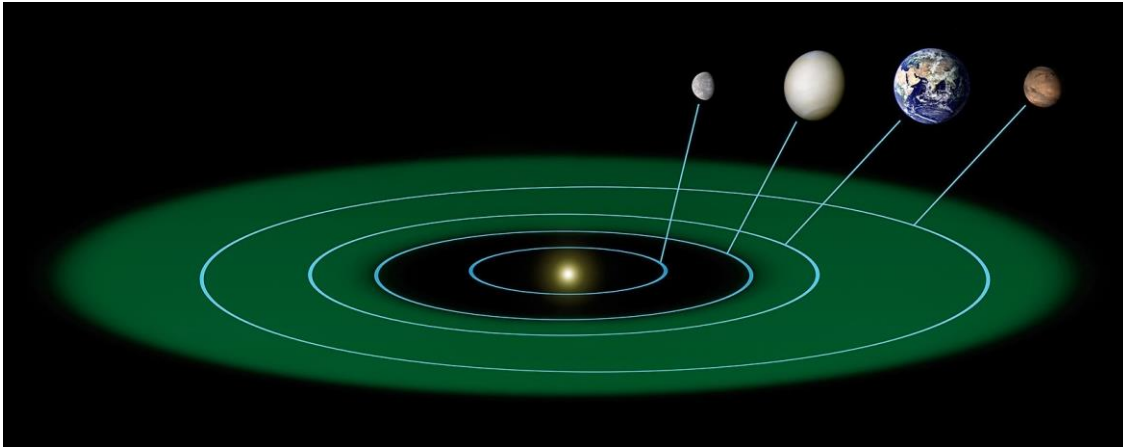


Figure 2-10 – Solar System’s habitable zone (credit: NASA / JPL-Caltech / T. Pyle)

It is now common to see the term “habitable zone” applied to the increasing number of planetary systems that exoplanet surveys are detecting. In its simplest formulation, it identifies the family of orbits where, given favourable atmospheric conditions, liquid water can exist on the surface of a planet. This reasoning is rarely used in our own planetary system because we know with confidence that it contains only one habitable planet: Earth. However, if the same considerations were applied to the star Sol, the situation in Figure 2-10 would be obtained, showing two planets orbiting within the habitable zone: Earth and Mars.

If the Solar System had been detected by one of our exoplanet hunting missions, we would be looking at two candidate habitable planets and, if we were unable to see their atmospheres (for example exploiting a transit in front of the parent star), they would be of equal interest. Therefore, the first questions that scientists ask themselves about Mars are why and how it turned out so different from Earth: whether it is due to its size, its geology, the lack of magnetic field, or the absence of a large moon, if it is linked to orbital mechanics, chemistry in its atmosphere or lithosphere.

On the other hand, Mars is not really that alien compared to our world. If we consider other planetary bodies, even without venturing outside of our system, the variety is striking: ranging from planets with incandescent, corrosive atmospheres, to glaciers of frozen nitrogen, volcanoes erupting liquid water and bottomless worlds, where no solid surface can be reached. In view of this diversity, Earth and Mars are, in fact, notably alike. Figure 2-11 provides an example of how certain areas of the planets can be remarkably similar, with the blue sky giving away Earth’s desert. As a matter of fact, the presence of vegetation and soil of organic origin are the main features that make terrestrial landscapes so different from other desert planets.



Figure 2-11 – Comparison between Mars and the Atacama Desert (credit: NASA / A. Airo, TU Berlin)

There is evidence that Earth and Mars have been significantly more alike in the past, when liquid water was abundant on the surface of the Red Planet. With this in mind, it is reasonable to ask further questions as to the wetter past of Mars, for example, if the planet has ever been able to sustain life as we know it, for how long, if life did actually emerge and if it is still present today.

The fact that it is so comparable, yet so different to the Earth, together with its relative proximity and ease of travel, are the reasons why Mars is such an interesting destination. It is the objective of this PhD project to develop the technology that will help to answer some of the questions listed above.

2.3.3 The outer planets

Outside the orbit of Mars, beyond the Asteroid Belt, reside the four outer planets of the Solar System, which are radically different from the inner ones in the fact that they are many times as massive and primarily composed of volatile substances. Today we identify two gas giants, Jupiter and Saturn, containing primarily hydrogen and helium, and two ice giants, Uranus and Neptune, composed by heavier volatiles (water, ammonia, hydrocarbons).

2.3.3.1 Jupiter

The four rocky planets of the Solar System are all located within a radius of approximately 228 million km from the Sun, but it is necessary to travel more than three times that distance to encounter another planet beyond Mars. In the outer Solar System distances expand significantly and so do flight times. Solar irradiation gets weak, and communication delays become substantial, since light – and hence radio waves – from Earth can take hours to reach a craft in this region. The orbit of Jupiter is the furthest point from the Sun where solar panels can still be used to power a probe, even though at their very limit. As a matter of fact, nuclear power sources, despite their outdated technology, are the most advantageous choice from Mars onwards, and when they are not used it is simply to avoid the political and cost implications of handling radioactive material.

In the cold expanse of the outer Solar System, Jupiter presents itself as a miniature planetary system in its own right. With a massive central object, composed by the same stuff of stars (hydrogen and helium) and dozens of smaller bodies orbiting around it. Similarly to a star, Jupiter also manifests a powerful magnetosphere, so vast that, if it was visible to the human

eye, it would appear larger than a full moon in the Earth's sky [14]. At approximately 318 Earth masses, Jupiter is by far the most massive planet in our system, but still two orders of magnitude away from being able to ignite nuclear fusion in its core and light up as a star.

As it happens with most gaseous planets, on Jupiter it is impossible to identify clearly a surface. We can recognise the cloud tops, whose distinctive colours, caused by small concentration of gases mixed with hydrogen and helium, act like a flow tracer and allow to observe the intricate circulation patterns. Jupiter is an ideal test bed for our understanding of weather dynamics and planet-wide climates: one that keeps proving how our models of these phenomena are, in fact, still lacking. Below the clouds, the gases gradually fade into liquid phase as the density increases, until, under the mounting pressure, hydrogen transitions to its metallic state [15]. This exotic form of matter is an atomic superfluid (i.e., with no viscosity or friction), likely superconductive as well, although it still eludes detailed studies, as it manifests itself only in the extreme pressure conditions that exist inside giant planets like Jupiter and Saturn. What is at the centre of Jupiter is not yet defined: recent measurements suggest a “fuzzy core”, i.e., an increasing concentration of heavy elements dissolved in the metallic hydrogen, but a classical rocky core is not excluded [16].



Figure 2-12 – Vortices in Jupiter's North North Temperate Belt imaged by NASA's Juno spacecraft at low altitude (credit: NASA / JPL-Caltech / K. M. Gill)

It is certainly the peculiar interior of Jupiter that produces its strong magnetic field, but how that happens is still being studied by probes, along with the dynamics of its atmosphere. The only spacecraft currently operating in the Jovian system is NASA's Juno mission, which reports spectacular views of the cloud patterns from close passes in its elliptical orbits around the planet, like the one in Figure 2-12. The planet's magnetic field is extremely problematic for spacecraft flying in its proximity, because it captures charged particles and accelerates them creating intense radiation belts, similar to Earth's Van Allen belts, but thousands of times more powerful. This radiation is destructive for the semiconductor materials at the basis of our electronic technology, so any probe approaching Jupiter needs to carry heavy shielding (usually metallic, e.g., lead enclosures) and try to spend as little time as possible in the radiation zone (for example by flying highly elliptical orbits).

Not many spacecraft have flown to Jupiter before Juno, due to the challenges of pushing a probe this far from home. These are: Pioneer 10 and 11 (NASA, flyby), Voyager 1 and 2 (NASA, flyby), Galileo (NASA, orbiter and entry probe), Ulysses (ESA/NASA, gravity assist only) and Cassini (NASA/ESA, gravity assist only). All of them were designed to face similar challenges: large propellant needs, lack of solar power, cold environment, communication delay, and very high radiation (at exception of Pioneer, which discovered the radiation, and was just fast enough to fly through it before receiving severe damage). Remarkably, 100%

of these missions have been successful. Future missions to Jupiter like ESA's JUICE and NASA's Europa Clipper will be shifting the focus from the planet to its moons.

The natural satellites of Jupiter have attracted attention since the early flybys, in particular the four large Galilean moons¹⁴, which, differently from the others, have shown to be active, complex worlds in their own right. With the exception of Io, which is a tumultuous volcanic world, it is believed that Callisto, Europa and Ganimede all host subsurface oceans of liquid water. These oceans would be kept permanently liquid by the tidal forces of the giant planet, which dissipate deformation energy into the moons' interiors. They might be some of the most hospitable place for microbial life currently present in the Solar System, excluding Earth. Figure 2-13 shows a view of Europa from the Galileo spacecraft: this striped surface of water ice might be hiding a vast salty ocean.

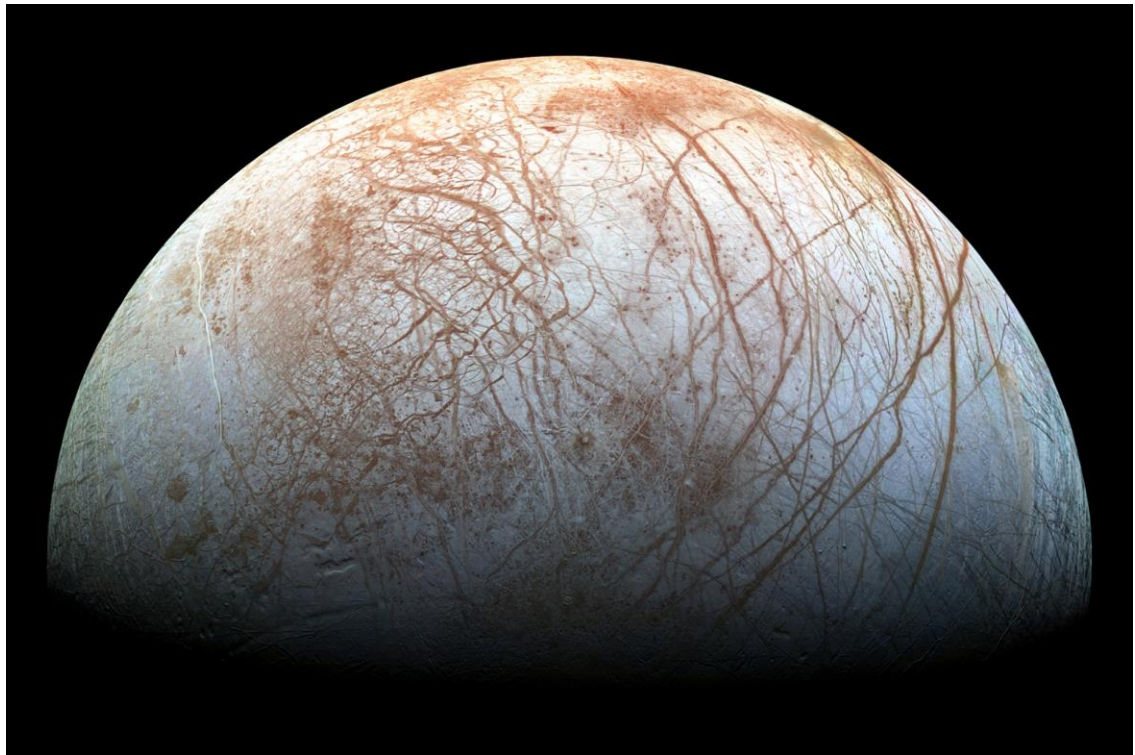


Figure 2-13 – A composite view of Europa obtained by images from the Galileo probe (credit: NASA / JPL-Caltech / SETI Institute)

2.3.3.2 Saturn

In the history of space exploration, only six probes have ventured beyond the orbit of Jupiter: Pioneer 10 and 11 (NASA), Voyager 1 and 2 (NASA), Cassini-Huygens (NASA/ESA) and New Horizons (NASA). These names denote some of the most daring crafts ever produced by human ingenuity and, remarkably, all have performed successfully in the face of extreme odds. So far, humankind's boldest strides towards the stars have been rewarded by the most wondrous achievements. Four of these historic probes have encountered the planet Saturn and one of them, Cassini, has spent more than 13 years orbiting around it.

¹⁴ The largest natural satellites of Jupiter were discovered by Galileo Galilei in 1610 and are called Galilean moons.

Since the invention of the telescope, Saturn has presented itself as one of the most visually impressive features of our planetary system and, when finally visited up close, it certainly lived up to expectations. Saturn is a gas giant encircled by a magnificent ring system and dozens of moons. It has a similar composition and internal structure to Jupiter, although smaller in size, at approximately 95 Earth masses. Saturn's magnetosphere is not as powerful as Jupiter's and its atmosphere does not appear as dramatic to the naked eye, but its climate and storms are not dissimilar. As it happens for Jupiter, an increasing amount of scientific interest is being captured by the objects in orbit around the planet. Figure 2-14 offers a stunning backlit view of Saturn from the Cassini probe: the Sun is behind the planet and the vast ring system shines in scattered light. The night side of planet is partly illuminated by the "ringlight"¹⁵.

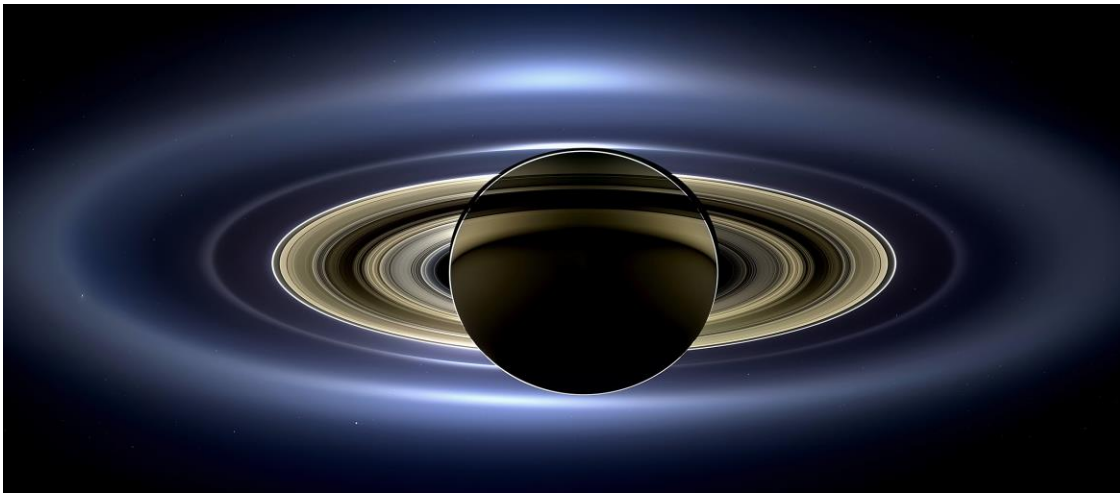


Figure 2-14 – View of Saturn transiting in front of the Sun from the Cassini orbiter (credit: NASA / JPL-Caltech / Space Science Institute)

Orbital dynamics suggest that a ring system like that of Saturn is not a long-lived phenomenon – in planetary terms – and should be stable for a few hundred million years at most. This implies that whatever created it should be a fairly recent event, possibly the disintegration of a moon or the capture of an external body, or perhaps today's rings are the decaying leftovers of a much larger ring structure [17]. The answer is still an object of research. What we know today is that the ring is composed mostly of water ice, like Saturn's moons, and is stabilised by small moons orbiting within its gaps, also called "shepherd moons". One of these bodies, Daphnis, can be seen orbiting in the Keeler gap in Figure 2-15, followed by waves of ring material disturbed by its gravity.

¹⁵ Saturn's ringlight, analogous to Earth's moonlight, is caused by the diffuse reflection of the rings illuminated by the Sun.

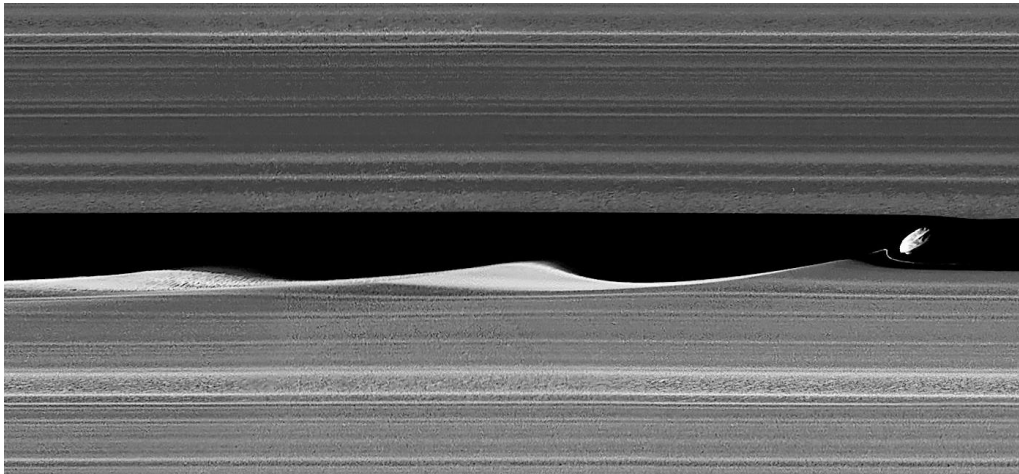


Figure 2-15 – Saturn’s moon Daphnis raising a trail of waves in the ring material imaged by Cassini (credit: NASA / JPL-Caltech / Space Science Institute)

Beyond the rings lays a varied population of satellites, some of which have been subject of a few of the most sensational discoveries in planetary exploration. Inside the faint outermost ring, identified as E ring, orbits Enceladus (on the far left in Figure 2-14), an icy moon with a global underground ocean of liquid water. In fact, the E ring is not only inhabited by Enceladus, but created by it: the moon emanates large plumes from its south pole, ejecting the underground water through the icy crust into open space (Figure 2-16).



Figure 2-16 – Water plumes rising from Enceladus imaged by Cassini (credit: NASA / JPL-Caltech / Space Science Institute)

Scientists realised that, differently from Jupiter’s moons, Enceladus’ ocean would be easily accessible even for spacecraft in flight. Fortunately, a ship with sufficient manoeuvring capability was already available: in March 2008, Cassini altered its course and performed an incredible passage through Enceladus’ plumes at over 51 000 km/h and a mere 52 km above its surface. The measurements obtained echo in the scientific community to this day: 1.6 billion km away from Earth, in the cold outskirts of the Solar System, Enceladus harbours an ocean of salty water, rich in complex organic compounds [18].

When NASA’s Voyager 1 reached Saturn in 1980, the mission team faced a hard decision: an onwards journey to Pluto or a flyby of Saturn’s moon Titan, as the trajectory for the latter

would have flung the spacecraft out of the plane of the Solar System, never to return. In the end, Titan was selected. The choice paid off and revealed a world so interesting to become one of the key motivations behind the Cassini mission and even get its own dedicated lander, the European Huygens probe.

Titan is a planet-sized moon with a thick nitrogen atmosphere and a surface pressure of 1.5 bar. Figure 2-17 shows an image of its surface from the Huygens lander, which is the only existing photograph from the surface of a planetary body in the outer Solar System. The picture portrays a riverbed: Titan is the only other world beyond Earth known to have a liquid cycle, but instead of water, that liquid is mostly methane, which, at the typical surface temperatures of -180°C , can evaporate into clouds, fall as rain or snow and flow through rivers into large lakes [19]. At this temperature, water ice plays the role of rock, forming the moon's lithosphere. The potential for life of this environment remains difficult to assess, as the chemistry is so exotic that might challenge our definition of life itself.

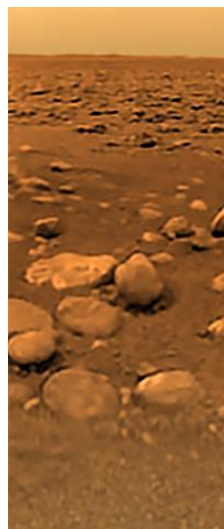


Figure 2-17 – Titan's surface from the Huygens probe (credit: ESA / NASA / JPL-Caltech / University of Arizona)

The probes that flew to Saturn share a similar architecture: they are all powered by a Radioisotope Thermoelectric Generator (RTG), mounted on an appendage to minimise irradiation to the spacecraft components, and their appearance is dominated by a high-gain antenna dish, as large as 4 m in diameter, which is required to maintain contact with the distant Earth. They carry a fair amount of fuel on board for trajectory corrections during their long interplanetary cruise and their thermal control is based on the need to manage precious heat when far from the Sun but also avoid overheating while in transit through the inner system. This is at exception of the Huygens probe, which was a mostly passive lander running on primary batteries¹⁶ with an autonomy of a few hours.

The next planned mission to the Saturn system will likely be very different from the previous ones, and in fact from any other spacecraft ever flown before: Dragonfly is a nuclear rotorcraft designed to land on Titan and explore it through powered flight, taking advantage of the dense atmosphere. NASA is planning to launch this ambitious mission in the late 2020s. It would be the seventh human-made object to operate beyond the orbit of Jupiter.

¹⁶ A primary battery is a battery not intended to be recharged after use.

2.3.3.3 Uranus

With Voyager 1 leaving the Solar System on an out-of-plane slingshot after the encounter with Titan¹⁷, only Voyager 2 remained on its Grand Tour trajectory¹⁸ after 1980. It is the only probe to have visited the last two planets of the Solar System. Yet most of the planets found around other stars are Uranus and Neptune-sized, so studying them improves our understanding of other planetary systems and explains whether our own is a rare case. Because they were observed only through brief flybys and they are too far to resolve in detail through Earth-based telescopes, Uranus and Neptune are still rather mysterious objects.

Uranus presents itself as an almost featureless light blue orb (Figure 2-18), encircled by 27 known moons and a set of very faint rings, whose arrangement hints at one of the peculiar characteristics of the planet: its equator is tilted by 98° compared to its orbital plane, meaning that the planet “spins on its side”. From this follows that Uranus’ diurnal cycle is largely unaffected by its spin and its day is as long as its year, i.e. 84 terrestrial years.

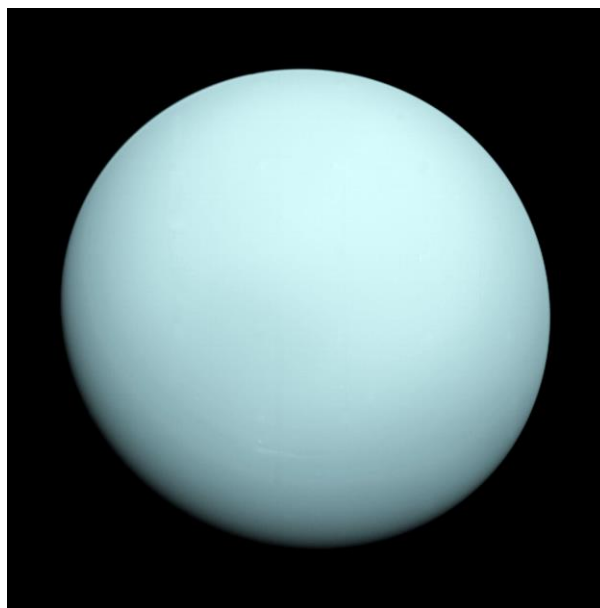


Figure 2-18 – Uranus from Voyager 2 (credit: NASA / JPL-Caltech)

Uranus’s atmosphere is mostly hydrogen and helium with traces of methane, which provides its pale blue hue. Beneath the atmosphere, the bulk of the planet is composed by water, ammonia and methane in a partially frozen state, which forms a dense fluid under extreme pressures and temperatures of thousands of degrees [20]. At its centre, it is believed to be a small rocky core. The inner workings of Uranus became significantly more puzzling when its magnetic field was measured as off-centre by more than 7000 km and tilted by 60° from its rotation axis, meaning that its magnetosphere is constantly twisting and tumbling through space [21]. Uranus also features the minimum internal heat emissions of all planets, making it home of the coldest naturally occurring¹⁹ temperature among all planets, at just

¹⁷ See Section 2.3.3.2.

¹⁸ The Grand Tour is a chain of gravity assists allowing one spacecraft to visit all the outer planets in sequence, see Section 2.1.2.

¹⁹ The absolute coldest temperatures in the Solar System are reported on Earth, but they are created by human technology.

49 K. All of the above hints at some cataclysmic events in Uranus' past that significantly altered the planet's structure: possibly one or more impacts with fully formed planets as large as Earth. It is believed that both Uranus and Neptune formed closer to the Sun and gradually migrated to where they are today, which might explain some planetary accidents along the way.

With just one in-situ data point, it is difficult to say more about Uranus' past. The only spacecraft that encountered the planet, NASA's Voyager 2, was not officially meant to survive this far from Earth, but it succeeded thanks to the ingenuity of its mission designers. The twin Voyager probes are three-axis stabilised systems that use celestial or gyro references to maintain pointing of a large high-gain antenna toward Earth, as shown in Figure 2-19.

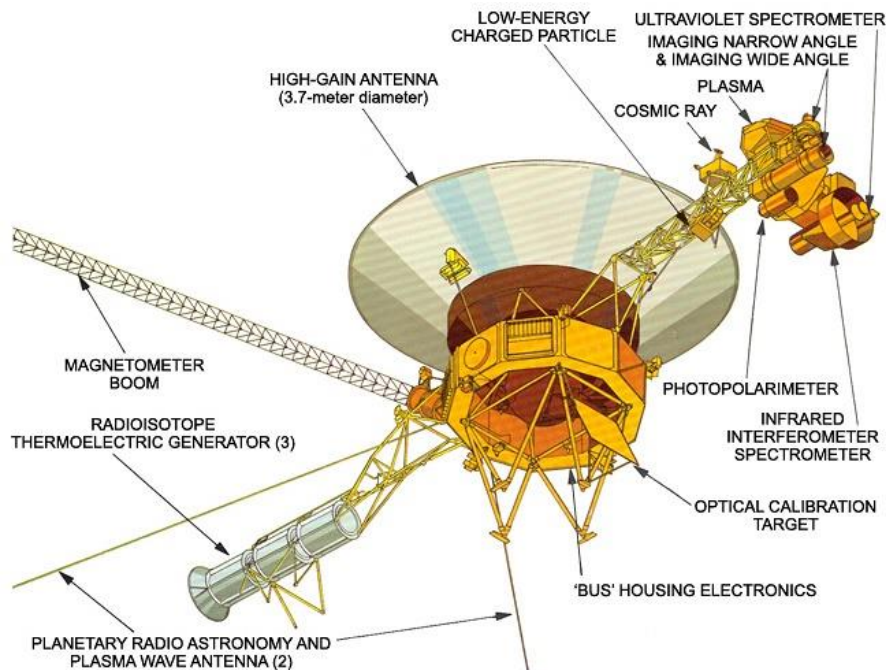


Figure 2-19 – The architecture of the Voyager spacecraft, including main scientific instruments (credit: NASA / JPL-Caltech)

The key challenge at this distance from the sun, besides the lack of sunlight and heat, which are addressed by the RTG power source, is communication. A radio signal takes approximately 2.5 hours to reach Uranus from Earth, so mission controllers need at least 5 hours to get confirmation that each command is executed. This means that the spacecraft had to be highly reliable and autonomous despite their simple technology: the Voyager computer command subsystem, in fact, has less processing power than the battery charger of a modern phone and its memory is a simple magnetic tape that is continuously rewritten. It has been playing without fault for 45 years. To this date, there are no other missions planned to follow the path of Voyager 2 to Uranus, apart from some preliminary studies.

2.3.3.4 Neptune

Neptune, the eighth and outermost planet of the Solar System, is very similar to Uranus in size and composition (see section 2.3.3.3). Different concentrations of gases in the atmosphere are believed to be at the root of its deeper blue colour and more noticeable clouds, which highlight one of the distinctive features of Neptune: its remarkably strong winds. Voyager 2 measured winds as fast as 2100 km/h, which is faster than any other planet and nearly supersonic for the Neptunian atmosphere. The source of all this kinetic energy is still

a mystery, considering that Neptune receives three orders of magnitude less solar energy than the Earth. Some common models suggest that the planet's deep circulation could be feeding a colossal, highly efficient Brayton cycle that powers the high-speed currents [22]. As Uranus, Neptune has been visited only by the Voyager 2 probe and no other missions are expected in the near future. An image from that encounter is reported in Figure 2-20.

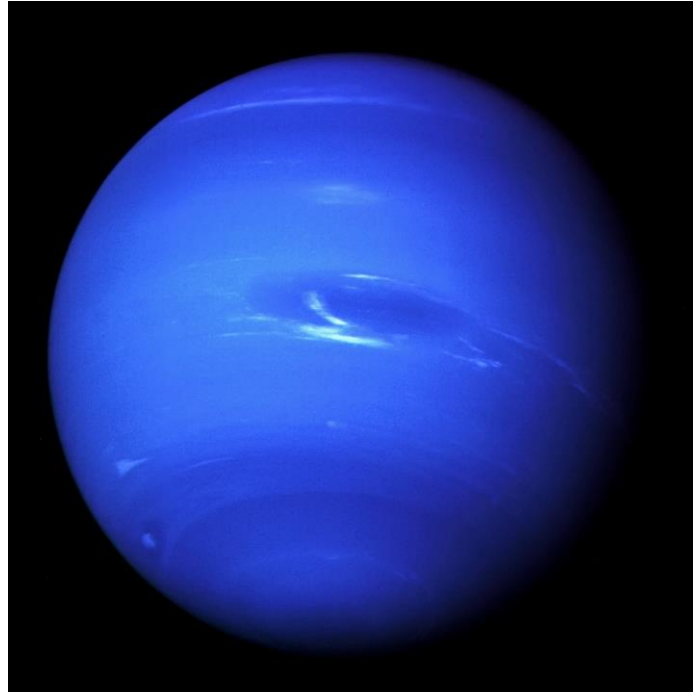


Figure 2-20 – Neptune from Voyager 2 (credit: NASA / JPL-Caltech)

Like all the other giant planets, Neptune is encircled by moons, although not as numerous. 14 have been discovered so far and one in particular stands out from the rest: Triton. This moon is much larger than the others and follows a retrograde orbit²⁰ around the planet, which means that it cannot have been created around Neptune, but it must have been captured after its formation [23]. This is probably true for about half of the moons in the Neptune system, but, while the others have the appearance of small irregular asteroids, Triton is really a world on its own. Larger than Pluto, it displays an active, complex geology with geysers of nitrogen and a surface of water ice, perhaps hiding an underground ocean of liquid water. Figure 2-21 shows a high-resolution image of Triton, with dark plumes from its geysers visible in the top portion. It is believed that Triton was a dwarf planet formed in the Kuiper Belt²¹ and captured by Neptune during its migration outwards in the Solar System. The arrival of such a massive object most likely caused collisions and ejections among the pre-existing moons, leaving the small population that can be observed today.

²⁰ A retrograde orbit is an orbit whose direction of motion is opposite to the rotation of the primary body.

²¹ The Kuiper Belt is a circumstellar disc of mostly small, icy bodies extending outward from the orbit of Neptune see Section 2.3.5.

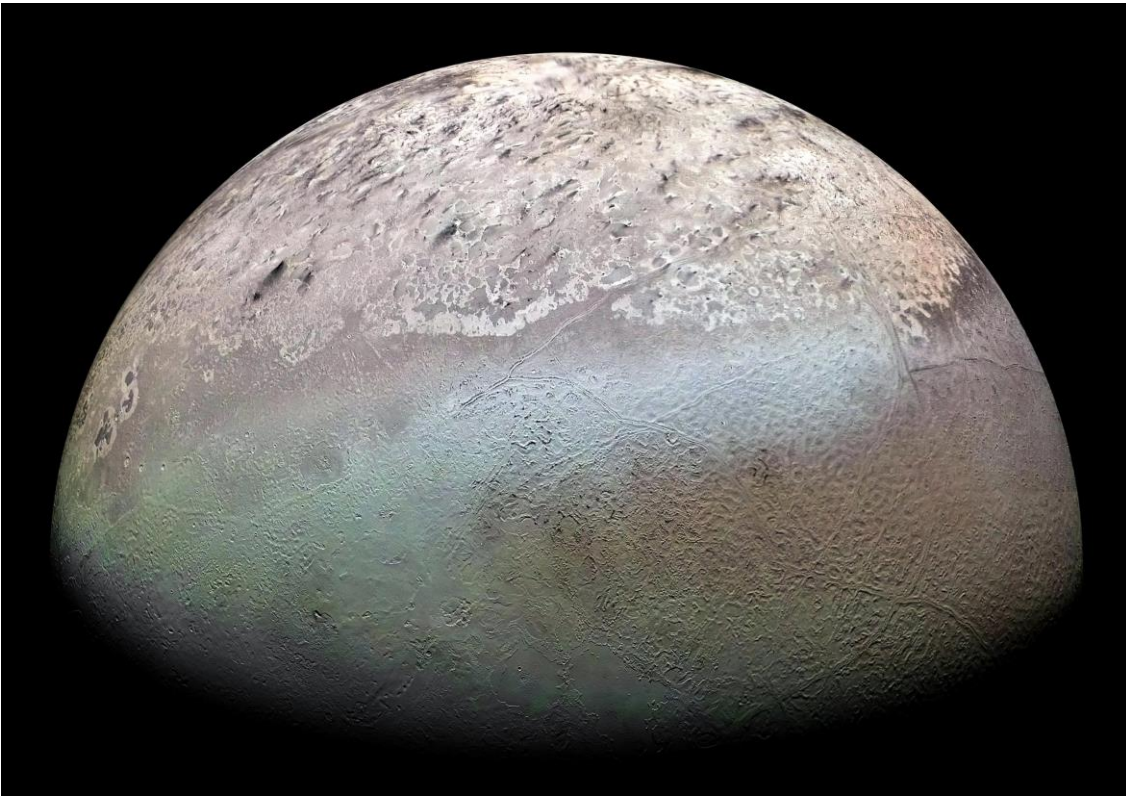


Figure 2-21 – A mosaic view of Triton obtained by Voyager 2 imagery (credit: NASA / JPL-Caltech)

The mission design that is required to fly this far from our Sun has been already mentioned in Section 2.3.3.3, with additional operational challenges caused by the growing distance. The Sun at Neptune is 1000 times fainter than on Earth, meaning no appreciable heating and scarce illumination for photography in visible light. By the time Voyager 2 reached the last planet, it was 12 years old and the decay of its radioactive power source had appreciably reduced the power output. From that moment onwards, it became necessary to start switching off instruments to save power for the spacecraft's vital systems. Communication proved increasingly more challenging, since the Voyager radio transceiver has a power of just 23 W, not much greater than that of a mobile phone, and it was becoming hardly distinguishable from the background cosmic radiation. As both Voyager probes kept flying farther from Earth, ground-based antennas had to increase in size and number, reaching more than 70 m in diameter and eventually forming what is known today as the Deep Space Network (DSN), humanity's key asset in establishing contact with all interplanetary spacecraft.

2.3.4 The minor bodies

Even if this summary is focused on planetary exploration, it is worth mentioning briefly some key categories of smaller bodies which are not planets. These can be identified as:

- Asteroids
- Dwarf planets
- Comets
- Kuiper Belt objects

2.3.4.1 Asteroids

The term “asteroid” is a generic name for any rocky object orbiting the Sun that is not active and not massive enough to assume a spherical shape. Asteroids are scattered across the whole Solar System but are found in particularly high concentration in the Asteroid Belt, between Mars and Jupiter. The belt is essentially a rocky planet that never formed, because the coalescence of its material was disturbed by the gravitational influence of the nearby gas giants. Thanks to that, it provides a window on the early history of the Solar System. The asteroids of the belt are relatively easy to reach and, thanks to their large number, it has been possible to perform close approaches with more than one object in a single mission. Solar illumination is sufficient to power spacecraft and the thermal environment is relatively benign for space standards.

2.3.4.2 Dwarf planets

As described above, the Asteroid Belt is the snapshot of a planet in formation and, in fact, a planetary embryo hides in the belt: Ceres. Almost 1000 km in diameter, Ceres is identified as a dwarf planet, a term that addresses a world sufficiently massive to be in hydrostatic equilibrium, i.e., take a spherical shape under its own gravity, but not large enough to have cleared its orbit from the debris of its formation. Ceres is the only object of this type in the inner system, while several others are found beyond the orbit of Neptune, in the Kuiper Belt.

2.3.4.3 Comets

Comets are minor bodies of the Solar System primarily composed by water ice and dust, which, when in proximity of the Sun, warm up and release volatiles, forming a coma and often a tail pointing away from the Sun. Comets usually move on highly eccentric orbits that keep them far from the Sun for most of the time. Compared to asteroids, they are more pristine remnants of the formation of the Solar System, since they have not been considerably aged by the solar irradiation. They are divided in two categories, based on their origin:

- Short period comets, originating from the Kuiper Belt, which take less than 200 years to orbit the Sun
- Long period comets, originating from the Oort Cloud²², which take more than 200 years to orbit the Sun

It is possible to intercept a comet for a brief flyby as it approaches the Sun and it has been done by several probes. It is significantly more challenging to match a comet’s orbit with a spacecraft since its trajectory can be very different from planet’s orbits. This has been achieved only once, by ESA’s Rosetta mission, which orbited Comet 67P Churyumov–Gerasimenko (Figure 2-22) for two years and landed a probe on its surface.

Rosetta was a solar-powered spacecraft, but matching the comet’s orbit required flying along an arc beyond Jupiter’s orbit. This pushed the craft’s power system beyond its ability to sustain normal operations and it became necessary to put the orbiter into hibernation for 2.5 years. During this period, only basic thermal control was active and the spacecraft was

²² The Oort Cloud is a scattered collection of icy bodies which is believed to occupy a vast region around the Solar System, with a diameter in the order of 1 light year. It has never been directly observed, but comets trajectories indicate its likely existence.

unable to send or receive data. Simple on-board timers were set to reboot the system after 2.5 years, which they did successfully and full operational capacity was restored [24].



Figure 2-22 – Comet 67P Churyumov-Gerasimenko showing significant outgassing activity imaged by the Rosetta orbiter (credit: ESA / Rosetta / NavCam)

2.3.4.4 Kuiper Belt objects

Outside the orbit of Neptune lays a disk of icy bodies widely ranging in size. These are the most preserved remains of the early Solar System and they haven't changed much since they formed as part of the nebula that gave birth to our star. Too heavy to be blown away by the ignition of the young Sun, too scattered to coalesce into planets, the sheer distance of these objects makes them the least known in our planetary system. One ship braved this distance and travelled the 5 light-hours needed to encounter some of the nearest Kuiper Belt objects. That ship is NASA's New Horizons and its target is Pluto.

Although now classified as a dwarf planet, in front of New Horizons Pluto presented itself as a surprisingly complex world, rich and dynamic as the ones in the inner system. During the brief flyby, the probe observed an active geology with mountain ranges of water ice, glaciers of nitrogen, a thin, hazy atmosphere and an intricate interaction with the large moon Charon. One of these dramatic portraits taken by New Horizon as it was leaving the dwarf planet can be seen in Figure 2-23.

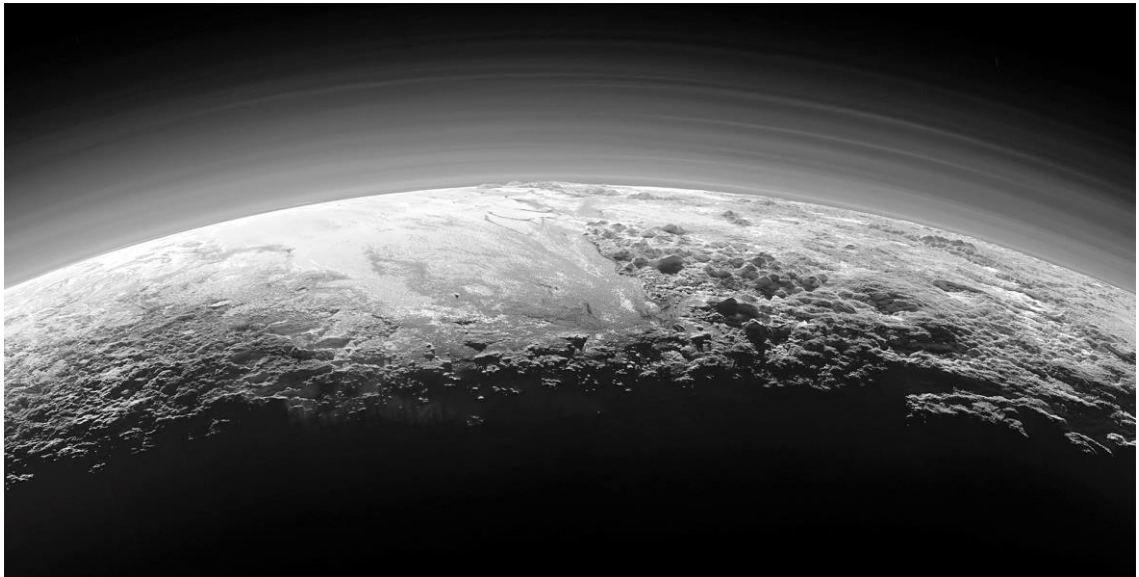


Figure 2-23 – View of Pluto under a low illumination angle by New Horizons (credit: NASA / JHUAPL / SwRI)

Given the similar mission profile, the New Horizon spacecraft architecture is comparable to that of Voyager, described in Section 2.3.3.3, but smaller in size thanks to the more recent technology. The limited launch mass was essential for this probe because, lacking the gravity assist sequence that benefitted Voyager, it had to be greatly accelerated at the beginning of his travel, with considerable propellant cost. New Horizon was launched by the largest Atlas V rocket available at the time, equipped with an additional solid rocket upper stage. At the end of the burn sequence the craft was released in a solar-escape trajectory at over 58 000 km/h, making it the fastest object to ever leave Earth [25]. 9 hours later, mission controllers had barely begun post-launch health checks while the spacecraft had already flown past the Moon. In two and a half months it was beyond the orbit of Mars.

To minimise mass, New Horizon’s main instrumentation is body-mounted instead than on an external motorised platform. This allows for a simpler design but it also requires an agile attitude control system that can swiftly reorient the spacecraft to perform various observations. It also means that antenna pointing was lost for the 22-hour duration of the Pluto flyby. New Horizons had to use a high degree of on-board intelligence to operate autonomously during this radio science. At the end of the sequence, the spacecraft re-established antenna lock on Earth showing a full on board memory, sign of a successful flyby. At a rate of 2 kb/s, it took more than a year to download the 6.25 GB of data acquired in those 22 hours, but it permanently changed our understanding of the Pluto system.

2.3.5 The boundaries of the Solar System

The Solar System is surrounded by a vast magnetic “bubble”, formed by the solar wind: the heliosphere. Inside this region, the particle and radiation environments are predominantly controlled by the Sun, while outside, the galactic environment dominates. The boundary of the heliosphere is called the heliopause and, beyond this limit, interstellar space officially begins. The Sun completes one revolution around the galactic centre (galactic year) every 230 million Earth years, which might appear rather slow paced, but, considering the immensity of the orbit, it corresponds to a velocity of 864 000 km/h. If the local galactic clouds are moving at a slower speed, this can form a bow shock in the direction of motion. Whether

this shockwave is fully developed or not in the current galactic medium is still subject of debate [26]. Figure 2-24 offers a diagram of these structures surrounding the Solar System.

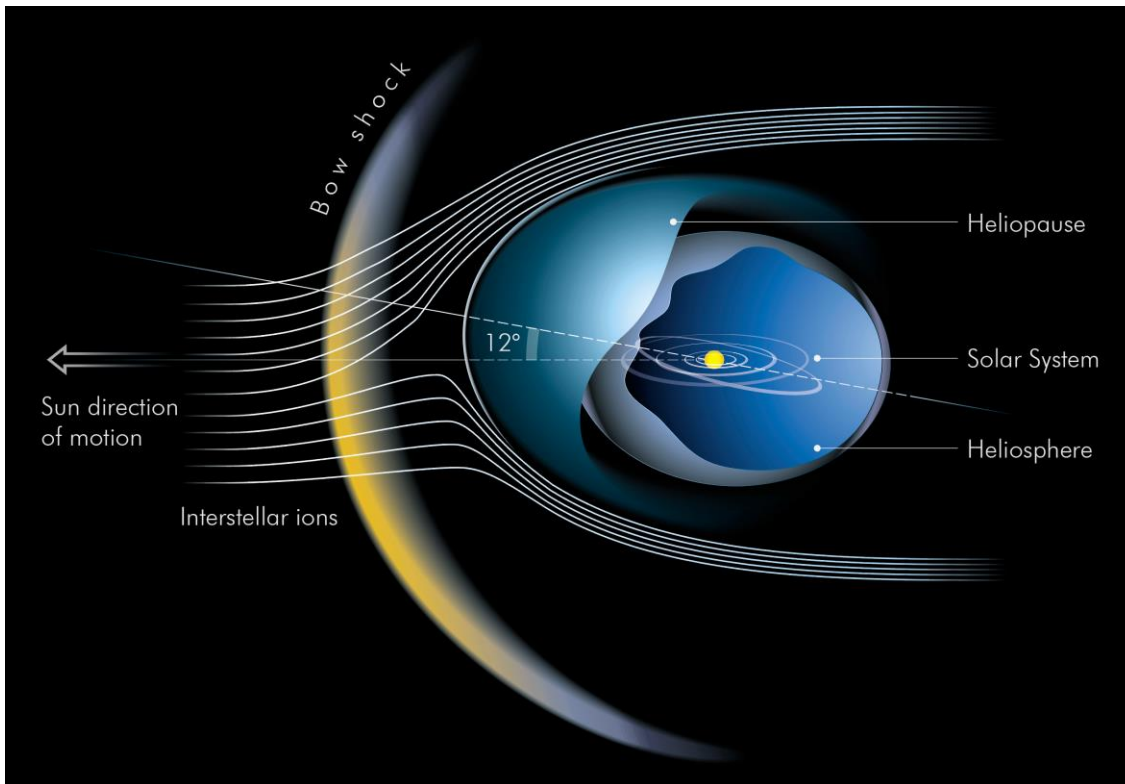


Figure 2-24 – Diagram of the heliosphere and large-scale structures around the Solar System (credit: ESA / L. B. Jaffel / M. Kornmesser / L. L. Christensen)

The scale of these structure is colossal, even in planetary terms. The heliopause is found no closer than 121 AU from the Sun, which is 18 billion km or nearly 17 light-hours. The flight time to that distance, with the current technology and the most favourable orbital configuration, is nearly four decades. The only two ships to have braved this journey are Voyager 1 and 2, which crossed the heliopause in 2012 and 2018, respectively, thus becoming the first human-made objects to venture into interstellar space. It is through these crossing that we have learned about the existence of these structures and about our place in the galaxy.

Nearly half a century after their departure, the probes are still radioing back their discoveries through the Deep Space Network as they speed outward into the galaxy. The ships have exceeded their design specification more than tenfold, but they have kept faithful to their design intent. After the completion of the Grand Tour of the Solar System, NASA approved support for an open-ended Voyager Interstellar Mission, aimed at following the probes just as far as they would be able to be communicate. It is probable that before the end of the 2020s their nuclear power sources will have become so weak to be unable to keep on the communication systems. From that point onwards the Voyager Interstellar Mission will continue in silence.

The last mission objective of the Voyagers is to bear a message to the stars. On each vessel is mounted a copy of the “Golden Record”, a 12-inch gold-plated copper disk containing sounds and images selected to portray the diversity of life and culture on Earth. The chances of some distant alien civilisation intercepting the probes are ridiculously small, but during their journey, the Voyagers have gradually acquired more symbolic meaning over practical use and have become an emblem of exploration, a signpost of how far humans have come

through their robotic ambassadors. Billions of years from now, after our species has become extinct, after the Earth and the Sun are gone, the Voyagers will fly on. Destined to sail indefinitely through the galaxy, they will be the last remaining proof that humankind ever existed.

3 MARS

Mars is often described as “Earth’s brother”, especially after the discouraging realisation that “Earth’s twin”, Venus, is one of the most inhospitable places in the Solar System. However, if the two planets are siblings, they must have grown apart a long time ago. Today Mars presents itself as a dusty, frigid desert, geologically dead, stripped of much of its atmosphere and water. And yet, it is the most familiar world that we have found so far. The sun rises and sets almost once every 24 hours, there are four seasons, there is wind and a surface made of rock and sand: phenomena and materials that are familiar to human senses. On that surface we could comfortably stand – as long as we wore protection from the cold and the low pressure – and use our limbs for locomotion and manipulation, like we do on our home planet. The truth is that, in our observation and exploration of the Cosmos, we have yet to find a place that more closely resembles our world.

As already noted in Chapter 2, these conflicting thoughts have driven significant interest and curiosity towards our colder planetary neighbour. The more we explore it, the more we long to understand why Earth and Mars appear so similar and yet so different. This chapter provides a summary of the history of the exploration of Mars and the scientific interests behind these undertakings. It also describes the environment that surface missions have to face, with particular attention to rovers, a type of spacecraft with a key role in the exploration of Mars and in this research.

3.1 History of the exploration of Mars

3.1.1 Early days and pioneering missions

Attempts to reach Mars began as early as 1960, with the Soviet Union commencing a series of launches that unfortunately did not match the initial ambitions: 10 Soviet spacecraft were lost in that decade without ever reaching the planet. Meanwhile, the USA accomplished a flyby on their second attempt in 1964, with the Mariner 4 probe, and continued to succeed with Mariner 6 and 7 in 1969.

At the time when Mariner 4 was headed for Mars, human knowledge of the planet was limited to what could be observed through the telescopes of the time. Scientists still thought possible, however unlikely, that the planet hosted complex life on its surface. During the

brief flyby – less than half an hour of observation time – the television camera on board Mariner 4 acquired a total of 22 images, which were then radioed back to Earth. Each image was only 200 x 200 pixel in size and took more than 6 hours to download. A "real-time data translator" machine converted each Mariner 4 digital image data into numbers printed on strips of paper. Too anxious to wait for the official processed image, employees from the Telecommunications Section at NASA's Jet Propulsion Laboratory, attached these strips side by side as they were being received and hand coloured the numbers like a paint-by-numbers picture (Figure 3-1). Data from the probe confirmed the theory that Mars was a cold desert planet, with a thin atmosphere and a surface dominated by dust and craters and not by blooming life and water bodies. To the disappointment of the general public, Mars looked a lot more like our moon than our planet.

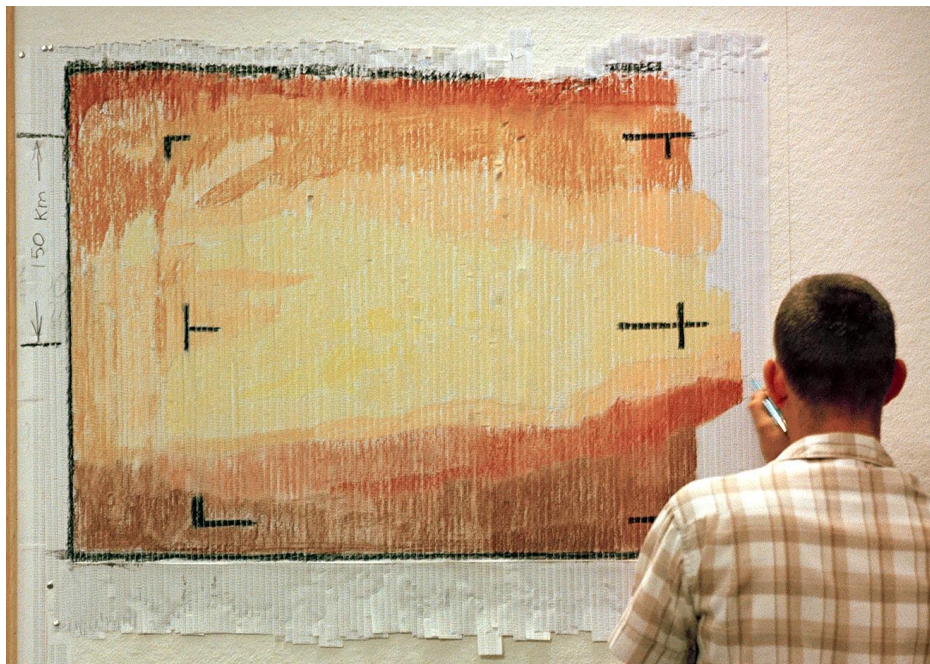


Figure 3-1 – A JPL engineer colouring by hand the transmission strips of the first television image from Mariner 4 (credit: NASA / JPL-Caltech)

During the '70s, the scene of the exploration of Mars was changed by a number of factors: firstly, the "Moon race" was settled, and Mars attracted more attention as the obvious next target. Secondly, the emphasis shifted from quick flyby missions to orbiters and landers, since, by that time, humankind had developed the technology to enter orbit around another planetary body and descend onto its surface. Orbital insertion around Mars was achieved by American and Soviet probes almost at the same time in 1971, with the American Mariner 9 on November 14th and the Soviet Mars 2 and Mars 3 on November 27th and December 2nd, respectively. The Soviet orbiters were also carrying landers on board: the one delivered by Mars 2 entered the Martian atmosphere with an incorrect angle and disintegrated upon impact, while the one delivered by Mars 3 correctly performed a soft landing, even though it operated only for 20 seconds after touchdown. The cause of failure is still unknown, but possibly linked to an enormous dust storm that was raging at the time of landing.

A relevant fact to note is that, during this time, space agencies often sent probes to Mars in pairs, usually formed by identical spacecraft. Sometimes they travelled even in groups of

three or four. The departure window to Mars occurs approximately every 26 months²³, so during the '60s and '70s it was common to see a small fleet of spacecraft set sail together to the Red Planet every two years or so. This now unfamiliar approach was driven by the need for redundancy: the failure rate was so high that it seemed reasonable to duplicate entire missions in case one failed. The truth is that Mars remains a rather unforgiving destination to this day, and the failure rate never quite dropped to a comfortable level for modern space agencies, but modern space budgets rarely allow the duplication of entire exploration missions.

Orbiters launched in the early '70s relayed a far greater amount of scientific data compared to the early flybys, mapping the entire surface and picturing a much more complex and dynamic world than what initially appeared. These advancements led to NASA's Viking project, which delivered two more twin missions to Mars in 1976, each composed by an orbiter and a lander. Both landers were successful and transmitted the first, striking imagery from the surface of Mars, deeply transforming our understanding of the planet from remote sensing to in-situ analysis and observation at human scale. A panoramic image from Viking 2 is reported in Figure 3-2.

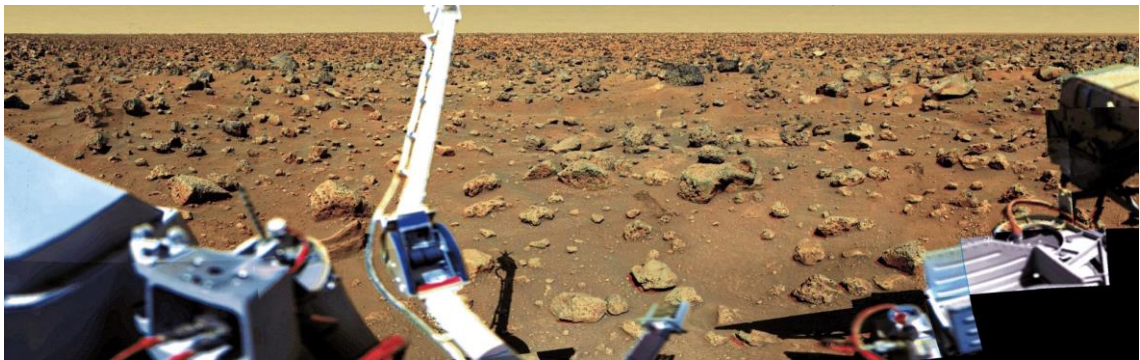


Figure 3-2 – Panorama of the Martian surface from Viking 2 (credit: NASA / JPL-Caltech)

The Viking landers produced a wealth of scientific data, from geological investigation to characterisation of the atmosphere, radiation environment, chemical, mechanical and even biological analysis of the surface material [27]. The three exobiology experiments on board the landers discovered unexpected and enigmatic chemical activity in the Martian soil, but provided no clear evidence for the presence of living microorganisms. Today, the interpretation of these results in the light of more findings from other missions leads us to believe that, while organic compounds are easily found on Mars, its soil is likely unsuitable for microbial life, at least in proximity of the surface.

The Vikings were powered by Radioisotope Thermoelectric Generators, which made them relatively long-lived: Viking 1 operated for approximately 6 years, Viking 2 for 4. Their extended permanence on Mars gave them the opportunity to observe the rotation of seasons and the changes in their environment. This was particularly true for Viking 2, which had landed at higher latitude and, on a cold winter day, took the picture in Figure 3-3. The frost

²³ The Earth-Mars departure window occurs when Earth is approaching Mars, moving faster on its inner orbit, approximately 2-3 months before the point of minimum distance between the two planets. It is possible to launch to Mars outside of this window, but the propellant requirements are much higher and generally do not allow to deliver any meaningful payload with present rocket technology.

visible on the surface is water ice: Mars had not completely lost its water after all. The portrayed area is the same one on the far right in Figure 3-2.

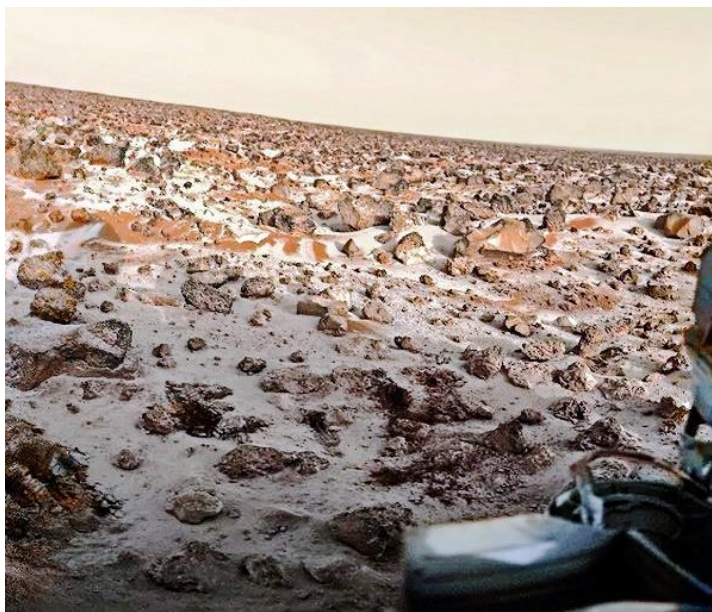


Figure 3-3 – Winter frost around Viking 2 (credit: NASA / JPL-Caltech)

These would be the last pictures from the surface of Mars for quite some time, since the launch rate towards the Red Planet almost came to a halt in the '80s. During the two decades that followed the launch of the Vikings, only a single spacecraft made it to Mars: it was the Phobos 2 orbiter, the last interplanetary probe from the Soviet Union before its collapse.

3.1.2 Modern exploration of Mars

In the late 90's and early 2000s, the number of missions to Mars started picking up again, although it would never reach the pace of the '60s and '70s. The chart in Figure 3-4 summarises almost seven decades of Mars missions. It can be noted how the '60s and '70s take nearly half of it: a reminder that, despite recent positive signs, the planetary exploration effort has far from recovered its original strength. On the other hand, the chart also shows how the success rate has been improving, highlighted by the large number of dark dotted lines (failures) in the earlier times. The chart also provides an indication of how rare it is to attempt a landing, as opposed to an orbital mission, and how even rarer it is to succeed in that. Of these few successful landings, six carried rovers to the surface of Mars: Pathfinder²⁴, Spirit, Opportunity, Curiosity, Perseverance and Tianwen-1²⁵ (Chinese Mars Mission). Of these six, the last three are still operational to this day. The ExoMars 2022 rover, the Martian Moons eXploration probe (MMX) and the Mangalyaan 2 mission have yet to be launched at the time of writing.

²⁴ The rover delivered by Pathfinder is named Sojourner.

²⁵ The rover delivered by Tianwen-1 is named Zhurong.

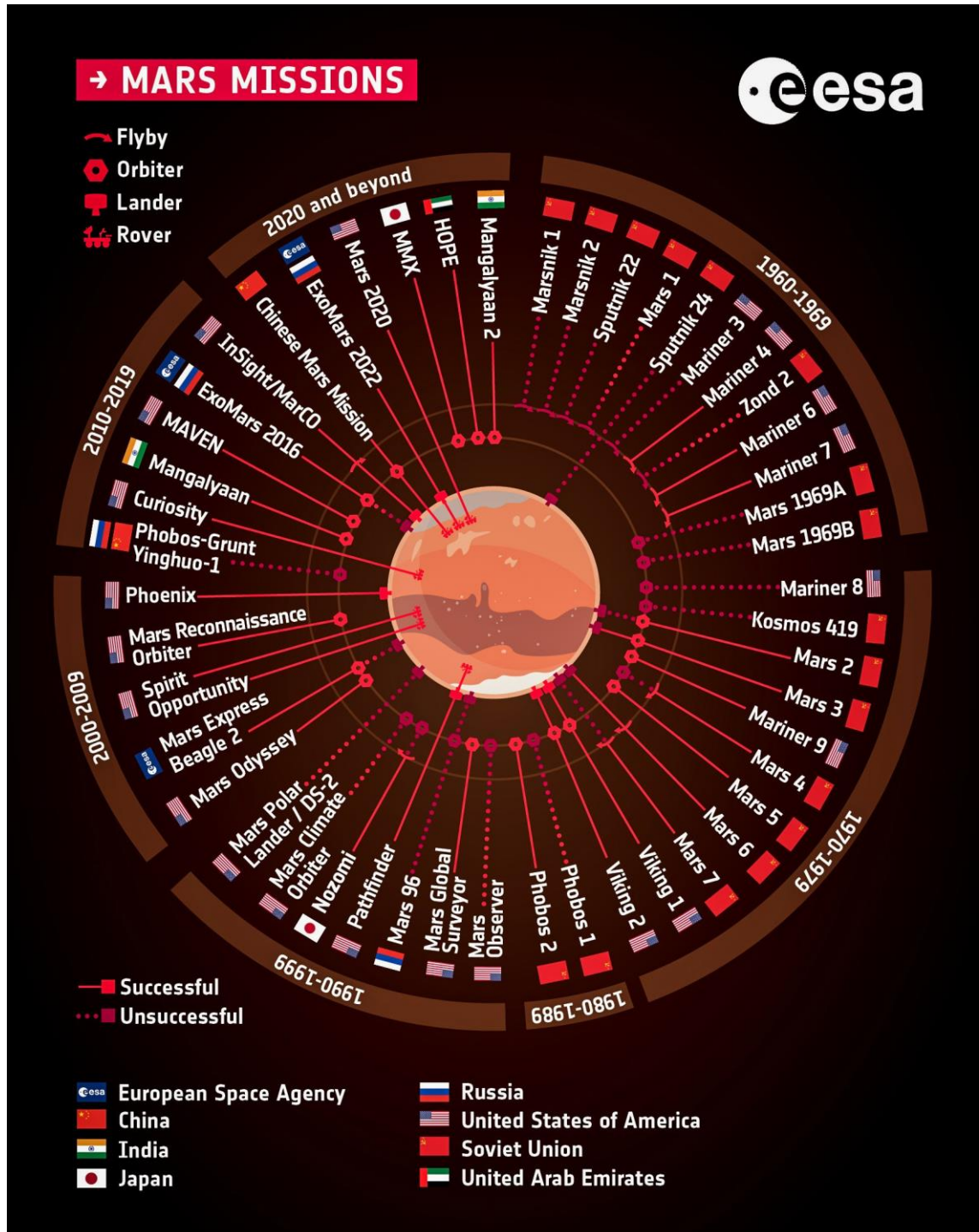


Figure 3-4 – Visual summary of all the missions in the history of Mars exploration, categorised as flybys, orbiters, landers and rovers, updated as of July 2020 (credit: ESA)

Whilst increasingly sophisticated orbiters were being sent to the Red Planet, it is the advent of rovers that would change the study of Mars so significantly to make these machines the most widely recognised symbol of its exploration. The first spacecraft of this type was a microwave-sized technology demonstrator riding on a lander with its own separate mission. The Microrover Flight Experiment (MFEX), delivered by NASA's Pathfinder lander and better known as Sojourner, is the ancestor of all planetary rovers.

Sojourner operated for 92 Martian days in 1997 and drove approximately 100 m, powered by the solar panel on its top deck. In that brief distance, it performed chemical analyses on 15 rock formations and returned thousands of images. Despite its elementary sensors, the small rover had achieved more than any stationary lander before and unquestionably proven the advantages of surface mobility for planetary exploration. Figure 3-5 shows Sojourner immediately after descending its egress ramp (on the left). On the right, it is possible to see part of the deflated airbags that decelerated the lander.

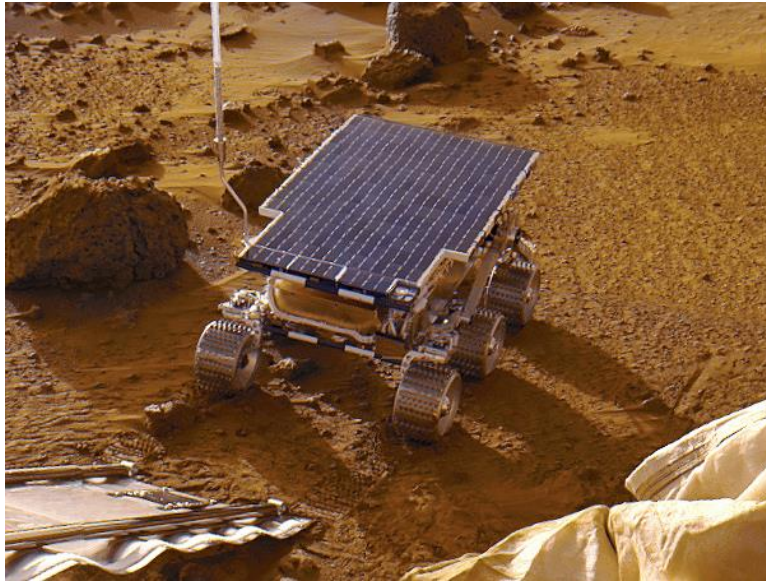


Figure 3-5 – NASA’s Sojourner rover imaged by the Pathfinder lander (credit: NASA / JPL-Caltech)

A second MFEX rover, identical to Sojourner had been built during the flight programme and was ready to be sent to Mars on another lander. However, NASA decided that the results of the first surface mobility experiment were sufficiently promising to justify the development of a new class of larger, solar-powered surface vehicles, christened MER, Mars Exploration Rovers. Two identical spacecraft of this class were built, named Spirit (MER-A) and Opportunity (MER-B). They landed in 2004 on two opposite sides of the planet and have been greatly successful. Spirit operated for 6 years and traversed almost 8 km, while Opportunity operated for over 14 years and logged 45 km, which is the current off-planet driving record. Its total traversed path seen from orbit is shown in Figure 3-6, with the Municipality of Bologna, Italy superimposed for scale. The planned nominal mission was only the first leg between Eagle Crater and Endurance Crater. Opportunity ultimately succumbed to a planet-wide dust storm in Perseverance Valley, just before the 15th anniversary of its landing.

Through their journeys, the MER rovers collected a huge amount of data on Martian geology, they found evidence of prolonged water presence, they deepened our understanding of the weather, the winds and how they sculpt the surface, they showed the diversity and complexity of the environment and, remarkably, they brought the general public along with them. Spirit and Opportunity reignited the interest on Mars and brought planetary exploration back onto the centre stage of space business.

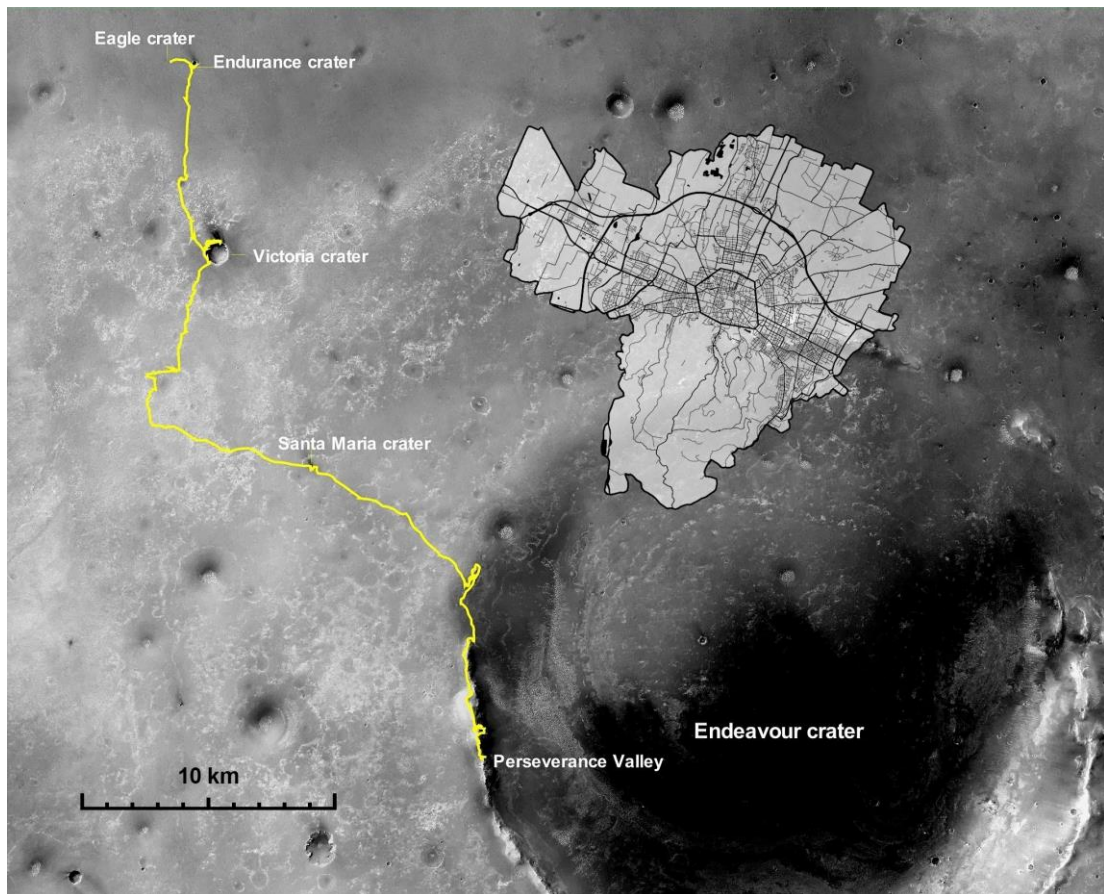


Figure 3-6 – Opportunity’s path (from top to bottom) on Mars with the City of Bologna for scale (credit: NASA / JPL-Caltech)

In 2003, the European Space Agency had already become the third agency to successfully deliver a spacecraft to Mars with the orbiter Mars Express, which is still operational to this day. Unfortunately, the lander that it was carrying, Beagle 2, failed to complete deployment after touchdown and never established communication with Earth. The following decade saw India achieving orbit as well, with its Mars Orbiter Mission Mangalyaan. In 2016, ESA succeeded in delivering another, more complex spacecraft, the Trace Gas Orbiter, but the associated lander, Schiaparelli, suffered a similar fate to its predecessor, crashing on the surface at high velocity.

Meanwhile, NASA had developed another class of rovers, significantly more capable than MER: the Mars Science Laboratory (MSL), better known as Curiosity. This SUV-sized rover has been exploring the area of Gale Crater since 2012, unaffected by dust storms or seasonal changes thanks to its nuclear power source. The MSL design is the highest performance mobile machine that has ever operated on Mars. Its ability to capture the environment in unprecedented detail has changed the way we study the planet: now scientists are able to immerse themselves in high-resolution panoramas and 3D reconstructions of the surface in virtual reality, allowing them to carefully choose the areas to sample and analyse. The rover’s highly autonomous mobility system then moves the virtual outpost to the desired location. Figure 3-7 shows one of these panoramic images, which includes the rover itself. The last launch window of the 2010s saw another successful NASA landing with the InSight surface platform to study Martian geology.



Figure 3-7 – Curiosity panorama in front of Mont Mercou (credit: NASA / JPL-Caltech / MSSS)

The 2020's are showing a very promising trend for the exploration of Mars, with more capable, more frequent missions and more space agencies involved. During the first Mars launch window in 2020 a fleet of three ships embarked on the interplanetary trip together and all have reached their objectives successfully: the Emirati orbiter Hope, the Chinese orbiter and rover Tianwen-1 and the American rover Mars2020, now known as Perseverance.

Perseverance is an enhanced version of the MSL design, overall similar to Curiosity, but it carried another, unique spacecraft: Ingenuity, the Mars helicopter. On April 19 2021, the small rotorcraft accomplished the first powered flight on another planet in history, adding a new dimension to Mars exploration (Figure 3-8).



Figure 3-8 – Ingenuity hovering 5 m above the ground, seen from Perseverance (credit: NASA / JPL-Caltech / ASU)

This summary of the exploration of Mars has reached the present day, but more missions are already under development for the immediate future, including the ExoMars Rover and, towards the end of the decade, Mars Sample Return, of which much more will be discussed in these pages.

3.2 Scientific interest

The study of Mars is a vast and constantly changing landscape that involves almost every branch of science, therefore, it would be impossible to present it in an accurate way within the scope of this document. A concise summary is provided below, touching upon the major areas of interest that often become scientific objectives for the missions sent to explore the planet.

3.2.1 Planetary formation and geology

With the remarkable variety of planets that can be observed within our Solar System, every time we visit a new world, one of the first things that we seek to comprehend is how it works and how it came to be like that. How did Mars form and develop into the planet it is today? What is its internal structure? These are some frequent questions that arise in the study of the Red Planet. We also aim to understand what geological activity was like on the planet and when did it cease or, in fact, if it has actually ceased completely or not.

We know that a magnetosphere is an effective barrier to protect terrestrial life from harmful radiation and Mars does not seem to have one, but did it have a global magnetic field in the past? Mars is an opportunity to better understand what makes a planet geologically active and what are the contributions of various factors, such as residual heat from the planet's formation, radioactive decay in its core and tidal forces from nearby massive bodies.

3.2.2 Climate and habitability

It is now consolidated that Mars once had abundant water on its surface, a thick atmosphere and mild temperatures. The planet has therefore undergone a momentous shift in its climate to become the cold desert that it is today. A significant investigation effort is concentrating on the cause and the process that led to this change: whether it was the weak gravity that failed to hold on to the atmosphere or the loss of a magnetic field that allowed the solar wind in.

Given that Mars and Earth were much alike in the past and that, as described in Section 2.3.2.4, they are on equally promising orbits for habitability, scientists seek to understand how the two planets evolved so differently. In the future, we might have to make resource-constrained decisions on what exoplanets to observe, or even send probes to, and we need to be able to recognise a "Mars" from an "Earth".

Even though Mars is far less hospitable than it used to be, it is still among the most promising places in the Solar System for human exploration and settlement. In our study of this world, we also strive to learn how to survive, and perhaps one day thrive, on its surface. Much is to be learned in this regard, since our technology, like our body, has evolved to function at its best on one planet only.

3.2.3 Exobiology

Our expectations for life on Mars have been progressively scaled down over the 20th century, from advanced alien civilisations to fossil remains of microbial activity. Nonetheless, it is impossible to talk about the study of Mars without talking about the search for life. Every single mission to the Red Planet has this quest captured in one or more of its primary objectives. It is known that the planet has had liquid water on its surface, possibly for hundreds of millions of years. However, that was billions of years ago, and what is left of that era is no more than faded geological footprints. Even so, no matter how small the chances, the prospect of finding some form of biology away from Earth is one of the strongest drivers for exploration.

It seems that, as Carl Sagan remarked, “We can't help it. Life looks for life.” [28] We perceive life as an exceedingly rare phenomenon. We have reason to believe that, for all practical purposes, our civilisation is alone in the dark expanse of space. What would then be the implications of finding a “second genesis” in our planetary neighbourhood? The logical consequence would be that the Universe around us is probably brimming with life. This is such a profoundly significant issue for humans that we cannot avoid chasing it, on Mars and wherever else there might be some chance of finding traces of life.

3.3 The Martian environment

What follows is an overview of the Martian surface environment and its influence on spacecraft design and operation. This analysis is focused on the planetary surface, since it is the most relevant for the systems developed in this project, and because the orbital environment is not radically different from any interplanetary space in the proximity of Earth, but with weaker solar irradiation and longer communication delay.

3.3.1 Gravity

The gravitational acceleration on the surface of Mars is 3.72 m/s, or 38% that of Earth. At this gravity level, humans can certainly stand and walk, although hopping might prove more efficient than walking, as Apollo astronauts realised on the Moon, with a gravitational acceleration 16% that of Earth. Differently from the Moon, the Martian gravity field should be strong enough for the sensory response of the human inner ear to be useful in maintaining balance, while Apollo astronauts had to rely heavily on their vision to correct their posture [29].

As to operating machinery, the relatively weak Martian gravity has some advantages: it reduces the power required for controlled flight (in particular during descent and landing operations), it leads to more benign loads for on surface mobility and generally does not constitute a challenge for structural design, which is more frequently driven by launch and Entry, Descent and Landing (EDL) loads. The low gravity can also lead to less compaction of the terrain material, meaning that Martian sand and dust can be much less cohesive than their Earth analogues: this poses a danger to surface vehicles, which can get trapped in patches of material as soft as talcum powder. For wheeled machines, lower weight means lower down-force to produce traction. These aspects lead to challenges in developing wheels for Mars, which often use a compliant design to create traction on a large contact

patch or implement grousers²⁶ on the wheel thread or, sometimes, a combination of the two, as will be discussed more in Section 4.2.4.

One peculiar aspect of developing spacecraft for the Martian gravity environment is that it becomes difficult to test them before launch under the stronger Earth gravity. For robotic arms, lightweight appendages and mobility systems, testing in 1 g can lead to excessive loads or non-representative behaviours. Sometimes the solution is to use off-loading devices, like cranes and helium balloons, or to build lighter, Mars-weight versions of the hardware. The latter is rather common for development of mobility systems, which can operate with most of the other spacecraft systems removed. The result is a skeleton model like the one depicted in Figure 3-9, showing an early prototype of the ExoMars Rover mobility system. The electronics are accommodated in a tower structure to reproduce the centre of mass of the vehicle, which would be otherwise too low because of the missing equipment.

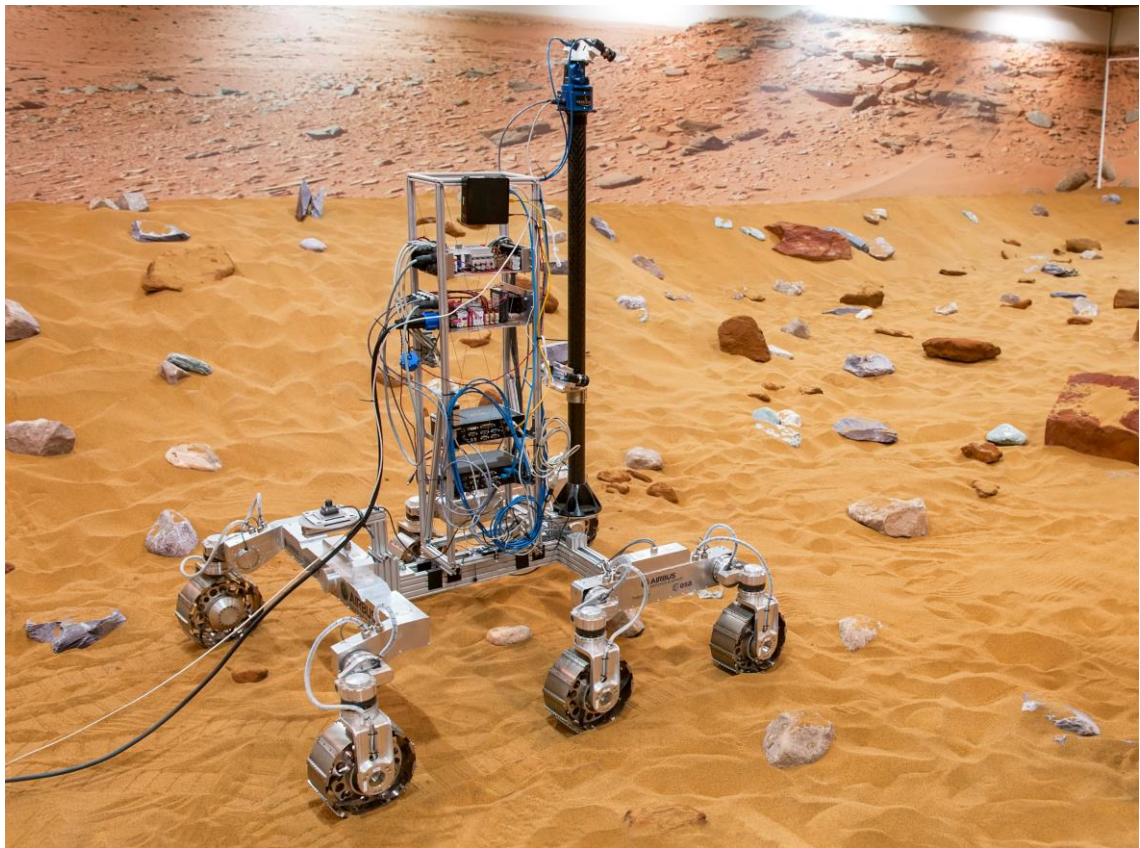


Figure 3-9 – Mars-weight prototype of the ExoMars Rover in the Mars Yard facility (credit: Airbus)

3.3.2 Atmosphere

The Martian atmosphere is significantly thinner than Earth's. With an average surface pressure of approximately 0.6% that of our planet, to human perception it would be largely equivalent to the vacuum of space. Its chemical composition is dominated by carbon dioxide, followed by molecular nitrogen, argon, molecular oxygen, carbon monoxide and other trace

²⁶ Grousers are protrusions designed to increase traction, common in tracked vehicles on Earth, often in the form of pads or plates attached to the tractive surface.

gases including water vapour. The concentration of these elements was measured accurately by the Sample Analysis at Mars (SAM) experiment on board NASA's Curiosity rover [30] and is reported in Table 3-1.

Species	Volume ratio
CO ₂	94.9%
N ₂	2.79%
Ar	2.08%
O ₂	0.17%
CO	0.06%

Table 3-1 – Composition of the Martian atmosphere measured by NASA's Curiosity rover

The fact that the surface pressure is so low does not necessarily mean that the atmosphere density is equally low. Because carbon dioxide is a rather heavy gas and it is kept cold by the Martian environment, the density of Martian air is relatively high, up to 0.02 kg/m³. For comparison, that is equal to the air density at approximately 35 km altitude on Earth. Combining this with the low gravity, it follows that aerodynamic flight should be possible on Mars, and so it was proven when NASA's helicopter Ingenuity performed the first powered flight on another planet on February 18th 2021.

The air density on Mars is sufficient to make the atmosphere a design driver for spacecraft operating on its surface. It is sufficient to generate convection and so can be a means of heat transport. Most importantly, Martian air is a vehicle for dust. Dust is one of the greatest concerns when designing surface platforms, as described in Section 3.3.4, and the wind is responsible for carrying it onto the hardware. The dust deposition by wind, or aeolian deposition, is a factor of incremental degradation of spacecraft performance, especially for the power output of solar arrays. Although in some cases it has been observed that strong wind gusts can actually clean solar arrays from the dust accumulated over time, as it happened to NASA's Spirit rover multiple times during its mission (Figure 3-10).

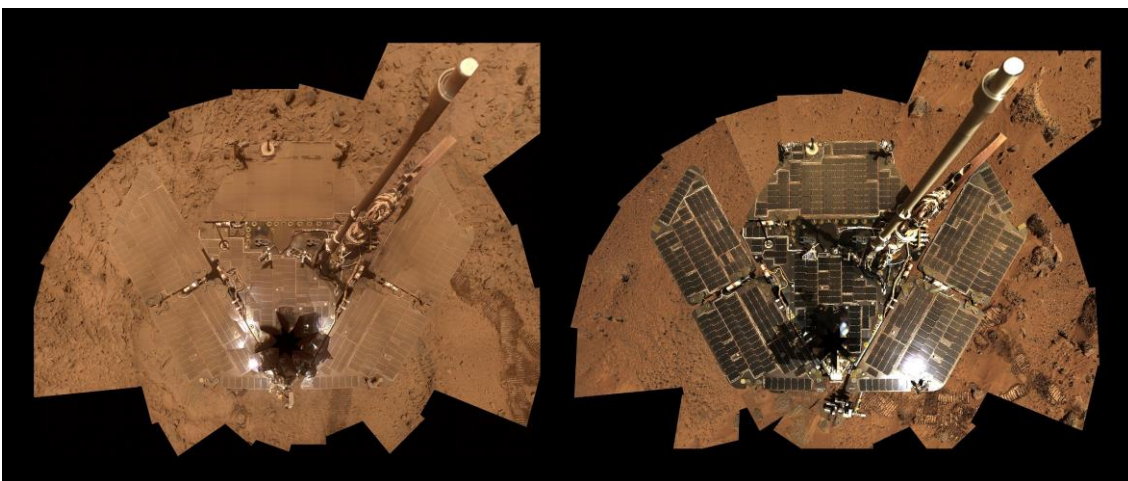


Figure 3-10 – Composite views of Spirit's top deck before (left) and after (right) a cleaning event (credit: NASA / JPL-Caltech / Cornell)

The atmospheric wind patterns are as varied as on Earth and they can give rise to high-intensity phenomena like dust devils (similar to Earth tornadoes, but usually smaller) and

dust storms, which can be local or global. Dust storms are a major risk to surface assets as they can obscure the sun and deposit large amounts of dust on the hardware. They are known to have ended several surface missions like the recent Opportunity rover. Even without dust storms, there is a constant presence of airborne dust in the planet's atmosphere, which affects a key parameter known as optical depth, generally defined as follows:

$$\tau = \ln\left(\frac{\Phi_i}{\Phi_t}\right)$$

where Φ_i is the incident radiant flux onto a certain substance and Φ_t is the radiant flux transmitted by that substance. In other terms, τ gives a measure of how "opaque" the atmosphere is. More suspended dust means a more opaque atmosphere and therefore less sunlight for power generation and lower ability to radiate heat towards the cold sky, so, somewhat counterintuitively, a hotter environment for spacecraft.

It is a common misconception, probably related to the scale of Martian dust storms, that winds on Mars are powerful and dangerous. In fact, wind speeds are generally moderate, with a maximum of approximately 100 km/h for the most intense storms, which is much less than Earth's hurricanes. Considering the low air density, these winds cannot generate any significant mechanical loading on spacecraft except for appendages with large surface area, like solar panels, which are sized to resist the strongest gusts.

The atmosphere of Mars is rarefied, but rather thick in terms of extension in altitude because of the low gravity. It is more than sufficient to stop micrometeoroids²⁷ from reaching the surface at high velocity, but not dense enough to filter the solar radiation, which is intense even at ground level. The high-energy component of the solar spectrum constantly bakes the topsoil of Mars in harmful radiation, altering its chemical composition and making it inhospitable for life. This radiation has to be considered in the design of spacecraft, which require radiation-hardened electronics, but rarely need any dedicated shielding.

One last peculiarity of the Martian atmosphere is that it can freeze out onto the surface, i.e., the CO₂ that forms 95% of the air solidifies into dry ice. It is estimated that, every winter, as much as one third of the atmosphere can freeze onto the polar caps, which are composed by permanent water ice and are visibly expanded by this seasonal CO₂ ice [31]. The CO₂ then starts to sublimate in spring and is returned to the atmosphere.

3.3.3 Temperatures

Much like Earth, Mars exhibits diurnal and seasonal temperature variations, but with markedly lower temperatures because of the greater distance from the Sun and the rarefied atmosphere. One Martian day, or sol, is approximately 24 hours and 40 minutes long. During this time, the air temperature changes quite significantly due to the thin atmosphere that allows the planet to radiate heat to deep space and cool down during the night. Figure 3-11 shows the temperature ranges recorded by NASA's Curiosity rover during its first two Martian years in Gale Crater. The typical daily variation is in the order of 60°C, with the hottest summer day reaching close to 0°C and the coldest winter night down to -90°C. The temperature ranges in Los Angeles (where Curiosity was built) are superimposed to highlight the

²⁷ Micrometeoroids are small particles of rock, typically less than a gram, that populate interplanetary space. They originate from comets and asteroids and they pose a threat to spacecraft in orbit.

much wider variation present on Mars. Gale Crater is a relatively warm region near the equator, while other areas of the planet have a more frigid climate. Nonetheless, minimum temperatures generally do not go below -125°C , since that is the point at which the planet's atmosphere begins to freeze down onto the surface, and the temperature remains on that transition point until a significant portion of the atmosphere's mass has solidified (see Section 3.3.2).

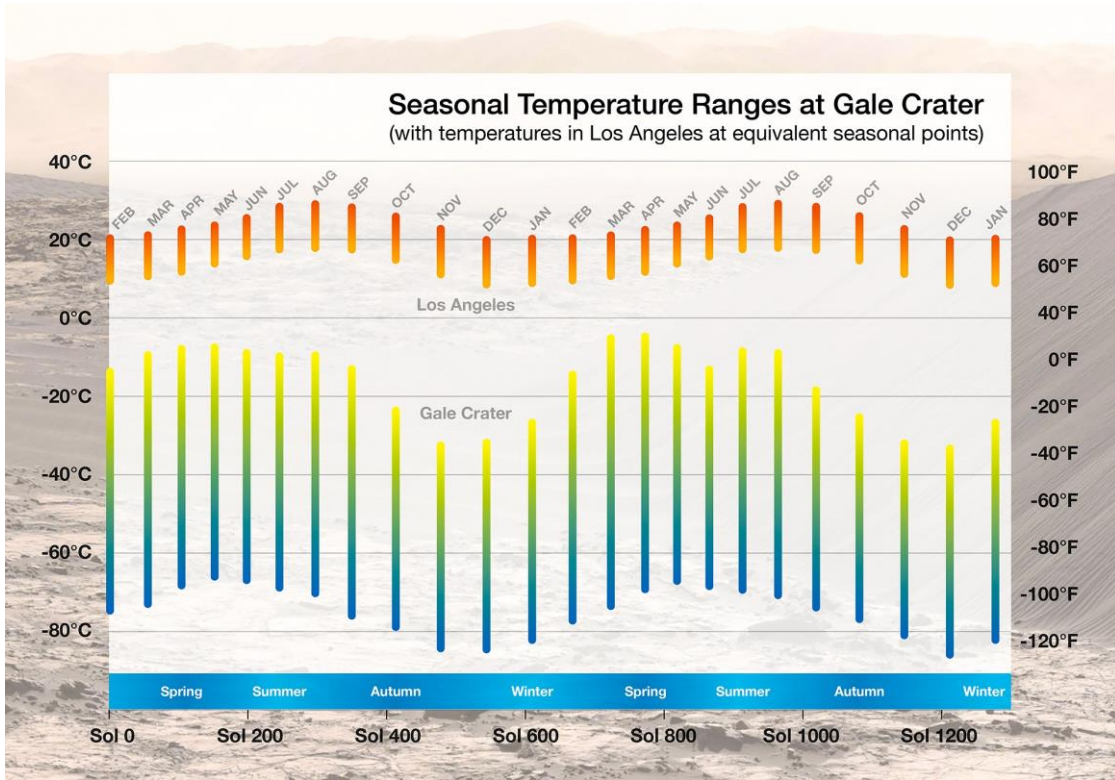


Figure 3-11 – Temperature ranges at Gale Crater by NASA’s Curiosity rover, with temperatures in Los Angeles at equivalent seasonal points (credit: NASA / JPL-Caltech / CAB)

Martian night temperatures are one of the most notorious challenges for spacecraft design. Most of the surface probes reach their end of mission when, for one reason or another, their sensitive components get cold during the night and become too damaged to reactivate in the morning. Spacecraft for Mars are designed to survive down to approximately -125°C , although their functionality at this temperature is very limited, and they typically do not commence nominal operations until -60°C . These spacecraft usually have “warm” and “cold” components: the warm ones need to be actively maintained above a certain threshold or they will sustain irreversible degradation, while the cold ones are designed to withstand the natural temperature range without any active thermal control (not necessarily operate, but survive). The former must be protected inside an insulated and heated enclosure and include sensitive elements like batteries and on board computers; the latter can be mounted on the outside of the spacecraft and include mechanisms and cameras. For some components, the cold itself is not the main threat, but rather the daily cycling over a large temperature range, which produces mechanical stress and fatigue.

Due to the presence of an atmosphere, heat exchange by radiation and by convection are equally relevant on the surface of Mars. Both of them tend to cool down spacecraft during the night, which is particularly undesirable for solar-powered systems that count on the energy stored in their battery for heating. Nuclear-powered vehicles benefit from a constant

output of energy, although it is still a precious resource. These considerations lead to implement as much insulation as possible to protect any sensitive hardware. However, this can become counterproductive during daytime operations, when active components dissipate energy and tend to overheat. To balance the two conflicting requirements, more sophisticated thermal control solutions are often required, such as heat pipes²⁸, active cooling or heat capacitors.

3.3.4 Regolith and dust

On top of Mars' bedrock layer, sits a variety of more or less unconsolidated terrain materials with different characteristics, which is broadly referred to as regolith. Differently from Earth's soil, which is often of biological origin and has a high water content, Martian regolith is the product of surface erosion or meteoritic impacts and is almost completely dry. The terrain material is often classified depending on its granulometry and mechanical properties, as they define its ability to support spacecraft, especially mobile vehicles. During the development of the ExoMars Rover, the European Space Agency carried out a study to identify the most relevant classes of soil types found on Mars and produce simulants that replicate their properties to the best of our knowledge [32]. As a result of that work, four Engineering Soils (ES) were developed: their characteristics and occurrence on Mars are illustrated by Table 3-2 and Figure 3-12.

Regolith	Occurrence	Simulant
Type 1	Very fine-grained, soft and compressible dust. Occurs locally outside main wind fields where the wind slows down.	ES-1
Type 2	Fine sand, non-cohesive and with low internal friction, very common on wind-blown ripples and dunes.	ES-2
Type 3	Medium – coarse sand, gravelly and compact, often encountered near bedrock.	ES-3
Type 4	Compacted regolith, cohesive and with high bearing capacity, prevalent on flat and gently sloped terrain.	ES-4

Table 3-2 – Characteristics of Martian regolith types and corresponding ES simulants

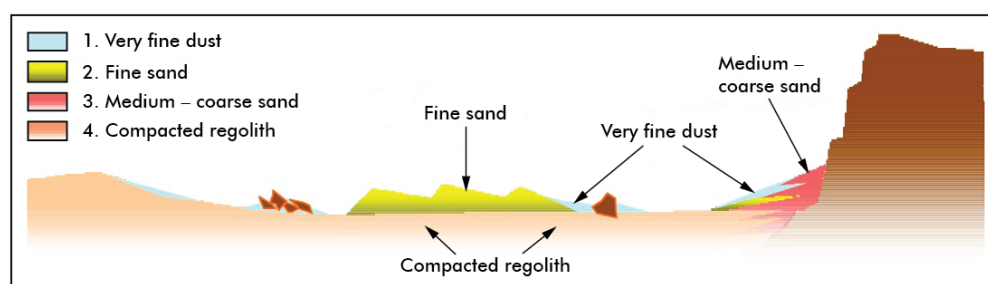


Figure 3-12 – Examples of occurrence of different regolith types on Mars (credit: G. Kruse)

²⁸ A heat pipe is a passive (i.e., non-motorised) heat transfer device that exploits the phase transition of the working fluid inside its cavity to transfer heat between a hot interface and a cold interface.

The bearing capacity, i.e., the ability to sustain weight, of the surface material influences the design of landers and rovers in that it requires them to spread the ground contact forces over a suitably large surface and possibly implement mechanical compliance to reduce peaks in the pressure distribution. Of particular concern are the regolith types 1 and 2 in Table 3-2, which are the least stable materials in that classification. For comparison with everyday experience, they remind of talcum powder or very fine, sifted beach sand. They are transported by the wind and receive little compaction from Mars' low gravity. This makes them perfect traps for rover wheels, which can sink deeply in the soil if the control system does not react quickly enough. One such occurrence was particularly severe for NASA's Opportunity rover. In 2005, the vehicle drove into a deep patch of wind-blown sand where its wheels sank almost completely and became unable to provide traction. Figure 3-13 shows a view of the rover wheels as it was attempting to escape the sand trap: it can be observed how the material provides little support and sticks to the wheel threads, making them less effective. It took mission controllers 5 weeks of careful, step-by-step motions to pull back the rover from the area, now named Purgatory Dune.



Figure 3-13 – View from Opportunity's Hazcams on Purgatory Dune (credit: NASA / JPL-Caltech)

The finest component of these materials, commonly referred to as dust, is the most easily airborne and, in fact, it always pervades the atmosphere to a varying degree, as described in Section 3.3.2. Because it is so omnipresent, every component of Mars surface probes needs to be designed to withstand a certain level of contamination by dust, even those that have nothing to do with mobility or soil interaction. Martian dust is an abrasive, insulating material that adheres easily to most surfaces. It reduces the performance of solar arrays, optical and thermal surfaces, which need to be oversized to account for this degradation, and it can cause wear or clogging of mechanisms, requiring suitably sealed designs.

3.3.5 Seasons

By a rather peculiar coincidence, Mars today has almost the same rotation period as Earth (within 1 hour) and the same tilt to its rotation axis (within 2°), even though the latter is less stable than that of our planet and wanders significantly over geological timescales. As a result of this similarity, Mars currently undergoes a seasonal cycle not too different from that of our planet. We observe polar ice caps expand during winter and contract during summer (up to almost disappearing if not for the water ice that remains under the carbon dioxide ice).

There is one feature of the Martian climate that is completely alien to Earth and, as a matter of fact, to any other planet in the Solar System: the dust storm season. Mars' orbit is more elliptical than Earth's, meaning that the amount of solar irradiation varies conspicuously as it moves closer or further from the Sun. During the northern autumn and winter, which correspond to the closest approach to the Sun, large thermal gradients between the north pole and the mid-latitude plains generate strong winds that begin to pick up dust [33]. Dust absorbs solar light and warms up the air, producing a self-amplifying phenomenon that gives rise to immense storms, like that in Figure 3-14, which extends more than 500 km across.

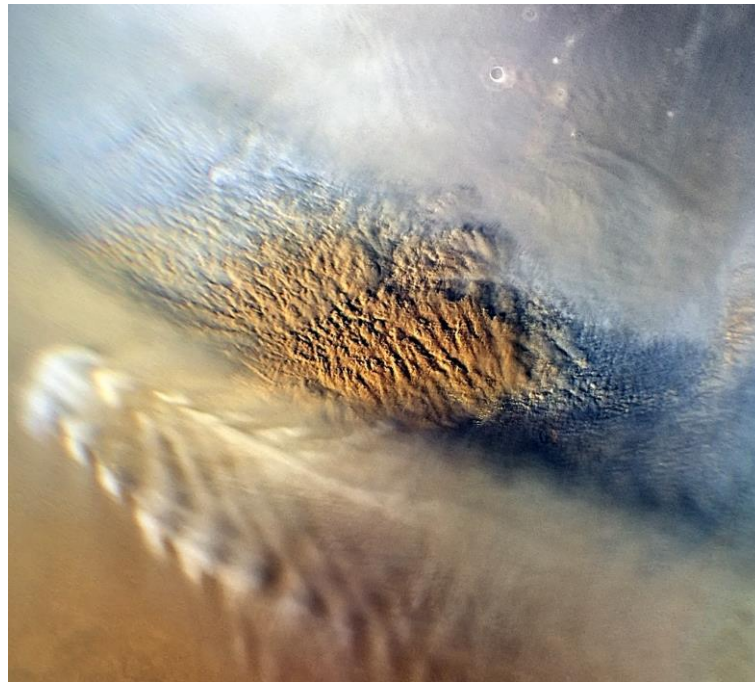


Figure 3-14 – A regional dust storm imaged by NASA's Mars Reconnaissance Orbiter (MRO) in 2007 (credit: NASA / JPL-Caltech / MSSS)

Occasionally, multiple regional storms can merge and expand in a runaway global dust storm that encircles the entire planet from pole to pole. These phenomena can last several weeks, during which they change completely Mars' appearance, as shown in Figure 3-15 by images taken before and during the 2001 global dust storm. Eventually, the dust coverage homogenises the planet's temperature and the winds fade away. However, in the process, global dust storms can be deadly for solar-powered probes and have claimed numerous missions already, last of which NASA's Opportunity rover. The spacecraft was met by a global storm in Perseverance Valley, from where it sent its last communication on June 10th 2018, before the sky became so obscured that the robot depleted its battery in the attempt to keep warm and succumbed to the rigours of the Martian night.

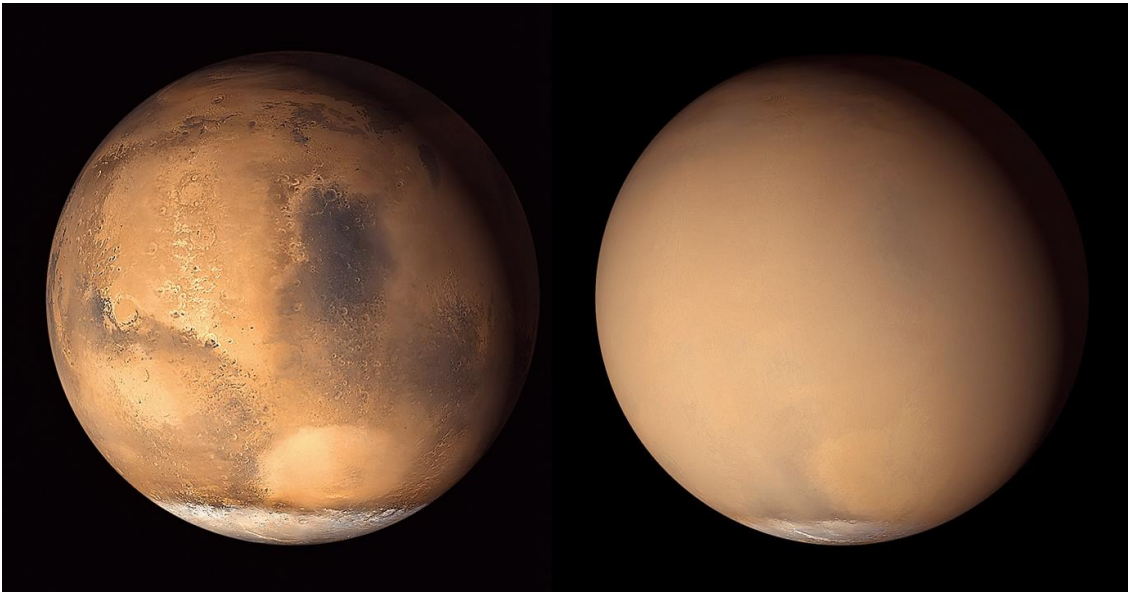


Figure 3-15 – Mars imaged by NASA's Mars Global Surveyor in June (left) and July (right) 2001 (credit: NASA / JPL-Caltech / MSSS)

Given the unpredictable nature of dust storms and their possible long duration, it is not practical to design solar-powered systems that can survive them, as they would have to carry an unrealistic amount of batteries. The only workable solutions are the acceptance of the risk to the mission or the provision a nuclear power source, at least for heating the craft.

3.3.6 Radiation

Due to the thin atmosphere and the lack of a global magnetic field, the radiation environment on the surface of Mars is rather harsh. Solar radiation is less intense compared to Earth because of the greater distance from the Sun, but it also encounters far less resistance along its path. This is even more true for cosmic rays²⁹ that can easily reach the ground thanks to their higher energy. Low-altitude regions benefit from additional attenuation by the slightly thicker mass of air overhead. In-situ measurements show that these effects combined lead to an average yearly radiation dose on Mars almost 80 times that from natural sources on Earth [34]. This is roughly the same radiation level that is measured inside the International Space Station in low Earth orbit. While it is not particularly challenging for hardware, it has always been one of the key objections to human exploration Mars, which would expose astronauts to relatively high doses, especially considering the long travel time. Figure 3-16 reports a comparison of radiation doses that would be accumulated by an average human being in some example scenarios including travel and stay on Mars.

The radiation levels on the Martian surface pose some constraints on the selection of materials and components for spacecraft. In particular, polymers like rubbers and adhesives are quickly damaged and lose their mechanical properties, becoming frail and brittle. Electronic devices are especially sensitive to radiation, and only radiation-hardened components can

²⁹ Cosmic rays, or galactic cosmic rays, are a major contributor to radiation in space in addition to solar particles. They generate in the most active regions of the Universe and they are composed by protons and atomic nuclei with far greater energy and penetration power than solar radiation.

be used with confidence. This translates into constraints on the size and computing power of the electronics, since robustness against radiation typically comes with bulkier and less performing hardware.

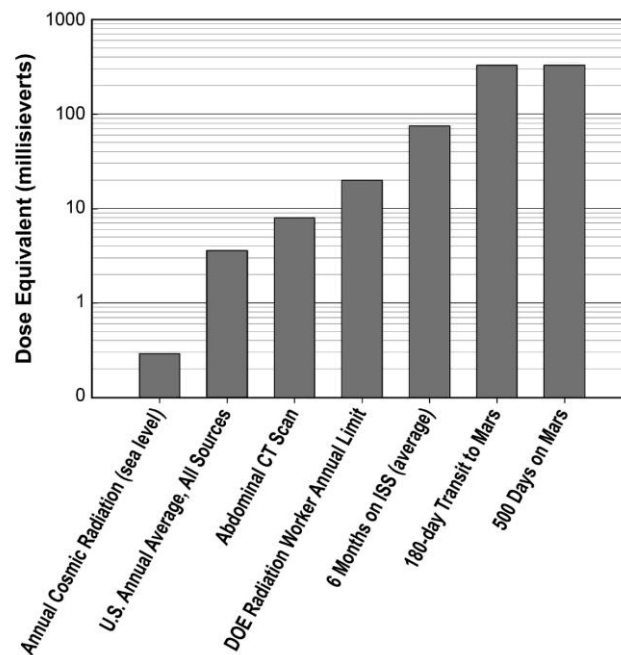


Figure 3-16 – Examples of radiation doses for different scenarios (credit: NASA)

One further consequence of this radiation environment is that the top layer of Martian regolith is constantly bombarded by ultraviolet light and high-energy particles. With little replenishment of material beyond what is offered by the wind, the terrain absorbs radiation over time and becomes chemically altered, assuming a composition that is highly toxic to any known terrestrial life [35]. This pushes the search for past and present life to look deeper into the ground, where the radiation cannot penetrate. Recently studied missions, like the ExoMars Rover (see Section 4.4), are designed to carry drills and other instruments to investigate the subsurface of Mars from a few centimetres to a few metres deep, with the aim to find a more benign and biologically interesting environment.

4 MARS ROVERS

Over the last decades, wheeled robotic vehicles have become the symbol of the exploration of Mars. They are the kind of spacecraft that the general public can easily identify at a glance, like the Space Shuttle or the Apollo Lunar Module. Rovers have not become so popular for their number, as they are, in fact, quite uncommon spacecraft even for Mars: only six have reached the planet so far, compared to dozens of other probes. It was rather their roaring success and their ability to bring a human scale to planetary exploration that made them so iconic. Rovers have a speed that we can understand and replicate with our bodies (although it might require some patience), they observe the world from a vantage point approximately two meters above the ground, they interact with rocks as we would do with our hands, they touch, they drill and dig. It is unavoidable that human senses engage with these vehicles much more easily than with a probe skimming the Sun a thousand times faster than a bullet.

What made these vehicles so desirable for scientists is certainly not just their appeal to the public, but also their ability to perform detailed, in-situ analyses at a variety of locations. This makes the scientific return of a rover mission potentially equivalent to that of many lander missions, as already noted in Section 3.1.2. The following pages offer some considerations on the technologies at the basis of surface mobility and discuss a few examples of vehicle designs successfully operated on Mars; lastly, they provide a brief overview of the European rover ExoMars, which established the foundation for much of the experience and technology that will be used in this project.

4.1 Mobility on planetary surfaces

Planetary mobility can be achieved in a number of ways, depending on the properties of the planet under consideration. For example, on Earth, with its variety of environments, mobile machines have been developed to operate on the surface of solid bodies, on the surface of liquid bodies, suspended in gas and also immersed in liquid. Other planets offer one or more similar environments, therefore, it could be expected for mobile machines to be adapted in a similar fashion. In reality, the only type of mobility broadly used the exploration of other planets is that on a solid surface, i.e., vehicles moving on rocky ground. Only very recently, powered flight through the atmosphere was added to this traditional type of locomotion by

NASA's Ingenuity helicopter. This section focuses on the more conventional mobile machines that operate in continuous contact with the terrain, commonly known as rovers.

A number of locomotion strategies can be evaluated when designing a rover for a planetary surface like that of Mars. Below are some of the most frequently considered:

1. Wheeled locomotion
2. Tracked locomotion
3. Legged or walking locomotion
4. Unconventional locomotion strategies (e.g. snaking or hopping)

The following sections provide a brief description of these approaches.

4.1.1 Wheeled locomotion

Wheeled locomotion is the solution most frequently associated to planetary exploration and it is, in fact, the only one implemented successfully beyond Earth to date. Having been in use on our planet for a few millennia, wheels are a simple and well-consolidated technology: they are a 1-degree-of-freedom mechanism where the only joint is the central rotary coupling, which might be motorised or not. The control of a wheeled vehicle is not complex and usually consists in commanding the desired velocity³⁰ to the active wheels or, when steering joints are present, also the desired orientation. Provided a number of wheels greater than 3, the vehicle is in static equilibrium under its weight and can be controlled at low speed and stopped at any moment if necessary.



Figure 4-1 – Spare wheel of NASA's Apollo LRV (credit: Smithsonian National Air and Space Museum / E. Long)

³⁰ The control of manned vehicles, like cars, usually works by commanding torques rather than velocities. However, that is influenced by historic reasons related to the combustion engine and the fact that the human brain processes loads better than speeds. The simplest control for autonomous vehicles is a velocity control.

One of the disadvantages of wheeled locomotion is that it usually produces small contact patches between the vehicle and the ground, thus leading to risk of sinkage and poor traction. Figure 4-1 shows one of the spare wheels for NASA's Lunar Roving Vehicle (LRV), left on Earth at the end of the Apollo programme. The tyre is composed by a woven mesh of zinc-coated steel piano wire to which titanium treads are riveted in a chevron pattern, with an overall diameter of 818 mm. The hub is made of aluminium, with a titanium frame to limit the tyre deformation upon impact. This wheel was developed for human transportation and it aimed at reproducing the automotive technology of the time. It uses a compliant tyre, which partly addresses the issue above of the small contact patch with the ground.

4.1.2 Tracked locomotion

Tracked locomotion is not uncommon on Earth, especially in rough off-road terrain. Tracks help mitigate the issue of limited contact surface on wheels and distribute the weight of the vehicle on a large area, which is why they are frequently used on heavy machinery. However, they are most useful when the terrain is either wet or of organic origin, which are conditions very common on Earth but not on any other place in the Solar System, except for some regions of Titan (see 2.3.3.2). The regolith in most areas of the rocky planets has sufficient bearing capacity not to require tracks.

The key disadvantage of tracks is their mechanical complexity: one single track requires approximately a dozen wheels to operate and a similar number of mating surfaces that can get damaged or clogged by terrain material. Furthermore, the track itself is either built with some type of flexible rubber (which would be unsuitable for planets other than Earth due to the radiation and temperature environment) or composed by a large number of rigid segments, linked by equally numerous mechanical joints. For this reason, tracked vehicles require considerable maintenance on Earth, which would not be easily available on other planets. Figure 4-2 captures well the complexity of the continuous track suspension of a 1950s medium-size tank.

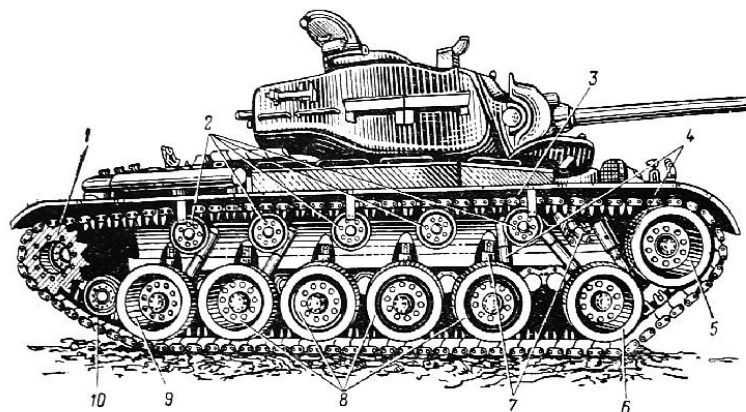


Figure 4-2 – Schematic of the track drive system and suspension of a 1950s tank (credit: allworldwars.com)

4.1.3 Legged or walking locomotion

Legged or walking locomotion is most frequently observed in mobile systems of biological origin, including human beings. The fact that it has been favoured by natural selection does not signify that it is the best performing locomotion strategy, as even natural selection is

limited by the constraints of what Terrestrial biology can produce. For instance, complex life forms rely on internal fluid networks to operate and thus cannot develop rotating joints with unlimited range. Legged locomotion does have its advantages, in particular on very rough terrains, as it allows to place the robot's "feet" into carefully selected places, avoiding too steep or hazardous features.



Figure 4-3 – Testing of a walking robot prototype aimed at exploring Martian and Lunar caves (credit: NASA / JPL-Caltech)

There are today numerous implementations of walking machines, with varying mechanical complexity and effectiveness. Some of the most attractive ones are those that somehow mimic four-legged animal locomotion, due to their agility and operational flexibility. Robots of this kind have recently become popular on Earth, and even studied for Mars missions, like the one in Figure 4-3, showing a prototype called NeBula-SPOT, developed by JPL on a commercial walking robot from Boston Dynamics. However, these machines are characterised by non-insignificant mechanical complexity and are very challenging to control, especially when it comes to maintaining dynamic equilibrium. This level of reactivity is not compatible with current standard space electronics and therefore has never been implemented in planetary exploration.

In some cases, walking actuators are coupled with other locomotion means, such as wheels, creating a hybrid configuration. These can be used for backup mobility in difficult situations or as a way to change the load distribution of the vehicle. The ESA ExoMars Rover is an example of such a hybrid architecture with a backup "wheel walking" capability, as described in Section 4.4.3.

4.1.4 Unconventional locomotion strategies

Other, more exotic types of locomotion have been considered for planetary surfaces, but rarely developed past the stage of initial research. Some examples are snake-like devices, which offer great flexibility with respect to the environment but also lead to extreme mechanical complexity. Another mobility scheme worth dwelling on is hopping: rather unusual on terrestrial robots, but promising for very low-gravity environments, such as asteroids

and small moons. If the robot can be designed to be robust to falls, a very simple hopping strategy can be implemented through elastic means or thruster propulsion, potentially covering significant distance in a single hop.

4.2 Locomotion of wheeled planetary rovers

Given the discussion above, it can be appreciated how wheeled locomotion has become one of the preferred strategies for planetary mobility, especially for environments like Mars. The simplicity of the mechanical implementation and the control scheme, together with the overall reasonable bearing capacity of the regolith, have made wheels the solution of choice for Mars exploration.

The arrangement of wheels and the structure connecting them to the vehicle – broadly referred to as suspension – is defined in response to the terrain and velocity requirements of the vehicle [36]. Planetary rovers are characterised by low speeds and the only highly dynamic events during their operation are the impacts that can happen when descending obstacles. Because of this, rovers do not generally require dynamic³¹ suspensions like those typical of the automotive industry, but more often rely on a set of freely rotating joints. The only exception to this is the Apollo Lunar Roving Vehicle, which needed to move at speeds useful for its human drivers, whilst maintaining stability and some degree of comfort, and therefore mounted sprung suspensions similar to those of a car.

All the autonomous planetary rovers rely on non-elastic suspension mechanisms that have as main objective to make the vehicle statically determined³². In practical terms, this means adding one degree of freedom for each additional wheel above the minimum stability requirement of three wheels. These mechanisms also aim to distribute as evenly as possible the loads between different wheels to homogenise traction and sinkage. The suspension architectures below are the most frequently studied for Mars rovers:

1. Rocker arm suspension
2. Rocker bogie suspension
3. Triple bogie suspension

The following paragraphs offer a high-level summary of these three common implementations and some further considerations on their design.

4.2.1 Rocker arm suspension

The rocker arm, depicted in Figure 4-4, is a four-wheeled suspension where the wheels on each side are attached to an arm that is in turn connected to the vehicle body through a hinge. To prevent the vehicle from oscillating freely around said hinge, the pitch angle of the

³¹ The term dynamic here refers to a suspension designed to operate in a predominantly dynamic regime during locomotion, i.e. not in static equilibrium and constantly affected by inertial forces.

³² A statically determined system is one that is stable and whose reactive forces can be determined from the equations of equilibrium alone.

body needs to be combined with the rotation of the arms. This can be achieved with a differential³³ mechanism, such as, for example, one further oscillating arm as shown in Figure 4-4 (b). With this linkage, the vehicle body always sits at an average angle between the two arms and the solution is thus defined pitch-averaging suspension (for further details on the kinematics, see Figure 7-13 in section 7.2.1). It is common to see the main suspension arms referred to as “bogies”, although that term comes from the rocker bogie design (Section 4.2.2). In cases like this, where there is only one oscillating element per side, there is no real distinction between a rocker and a bogie and so both terms are equally accepted.

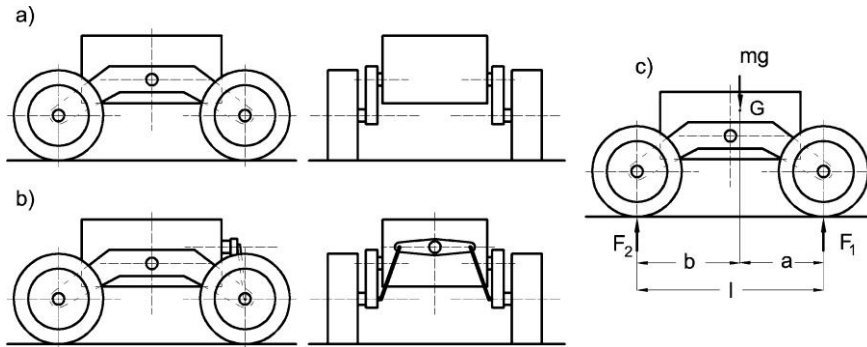


Figure 4-4 – Rocker arm suspension for a four-wheeled rover: (a) general layout, (b) with differential arm, (c) forces on level ground (credit: G. Genta)

With reference to Figure 4-4 (c), the forces acting on each wheel on level ground can be calculated from moment equilibrium as:

$$F_1 = mg \frac{b}{2l} \quad F_2 = mg \frac{a}{2l}$$

where m is the mass of the vehicle and g is the gravity acceleration (e.g., 3.72 m/s^2 on Mars), taking into account that the wheels on each side support half of the total weight. It derives that, if $a = b = l/2$, then each wheel carries $1/4$ of the weight of the vehicle.

The rocker arm suspension is rather simple system, both from the mechanical and control point of view. However, its capability to overcome obstacles is limited by the number of wheels: when one of them encounters a rock, there are only three left to provide the traction required to push it over the obstacle. Systems with more wheels provide more traction to surmount discontinuities in the terrain and tend to be preferred for planetary exploration because of this and other reasons, as discussed in Section 4.2.4. The four-wheeled rocker arm design has always received serious consideration but has never been selected for implementation on spacecraft. That is, until it became the baseline for the Sample Fetch Rover, subject of this work and discussed in depth in Chapter 7.

4.2.2 Rocker bogie suspension

The six-wheeled rocker bogie is the suspension of choice of all NASA rovers on Mars and it is shown in Figure 4-5. This architecture can be considered an evolution of the rocker arm,

³³ This type of mechanism has similar properties to the classical automotive differential, insomuch that the rotation of one element (the rover’s body or the car’s engine shaft) is the average of the rotation of the other two (the rover’s rocker arms or the car’s wheels). However, while in automotive applications its function is to add one degree of freedom to the system, on planetary rovers it is to remove it.

since each side features a rocker carrying a wheel on one end, while the opposite end is hinged onto another oscillating element, the bogie, connected to two wheels. Like the rocker arm configuration, the body needs to be coupled to the arms by a differential mechanism to constrain its pitch angle.

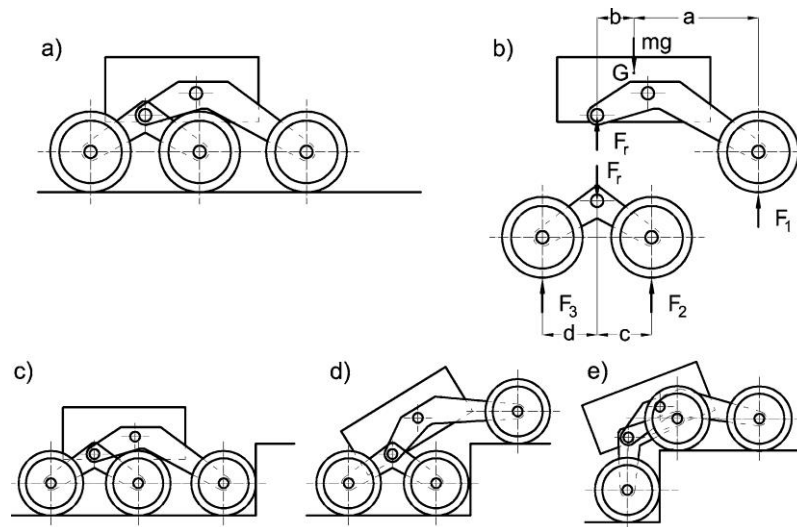


Figure 4-5 – Rocker bogie suspension for a six-wheeled rover: (a) general layout, (b) forces on level ground, (c) – (e) overcoming a step (credit: G. Genta)

Considering Figure 4-5 (b), the forces acting on the front wheel and the rocker pivot on level ground can be calculated from moment equilibrium as:

$$F_1 = mg \frac{b}{2(a+b)} \quad F_r = mg \frac{a}{2(a+b)}$$

The forces acting on the other wheels are:

$$F_2 = mg \frac{ad}{2(a+b)(c+d)} \quad F_3 = mg \frac{ac}{2(a+b)(c+d)}$$

It derives that, if $a = 2b$ and $c = d$, then each wheel carries $1/6$ of the weight of the vehicle.

The rocker bogie has proven very successful on NASA's rovers and also the Chinese National Space Administration (CNSA) has started using it on the Moon and Mars. This architecture shows good static stability, adequate load distribution among wheels and, in good traction conditions, it is capable of surmounting obstacles as high as a wheel diameter. It also is possible to obtain an eight-wheel version of this architecture by simply adding another bogie in place of the wheel that is directly connected to the rocker. The result is shown in Figure 4-6, although this design has never been used in planetary exploration.

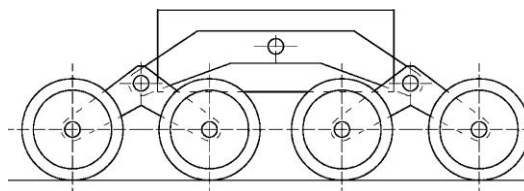


Figure 4-6 – Rocker bogie suspension for an eight-wheeled rover (credit: G. Genta)

4.2.3 Triple bogie suspension

The triple bogie suspension can be considered the result of directly applying the rocker arm concept to a six-wheeled vehicle. It is, in fact, also defined triple rocker arm or six-wheeled rocker arm, recalling that, as noted in Section 4.2.1, there is no real distinction between a rocker and a bogie when all the hinges are on the vehicle body. This architecture, shown in Figure 4-7, simply uses a third transversal rocker arm to accommodate the two additional wheels. Differently from the previous designs, the vehicle configuration is statically determined without the need for a differential linkage, making this a very simple mechanical implementation.

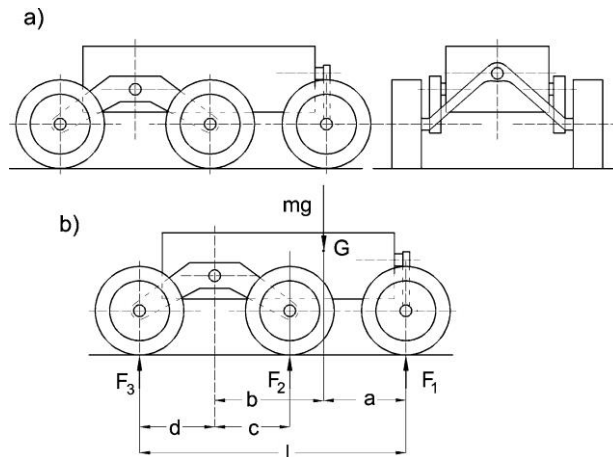


Figure 4-7 – Triple bogie suspension: (a) general layout, (b) forces on level ground (credit: G. Genta)

With reference to Figure 4-7 (b), the forces acting on the wheel connected to the transverse arm and the arm pivot on level ground can be calculated as:

$$F_1 = mg \frac{b}{2(a + b)}$$

The forces acting on the other wheels are:

$$F_2 = mg \frac{ad}{2(a + b)(c + d)} \qquad F_3 = mg \frac{ac}{2(a + b)(c + d)}$$

The force distribution is exactly the same as the rocker bogie and, as in the previous case, if $a = 2b$ and $c = d$, then each wheel carries 1/6 of the weight of the vehicle.

The triple bogie offers the same force distribution on level ground and stability as the rocker bogie, but with lower mechanical complexity. The obstacle capability of the two suspensions is comparable, with some minor disadvantages for the triple bogie due to the transversal behaviour of the third bogie. For its simplicity and low mass, together with the absence of a differential linkage that would interfere with solar arrays or other hardware mounted on the rover, the triple bogie was selected for the ESA ExoMars Rover [38].

4.2.4 Number and types of wheels

When it comes to the number of wheels for Mars rovers, there seems to be a clear preference for six-wheeled platforms, since all rover designs use this approach at exception of the Sample Fetch Rover, subject of this study, which is based on a four-wheel platform. There are

multiple reasons behind the choice of six wheels for most exploration rovers, the following being the key ones:

1. **Load distribution.** As discussed in Section 4.2, the average load on each wheel of a six-wheeled vehicle is $2/3$ that of a four-wheeled vehicle of equal mass, leading to less sinkage and lower risk of becoming trapped in loose sand.
2. **Traction.** More contact points with the ground mean more interfaces available to produce traction.
3. **Obstacle climbing ability.** As one wheel encounters a rock, in a six-wheeled rover there are five more to provide useful traction to push it over the obstacle, while on a four-wheeled rover there are only three.
4. **Redundancy.** In case one wheel fails, the vehicle might attempt to continue the mission with the remaining ones, potentially dragging the damaged wheel. If there are five wheels available to drag the failed one, the performance degradation is smaller than if only three are left.

The obvious drawbacks of increasing the number of wheels of a vehicle are the associated additional complexity, mass and volume. For example, moving from six to eight wheels is often considered not sufficiently advantageous to justify the associated impacts to the mission design. While point 4 above is a mission-level decision that depends on the required traverse profile, the first three are performance parameters influenced by other contributors beyond the number of wheels, a fundamental one being the wheel design. If that can be streamlined to improve load distribution, traction and obstacle capability, then the need for a high number of wheels is reduced. In particular, all of the three performance indicators can be increased by tuning the level of mechanical compliance in the wheel.

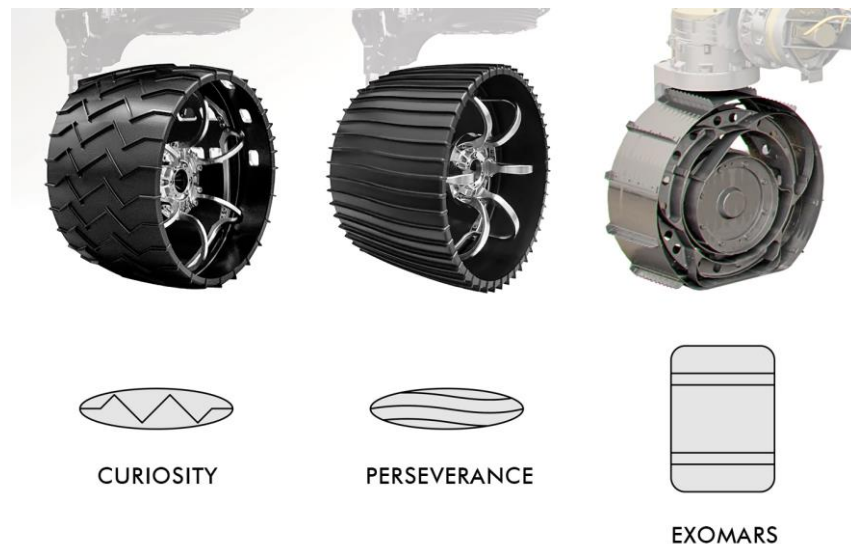


Figure 4-8 – Comparison between Curiosity, Perseverance and ExoMars wheels (not to scale) with approximate contact patches on firm soil.

The choice between rigid wheels and compliant wheels is a defining factor of a rover's architecture. Rigid wheels have a much simpler design, but they lead to a high contact pressure on the ground, reducing the traction and obstacle performance. To compensate for that, the size or the number of wheels needs to increase. NASA's Curiosity and Perseverance rovers, for example, have a rigid wheel design. Their threads are covered in grousers to provide traction, whose geometry was changed between the first and the second rover to improve

durability. Figure 4-8 shows a comparison between these wheels and the ExoMars Rover wheel, not to scale.

The ExoMars wheel, more constrained in size by the accommodation on the landing platform, had to use significantly more mechanical compliance. This reduces the contact pressure and increases the useful surface to produce traction, mitigating the downsides of the smaller size. This wheel is also equipped with larger grousers to improve the engagement with the terrain and obstacle surfaces. It was observed in Section 4.1.2 that tracked locomotion is generally unnecessary for Mars, but the contact patch of the ExoMars wheel does resemble a short track. It is also evident how this wheel is mechanically more complex than the others, although nowhere near as complex as a continuous track.

Considerations like the ones above have led to the unusual choice of four wheels for the Sample Fetch Rover design, in light of an equally unusual wheel technology and a mission profile that allows this redundancy approach. This is discussed in detail in Section 7.1.1.

4.2.5 Actuators

The ideal configuration for any off-road vehicle is to have all wheels motorised to maximise the traction available, and the control of the vehicle is most effective if each wheel is independent from the others. This solution is common across all planetary rovers, which typically accommodate an electric drive actuator³⁴ inside each wheel hub.

The implementation of steering actuators is subject to more variation: in theory, it is possible to avoid them entirely if a skid-steering strategy is chosen, which makes the vehicle turn by driving the wheels on either side at different speeds. This technique is very simple, but, while it is suitable for tracked vehicles, it is usually considered too coarse for wheeled rovers, which have the potential to achieve significantly greater agility. In order to do that, dedicated steering actuators are provisioned.

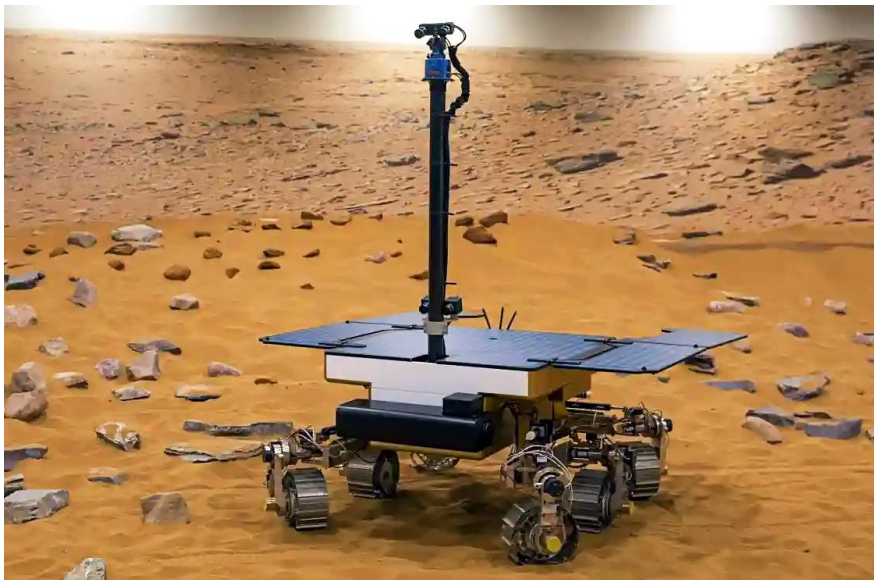


Figure 4-9 – A prototype of the ExoMars Rover performing a point turn (credit: Airbus)

³⁴ The term actuator here indicates the assembly of motor, gear train, sensors, bearings and housing.

Six-wheeled rovers need at least four steering actuators to prevent wheels from slipping and ensure an accurate trajectory control. All of NASA's rovers, in fact, have steering actuators on their front and rear wheels, and not on the middle wheels. The steering joints have sufficient range to allow the vehicle to turn on the spot if needed (approximately $\pm 45^\circ$, see Figure 4-9). The ExoMars Rover, on the other hand, has steering actuators also on the middle wheels, allowing it to choose more freely its centre of curvature and to perform "crabbing"³⁵ manoeuvres, which are required during scanning with its ground penetrating radar. All six wheels can steer $\pm 90^\circ$ so the vehicle can crab at any angle.

Another area where the use of actuators is considered is the suspension itself: if parts of the structure can be moved to modify its geometry or load distribution, this allows to achieve alternative locomotion strategies. Section 4.4.3 describes the implementation of such a feature on the ExoMars Rover, which reuses the already-present deployment joints. The Chinese rover Zhurong, for example, has dedicated actuators in the rocker hinges of its rocker bogie suspension to achieve this functionality.

On both rovers above, the active suspension modifies the geometry of the vehicle, for example to break free from sand traps. Other strategies, controlling the load distribution instead of the position of the wheels have proven highly advantageous for obstacle climbing [37]. Figure 4-10 shows an example of a triple bogie rover prototype climbing an extremely challenging step obstacle thanks to actuators that apply torques to its front bogies. However, these strategies are rarely implemented in flight since they require a rather sophisticated on-board perception of the obstacle or a slow step-by-step approach by ground control.

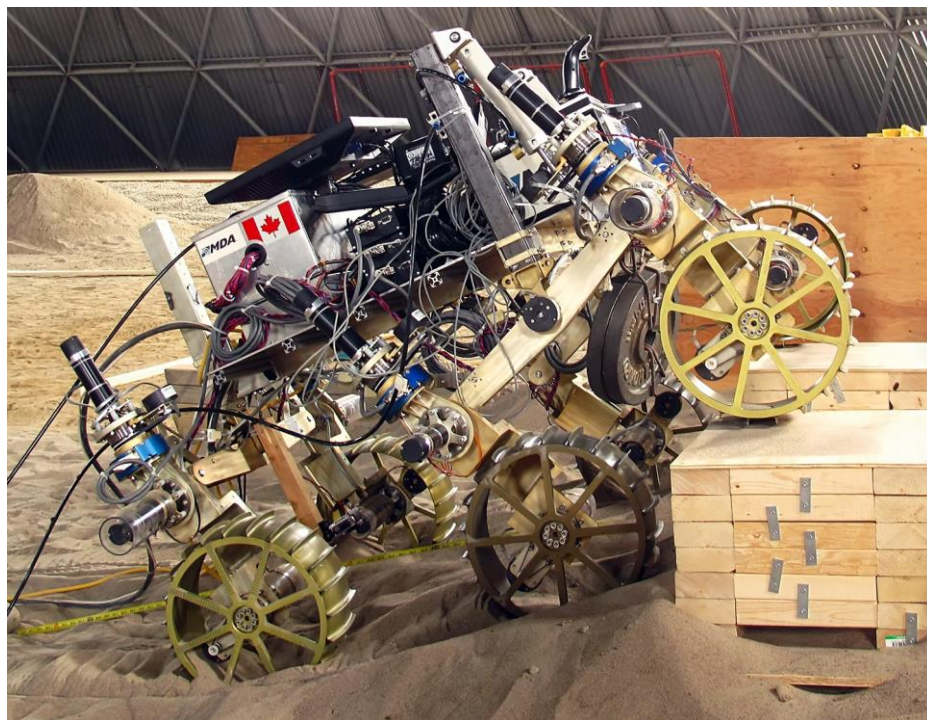


Figure 4-10 – Rover prototype climbing a large obstacle thanks to active front bogies (credit: B. Ghotbi)

³⁵ Crabbing is a manoeuvre in which a vehicle follows a linear motion not coincident with its longitudinal direction, often in a perpendicular one, but more generally in any direction that is not the traditional driving one.

4.3 Rover designs operated on Mars

The six rovers operated on Mars to date can be categorised in terms of size and capability into three main classes. This also applies, with some adjustments, to the major rovers currently under development. These three classes can be defined as follows:

1. Microrovers (MFEX class)
2. Medium solar rovers (MER class)
3. Large nuclear rovers (MSL class)

The following pages outline the salient features of these vehicles.

4.3.1 Microrovers

The only microrover successfully operated on Mars is NASA's Microrover Flight EXperiment (MFEX), deployed from the Pathfinder lander. More commonly known as Sojourner, it was a microwave-sized, solar-powered robot. Other similarly sized vehicles have been studied and even launched, for example the Soviet PrOP-M rovers on board the Mars 2 and 3 landers, which both failed. Sojourner was the first rover to be operated on Mars and is taken as an example of the key parameters of this class of vehicles, summarised in Table 4-1.

Feature	Description
Mass	11.5 kg
Science payload	0.6 kg
Ground footprint ³⁶ (L x W)	0.5 m x 0.4 m
Power	Solar, 16 W on Mars at noon
Locomotion architecture	Six-wheeled rocker bogie
Maximum speed	0.7 cm/s
Mission duration	Planned: 7 sols Achieved: 83 sols
Traverse distance	104 m

Table 4-1 – Key features of NASA's Sojourner rover

As the table above illustrates, on board a vehicle of this size there is limited room for scientific instruments. This type of vehicle is typically experimental in nature and capable of performing only limited observations. Solar power is limited by the small surface area, so the spacecraft is usually unable to communicate with Earth or even Mars orbit without the support of a nearby communication relay, for example its mothership lander. The Soviet microrover design was not even independent in terms of power generation and was connected to the lander through a tether that transferred power and telecommunications. The opera-

³⁶ Ground footprint here indicates the distances between the centroids of the contact patches of the corner wheels and not the overall length or width of the vehicle.

tional autonomy of a microrover is limited by the power of the computer that can be accommodated aboard. This usually implies frequent intervention by ground and a limited traverse range.

4.3.2 Medium solar rovers

The first microrover experiment demonstrated that this kind of robot could significantly increase the scientific return of a surface mission and so it was soon followed by larger, more capable rovers. The first ones were the Mars Exploration Rovers (MER), named Spirit (MER-A) and Opportunity (MER-B). The two identical vehicles were the size of a golf cart and some of their salient features are summarised in Table 4-2.

Feature	Description
Mass	185 kg
Science payload	9 kg
Ground footprint (L x W)	1.2 m x 1.1 m
Power	Solar, 140 W on Mars at noon
Locomotion architecture	Six-wheeled rocker bogie
Maximum speed	5 cm/s
Mission duration	Planned: 90 sols Achieved: 2208 sols (MER-A) Achieved: 5352 sols (MER-B)
Traverse distance	7.73 km (MER-A) 45.13 km (MER-B)

Table 4-2 – Key features of NASA’s MER rovers

It is evident how MER-class rovers were designed to carry a sizable science payload over a long distance. They both ended up far exceeding even the best expectations in terms of durability and quality of their observations. Like their predecessor, these robots are solar powered, but they mounted much larger, deployable solar panels, which ensured sufficient power for prolonged traverse and direct communication to orbit. The rovers had a certain degree of autonomy, with the ability to cover hundreds of meters on easy terrain without ground intervention.

The Chinese rover Zhurong and the European ExoMars can be considered part of the same class of spacecraft. They are both slightly heavier and incorporate more modern technology, but they are otherwise similar in their capabilities. Despite the risks associated to solar power in dusty conditions (see Section 3.3.5), this type of vehicle has proven rather sturdy and relatively simple, and so it is often taken into consideration by many space agencies that venture to explore the Red Planet. The Sample Fetch Rover is also a MER-sized vehicle, although it is not designed to carry any science payload to Mars, but rather to retrieve one to be sent to Earth.

4.3.3 Large nuclear rovers

The largest class of robotic vehicles on Mars was developed by NASA in the late 2000’s and named Mars Science Laboratory. Also known as Curiosity, the first vehicle of this class is in

fact a fully-equipped mobile laboratory, with the size of a large car and a broad array of scientific instruments on board. Differently from previous rovers, this spacecraft is powered by nuclear reactions inside its Radioisotope Thermoelectric Generator (RTG), which ensure a reliable power output in any environmental condition. Some key specifications of the vehicle are reported in Table 4-3.

Feature	Description
Mass	899 kg
Science payload	80 kg
Ground footprint (L x W)	2.3 m x 2.3 m
Power	Nuclear, 100 W beginning of life
Locomotion architecture	Six-wheeled rocker bogie
Maximum speed	2.5 cm/s
Mission duration	Planned: 668 sols Achieved: >3500 sols (ongoing)
Traverse distance	>27 km

Table 4-3 – Key features of NASA’s Curiosity rover

NASA’s Perseverance rover is of the same class as Curiosity, with a very similar architecture and a slightly higher mass. These spacecraft are the heaviest payloads ever delivered to the surface of Mars and their size necessitated a unique type of descent module, called Sky Crane, which lowers the rover on tethers and then flies away. Both vehicles are currently operating on Mars and constitute humanity’s most technologically advanced outposts on the planet. Perseverance carries a slightly heavier scientific payload than Curiosity’s, which includes the systems that collect, prepare and seal the samples to be returned to Earth as part of the work described in the next chapters.

4.4 ExoMars Rover design

At the time of writing, European and Russian collaboration on joint space programmes, like ExoMars, is heavily affected by the unsettled political context. The ExoMars Rover was intended to be launched on a Russian rocket and delivered to Mars by a Russian lander. Following Russia’s invasion of Ukraine on 24th February 2022, the European Space Agency has halted preparations for the 2022 launch, now officially cancelled, and a backup strategy remains to be defined. Nonetheless, the vehicle was built, tested and delivered on time for a 2020 launch, then delayed by issues with the descent module. This means that all the technology on board the ExoMars Rover is formally qualified for operation on Mars. The know-how acquired during the design, construction and testing of the spacecraft constitutes the foundation for the development of the Sample Fetch Rover, hence a brief summary of its design is provided in the following pages.

4.4.1 Spacecraft architecture

The ExoMars Rover was built by Airbus for the European Space Agency in 2019. It is a solar-powered spacecraft, slightly larger than the NASA MER vehicles described in Section 4.3.2. Its physical architecture is based around a central, box-like body, which provides structural

integrity and creates a thermally-controlled environment for sensitive electronics and scientific experiments.

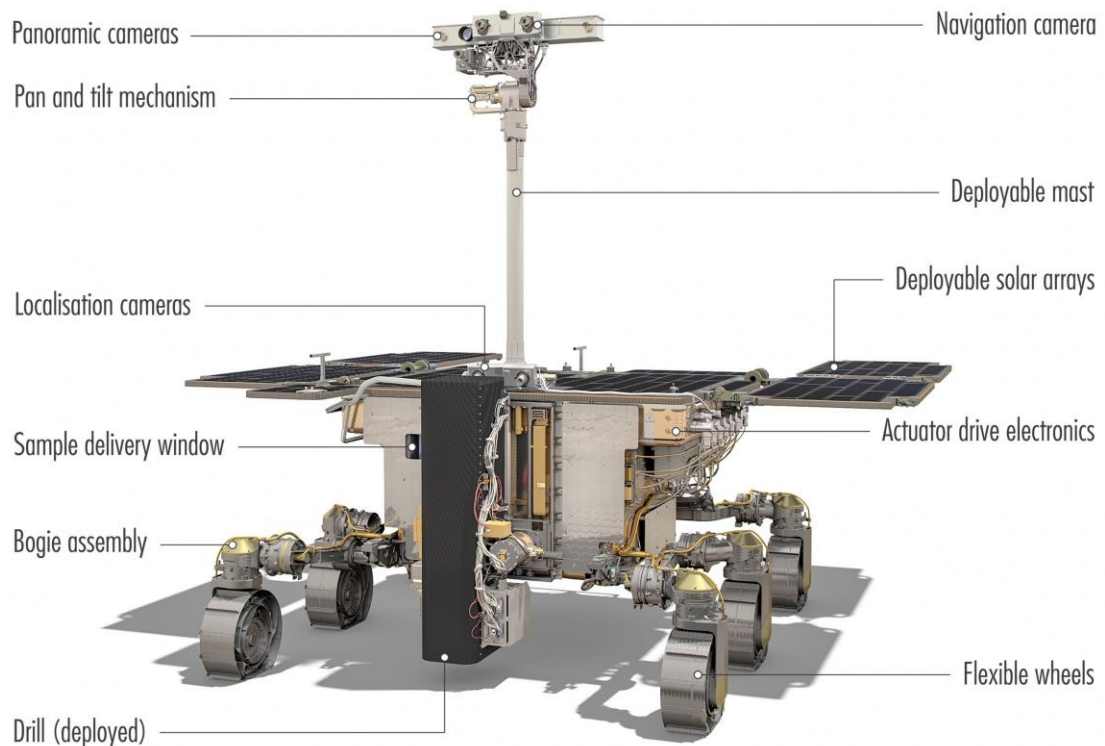


Figure 4-11 – Overview of the ExoMars Rover with some key features (Credit: ESA / ATG Medialab)

With reference to Figure 4-11, at the sides of the rover body are accommodated the suspension system and the drive electronics that control all mechanisms on board. On the front, the large drill system is visible, which extracts the samples for analysis in the internal scientific laboratory. On the top deck are the solar arrays that power the craft and the mast that holds camera payloads at a height of approximately two metres.

Feature	Description
Mass	310 kg
Science payload	47 kg ³⁷
Ground footprint (L x W)	1.3 m x 1.4 m
Power	Solar, 140 W on Mars at noon
Locomotion architecture	Six-wheeled triple bogie
Maximum speed	1 cm/s
Mission duration	218 sols
Traverse distance	4 km

Table 4-4 – Key features of ESA's ExoMars Rover

³⁷ Including 21 kg of drill system.

For comparison with the vehicles described in Section 4.3, the main characteristics of the ExoMars Rover are summarised in Table 4-4. It can be noted how several aspects are very similar to the MER vehicles, but the science payload is remarkably large for a spacecraft of this size.

4.4.2 Mission profile

Like any spacecraft on the surface of Mars, the ExoMars Rover’s mission is planned to start with the so-called “seven minutes of terror”, a colourful expression to identify the Entry, Descent and Landing (EDL) sequence. They are seven because that is the approximate time between first contact with the planet’s atmosphere (entry interface) and touchdown on the surface, and they are “of terror” because this critical and highly dynamic series of manoeuvres has to be executed in complete autonomy. The one-way light time between Mars and Earth during EDL is, in fact, in the order of 13 minutes, so mission controllers on Earth can only watch the sequence unfold after the spacecraft has already reached the surface – successfully or not. Figure 4-12 illustrates the EDL sequence of the ExoMars Rover, where t is the elapsed time since entry interface, H the altitude, V the velocity, θ the angle between the trajectory and the ground plane, Q the pressure on the aeroshell and M the Mach number.

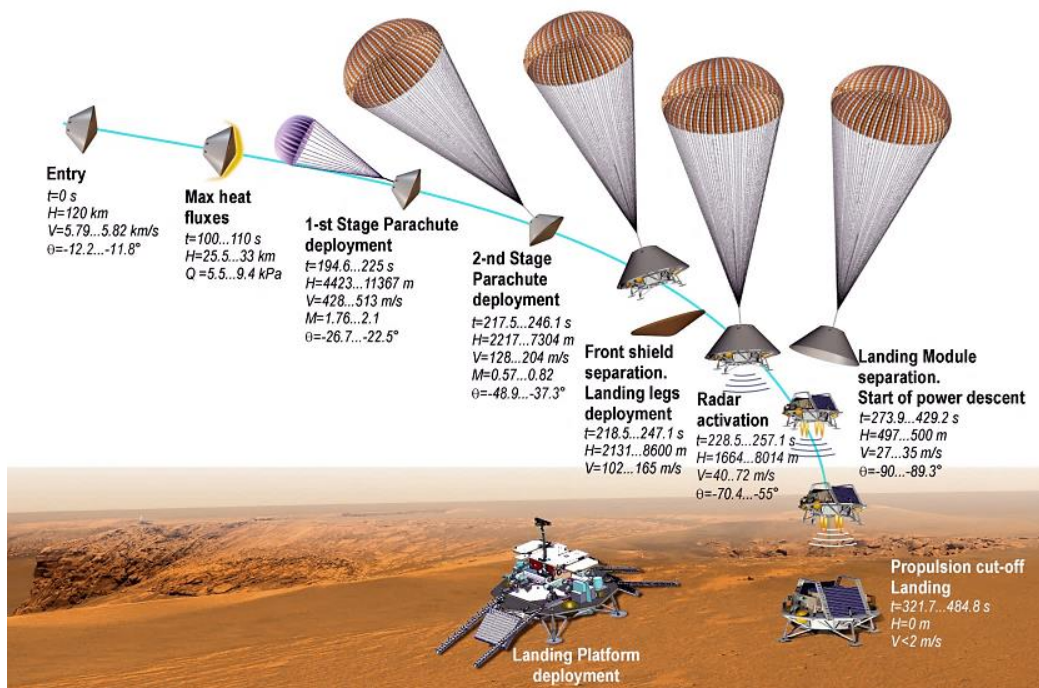


Figure 4-12 – ExoMars Rover entry, descent and landing sequence (credit: ESA)

The descent trajectory leads to a region named Oxia Planum and chosen as landing site for its geological interest. For the entire duration of the travel, the rover is stowed inside the descent module in a very compact configuration, which can be seen in Figure 4-13, depicting a qualification model of the rover during vibration testing. The difference with the on-surface configuration of Figure 4-11 is evident. Once landed, the rover must transition from the first to the second one. The deployment sequence includes unfolding the solar arrays, the mast, standing up on its wheels and disconnecting from the lander. The vehicle is then free to descend onto the surface through ramps.

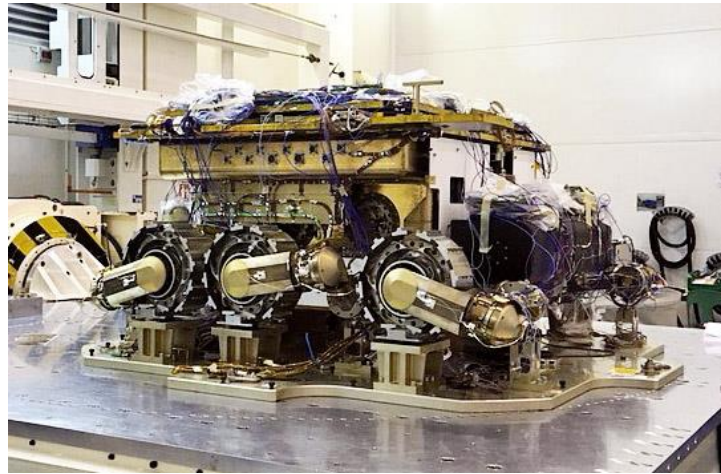


Figure 4-13 – ExoMars Structural and Thermal Model (STM) during vibration testing
(credit: Airbus)

Following egress from the lander and commissioning, the rover will commence its traverse and science phase, during which it will travel up to 100 metres per sol and perform scientific observations. The primary science objectives of the mission are the following:

- To search for signs of past and present life on Mars
- To characterise the water and geochemical environment as a function of depth in the shallow subsurface

One instrument is particularly relevant to the pursuit of these objectives and, in fact, unique to this rover: the multi-stage drill visible at the front in Figure 4-11. It is designed to gather samples from up to two metres underground, reaching areas that are protected from the hostile surface radiation and are much more likely to contain water or traces of potential biological activity.

4.4.3 Locomotion

The locomotion architecture of the ExoMars Rover is based on a triple bogie suspension, already described in Section 4.2.3. This was chosen for being a relatively light and simple design and not needing a differential mechanism, although its obstacle performance is marginally lower than that of a rocker-bogie system. The ExoMars wheel uses a highly compliant design to overcome its small size, constrained by the accommodation on the lander to a diameter of 280 mm. This is achieved through a complex assembly of flexural elements in steel and titanium alloy, shown in Figure 4-14. The result is a wheel that behaves almost like a track when interacting with the terrain, obtaining a large contact patch to support weight and provide traction (see Section 4.2.4).

Each wheel can drive and steer independently, making the rover able to follow trajectories with any curvature, turn on the spot, and “crab” in any direction. Sharp grousers on the tyre thread provide good traction on compact and loose soil. The vehicle’s suspension, also referred to as the Bogie Electro-Mechanical Assembly (BEMA) can surmount obstacles almost as large as a wheel diameter and maintain the rover stable on slope angles up to 45°, although the autonomous navigation system would never allow the vehicle on such steep slopes.



Figure 4-14 – ExoMars wheel climbing a large obstacle (credit: Airbus)

The ExoMars Rover uses three rotary actuators for each wheel, sharing a broadly similar design [39]: driving, steering and deployment. The latter commands a rotation of the entire wheel leg assembly and is used to unfold the locomotion mechanism from its stowed configuration, essentially acting as the rover’s “knee”. This actuator was originally intended to be used only at the beginning of the mission and then latch into position, however, during the development of the locomotion subsystem, it was chosen to leave the actuator free to rotate and available to move again if necessary, for example to pull the rover out of a sand trap. This mode of operation is defined “wheel walking” and uses alternating motions of the deployment actuators to produce thrust on the wheel legs [40]. The types of actuators and their location on the rover are shown in Figure 4-15, where DRV indicates driving, STR steering and DEP deployment.

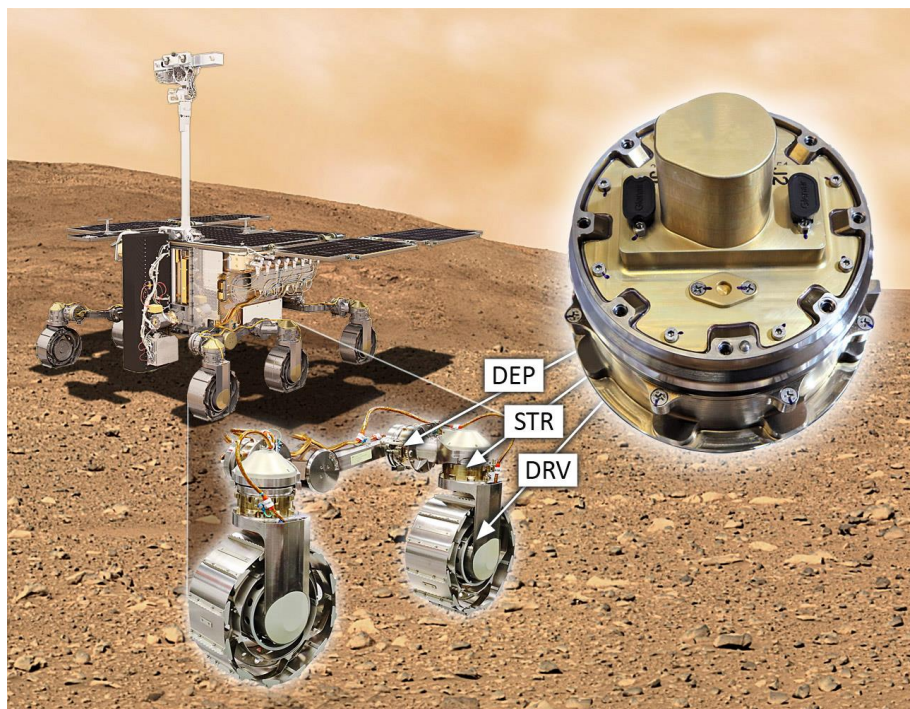


Figure 4-15 – BEMA actuator types and locations (credit: MDA)

4.4.4 Actuator Drive Electronics

To fulfil its mission, the ExoMars Rover needs to operate a variety of mechanisms, including locomotion actuators, solar panel hinges, camera pan and tilt axes³⁸. All of these mechanisms are powered by electric actuators, which need their control electronics to operate. The ExoMars Actuator Drive Electronics (ADE) fulfil this purpose by controlling all motors and separation devices according to the commands coming from the On-Board Computer (OBC, Section 4.4.6).

The electronics are accommodated in two boxes mounted onto the sides of the rover body. For this reason, they are defined “cold electronics”, i.e. not contained in a thermally-controlled enclosure and therefore exposed to the diurnal temperature variation. This choice is driven by challenges in maintaining thermal control if the electronics were inside the rover. In fact, the ADEs would require significant energy to be kept warm, but especially they would constantly leak that energy out of the rover, since they have far too much harness going to the mechanisms to remain isolated. The units would also pose an issue of overheating during the day when they can handle considerable power. The exposure to an extreme thermal range, from the frigid Martian night to the heat of components under high current load, makes the development of this type of electronics particularly challenging.

On the ExoMars Rover, motion control is implemented through an unusual architecture: there are no electronics dedicated to specific mechanisms, but instead the same board is shared among various motors and can be configured to drive only a subset of them at a time. This is acceptable because not all mechanisms are active at the same moment, however, it means that the design of the control system is not optimised for the individual actuator, but rather a compromise between the needs of multiple ones. The reason behind this implementation is to save mass and volume on the ADE by reusing the same board for multiple motors, even if it implies more complex interfaces.

4.4.5 Guidance, Navigation and Control

In order to manoeuvre the locomotion subsystem and travel safely to a chosen destination, the ExoMars Rover is equipped with a highly autonomous Guidance, Navigation and Control (GNC) system. This is based on a set of algorithms running on the On-Board Computer (see Section 4.4.6), which gather data from a variety of sensors to make decisions on the rover path and issue commands to manoeuvre the rover. The commands are picked up by the Actuator Drive Electronics that translate them into movement of the locomotion actuators, driving the vehicle along the desired route. Sensors are regularly interrogated to measure the actual traversed path and make corrections. The GNC system offers various functions and modes of operation to mission controllers. A typical use case foresees a target location set by ground and potential waypoints along the route: the rover then plans a path and follows it whilst avoiding any hazardous areas. A visualisation of this scenario is offered in Figure 4-16.

³⁸ These are the mechanisms on the “rover platform”. The mechanisms that are part of scientific payloads, like the drill, are controlled by their own dedicated electronics.

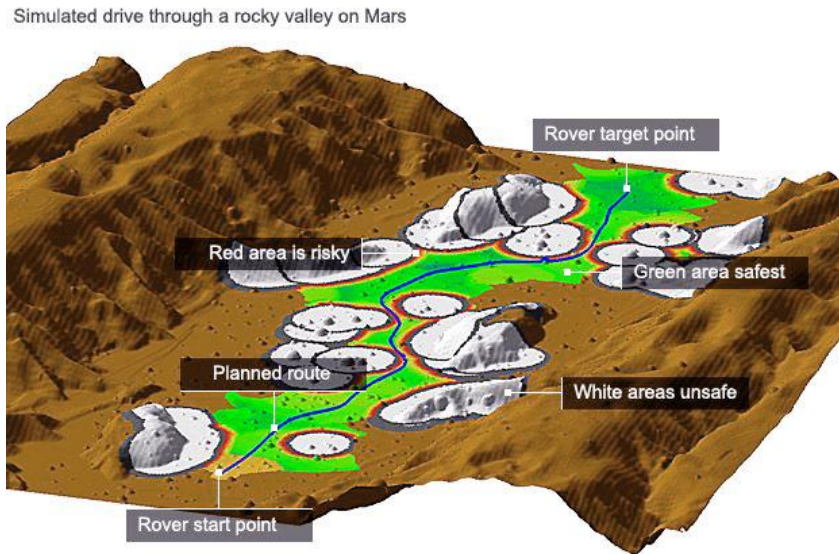


Figure 4-16 – Visualisation of the ExoMars GNC system planning a path and identifying hazardous terrain (credit: BBC)

The GNC system controls and gathers data from the following hardware:

- **Navigation Camera (NavCam).** Mounted on the mast head, at approximately two metres height, and steered by a pan and tilt mechanism, it captures panoramic stereo images to build a 3D map of the rover’s surroundings. It also detects the position of the sun in the sky to establish the vehicles heading.
- **Localisation Camera (LocCam).** Fixed to the rover’s top deck, at approximately one metre height, it captures stereo images of the terrain immediately in front of the vehicle at a relatively high frequency to watch for hazards and monitor progress.
- **Inertial Measurement Units (IMU).** Accommodated inside the rover, they consist of gyroscopes and accelerometers that measure the rover’s attitude and estimate its movement.
- **Locomotion subsystem.** The actuators and the drive electronics that execute the commands of the GNC system, in addition to the sensors that measure the position and velocity of the actuators and the rotation of the suspension linkages.

Information from all these sources is fused by the GNC algorithms to ensure rover safety and make decisions on its trajectory, which are then translated into commands to the locomotion subsystem [41]. During a typical autonomous traverse, the vehicle stops every 2.3 metres (roughly its own length) to acquire panoramic images of its surroundings with the NavCam on the mast. These are elaborated by feature-matching algorithms and transformed into a Digital Elevation Model (DEM) of the area, which is used by the GNC system to identify obstacles and plan a path towards the assigned target location. The NavCam also detects the position of the sun in the Martian sky that, combined with knowledge of the local time, provides the true heading of the vehicle, much like early navigators used to do when sailing the open seas of planet Earth. The LocCams acquire images at higher frequency, approximately one every 0.1 metres, to monitor progress of the rover and detect unexpected hazards or deviations from the path. The other sensors, like IMUs and position sensors, are acquired at a much higher frequency. The data from all these sources is constantly checked against the expected drive profile and against each other for consistency.

Like any Mars rover, ExoMars is designed to venture into unknown territory, which is seen for the first time only as the cameras on the mast gaze upon it. It is therefore necessary to “expect the unexpected” and have a strategy for unforeseen features that the terrain might present. The GNC system reacts to anomalies and hazards according to their severity, for example, by triggering additional camera images, choosing an alternative route or, in the most critical situations, calling for ground to intervene. The involvement of the human operator is kept as a last resource since it has a considerable cost in terms of mission timeline: the ground controllers need to receive and review telemetry, develop a new activity plan and radio it back to the rover, considering communication delay, availability of relay satellites and diurnal cycle on Mars.

4.4.6 On-Board Computer

The “brain” of the rover, responsible for all the high-level decision making and planning, consists in an On-Board Computer (OBC), mounted inside the rover body to protect its relatively sophisticated components from the harsh thermal environment. The OBC is in charge of the management of the mission, the interface with ground control, the high-level commanding and monitoring of all equipment on board, including scientific payloads. The computer also hosts complex algorithms like those required for GNC and image processing. Furthermore, it provides the central memory that stores all the data collected by the rover until it is sent to ground. Figure 4-17 shows the completed flight model of the ExoMars OBC before integration into the rover.



Figure 4-17 – ExoMars Rover On-Board Computer (credit: RUAG Space)

The OBC interfaces with components characterised by a high data rate, like cameras or other optical instruments, through a SpaceWire protocol. For the data bus connecting the other devices with a lower data rate, like the Actuator Drive Electronics or scientific payloads that do not generate high data volumes, a CAN (Controller Area Network) interface is chosen for its low power needs and suitability for motion control applications. The on board computer also manages the only interfaces between the rover and the outside world, through the radio transceivers, allowing to exchange data with ground during mission, and the connection with the descent module³⁹, providing a link to the rover during interplanetary cruise. For these two interfaces, an RS-422 serial protocol is used [42]. The computer, like its interfaces,

³⁹ The descent module is the capsule that contains the rover, together with all the supporting systems to perform entry descent, and landing on Mars.

is fully redundant. This means that, if any one element suffered a failure, the mission could continue on a redundant chain of components.

One of the key design drivers for the ExoMars OBC is the power consumption, which has to be kept to a minimum since the computer remains on also during the night, when energy is most precious. On the other hand, the computer has to be sufficiently powerful to run the image processing and 3D reconstruction algorithms used by GNC (Section 4.4.5). The result is a modular architecture, with high-performance processors used only for the computationally-heavy tasks and lower power processors constantly used for the routine mission management. As mentioned before, these components are far too sophisticated to survive the extreme Martian temperatures, so they are accommodated inside the rover. From this derives another key design driver: volume, which is particularly constrained inside the rover body. This has determined the flat aspect ratio of the unit, visible in Figure 4-17.

4.4.7 Telecommunications

Telecommunication with Earth is a particularly critical aspect of any space mission since, when a radio link is lost, there is nothing that can be done to recover the spacecraft until that link is re-established. One striking example on Mars is the Beagle 2 lander, delivered by the ESA Mars Express orbiter in 2003, which performed a successful landing but only partially deployed its solar panels, failing to expose its antennas to the sky. The spacecraft remained awaiting for commands from ground, eventually aged on Mars and failed when its battery was depleted, without returning one single bit of information⁴⁰.

The most effective way to establish a radio link across interplanetary space is through a high-gain antenna, typically using X band frequency⁴¹, which can produce a tight beam and maintain relatively high power density. However, these antennas require large dishes (often 2 metre or more in diameter) and accurate pointing, which is impractical on surface vehicles. For this reason, Mars rovers are equipped with smaller antennas, typically using UHF (Ultra High Frequency)⁴², which communicate through orbital relays around Mars. It is relatively easy to establish a low power link with an orbiter around the planet that then provides the communication channel with Earth through its high-gain antenna.

The ExoMars Rover uses the relay strategy just described and carries two monopole UHF antennas on the top deck. The antennas are compact to contain the height of the launch package and are connected to dedicated communication electronics, called transceivers. Two transceivers are present inside the rover for redundancy, each one serving one antenna and producing approximately 5 W of radio power output. The ExoMars Rover's telecommunication system is designed to be compatible with at least four orbiters: NASA's Mars Odyssey and Mars Reconnaissance Orbiter, ESA's Mars Express and Trace Gas Orbiter [43].

Orbiters around Mars are clearly a scarce resource and surface assets need to be flexible to make the best of any available spacecraft that flies overhead. Vice versa, as new orbiters are sent to the planet, they are prepared to serve as a relay for various surface missions that are

⁴⁰ It was possible to reconstruct these events from orbital imagery of the spacecraft. No information was ever retrieved from Beagle 2.

⁴¹ X band signals are radio signals in the frequencies between 8 and 12 GHz.

⁴² UHF signals are radio signals in the frequencies between 0.3 and 3 GHz.

in progress or planned. Such arrangements are a notable example of international cooperation between space agencies like NASA and ESA, whose spacecraft support each other in exploring the Red Planet. The communication architecture thus established by American and European orbiters around Mars is called the Mars Relay Network.

Planning the sessions to download and upload data through certain relays requires a precise choreography by mission controllers, and, as seasons pass and orbital patterns evolve, links might occasionally be scarce. The ExoMars Rover is designed to use typically two communication passes per sol, but it can be programmed to operate for much longer without ground intervention.

4.4.8 Scientific instruments

The ExoMars Rover carries a wide suite of scientific experiments, with a remarkably high payload-to-mass ratio for a Mars rover. Part of the instruments are accommodated outside the rover (mostly on the mast and drill) and part of them inside the rover, where they occupy more than half of the body volume [44]. The front section of the rover structure contains the so-called Analytical Laboratory Drawer (ALD), shown in Figure 4-18.

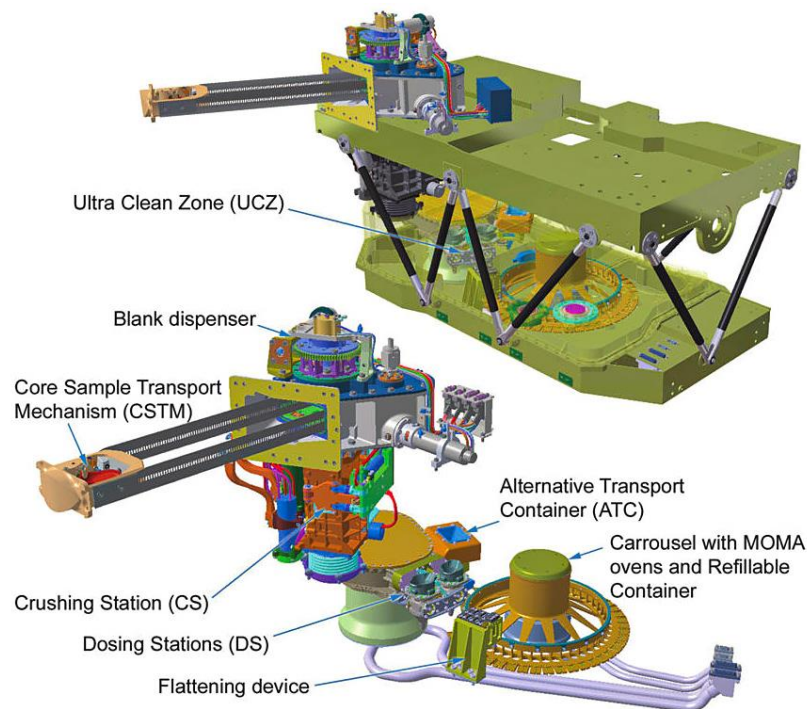


Figure 4-18 – ExoMars Analytical Laboratory Drawer and detail of the Sample Preparation and Distribution System (credit: ESA)

The instruments on board the rover and their purposes are listed below:

- **Panoramic Camera (PanCam).** Located on the mast head, includes two wide-angle cameras for multi-spectral stereoscopic panoramic imaging, and a high-resolution colour camera.
- **Infrared Spectrometer for ExoMars (ISEM).** Placed just below PanCam, analyses the mineralogy and water content of areas of interest.
- **Water Ice Subsurface Deposits Observation on Mars (WISDOM).** A ground-penetrating radar mounted on the rear face of the rover. It builds a stratigraphic map of

the subsurface up to a depth of 3 metres, allowing to identify interesting areas for sampling through the drill.

- **Adron-RM.** A neutron spectrometer housed inside the rover. It is used in combination with WISDOM to search for subsurface water ice and hydrated minerals.
- **CLOse-UP Imager (CLUPI).** Mounted on the drill housing, it provides imaging at close range of the terrain and sample material.
- **Mars Multispectral Imager for Subsurface Studies (Ma_MISS).** An infrared spectrometer located inside the core drill. It allows to analyse the walls of the borehole created by the drill and study the subsurface stratigraphy and distribution of water-rich material.
- **MicrOmega.** Accommodated inside the rover's ALD, it is an infrared hyperspectral microscope that can observe the mineral grain of crushed sample material at high magnification.
- **Raman Laser Spectrometer (RLS).** A spectrometer located within the ALD that analyses the mineralogy of the sample and identifies organic and water-related compounds.
- **Mars Organic Molecule Analyser (MOMA).** The rover's largest instrument, also accommodated inside the ALD. It contains an ion trap mass spectrometer and various extraction tools to perform high-sensitivity search and identification of organic compounds.

In addition to the scientific payloads listed above, the ExoMars Rover also includes extensive payload-servicing equipment. The most notable elements are the multi-stage core drill, which acquires soil samples down to a depth of 2 metres, and the Sample Preparation and Distribution System (SPDS), which transports the core sample inside the rover, crushes it, doses and distributes the powder to the various instruments. The drill is a highly distinctive feature of the ExoMars mission, however, it is also a rather risky device since previous experience with drilling on planetary surfaces shows how it is a particularly challenging and unpredictable process. The worst-case scenario would be the drill getting stuck in the borehole so that it cannot be extracted and permanently immobilising the rover. In response to this potentially mission-ending event, a separation device was built into the drill as a last resort: its activation allows the rover to jettison the drill and continue with at least part of its mission.

4.4.9 Structure

The largest structural element of the ExoMars Rover is the rover body frame, which is composed by a carbon fibre monocoque open on the top side, nicknamed "bathtub" for its peculiar shape and shown in Figure 4-19. The structure is shown here in an intermediate step of its construction where the bare carbon skin is still visible, but this surface would be later covered in sputtered gold to increase its reflectivity and decrease its absorptivity, thus making it a thermally-insulated enclosure.

During integration, the internal equipment is lowered into the body structure and then sealed in by the addition of the top deck panel, which forms part of the solar arrays. The solar panels, another prominent structural element of the rover, are composed by honeycomb sandwich panels with carbon fibre skin and aluminium core, connected by motorised hinges. The rover body structure also provides the main interface for launch loads through the rover body Hold-Down and Release Mechanisms (HDRM). These are three separation

devices positioned on the bottom of the rover that secure it to the landing platform until it has reached the surface of Mars. In Figure 4-19 are also visible the titanium brackets for bolting the pivot points of the triple bogie suspension (see Section 4.4.3).

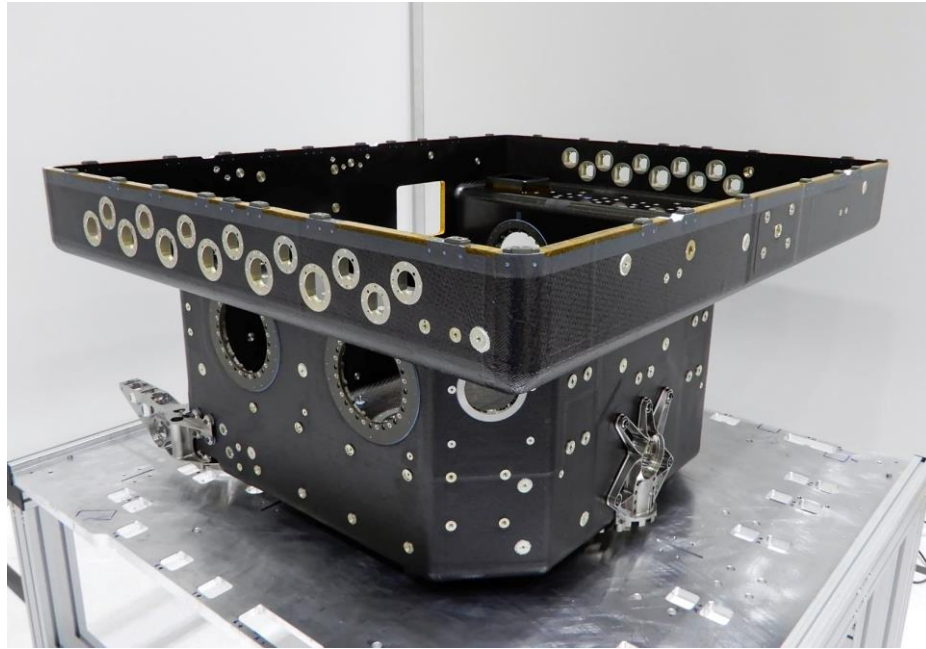


Figure 4-19 – The ExoMars Rover body structure during construction (credit: RUAG Space)

The internal volume is split in two sections, the front one hosting the internal science payload, described in Section 4.4.8, and the rear one containing a service module with the vital hardware needed to operate the spacecraft, including on board computer, battery, power conditioning electronics, inertial measurement units and transceivers.

The choice of carbon fibre composite for the frame of the rover was driven by its mechanical strength and low mass, although the benefits of this type of construction fade as the number of mechanical interfaces grows and the weight of inserts and brackets outbalances the mass savings. In Figure 4-19 it is evident that the quantity of interfaces on the rover body structure is significant. However, carbon fibre also brings great advantages in terms of stiffness, helping maintain a high natural frequency (desirable for launch vibration), and in terms of thermal stability, meaning that the deformation caused by the extreme temperature range is minimised.

Even if the structure is very stable over temperature, the issue of thermally-induced loads remains a major one, since the hardware mounted to the structure can be made of different materials and subject to different temperatures. To address the problem, the interfacing hardware largely uses isostatic mounts, i.e., mechanical constraints that maintain the system approximately statically determined across temperature, typically through the use of compliant elements. The two round openings in the body visible on the left in Figure 4-19 are in fact the interface points of two large isostatic mounts: one supporting the scientific payload and one supporting the service module.

4.4.10 Thermal control

As described in Section 3.3.3, the key challenge for the thermal control system of a Mars rover is to protect the Terrestrial technology on board from the frigid Martian temperatures. The ExoMars thermal control does so by implementing a typical architecture with a heated enclosure (inside the rover body frame), containing the most sensitive hardware, and less vulnerable components outside, exposed to the Martian environment. This does not mean that the devices outside can always operate across the thermal range: while they are designed to withstand the -125°C night temperature without survival heating, most of them need to be significantly warmer to function, typically -60°C or more. The rover's thermal control system also includes external heaters to warm up these items before they can be switched on in the morning.

Active heating on board the rover is generally implemented through electrical resistance heaters powered by the battery, at exception of two Radioisotope Heater Units (RHU) housed inside the rover that provide a baseline heating power (approximately 8.5 W each). One of the most temperature-sensitive elements is the rover's battery, which must never drop below -40°C or it would suffer irreparable damage. This is a remarkably cold temperature for a battery, but still more than 80°C warmer than the coldest Martian night. Consequently, good insulation is essential to minimise heat leak whilst maintaining this temperature inside the rover. Insulation is achieved through physical separation between the internal components and the walls of the body frame, thus preventing conduction. While this would be sufficient on an orbital probe, on Mars the atmosphere fills this gap and generates convection, which is rather effective at extracting heat. To prevent convection, some baffles are placed in the air gap to inhibit air circulation. Lastly, the optical properties of the exposed surfaces are tuned to minimise heat exchange by radiation.

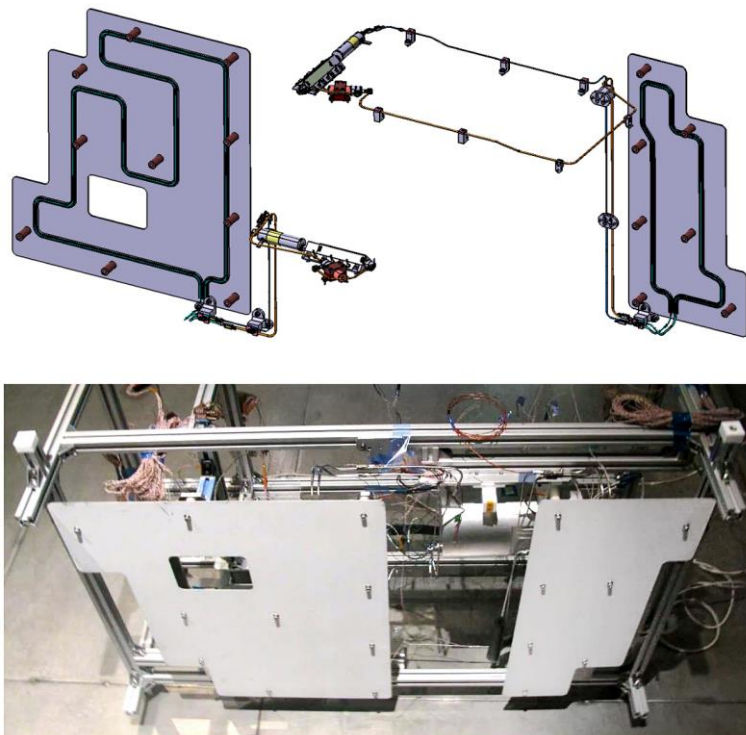


Figure 4-20 – ExoMars Rover ALD loop heat pipes layout (top) and test rig (bottom)
(credit: IberEspacio)

This insulation from the outside world is very effective in retaining heat inside the rover, which is crucial to survive the night, but it also highly undesirable during diurnal operations, when the active components would quickly overheat without a way to cool down. A solution is provided by four loop heat pipes linking to external radiators: two of them connected to the service module and two to the scientific payload. The heat pipes are fitted with thermostatic valves that switch them off automatically when the hardware has cooled down, in order to restore the protective insulation when needed [45]. These thermal control loops use propylene as a working fluid and their layout can be seen in Figure 4-20.

4.4.11 Electrical power system

The power architecture of the ExoMars Rover is similar to that of a classical satellite, with the solar arrays on the top deck generating electrical power for the craft and a battery to provide energy storage. The Power Conditioning and Distribution Electronics (PCDE), mounted on top of the OBC inside the rover, supply power to all the subsystems and secondary power converters.

The photovoltaic assembly is composed by 40 strings of 18 solar cells each, for a total of 720 cells arranged over five panels: a central fixed panel and four deployable segments. The assembly can be seen in Figure 4-21 just before integration onto the flight rover. The selected cell technology is an Azur Space 3G30 triple junction InGaP/GaAs/Ge, which provides a remarkable power generation efficiency of approximately 30% at the beginning of life [46]. On Mars at noon, they can generate more than 260 W at the beginning of life and approximately 140 W at the end of life, considering dust coverage and radiation aging.



Figure 4-21 – ExoMars Rover solar array assembly partially deployed (credit: Airbus)

Compared to a typical satellite, which only has to withstand limited eclipse times, the rover's battery has a considerable size, since it needs to provide survival power over several hours of darkness. Furthermore, the power profile of the rover during operations is highly variable, with frequent spikes and dips due to the traverse on rugged terrain and science operations. Since the solar arrays provide a rather steady power output, it is up to the battery to fill in the extra demand and absorb the surplus production. The ExoMars battery fits 56 SAFT MP 76065 XTD Li-ion cells into a package of 300 x 375 x 100 mm (Figure 4-22), for a total mass of 10.5 kg [47]. The overall nominal capacity is 1140 Wh and the voltage range is between 21.0 V and 29.4 V. One of the most challenging requirements for this battery is the extreme operational temperature range, reaching from -40°C to +50°C.

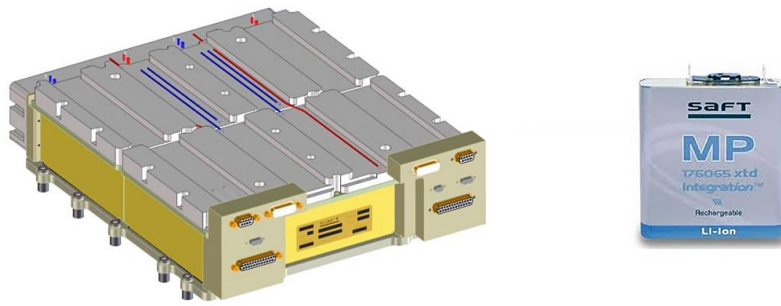


Figure 4-22 – ExoMars Rover battery assembly (left) and unit cell (right) (credit: SAFT)

The PCDE is the element that regulates how the power from the solar arrays and the battery is fed to the various subsystems and payloads. These electronics have to support the operation of power-hungry mechanisms, like the 18 locomotion actuators, and so must be capable of sustaining significant currents, in excess of 15 A in total. They also need to maintain the power bus stable and guarantee spacecraft safety in case of anomalies in the power profile of any unit. To do so, they are fitted with Latching Current Limiters (LCL) dedicated to the various power channels. The LCLs are solid-state switches that can interrupt circuits if the current draw is too high or exhibits non-nominal behaviour. They can also be reset to their normal condition once the fault is resolved.

4.4.12 Planetary protection

While not an immediately obvious feature of the spacecraft hardware, planetary protection has been a major design driver for nearly every aspect of ExoMars Rover. Planetary protection is a set of guiding principles in the design of interplanetary missions aimed at protecting Solar System bodies against biological contamination from Earth and, in case of sample return missions, protecting Earth against biological contamination from other bodies. The COmmittee on SPace Research (COSPAR) has identified a set of categories that are widely adopted when developing interplanetary missions [48]. These are based on the biological potential of target location and the type of mission under consideration. They are summarised below:

- **Category I.** Any mission to a target body which is not of any particular biological interest. No planetary protection requirements apply. Examples: any mission to the Moon or Venus.
- **Category II.** Any missions to a target body where there is interest relative to the process of chemical evolution and the origin of life, but where there is only a remote chance that contamination carried by spacecraft could affect the environment. Planetary protection only requires risk assessment and documentation. Examples: comets, gas giants and ice giants.
- **Category III.** Specific types of missions (generally flybys and orbiters) to a target body of biological interest where contamination carried by spacecraft could alter the environment and jeopardize future exploration. Planetary protection requires basic cleanliness standards, detailed documentation and end-of-mission plan. Examples: flyby or orbiters for Mars and Europa.
- **Category IV.** Specific types of missions (generally landers and other surface probes) to a target body of biological interest where contamination carried by spacecraft could alter the environment and jeopardize future exploration. Planetary protection

requires high cleanliness and contamination control, bioburden⁴³ monitoring and bioburden reduction or sterilisation. Examples: landers, rovers or other surface probes on Mars and Europa.

- **Category V.** All Earth-return missions. This category aims at protecting the Earth's biosphere from contamination by alien biological material. Two sub-categories are defined:
 - **Unrestricted.** Return from Solar System bodies that scientific consensus judges incapable of hosting any life forms. Only the requirements for the out-bound mission apply as per categories above.
 - **Restricted.** Return from Solar System bodies that could potentially host life. Strict biological containment of contaminated spacecraft hardware or sample material⁴⁴ must be guaranteed during the return and after landing. Timely analysis must be performed in a high-containment facility and the samples cannot be released unless no sign of alien replicating entities is found by the most sensitive techniques or it is fully removed by effective sterilisation.

According to this definition, the ExoMars Rover mission is classified as Category IV and thus is subject to strict cleanliness and contamination control, including biological contamination. The response to these requirements is to strive to build the hardware in a clean and controlled environment, although that might not be always possible, especially for the low-level components, like off-the-shelf products or parts fabricated on metal work machinery. For these cases, effective sterilisation methods have been identified, such as powerful surface disinfectants or Dry Heat Microbial Reduction (DHMR), which is a bioburden reduction method based on temperature. It typically involves heating the hardware to 125°C in controlled atmosphere for several hours and has been adopted as the standard sterilisation process for the ExoMars Rover for the fact that it can be applied to complex assemblies without stripping them down.

However, there are some elements that would be permanently damaged by DHMR temperatures, for example, the battery. For these items the only option is to build them in exceptionally clean conditions and employ thorough manual cleaning methods. There are also some components for which it is simply impossible to meet all the cleanliness and contamination requirements, for example, fluid-lubricated transmissions: these can be subject to DHMR to eradicate any terrestrial life, but the lubricant will remain an organic compound and, if transferred to scientific instruments, it could generate false positives in the detection of organic chemistry. For cases such as these, the cleanliness requirements can be relaxed as long as the cavity is sealed. If the cavity needs to be vented to release internal pressure during launch from Earth, this shall be done through High-Efficiency Particulate Air (HEPA) filters to prevent the egress of any contaminants.

The final integration of the rover is such a complex, large-scale operation that even DHMR becomes impractical at that stage. To address this challenge, a new, specially-designed building was erected: the Airbus Bio-Clean Facility. The building includes a high cleanliness environment for the integration of the rover, which can be seen in Figure 4-23. This main

⁴³ Bioburden indicates the quantity of microorganisms found on a particular surface or material.

⁴⁴ The same containment measures apply to human beings in the case of crewed spaceflight.

room is accessed through a system of airlocks connecting other rooms with increasing levels of cleanliness, all equipped with sterilisation ovens. Only thoroughly sterilised hardware and selected materials are allowed inside. The walls are made of surgical steel and all openings are tightly sealed, so air circulation has to be provided by a dedicated laminar flow system. Human operators can access only following a strict cleaning and preparation process, which includes air showers and two layers of full-body garments. Regular assays on the rover have shown how the facility has been successful in maintaining the cleanliness throughout the assembly and up to rover delivery.



Figure 4-23 – ExoMars Rover under test in the Airbus Bio-Clean Facility (credit: BBC)

5 MARS SAMPLE RETURN

The previous chapters have analysed the scientific interest driving the exploration of the Solar System and of Mars in particular, they have summarised the progress made so far in this field and presented the technologies used to achieve it. Considering the present status of the study of Mars and the means available to advance it, the logical next step, which scientists have been promoting for decades, is deemed to be returning Martian material to our planet for more in-depth analysis. A Mars Sample Return (MSR) plan was developed to pursue this aspiration.

The scheme took multiple forms, involving different organisations through history and culminating in the definition of a complex international campaign in cooperation between NASA and ESA, hailed as one of the most ambitious undertakings in the history of robotic spaceflight. This chapter presents the evolution of the campaign before and during the timeline of this PhD work. MSR is the setting in which this project takes place: it shapes and is shaped by the unfolding of the work discussed in this document.

Nevertheless, by the time this work will be published, MSR will have changed. The Sample Fetch Rover (SFR), main subject of this study, will no longer be part of the campaign. Affected by technical challenges in securing a lander system and hit by a deteriorating geopolitical situation that forced space agencies to rethink their planetary exploration programmes, the SFR project was cancelled in the summer of 2022. Towards the conclusion of this PhD project, the lander meant to deliver SFR to Mars was already facing serious mass issues, driving the decision to use an additional lander for the rover.

While ESA and NASA were looking for a way to develop this new lander in time for launch, the Russian invasion of Ukraine left another mission without a lander: the ExoMars rover, due to launch in September 2022. An assessment on the health of the Perseverance rover, already collecting samples on Mars, led to the forecast that it would likely be still operational at the time of MSR and so it could be used to deliver the samples in place of SFR. The removal of SFR allowed the agencies to concentrate their efforts in salvaging the ExoMars mission.

The research presented in these pages all happened before these events and depicts the Mars Sample Return architecture as defined in 2019, for which SFR was developed. This work is described in the following chapters.

5.1 History of Mars Sample Return

Over the last few decades, vehicles for the exploration of Mars – and of space in general – have seen considerable advancements in their payload capacity, carrying increasingly large and sophisticated instrumentation on their journeys. One notable example is the ExoMars Rover with more than half of its body filled with instruments, in addition to those mounted externally, as described in Section 4.4.8. However, even the nearly 50 kg ExoMars science payload is dwarfed by common geochemical or biological analysis laboratories on Earth, which can count on entire buildings filled with instrumentation, preparation facilities and skilled personnel to treat the samples and gather observations.

For how far miniaturisation has gone, the tools that can fit on a mass-constrained spacecraft are no match for even the average commercial laboratory. Planetary scientists have always had to work with these limitations, so returning samples to Earth naturally becomes desirable for any interesting location that is visited by spacecraft. Furthermore, returned material will remain available for future research, allowing to carry out experiments yet to be imagined, without needing a dedicated mission.

During the Apollo programme, astronauts returned approximately 382 kg of lunar material to be studied in Earth laboratories. Despite not showing any biological content, its analysis proved vitally important in understanding the history of the Earth – Moon system and the rocky planets in general. Those samples, some of which are still sealed, are yielding discoveries and technological advancement to this day. On Mars, the only other planetary body extensively visited by surface probes, the biological potential greatly increases the significance of such undertaking. Truth is, the instruments in-situ have provided so far only a crude grasp of the planet’s geochemical environment and history. Exobiology experiments have sometimes returned inconclusive results, only fuelling a desire for more. It quickly became clear that, after making observations in the field, the time had come to send some samples to the lab: the advocates of Mars exploration began urging to do just that.

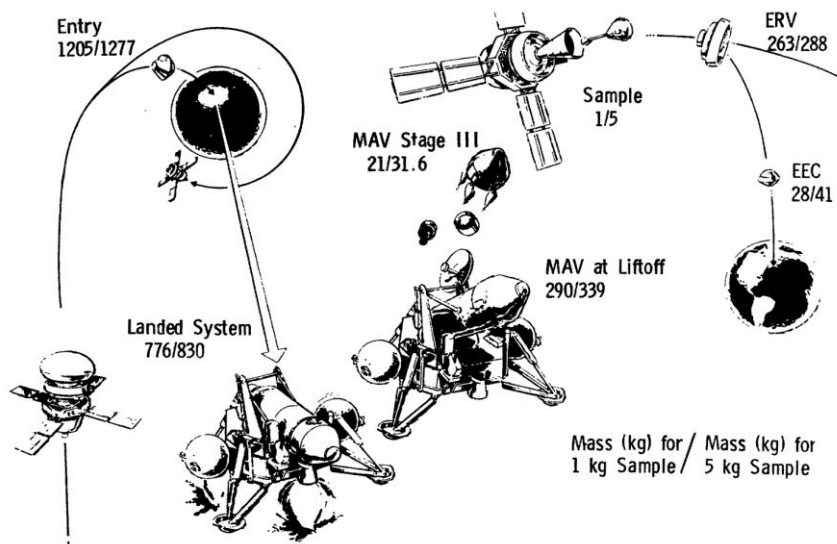


Figure 5-1 – Mission architecture for a 1984 Viking-based Mars Sample Return (credit: Martin Marietta)

The scientific community has identified a sample return mission from Mars as a top priority since the Viking landers reported the first observations from the surface of Mars in 1976. As a matter of fact, even before the Vikings had launched, a study [49] had already been

prepared on an adaptation of that same lander design to collect and launch surface samples into Mars orbit. The mission was assessed for a launch in 1984 and its architecture is shown in Figure 5-1, with mass figures for the various systems for a 1 kg sample payload and a 5 kg sample payload. In the illustration, MAV indicates the Mars Ascent Vehicle, ERV the Earth Return Vehicle and EEC the Earth Entry Capsule.

A number of iterations of this architecture were studied in the years following the Viking landings, but they all failed to proceed past the initial concept phase. Any sample return mission required very challenging technology developments, such as autonomous launch and orbital rendezvous at Mars. These risky development proposals did not gain much traction on space agencies that were experiencing a general decline in their budgets and ambitions at that time (see Section 3.1). The situation remained largely unchanged until the late '90s, when the first rovers were sent to Mars and demonstrated how mobility could augment the scientific return of a mission to the surface. It was natural to apply the same considerations to sample return, making rover-based sample collection a highly desirable approach and strengthening the support to such missions.

If the samples are carefully selected over enough time and a sufficiently large area, then they offer credible prospects of answering the open questions on past and present biology on Mars. Following this reasoning, new Mars Sample Return architectures were outlined in the early 2000s, involving one or more sample-caching rovers. These proposals varied in complexity, some involving up to 15 spacecraft [50], others aiming to minimise the number of flight elements to the point of merging Mars Ascent Vehicle (MAV) and the sample caching rover into one spacecraft. This latter architecture, named “Mobile MAV” is a particularly unique concept, where a rover would carry the rocket on its back during its surface mission and launch it once loaded with samples [51]. This design is shown in Figure 5-2 and is based on a large, MSL-class vehicle, but powered by solar arrays (refer to Section 4.3.3).

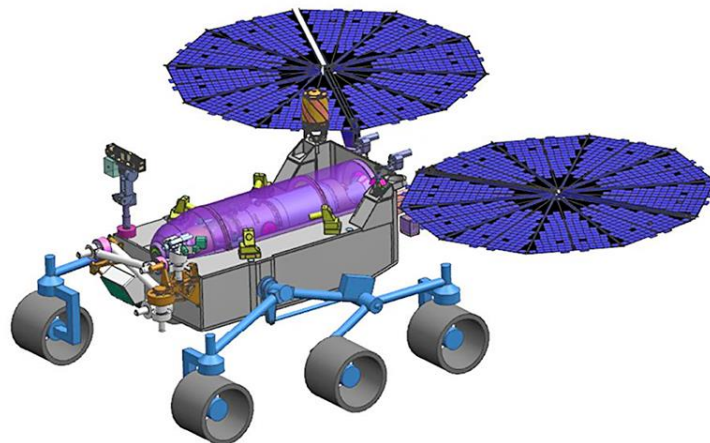


Figure 5-2 – Mobile MAV concept for Mars Sample Return (credit: NASA / JPL-Caltech)

Despite the variety of concepts, none of these proposals proceeded very far through the design phase, all stopped in their tracks for broadly similar reasons: the large budget requirements and the decades-long timelines, both not particularly appealing to space agencies and the associated governmental bodies. By 2009, a new idea had surfaced, which would become crucial to shaping the path of Mars exploration for the decades to come: if no single space agency could bear the risks of a Mars Sample Return campaign, then maybe a cooperation of multiple agencies could. NASA and ESA, two of the largest space agencies at the time,

teamed up to confront this challenge together and, for the first time, elements of Mars Sample Return moved into the preliminary design phase [52].

A lander with two rovers was envisaged to be launched in 2018, which would collect samples and cache them on the surface. A second lander, launched in 2024, would carry a small “fetch rover” to recover the samples and the rocket that would launch them into orbit, where an interplanetary vehicle, launched in 2022, would be waiting to intercept them. Remarkably, one of the two rovers on the “Mars2018” mission was the ESA ExoMars Rover, initially developed specifically for this campaign. The ExoMars Rover would perform scientific observations to support sample collection and guarantee a more immediate scientific return, while the NASA Mars Astrobiology Explorer-Cacher (MAX-C) Rover would prepare the cache of samples to be sent to Earth. The launch configuration of the Mars2018 mission is depicted in Figure 5-3, which shows, starting from the top, the cruise stage, the back shell, the Sky Crane descent stage, the landing pallet with the two rovers (ExoMars on the left and MAX-C on the right) and the heatshield.

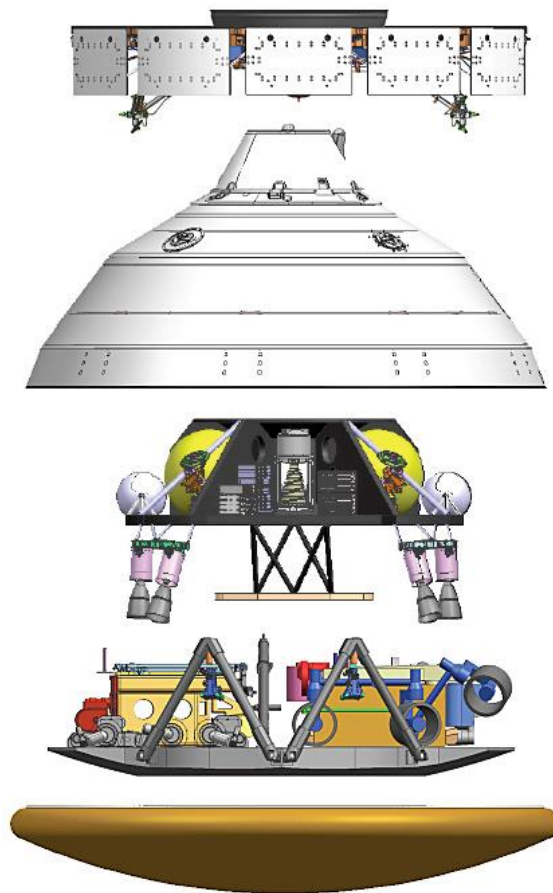


Figure 5-3 – Exploded view of the joint NASA / ESA Mars2018 mission (credit: NASA)

Unfortunately, due to a budgeting crisis, NASA withdraw from this collaboration in 2012, leaving the ExoMars Rover without a lander, for which ESA had to seek other, riskier partnerships (see Section 4.4). Despite being top scientific priority for almost half a century, Mars Sample Return was, once again, back to the drawing board because of government funding. Following this setback, one last attempt was made to revive the sample return effort, this time with one tweak that would prove decisive for the future of the campaign: instead of defining an entire architecture optimised for sample return, the sample collecting

system would be “squeezed in” another mission with its own scientific objectives. That mission would be NASA’s Mars2020, established briefly after the cancellation of the ExoMars / MAX-C joint mission in response to the uproar from the scientific community.

The Mars2020 rover, later named Perseverance, was fitted with an Adaptive Caching Assembly (ACA), shown in Figure 5-4. The system accommodates 43 tubes in total, 5 of which are witness blanks and the other 38 are to be filled with core samples for a potential Earth return. Policymakers who cut the budgets for previous sample return efforts would be hardly aware of the presence of this payload on the rover and, even so, the return mission would be sufficiently hypothetical and far in the future not to be perceived as an immediate commitment. However, scientists knew that, once the sample tubes would be on Mars, they would provide a far stronger argument for a return mission.

The sample tubes are indeed now on Mars, and the argument worked exactly as intended: NASA and ESA have been re-establishing an extensive collaboration to return those tubes to Earth. This multi-agency endeavour would be largely based on the previous NASA / ESA Mars Sample Return concept, with a second lander carrying a fetch rover and a rocket, and an interplanetary vehicle awaiting in orbit. Not having been planned as a whole sample return architecture since the beginning, all these systems now have to be designed to chase the elements that are already off-planet, i.e., Perseverance and its tubes. As eloquently put by R. G. Andrews on Scientific American [53], “*the “sample return” train has left the station with the tracks ahead of it still being built.*”

Such undertaking was captured in a joint statement of intent between NASA and ESA in April 2018 and is often referred to as “International Mars Sample Return”. This campaign is the setting of this PhD study and its elements are further discussed in the following paragraphs, including the one that lies at the centre of this work: the ESA Sample Fetch Rover (SFR).

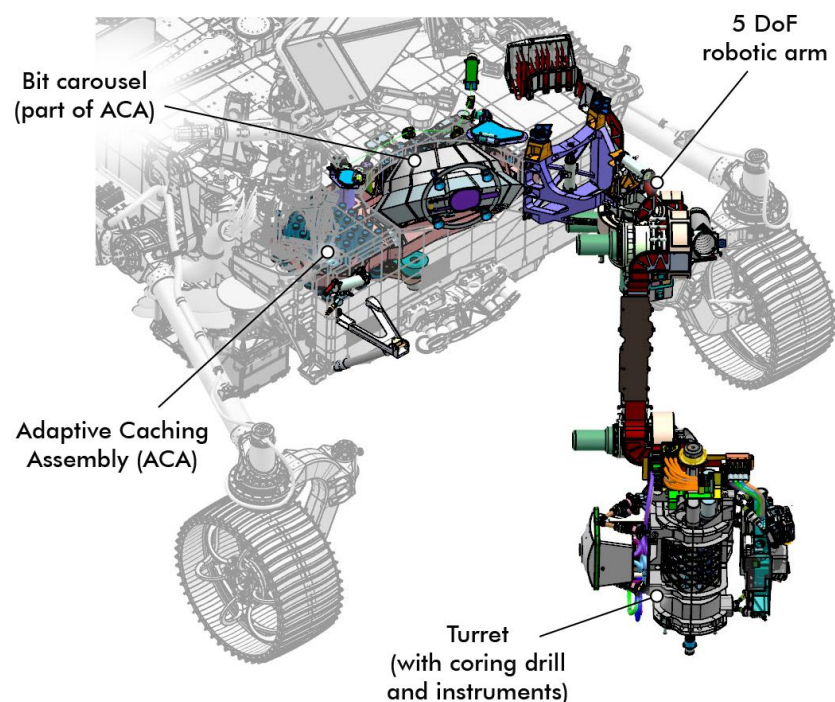


Figure 5-4 – Sample collecting and handling systems on board Perseverance (credit: NASA / JPL-Caltech)

5.2 International MSR architecture

The following paragraphs describe the architecture of the International Mars Sample Return Campaign and the roles of its key elements, including the Sample Fetch Rover. This description follows to the baseline architecture defined in 2019, which corresponds to the start of the SFR Project and this PhD work. An overview of all the major elements involved in this plan is provided in Table 5-1, where they are listed in the approximate order in which they are expected to perform their primary function in MSR [54].

MSR Element	Acronym	Provider	Function
Perseverance	-	NASA	Acquire, seal and cache samples
Returnable Sample Tube Assembly	RSTA	NASA	Contain and preserve the sample material
Sample Retrieval Lander	SRL	NASA	Carry SFR and MAV to the surface, support MAV launch
Sample Fetch Rover	SFR	ESA	Retrieve RSTAs from the surface and return to SRL
Sample Transfer Arm	STA	ESA	Transfer RSTAs from SFR to MAV and prepare it for launch
Mars Ascent Vehicle	MAV	NASA	Launch and deliver the RSTAs into Mars orbit
Orbiting Sample	OS	NASA	Contain the RSTAs during orbital manoeuvres and return to Earth
Earth Return Orbiter	ERO	ESA	Capture the OS and return to Earth
Earth Entry Vehicle	EEV	NASA	Transport the samples to the Earth surface
Sample Receiving Facility	SRF	NASA	Contain, analyse and preserve samples

Table 5-1 – Summary of key MSR elements and their functions

The sequence of events in which these elements play their part unfolds over more than a decade and can be divided in three main phases:

1. A sample caching mission, which collects and seals the samples, then deposits them in a selected location
2. A sample retrieval mission, which recovers the samples and launches them into Mars orbit
3. A sample return mission, which transfers the samples back to Earth and delivers them to the surface

A visual representation of this plan is provided in Figure 5-5, where the Earth is on the bottom, Mars is at the top and time goes from left to right. In the illustration “Mars 2020” indicates the Perseverance mission. Each phase is discussed in further detail in the following paragraphs.

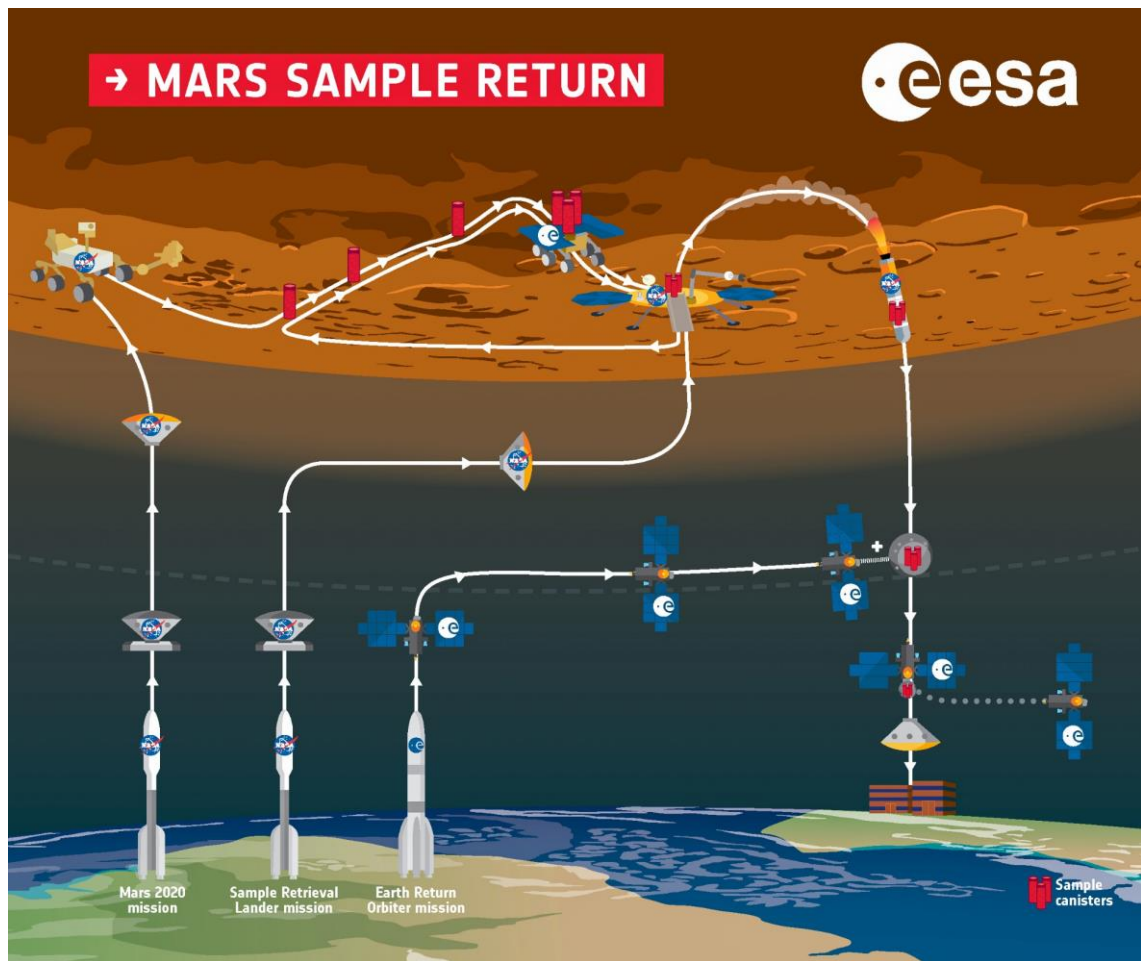


Figure 5-5 – Mars Sample Return campaign overview (credit: ESA / K. Oldenburg)

5.2.1 Sample caching

In the International MSR campaign, the sample caching operations are carried out by NASA's Perseverance rover and, at the time of writing, they are already under way. The rover is exploring the region of Jezero Crater and collecting samples from sites of high scientific interest. These activities overlap with the in-situ science mission and are supported and augmented by the other instruments on board. Jezero Crater was chosen as a landing site for the likely presence of water in the past and this expectation has been now confirmed by Perseverance: Jezero is indeed an ancient lake, fed by an intricate river delta, and the rover is currently standing on its floor. This contributes to the relevance of the samples being collected and the potential for discoveries if analysed by powerful instruments on Earth.

The system that collects and stores the samples is shown in Figure 5-4. Inside the rover is located a magazine of tubes (more precisely RSTAs, Returnable Sample Tube Assemblies), from which they can be selected and transferred to the bit carousel [55]. The chosen tube is inserted inside the coring bit so that it forms integral part of the drilling tool. The sample material is pushed directly into the tube as it is cut, ensuring that the sample is subject to minimal handling and the potential for contamination or alteration is reduced. The bit carousel is the main interface between the Adaptive Caching Assembly and the exterior of the rover. The robotic arm can access the coring bit and the tube from the carousel opening and mount them into the percussion drill on its end effector. The sampling operation is then performed on the desired target to a depth of approximately 70 mm, collecting a core 13

mm in diameter. A regolith bit is also available for the drill to collect softer material, which is scooped up rather than cut. Once filled, each tube is fitted with a seal that is pressed into position. The process produces permanent deformation of the tube shaft to ensure tight sealing of the material inside. Figure 5-6 shows a section of the tube inside the coring bit, a built flight tube and an X-ray of a filled and sealed tube.

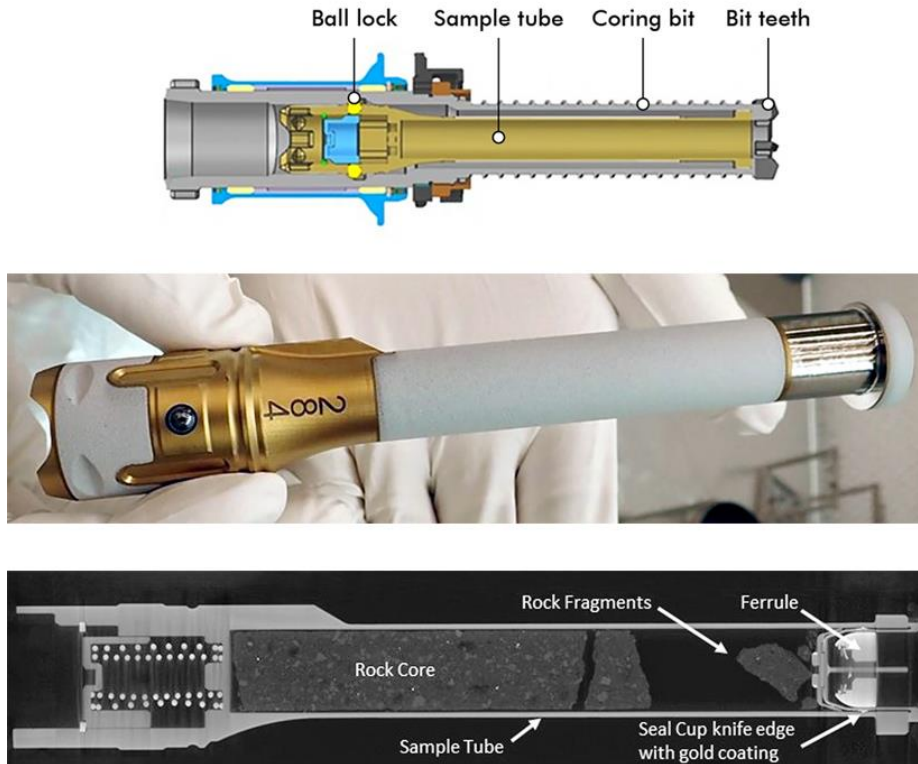


Figure 5-6 – Cross section of an RSTA mounted in the coring bit (top), one of the flight RSTAs before integration into Perseverance (middle) and an X-ray of a sealed RSTA after a drilling test (bottom) (credit: NASA / JPL-Caltech)

When commanded to do so, Perseverance is able to drop each tube individually through an opening in its underbelly. The decision on when and how to do so will shape the entire Mars Sample Return campaign. One key aspect of this operation is that Perseverance can drop the tubes only if it is still functioning and able to drive. The baseline approach for MSR is to collect two copies for the initial samples, probably the first ten, and deposit the first set onto the surface early in the mission, to act as a backup in case the rover encountered sudden difficulties. The tubes will be scattered over a small area (tens of meters across or less), characterised by benign terrain⁴⁵ that would ease future identification and retrieval. Such arrangement is referred to as “sample tube depot”.

Perseverance will continue to gather samples for a few years and it is expected to travel significant distance as it does so. There is currently a strong interest in attempting to climb the nearly 700 metres high crater rim to explore the ancient river delta and the surrounding

⁴⁵ Benign terrain for tube caching is considered to be compact or rocky, without loose sand or large obstacles, but also not completely flat or featureless, since the topology of the terrain can provide visual hints for the localisation of the tubes.

upland [58]. This is a long and challenging path, which would push the rover close to the distance record of 45 km held by Opportunity (See Section 3.1.2). Therefore, it is reasonable to prepare the first contingency depot before tackling this climb. What happens after that will depend on how the scientific mission unfolds, the difficulty of the terrain and Perseverance's health. It is envisaged that a second depot will be created with all the new samples and the copies of the first ones. This might be laid out in a single instance or gradually built by the rover coming back multiple times with additional samples. It is also possible to keep tubes on board Perseverance for direct delivery to the Sample Retrieval Lander, although it relies on the rover being still healthy and able to traverse to the lander in the late 2020s – early 2030s.

The subsequent steps in Mars Sample Return will have to remain compatible with all these scenarios and additional contingency cases, so there is not a single mission profile but rather a combination of them, depending on how Perseverance's mission will unfold. This complexity is captured well by Figure 5-7, where the "green zones" mark areas of benign terrain, candidate for potential tube depots or landing sites, and the network of paths between them represents the routes that Perseverance could take (in white) and that SFR has to be compatible with (in green) [56].

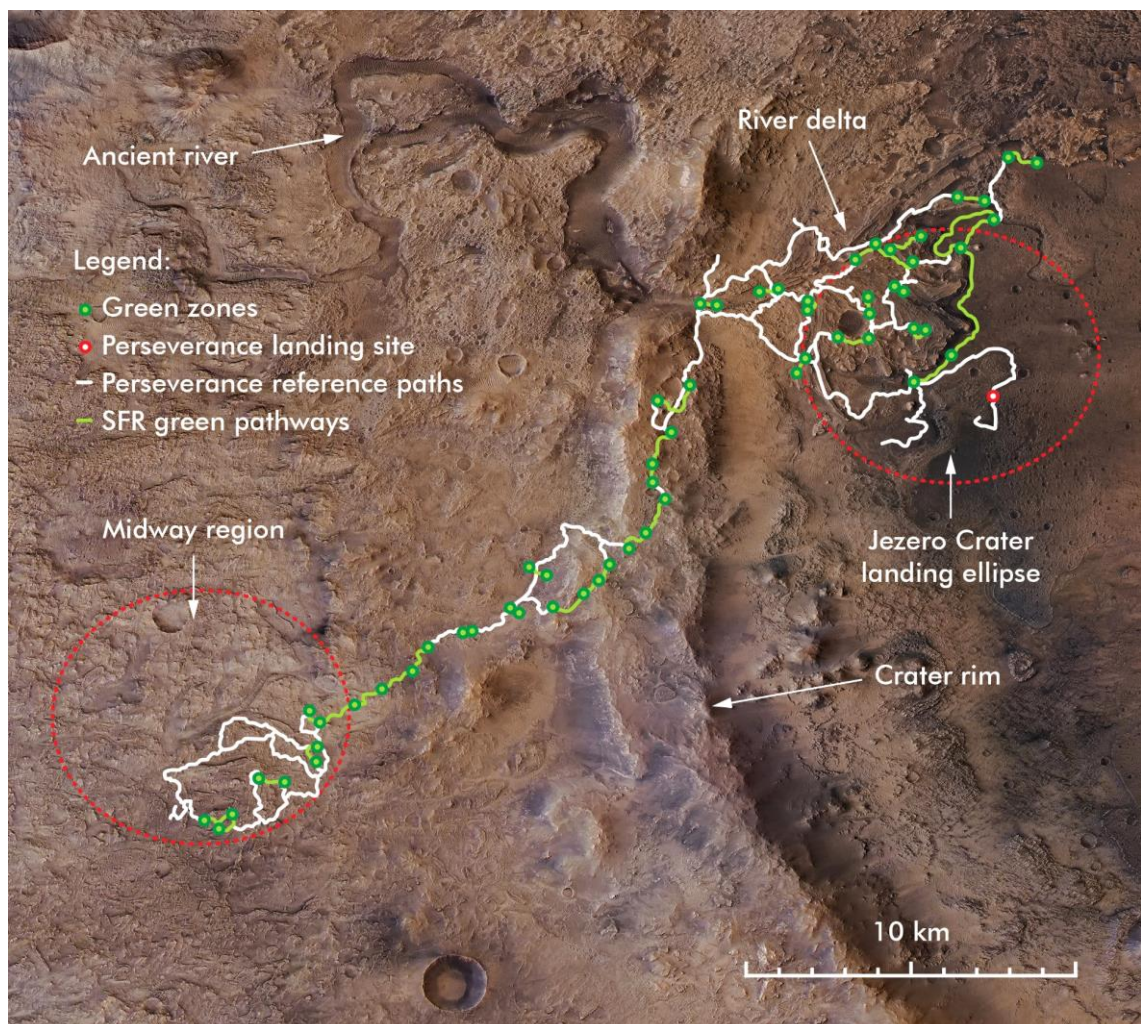


Figure 5-7 – Satellite view of the western rim of Jezero Crater with the potential routes for Perseverance and SFR (credit: NASA / JPL-Caltech)

As a last step in the sample caching phase, Perseverance will document the depot location as extensively as possible, acquiring detailed images of the tubes on the surface, the surrounding terrain and even Digital Elevation Models (DEM) of the area. This will aid future navigation in the depot and identification of the tubes. Perseverance will also scout target landing sites for the sample retrieval phase, looking for areas of flat and compact terrain as close as possible to the depot to minimise the distance to reach the samples. Naturally, it is undesirable to land directly on the depot as the gas outflow from the descent engines could scatter the tubes and render them impossible to find. These operations will be discussed further in the following section.

5.2.2 Sample retrieval

The sample retrieval phase is the second step in Mars Sample Return and it is expected to happen after a considerable amount of time from the caching phase. The main temporal link between the two missions is the fact that the tubes cannot be left on the surface indefinitely, as they would slowly get covered by dust and become increasingly difficult to identify and handle. The current understanding of the typical dust deposition rate, including dust storms, suggests that an exposure of less than 10 terrestrial years should bear relatively low risk in this regard. The objective of the retrieval mission is to recover a number of these tubes and deliver them to Mars orbit. The current target is to launch 30 tubes, corresponding to almost 0.5 kg of Martian material. This implies that only a subset of the cached tubes might be selected for return. On the other hand, it is also possible that less than 30 tubes might be actually available or reachable on the surface, especially in contingency situations.

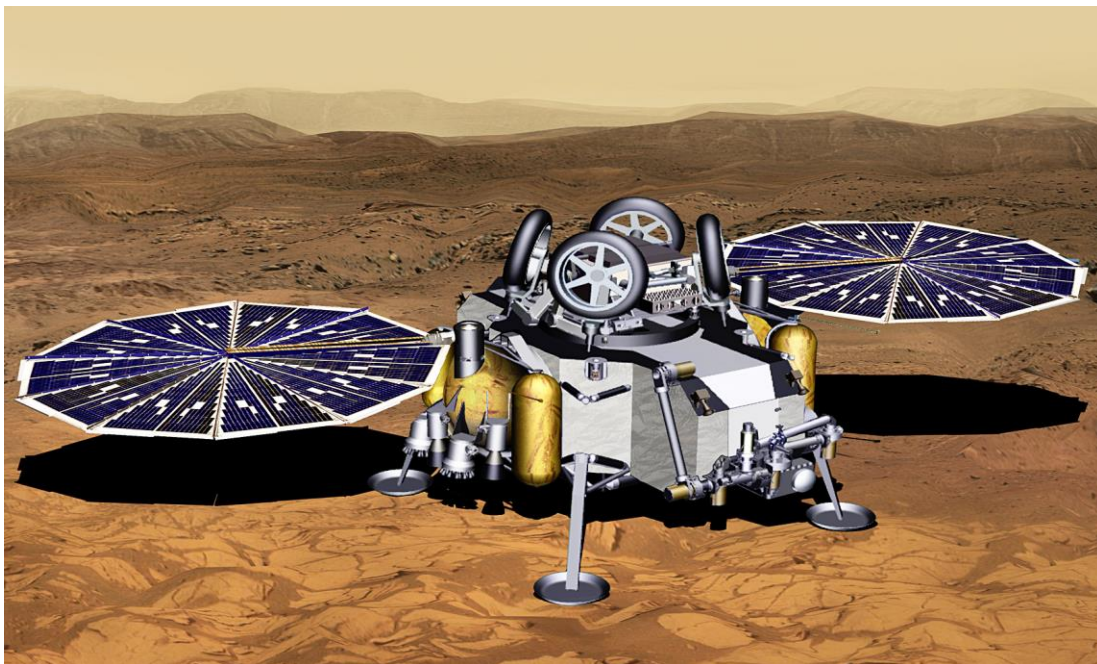


Figure 5-8 – Artist's impression of the Sample Retrieval Lander on Mars (credit: NASA / JPL-Caltech)

To achieve its objective, the sample retrieval mission would deliver a NASA lander to the surface: the Sample Retrieval Lander (SRL). SRL would carry the ESA Sample Fetch Rover (SFR) and the NASA Mars Ascent Vehicle (MAV). In the reference architecture for this study, a single SRL is considered, although there have been parallel studies for a dual lander approach, with SRL-1 carrying the MAV and SRL-2 carrying the SFR [57]. The lander is also

equipped with an ESA-provided Sample Transfer Arm (STA) to load the MAV and prepare it for launch. Figure 5-8 illustrates the reference concept for this spacecraft, with SFR stowed on top of the lander, the MAV (not visible) enclosed within its central body and the STA folded on the right-hand side in this view.

The high-level concept of operations at Mars follows the sequence below:

1. Entry, Descent and Landing
2. Critical SRL post-landing activities (solar arrays deployment, checkouts...)
3. SFR deployment and egress to the surface
4. SFR commissioning and checkout
5. Outbound traverse to the depot
6. Locate, acquire and stow the selected sample tubes
7. Return traverse to SRL
8. Transfer the tubes to the MAV with STA and prepare for launch
9. MAV launch
10. Release of the Orbiting Sample (OS) into Mars orbit

In Section 5.2.1 it was noted how there are still several unknowns around the unfolding of the caching mission and the resulting arrangement of tubes on the surface. The role of the Sample Fetch Rover is to accommodate this variability and ensure that SRL receives the desired set of samples regardless of the situation on the surface. Time is also crucial in this phase, since the MAV must launch before the Earth departure window, i.e. the moment when the configuration of the planets allows the orbiter to leave Mars and reach Earth with the propellant available on board. This time pressure reflects on all operations on the surface and especially those of the rover, which account for the greatest duration in the sequence. One key advantage with regards to this issue is the fact that Perseverance will have been in the same area before and will have recorded large amounts of data that can be used to plan the SFR mission, as already mentioned in Section 5.2.1.

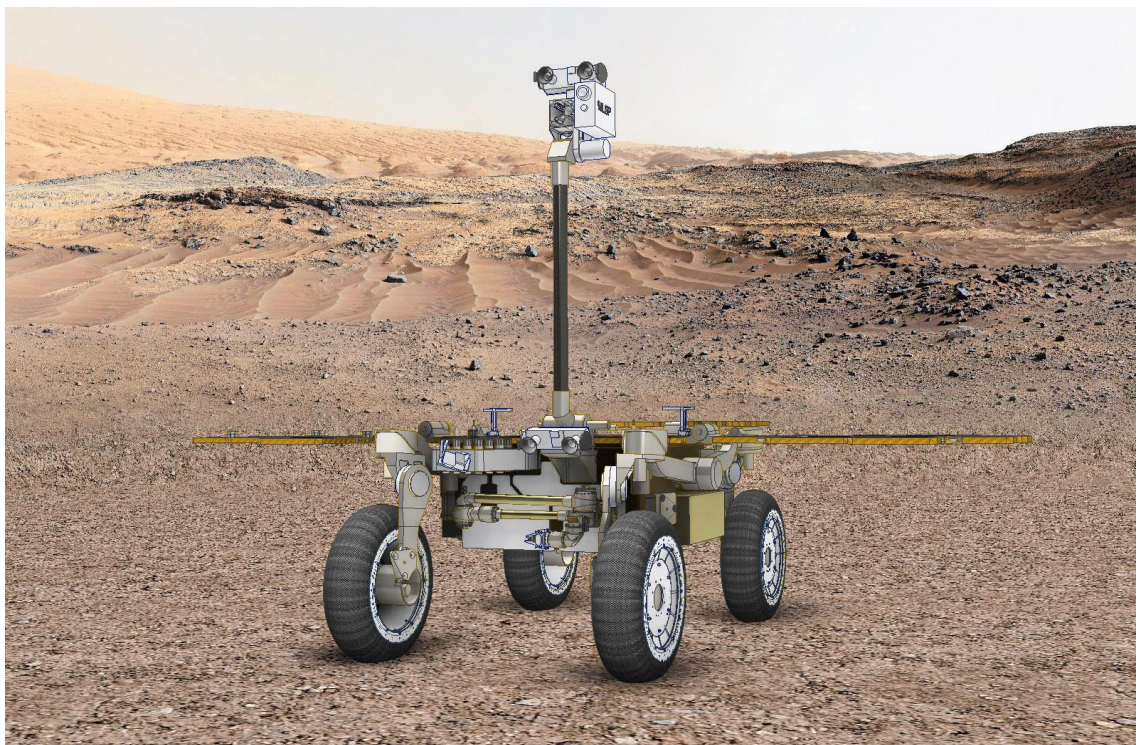


Figure 5-9 – Artist's impression of the Sample Fetch Rover on Mars

The primary objectives of SFR are to identify, retrieve and deliver the tubes on time to SRL, hence the rover can be seen purely as a transportation system, optimised for mobility performance, with no scientific instruments or experiments on board. The design response to this mission profile is the central subject of this research and the outcome is shown in Figure 5-9. The process that led to this design is discussed in detail in the following chapters.

At the end of its return journey, SFR would park in proximity of SRL, making the tubes available for transfer. The Sample Transfer Arm would then load them into the Orbiting Sample (OS), a sealed spherical structure, roughly the size of a basketball, which would contain all the tubes from that moment onwards, until recovered on Earth. The fully loaded OS is expected to have a mass of approximately 16 kg and is secured on top of the MAV in preparation for launch.

The MAV is a two-stage, solid-fuelled rocket provided by NASA [59]. It is roughly 3 metres long, with a mass of approximately 300 kg, and the fully assembled system can be seen in Figure 5-10. The MAV is accommodated inside a thermally-insulated enclosure at the centre of the SRL structure, which opens just before launch. The current concept for lift-off is to eject the rocket with a sprung mechanism and ignite it in mid-air to avoid the complexity of guiding mechanisms on the lander⁴⁶. Due to a combination of small payload, low gravity and thin atmosphere, the ascent will be relatively quick: the first stage would burn for 70 seconds, followed by a brief coast phase, and then the second stage would burn for another 27 seconds, after which the OS would be released in an orbit approximately 380 km in altitude. The choice of the orbit is an ongoing trade between the performance of the MAV and that of the return orbiter, which would struggle to depart from Mars if it ventured too deep into its gravity well to reach the OS.

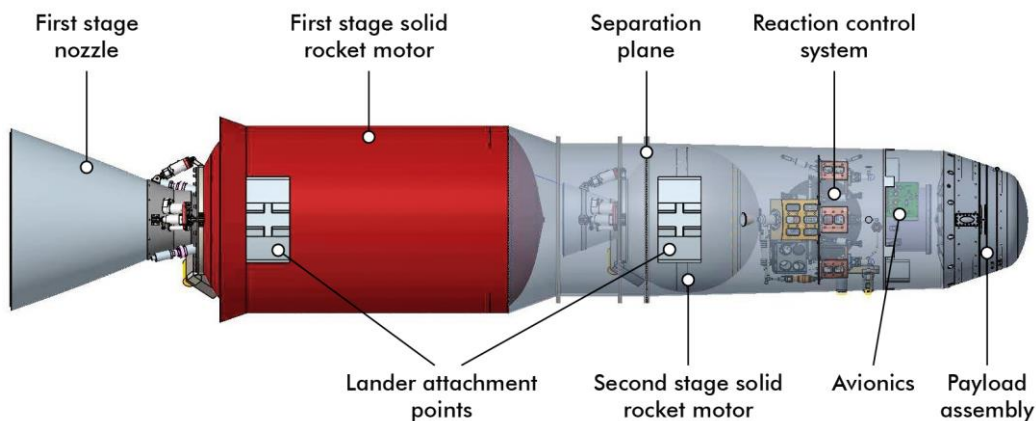


Figure 5-10 – Semi-transparent view of the MAV with key components (credit: NASA / MSFC)

5.2.3 Sample return

Once the samples have been delivered to Mars orbit inside the OS, it is up to the ESA Earth Return Orbiter (ERO) to capture them and bring them back to Earth. Due to mass con-

⁴⁶ This solution is also called “soft launch” or “cold launch” and is widely used in military applications for medium-sized missiles.

straints, the OS is an entirely passive system, with no manoeuvring capability, no radio beacons and no batteries, freely tumbling in orbit around Mars. The last estimated trajectory of the payload will be transmitted by the MAV after separation. ERO would have to rely on this telemetry to approach the OS and then attempt visual localisation once in range. In practical terms, that means shining a light and scanning the starry sky for the reflection of the basketball-sized object. At the end of the approach and rendezvous procedure, a NASA-provided payload on the orbiter would receive and capture the sphere.

All these complex operations are made even more challenging by the size of ERO, which, with solar arrays more than 40 metres in wingspan, would be by far the largest object ever flown to Mars (see Figure 5-11). The size of the solar arrays is driven by the power needed by its electrical propulsion system. ERO uses, in fact, a hybrid, multi-stage approach for its propulsion. The long interplanetary transfers rely on electric propulsion, which has high fuel-efficiency, allowing to move such a large payload, but provides low thrust, requiring very long “burn” times⁴⁷. The orbital insertion around Mars uses a chemical propulsion stage, which has lower efficiency but high thrust, making it possible to rapidly enter orbit before overshooting the planet. Once used, the orbit insertion module becomes undesirable dead mass for the return journey and so is jettisoned at Mars before the return trip⁴⁸.



Figure 5-11 – ERO over a regular-sized basketball field (left) and broken down into main elements (right) (credit: Airbus)

Once in proximity of Earth, ERO will guide the Earth Entry Vehicle (EEV), now containing the OS with the samples, on a precise trajectory to perform a purely ballistic descent towards the Utah Desert. Following release of the EEV, the orbiter would execute one last burn to avoid the planet and enter a solar orbit where it will remain indefinitely. The EEV will perform the final daring manoeuvres in the MSR campaign: entry into the Earth’s atmosphere at 12 km/s (43 200 km/h), aerodynamic deceleration and hard-landing onto the surface [60].

⁴⁷ ERO’s electric ion thrusters are actually active for almost the entire interplanetary flight, slowly altering the spacecraft course and velocity.

⁴⁸ The decommissioning of the orbit insertion module consists in passivating (i.e., depressurising) the propulsion system and then leaving it in a high orbit to minimise the risk of debris generation and uncontrolled re-entry.

The craft has, in fact, no propulsive capability and no parachute to maximise its simplicity and robustness (see Section 5.2.4) and is therefore designed to impact the ground at terminal velocity⁴⁹, acting essentially as an engineered meteorite. The OS and the tubes inside will be protected by a carbon-carbon composite structure filled with crushable material. The landed EEV would then be recovered and transported to the Sample Receiving Facility (SRF) where it will be gradually opened up and its wealth of science released. Figure 5-12 provides a cross-section of an EEV early concept and a still frame from impact landing test with an EEV prototype.

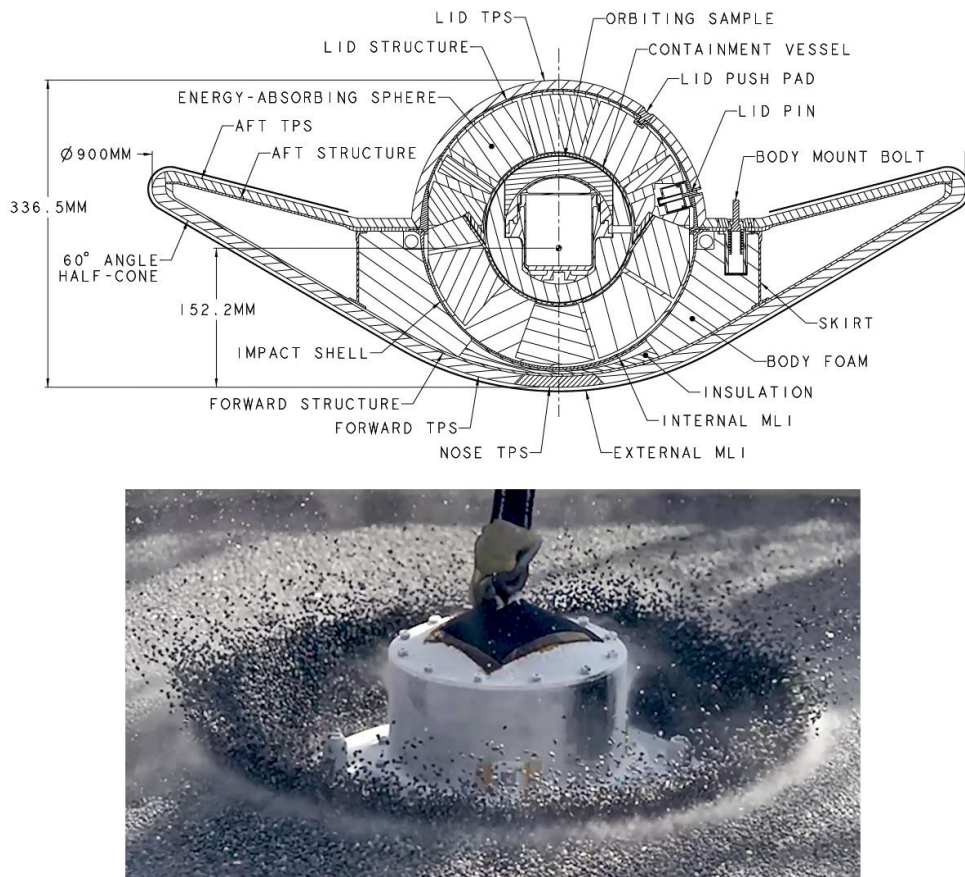


Figure 5-12 – EEV cross section (top) and impact testing (bottom) (credit: NASA / LRC)

5.2.4 Planetary protection

As described in Section 4.4.12, planetary protection rules apply to interplanetary missions according to five risk categories. Following the COSPAR classification, Mars Sample Return is identified as category V restricted, meaning that the most stringent requirements for contamination protection and bioburden control apply to the spacecraft involved in the sequence. The design and operation of these spacecraft responds especially to three primary objectives associated with planetary protection [52]:

1. **Protecting Mars from Terrestrial contamination.** Since there is a small, but non-null possibility that Mars might be currently hosting some form of biological activity,

⁴⁹ The terminal velocity is the steady-state speed of a free-falling body once the resistance of the medium through which it is falling equals its weight. For the current EEV design, it is in the order of 150 km/h.

it is mandatory to prevent contamination to its potential biosphere by terrestrial organisms. This translates into requirements on bioburden and contamination consistent with other missions to the surface, like those described in Section 4.4.12.

2. **Protecting the samples from Terrestrial contamination.** This is primarily to avoid false positives in case Terrestrial life is transferred to the sample material and is mistaken for indigenous life or pollutes existing chemistry, compromising science results. The associated requirements are similar to those in point 1 but generally have smaller contamination allowances, necessitating special cleaning and sterilisation of any hardware contacting sample material and some isolation from the rest of the spacecraft.
3. **Protecting Earth from Martian contamination.** This is one of the most demanding and certainly unique aspects of a sample return mission. Differently from Mars, Earth is known to host biological activity and its biosphere is isolated from any other life by the vacuum of deep space. Any returning interplanetary mission must first and foremost guarantee this isolation. The planetary protection requirements stemming from this mandate secure containment of the returned material and so-called “break-the-chain” events to interrupt any possible path of contamination. These are further elaborated below.

With particular reference to point 3 above, the sequence of events being considered has an extremely low combined probability: life being currently present on Mars, this life being captured inside the samples collected and it being able to survive and reproduce in the Earth’s environment. On the other hand, the potential consequences of a leakage could be so severe for all life on Earth that extreme measures must be taken to further reduce this already small probability. The mitigation approach is primarily to ensure that all Martian material remains contained and to interrupt the chain of contamination for any elements that might have come into contact with such material.

The tubes are hermetically sealed by Perseverance, but they are then dropped on the ground, so their exterior surfaces have to be treated as contaminated. Their sealing is more aimed at preserving the samples rather than avoiding contamination to Earth. The OS is loaded with the tubes and then sealed, providing a first step in breaking the chain of contamination. However, the OS is exposed to Martian atmosphere and dust during certain operations and its cleanliness cannot be fully guaranteed. The OS is therefore placed inside another sealed “biocontainer” once captured by the orbiter. The mechanisms in the orbiter that have come into contact with the bare OS are then jettisoned before returning to Earth. The orbiter is allowed to target Earth only after confirmation that sample containment has been established successfully.

The EEV is kept isolated behind a biological barrier until it receives the encapsulated OS and is then released for entry. The orbiter performs one last divert manoeuvre to prevent contact with Earth’s atmosphere in the unlikely event that it has become contaminated with Martian material. The EEV is designed with an ultra-safe entry profile to avoid any risk of breakup or loss of sealing. The capsule is entirely passive and has a self-righting shape, which would survive entry even if released backwards. To rule out any possible reliability concerns on parachute opening, the craft is designed to withstand impact with the ground at terminal velocity. The EEV is then secured immediately after landing and transported to the Sample Receiving Facility for quarantine before disassembly. Special protocols are being developed for gradual opening and assessment of the craft and its content.

6 OVERVIEW OF THE SAMPLE FETCH ROVER

The Sample Fetch Rover (SFR, sometimes referred to as Fetch Rover or simply “Fetch”) is the machine developed to acquire the sample tubes left on the surface of Mars by the Perseverance rover and thus enable the retrieval mission in the Mars Sample Return campaign. The robotic spacecraft is being developed for ESA by Airbus UK and this PhD covers the engineering work involved in the definition of its main systems, with a particular focus on mobility, robotics and mechanisms. The SFR mission patch is shown in Figure 6-1, providing an indication of the spacecraft appearance and its purpose. The following pages will attempt to describe the design of this machine and its major components.



Figure 6-1 – Sample Fetch Rover mission patch

The work involved in this study brought the project from initial concept to a preliminary design, going through the stages that in space programme management are called “phase A” and “phase B1”. A spacecraft of this kind is such an intricate machine that even its preliminary design requires volumes an order of magnitude larger than this dissertation to be described. For this reason, only certain areas are presented in detail, acknowledging that even those cannot be explored in full depth within the boundaries of this document. The overall architecture is briefly summarised in this chapter, using the ExoMars Rover design, discussed in Section 4.4, as a term of comparison.

ExoMars is, in fact, the origin of much of the technology on board the Sample Fetch Rover, sometimes reused as entire units “built-to-print”, sometimes just as basic principles adapted to a new design. The exploitation of heritage technology and components is one of the key premises to enable the fast-paced development of such a complex spacecraft in a mission architecture that has very little room for adjustment on the timeline. As will be evident in the next pages, the use of flight-ready items is often weighted against new bespoke developments with the aim to minimise risk, sometimes compromising on performance, but overall protecting the feasibility of the mission.

SFR does not only share some technology with ExoMars, but it is also developed by the same team and it takes advantages of the same facilities, in some cases highly specialised like the bio-clean facility described in Section 4.4.12. Even some contractors and industrial partners are the same ones from the ExoMars industrial setup, drawing on the know-how established by its predecessor. Lastly, some other technologies, not present on ExoMars but necessary for the SFR mission, were identified and adopted early in the development, as it was the case for the superelastic spring tyre design by NASA Glenn Research Centre (GRC), described in Chapter 7.

One aspect that does not have precedents in other projects and is unique to SFR is the fact that the rover is purely a transportation system, carrying no scientific instruments, and its primary mission objective is to collect a payload and deliver it on time. SFR would be the first logistic vehicle on the surface of another planet. From this point of view, the technology developed here can be seen as a precursor for more machines to follow in the future. As humankind’s spaceflight capability matures, robots of this kind are expected to become more common, supporting our exploratory effort across the Solar System. This focus on mobility and timeline performance will shape many aspects of the SFR development, as will be evident in the following pages.

6.1 Early concepts and trade-offs

The initial concept for SFR started off as a rather small vehicle. Like its predecessor studies, the rover was expected to travel not too far from the lander and have to deal with relatively easy terrain. It was a broadly reasonable expectation since the sample tubes would be cached in a region of benign terrain and the lander would aim to touchdown nearby. However, that assumption was gradually eroded as the mission became more defined.

Firstly, the study of the region of Jezero Crater highlighted challenges associated with the complex geography of the area. Unsurprisingly, the most desirable scientific targets are not found in the flat lowlands but in the more geologically and hydrologically complex structures around the crater rim. More areas of interest lie beyond the crater rim itself, reachable only through an arduous climb (see Figure 5-7). In this terrain, finding large, flat areas for

depots and landing sites would not be an easy task. Furthermore, landing ellipses can be quite large, even for the accurate NASA descent system, and potentially deliver the rover a long distance away from its target depot. Finally, even if the landing error could be reduced, the lander would never be able to target the same location as the sample tube depot, due to the risk of dispersing the tubes with the outflow from its powerful braking engines: it must then target the next closest favourable area, which, in this complex terrain, could be kilometres away.

The SFR design changed in response to these evolving traverse requirements as well as developments in its core technologies and improvements in the fidelity of the analysis of its operations on the surface. These had the effect of making the vehicle more capable, more autonomous, more durable but also more massive and power-hungry. Figure 6-2 depicts four snapshots of the rover design during the early development. The first concept (A) had a mass allocation of 120 kg, smaller than NASA MER (see Section 4.3.2), a ground contact footprint of 1 m by 1 m, six rigid wheels 200 mm in diameter and was expected to climb obstacles less than 200 mm in size (assuming that the obstacle meets one wheel at the time, i.e., it is only on one side of the vehicle). The second one (B), has similar mass and footprint, but had switched to four NASA spring tyres, increasing its obstacle climbing ability to approximately 240 mm.

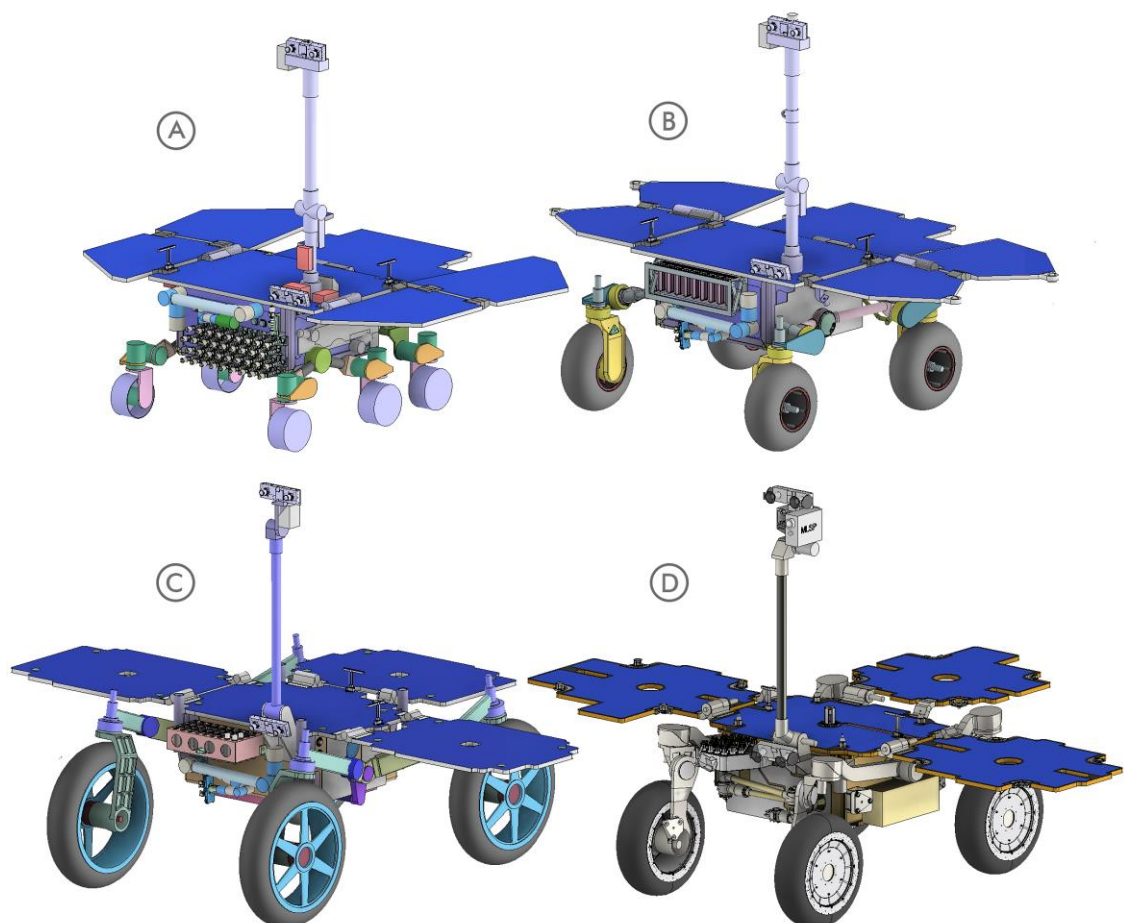


Figure 6-2 – Evolution of the SFR baseline during its early phases, to scale

The third design (C) represents the configuration of peak traverse performance for SFR: the vehicle used four spring tyres of 700 mm in diameter, arranged on a ground contact footprint of 1.6 m in length and 1.2 in width, and was able to negotiate harsh fractured terrain

with wide steps up to 250 mm encountering all wheels⁵⁰ on varying slopes. This locomotion design is further discussed in Section 7.1.4. The associated mission scenario was that SFR could land anywhere up to 15 km away from the sample tube depot and have to traverse the same terrain as Perseverance, but in a much shorter time. At that point, it had already become clear that the design of the rover and the lander were very closely coupled together, and the problem had to be tackled from an overall campaign perspective.

A series of trade-offs were performed, weighting the merits of augmenting the performance of SFR or SRL, and they led to the conclusion that it was more desirable to “transfer” some capability to the lander. In particular, the landing accuracy was greatly improved by increasing the manoeuvrability during the descent phase and implementing a terrain-relative guidance system like the one trialled by Perseverance. This meant that SFR could be delivered closer to the depot and on more favourable terrain. Careful evaluation of the terrain produced the network of potential depots and landing sites shown in Figure 5-7.

The new mission profile allowed to relax the mobility requirements on SFR, making the rover smaller and easier to accommodate in the volume available on the lander. The resulting design, on the lower right (D) in Figure 6-2, became the SFR baseline at the centre of this study and is characterised by a mass of approximately 260 kg (including the appropriate design and system margins), uses four spring tyres 550 mm in diameter arranged over a ground contact footprint 1.3 m in length by 1 m width in and stows in a cylindrical volume approximately 1.6 m in diameter and 0.7 m tall. The final SFR baseline, also depicted in Figure 6-3, is able to climb one-sided obstacles up to 295 mm high.



Figure 6-3 – Artist’s impression of SFR on Mars

⁵⁰ The fact that this configuration had to climb wide step features with two wheels simultaneously (as opposed to single-sided compact obstacles) is of great relevance, as it is far more demanding. The one-sided obstacle climbing ability of this rover was never explored in depth, but is expected to be well in excess of 350 mm.

6.1.1 Lander interface

As noted in the previous section, the mechanical architecture of SFR is intimately coupled to that of SRL and, as the rover grew in size, pushed by terrain requirements, it became more challenging to accommodate it on the lander. By observing closely Figure 5-8 it can be noted how SFR (pictured there as the baseline “C” in Figure 6-2) is stowed on the top deck of the landing platform in an upside-down orientation. The reason for this unusual layout comes from the fact that the interface between SRL and SFR is another major area of trade-off and re-configuration that has been evolving since early in the programme, along with the arduous activity of packaging multiple spacecraft into an entry capsule.

At this point, it is relevant to note that the diameter of the heatshield at the front of the capsule is heavily constrained by manufacturing issues and by the size of the launcher’s fairing. Aerodynamics define the shape of the rest of the aeroshell behind the heatshield, therefore the internal volume of the capsule is essentially fixed. The size of the heatshield also determines the opposing force that the spacecraft will get from the thin atmosphere of Mars, hence constraining how much mass it can carry whilst remaining able to decelerate before hitting the surface. From this derives that volume and mass of the stowed lander and rover are hard constraints.

As the rover was under pressure to improve its traverse performance and grow in size, the lander packaging was not producing a credible solution within these boundaries. An extensive trade-off exercise was set up to explore alternative mechanical configurations, where the key variables were the stowed layout and the rover deployment strategy. The primary objective was to find a robust packaging that allowed the largest possible locomotion subsystem on the rover. During this process, SFR had to follow a constantly changing lander interface and undergo numerous repackaging studies to assess the merits of each configuration. Figure 6-4 summarises the main steps in this complex study.

The first configuration Figure 6-4 (A) is the baseline with which SFR started its development: the rover would be attached on the side of the lander, just behind the MAV’s engine, and an egress mechanism, possibly in the form of an articulated arm, would move it a short distance to deposit onto the surface. This arrangement soon became problematic because having the rover in line with the MAV was pushing the capsule’s diameter beyond a feasible size. Two first alternatives were considered where SFR would be attached under the MAV: one with the rover deployed after landing (B) and one with the rover delivered to the surface before landing, with a Sky Crane⁵¹ manoeuvre (C).

⁵¹ The Sky Crane manoeuvre is a method of delivering payloads to the surface of Mars used by NASA for its largest rovers and consists in lowering the rover on tethers from a hovering propulsive stage. The tethers are cut immediately after touchdown and the Sky Crane descent module flies away.

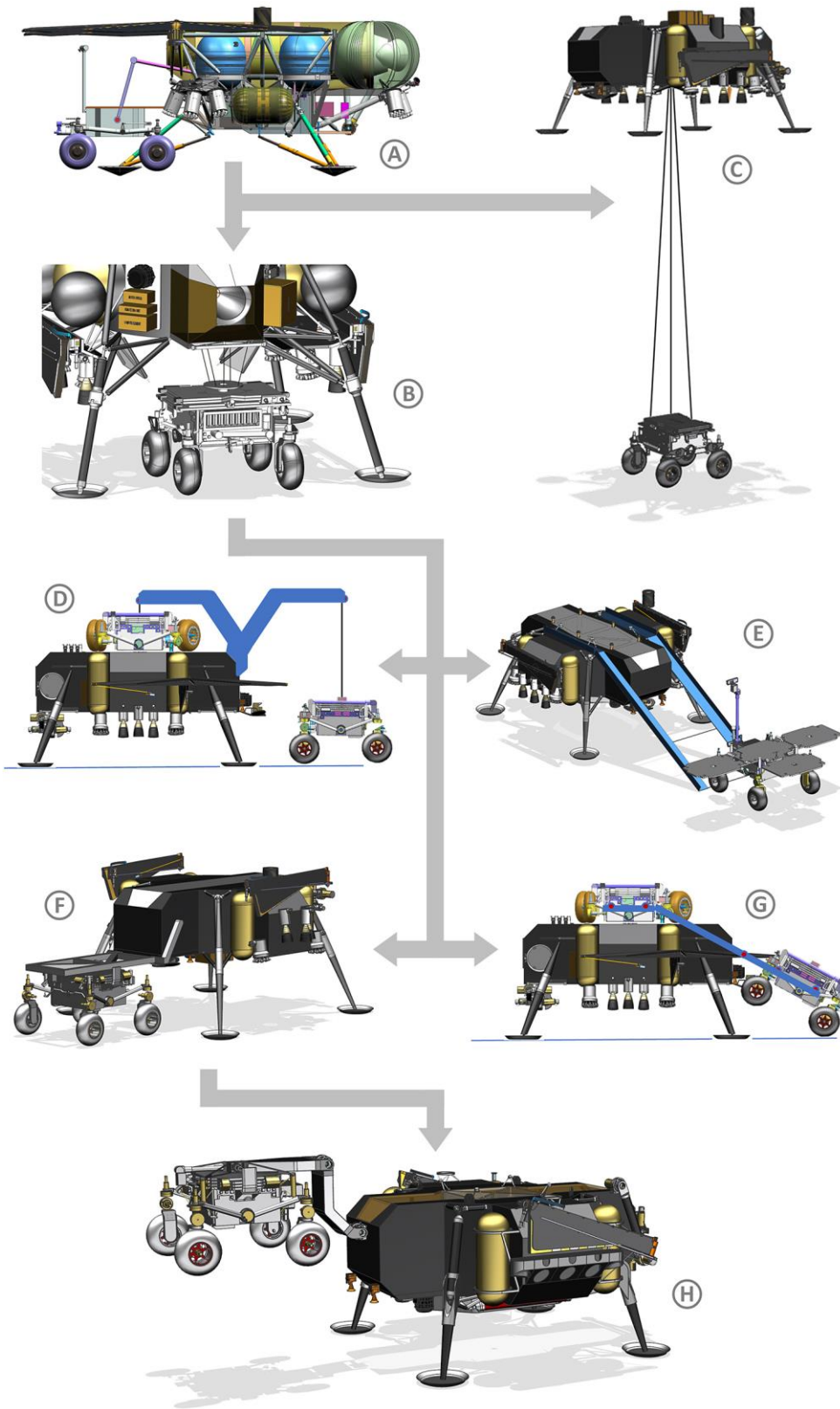


Figure 6-4 – Evolution of SRL architecture and SFR deployment concept (credit: NASA / JPL-Caltech)

In the following iteration, the Sky Crane approach was abandoned, but the vertical stacking (with respect to the landed configuration) was investigated further, this time placing the rover on top of the lander and exploring different egress mechanisms: a crane system (D), ramps (E), a turn over mechanism (F) and guiderails (G). The crane approach was judged

too complex and difficult to control in a deterministic way, while ramps and guidrails were too sensitive to the presence of large obstacles and, even though ramps have been used successfully in rover deployments, they did not appear advantageous considering the height of the SRL top deck (more than 2 meters above the ground). The turn over mechanism was judged to be a suitable egress method, although it did not offer much compliance to irregularities in the terrain. Configuration F was therefore chosen for further development, which led to a final, commonly-accepted baseline for the SRL mechanical configuration.

Option H is a refinement of option F and represents the conclusion of this trade-off. The rover would be stowed upside down on top of the lander and delivered to the surface by a 2-DOF arm. In Figure 6-4 the arm is shown attached to the rover's top deck, but later adjustments moved the interface to the aft panel of the rover body, so that it would be possible to partially deploy the solar arrays before separation. A third degree of freedom was also investigated in the egress arm to be able to adjust the roll of the vehicle on uneven terrain. The stowed configuration corresponding to this mechanical architecture is shown in Figure 6-5, where the advantages of placing the rover above the MAV enclosure become fully evident, as the stack naturally follows the conical shape of the entry capsule. The cruise module, providing power and propulsion during interplanetary transfer, would be attached to the top of the capsule in this view. The assembly is launched upside-down, i.e., with the heatshield facing up towards Earth's sky.

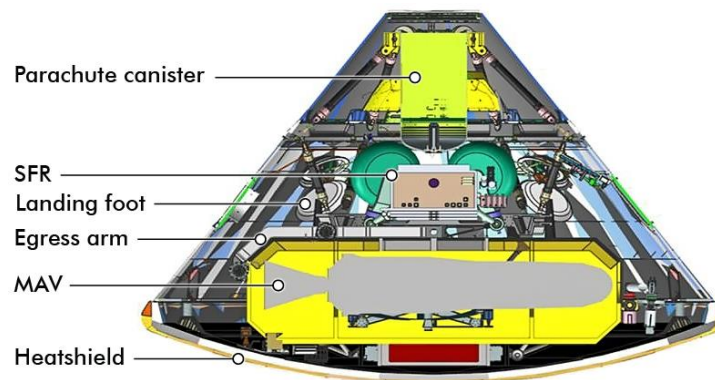


Figure 6-5 – Cross section of the SRL entry capsule (credit: NASA / JPL-Caltech)

6.2 Spacecraft architecture

SFR is a solar-powered surface vehicle, quite similar in size and architecture to the ExoMars Rover described in Section 4.4. Its mechanical configuration is based around a central, box-like body, which provides structural integrity and creates a thermally-controlled environment for sensitive electronics.

With reference to Figure 6-6, at the sides of the rover body are accommodated the suspension system and the drive electronics that control all mechanisms on board. The four large, compliant wheels dominate the external layout of the spacecraft and provide its distinctive appearance compared to other planetary rovers. At the front are mounted the systems to acquire the sample tubes from the surface: primarily a 6-DOF robotic arm and a storage assembly to host up to 30 tubes. Two stereo cameras are used for navigation and tube acquisition: one fixed at the base of the mast and one at the top, moved by a pan and tilt mechanism. On the mast head is also accommodated an engineering camera to film the MAV

launch. On the top deck are evident the large solar arrays that provide power to the craft, with one fixed panel and three deployable ones.

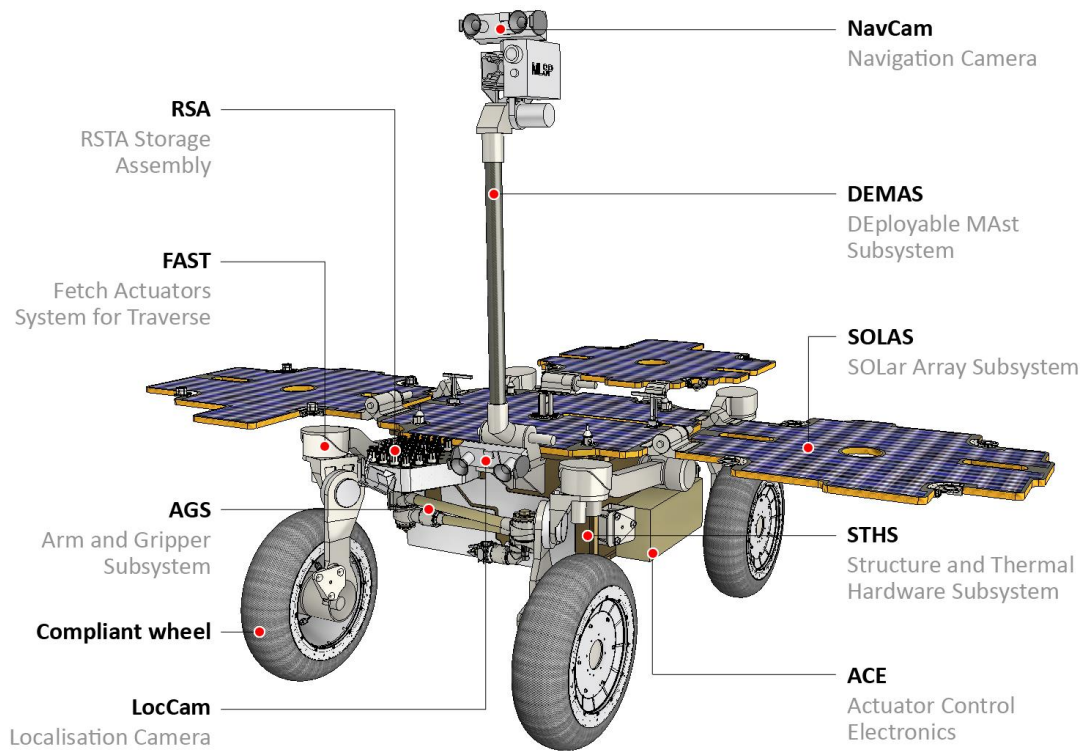


Figure 6-6 – SFR overview with major external components

Table 6-1 summarises the main characteristics of the vehicle. The most evident differences with the ExoMars specifications, reported in Table 6-1, are the new locomotion architecture, the much greater speed and the absence of scientific instruments on board.

Feature	Description
Mass	260 kg
Science payload	2.7 kg ⁵²
Ground footprint (L x W)	1.3 m x 1 m
Power	Solar, 120 W on Mars at noon
Locomotion architecture	Four-wheeled rocker arm
Maximum speed	6.7 cm/s
Mission duration	Varies, 345 sols max. ⁵³
Traverse distance	5 km

Table 6-1 – Key features of the Sample Fetch Rover

⁵² 30 tubes containing a total of 0.5 kg of sample material, to be acquired on Mars.

⁵³ The mission duration of SFR is not a pre-set target but it depends on the arrangement of landing site, depot and paths, which will not be known until late in the development.

Lastly, in Table 6-2 is reported a mass budget of the rover as it was at the beginning of phase B1 of its development, which generally corresponds to the design discussed in these pages. In the table, CBE stands for Current Best Estimate and DMM for Design Maturity Margin⁵⁴. The acronyms are defined in Figure 6-6.

Item	CBE (kg)	DMM	CBE + DMM (kg)
Rover body structure (part of STHS)	19.7	15%	22.7
Thermal control (part of STHS)	10.8	15%	12.4
SOLAS (incl. panels structure)	20.4	13%	23.1
Locomotion (FAST + wheels)	60.7	20%	72.8
Arm and Gripper Subsystem	9.6	16%	11.2
RSTA Storage Assembly	1.8	15%	2.1
DEMAS (incl. all cameras)	11.1	16%	12.9
Actuator Control Electronics	15.0	20%	18.0
Avionics	13.1	10%	14.4
IMU	1.9	5%	2.0
Telecommunications	2.5	5%	2.6
Battery	10.8	4%	11.2
Harness	4.7	30%	6.2
Lander interface hardware	11.0	20%	13.2
Sub-total (kg)			224.2
System margin (where applicable)⁵⁵			20%
Total with system margin (kg)			260.6

Table 6-2 – Sample Fetch Rover mass budget

6.3 Mission profile

SRL is a propulsive platform, so its entry, descent and landing profile is not dissimilar to that of the ExoMars mission described in Section 4.4.2. The main differences are that SRL uses only one parachute and its propulsive descent phase is longer, with more manoeuvres to perform a precision landing. The SFR mission begins once SRL has landed and completed its initial deployments and checkout activities, a high-level concept of operations can be summarised as follows:

⁵⁴ The DMM is established for each component based on how advanced its design is. For subsystems formed by multiple components, the subsystem-level DMM is the weighted average of the values at component level.

⁵⁵ On SFR, system margin is not applied to the locomotion mechanism, which is already sized to carry the vehicle's mass including system margin, hence the apparent discrepancy in the totals.

1. Egress to the surface
2. Deployment and commissioning
3. Outbound traverse
4. Acquisition of sample tubes
5. Return traverse
6. Transfer of sample tubes to SRL

The primary objective of the SFR mission is simply to retrieve up to 30 tubes and deliver them to SRL in time for launch. A secondary objective is still under evaluation and would be to film the MAV launch once the tube transfer is complete. As previously noted, SFR is not designed to perform any scientific observations and its role is essentially that of a transportation system. This concise overall objective enshrouds a complex maze of possible mission paths, operational scenarios and strategies to accomplish them.

Due to the uncertainty in the location of the sample tube depot and in how the Perseverance mission will take shape, SFR does not have a single traverse profile, but rather is designed as a multi-mission machine, capable of operating on different paths and combinations of various terrains. However, the candidate depot areas and landing sites have been already identified from orbit, so the space of combinations is defined. This situation lends itself to a statistical approach for mission analysis, hence a simulation tool was developed early in the project to rapidly explore thousands of paths, timelines, seasonal variations and operational scenarios. The analysis produces a statistical report showing which missions are successful, which are not and what factors determine the failures, helping to guide and verify the design as the development proceeds.

One last important aspect of the SFR mission profile is that, differently from any other exploration rover, it will drive in an area where another vehicle has driven before. Perseverance will have laid down the depot and scouted the landing site, therefore, it will have found a route between the two. That path might not be the absolute best one, but it would be very well documented, allowing to know what terrain features to expect at each step of the way. This is informally named “the highway”. Perseverance’s tracks might even still be visible on patches of compacted soil. Prior knowledge of the terrain significantly reduces the risk associated with high-level path planning for mission controllers, therefore, as soon as SFR lands, it will look for the highway and follow it to the depot.

6.4 Locomotion

Being a utility-driven transportation system, the Sample Fetch Rover’s locomotion function is unquestionably a central aspect in its design. The development of the electromechanical systems providing mobility to the craft is also a key part of this research and therefore treated in detail in a dedicated chapter. The SFR suspension mechanism is a rocker arm with a rear differential linkage. It uses four superelastic spring tyre wheels developed by NASA GRC, which are driven and steered independently. The design of these components is discussed in depth in Chapter 7.

6.5 Actuator Control Electronics

The Sample Fetch Rover’s Actuator Control Electronics (ACE) follow a similar architecture to the ExoMars ADE: they are two central units that serve all mechanisms on board, switching between groups of actuators. The centralised architecture is, as for ExoMars, driven by

mass constraints, which make shared electronics more mass-efficient, although not optimal in terms of control architecture. Like the ExoMars ADE, the ACE boxes are mounted outside, on the sides of the rover, making them “cold electronics”, exposed to the Martian environment. This is because the same thermal constraints apply, and placing them outside reduces the amount of harness going through the rover body walls, thus reducing the heat leak through these connections. It also avoids peaks in the internal heat dissipation due to ACE operation, overall reducing the strain on the thermal control system.

The ExoMars ADE are connected to 18 locomotion actuators (6 driving, 6 steering and 6 deployment), 4 solar array actuators (left and right primary and secondary hinges) and 3 mast actuators (deployment, pan and tilt), for a total of 25 brushed DC electric motors. The SFR ACE are connected to 8 locomotion actuators (4 driving and 4 steering), 3 solar array actuators (left, right and rear hinges) 3 mast actuators (deployment, pan and tilt) and 7 robotic arm actuators (6 DOF manipulator and gripper) for a total of 21 brushed DC electric motors. It derives that the ACE controls less axes compared to its predecessor, however, some of these actuators have much greater power needs (e.g., the locomotion, 6 times faster) or more stringent accuracy needs (e.g., the robotic arm, for precise tube handling), making the implementation of a common electronic design not less challenging. In addition to the electric motors, the ACE, like the ADE, control numerous Hold-Down and Release Mechanisms (HDRMs) and electric heaters spread over the vehicle.

The implementation of redundancy is different from ExoMars, where each unit contains internal redundancy and is connected to only about half of the actuators. On SFR, the ACE are two identical units, each redundant for the other and connected to all actuators. This implies more external harness to be routed around the rover, but a great advantage for the development of the hardware, which would have a single design, a single build process and would also allow testing of the whole system with just one unit. Figure 6-7 shows the location of one ACE on the rover (the other one is mounted symmetrically on the other side) and a detailed view of one unit. Each box has an envelope of approximately 480 x 200 x 120 mm and a mass of 9 kg.

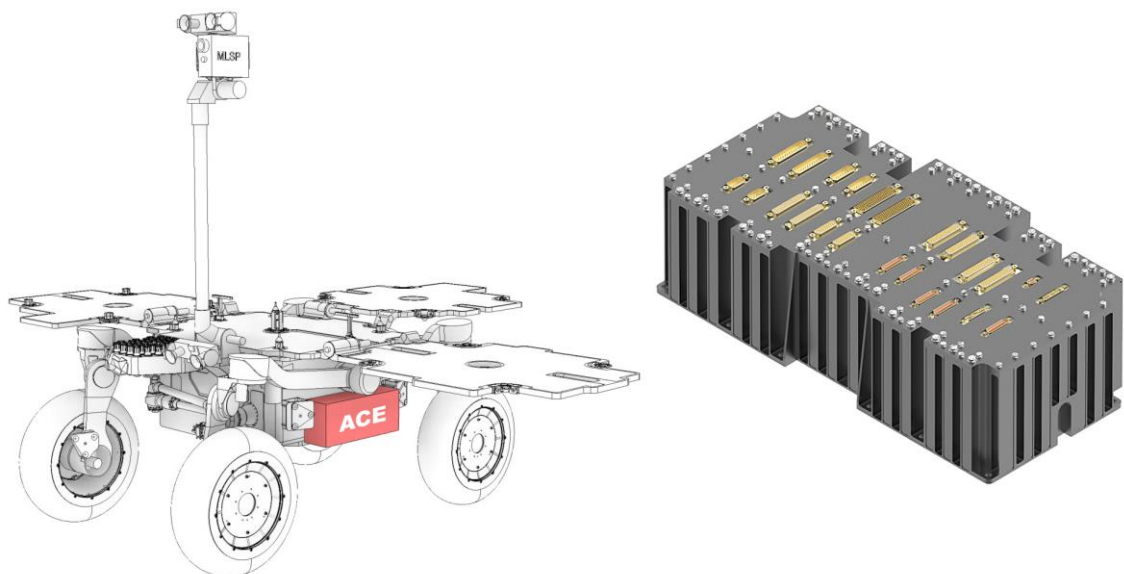


Figure 6-7 – Location of one ACE on SFR (left) and design of the unit (right) (credit: Sener)

6.6 Guidance, Navigation and Control

The ExoMars GNC, described in Section 4.4.5, can be reused on SFR with little modification for the most part. The GNC algorithms, running on the On-Board Computer (OBC), acquire data from very similar or identical components. In particular, they interface with the following hardware:

- **Navigation Camera (NavCam).** With the same geometry and optics of the ExoMars one (but using updated sensors), mounted on the mast head and steered by an equivalent pan and tilt mechanism. It builds a Digital Elevation Map (DEM) of the rover's surroundings to plan a path.
- **Localisation Camera (LocCam).** As the NavCam, with the same geometry and optics of the ExoMars one, it images the terrain from the rover's top deck to detect hazards and monitor progress. Since SFR is faster than ExoMars, the image acquisition frequency is also greater to maintain a similar spatial cadence of one picture every approximately 0.1 metres.
- **Inertial Measurement Units (IMU).** Essentially built-to print from the ExoMars units, they use the same gyroscopes and accelerometers to measure the rover's attitude and estimate its movement.
- **Locomotion subsystem.** This is the area that presents an obvious difference from ExoMars. While motors, sensors and control electronics use broadly similar technology, the architecture of the locomotion mechanism is clearly different and adaptations are necessary to control a four-wheeled vehicle. However, these modifications are mostly limited to the management of individual axes, since the two rovers have the same vehicle-level manoeuvring ability.

The data from the sensors above is fused exactly in the same way as on ExoMars. To be most effective, GNC algorithms have to be tuned to the response and the behaviour of the vehicle. In this respect, the heritage ExoMars GNC will necessitate a different tuning for the SFR platform, due to the different arrangement of wheels and their characteristics, such as size, radial deflection, lateral deflection, vibratory behaviour and traction profile on different materials. These parameters ultimately define how the vehicle responds to the terrain features that it encounters and so need to be accounted for in its control.

One notable difference with the ExoMars GNC is that SFR can use an additional mode of operation, devised to take advantage of the already-known path. The standard Autonomous Navigation (AutoNav) mode stops the vehicle every 2.3 metres to scan its surroundings, while this new autonomous follow-path mode would stop only every 5 metres to perform a safety assessment of the path ahead. The pause is also shorter since only two images are acquired rather than three, allowed by the fact that the route is broadly known and there is no need to scan a wide angle to look for alternatives. This enables SFR to cover more ground each sol and meet its strict timeline. If the rover encounters difficult terrain or it needs more precision, it can always switch back to the heritage AutoNav mode.

Unlike ExoMars and any other planetary rover before, SFR does not venture into the unknown. By the time the rover arrives on Mars, there will be various sources of information to build a three-dimensional map of its route: orbital imagery (resolution in the order of 1 m), Perseverance's navigation data (resolution in the order of 10 cm) and close-up depot imagery by Perseverance (resolution better than 1 cm). These products can be combined into a Digital Elevation Map (DEM) of the area and stored on board SFR, enabling another

new function of this spacecraft: Absolute Global Localisation (AGL). The rover drives along its path by regularly scanning the terrain, building consecutive DEM sectors that are stitched together to estimate its driven path. This approach is prone to error accumulation over time due to the accuracy of the DEMs and their merging. The AGL algorithm can overlap these DEMs with the global map stored on board and obtain the vehicle's true position on the Martian surface, thus resetting any cumulative error. This strategy is illustrated by Figure 6-8.

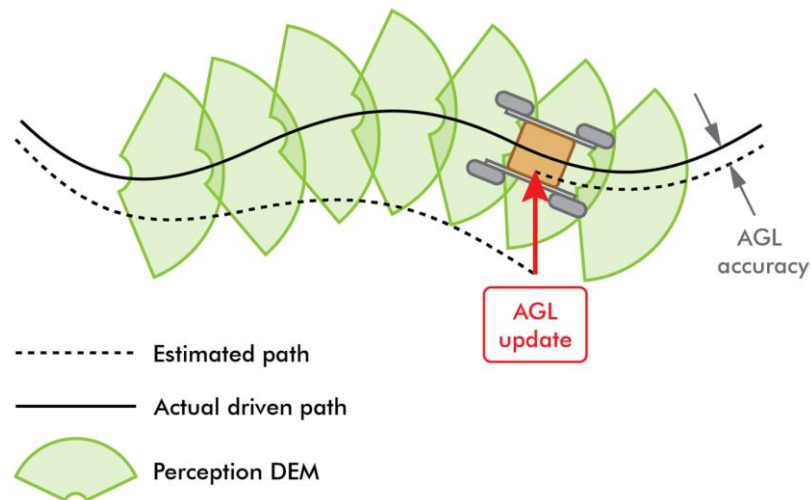


Figure 6-8 – Visualisation of a path following sequence with AGL update

6.7 Integrated avionics

The approach to core avionics is slightly different on SFR than on ExoMars. To maximise mass efficiency and simplify interfaces, the Power Conditioning and Distribution Electronics (PCDE) and On-Board Computer (OBC) have been combined into a single assembly, procured as a complete product. This device is identified as the Integrated Avionics Box Subsystem (IABS) and the design of its enclosure can be seen in Figure 6-9. The box is approximately 430 x 420 x 160 mm and 14.5 kg in mass, which is quite similar to the size of a common desktop computer. As on ExoMars, also on SFR these sophisticated electronics are accommodated inside the rover body to protect them from the cold environment.

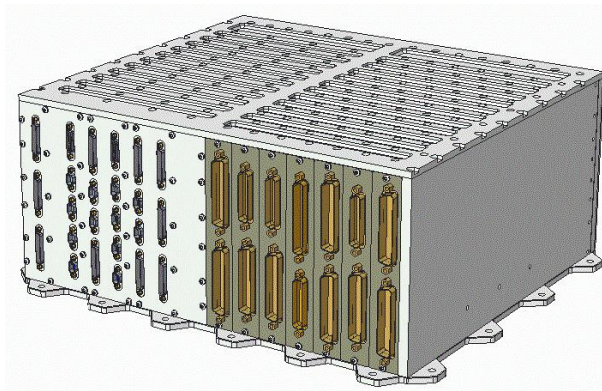


Figure 6-9 – Sample Fetch Rover IABS (credit: Beyond Gravity)

The unit is organised in a modular way, with several circuit boards of the same size stacked together and all connected by a mother board. Redundancy is achieved by duplication of boards or internal redundancy where possible. All connector interfaces on the housing are

also redundant. The IABS volume can be considered divided in two main areas (although there is no physical separation between them): one dedicated to the PCDE and one to the OBC. The key modules contained in the PCDE section and their functions are the following:

- **Solar array regulator.** Composed by power converters that regulate the input from the solar array and distribute it to the battery or to the primary power bus depending on the demand.
- **Battery management module.** It delivers to the battery the current generated by the solar array in excess of the primary power bus need, up to the maximum charging current according to the temperature. It also disconnects the battery from the main power bus if the level of charge gets too low.
- **Latching Current Limiters (LCL).** The circuits that take power from the primary power bus (fed by the battery or solar array) and distribute it to all the users. They provide numerous channels for different user groups, each with a maximum current allowance and rapid disconnection ability in case an anomalous current draw is detected. All these channels provide an unregulated nominal voltage of 28 V⁵⁶.
- **Heater drivers.** They activate heater channels based on the input from temperature sensors. They serve only the heaters internal to the rover body and those in the ACE, since the other external heaters are controlled by the ACE itself.

The key modules contained in the OBC section and their functions are the following:

- **Telemetry, telecommand and reconfiguration module.** The device that decodes commands, encodes telemetry packages and also keeps on-board time while the rest of the system is inactive is in sleep mode.
- **Processor module.** A radiation-hardened, failure-tolerant processor operating at 100 MHz and accompanied by 512 MB of SDRAM. It is a low-power processor and executes the core software functions of the rover.
- **Mass Memory.** A flash memory module with a capacity of over 40 GB.
- **Co-processor module.** A powerful processor dedicated to computationally-heavy tasks like image processing for GNC. It is based on a quad-core, radiation-hardened, fault-tolerant processor operating at 250 MHz.
- **Analog and bi-level interface.** A converter that transforms analogue signals into digital telemetry.

On SFR, power consumption is a crucial aspect, even more so than ExoMars, since its daily traverse range is almost always limited by the energy available. Every evening, the rover transitions to sleep mode with a certain minimum amount of energy stored in its battery to power internal heaters to survive the night. The power consumption of the components that remain active in this mode is the most critical, since it directly draws from this precious energy reserve. As a consequence, a carefully coordinated “sleep pattern” has been engineered for the IABS, where power is removed from most of the components listed above, maintaining only a handful of critical LCLs and heater drivers for survival, and deactivating most of the OBC, at exception of the telemetry, tracking and control module that keeps on-

⁵⁶ This means that the voltage is not actively maintained to a certain level, but varies depending on the battery level and the power draw. On SFR this can typically range from 21 V to 29.4 V.

board time and wakes up the rover with a pre-programmed alarm or if a “hail” radio signal is received.

The external interfaces of the IABS use the same architecture and protocols of the ExoMars OBC described in Section 4.4.6, with the addition of the power lines connecting the PCDE with the solar array, the battery and the various users on board.

6.8 Telecommunications

The communication system on SFR is identical to that on ExoMars, with the same redundant UHF transceivers and antennas as described in Section 6.8. The communication strategy, however, is different. Since the SFR mission is planned towards the end of the 2020s, it is uncertain what American or European orbiters will be still operational and able to provide relay service. One orbiter will undoubtedly be available: the MSR Earth Return Orbiter (ERO), which will be already waiting around Mars when SRL arrives.

Having to rely on only one orbiter makes communication passes particularly critical, as there might be only one or two per sol and might be too short to exchange the desired data volume every time. This necessitates significant autonomy on board, making the rover capable to operate for longer without ground intervention, but also the ability to be woken up during the night to communicate with ERO, which is undesirable due to the energy consumption, but necessary in some mission scenarios.

6.9 Sample tube acquisition

The acquisition of the sample tubes left by Perseverance on the surface is the defining function of the Sample Fetch Rover and a central aspect of the work discussed here. The system that is in charge of executing this function is called RSTA Acquisition System (RAS), where RSTA stands for Returnable Sample Tube Assembly, indicating the individual sealed tube prepared by Perseverance. The RAS is composed of the following elements, some of which are shared with other functions:

- **Arm and Gripper Subsystem (AGS).** A 6-DOF robotic manipulator to acquire and manipulate the tube, equipped with a camera on the wrist and a temporary tube holding station to switch the gripping orientation.
- **Navigation Camera (NavCam).** The same camera on the mast head used by the GNC system. It images the terrain in front of the rover to identify the position of the tube.
- **RSTA Storage Assembly (RSA).** A storage mechanism to accommodate up to 30 tubes during the return traverse and allow exchange with the lander’s robotic arm.
- **RAS software.** Specialised algorithms that coordinate the tube acquisition sequence, process camera imagery to guide autonomous operations and deal with unexpected events and faults. They run on the processor and co-processor modules in the OBC (see Section 6.7).

The acquisition of tubes from unprepared terrain requires carefully choreographed robotic operations, which would take an impractical amount of time if commanded by ground in a step-by-step fashion. Therefore, the level of autonomy associated with these functions is very high and the system is able to cope with uncertainties and try alternative strategies in

case of failure. These operations and the components that execute them are described in detail in Chapter 8.

6.10 Structure

The SFR structure relies heavily on ExoMars technology. It uses the same materials, same construction and integration approach described in Section 4.4.9. Since SFR does not contain scientific instruments, the main carbon fibre frame is smaller and has a simpler shape than the ExoMars' "bathtub". It is simply a rectangular parallelepiped measuring 800 mm in length, 750 mm in width and 420 mm in height. These dimensions are heavily constrained by the packaging on the lander, especially the height, which is compressed between the parachute canister and the lander's top deck inside the descent capsule, as shown in Figure 6-5. Another notable difference is that on SFR the body HDRMs are located on the rover's top deck since it is stowed upside down, but they use similar technology to the ExoMars ones. Beyond these implementation-specific differences, the same general considerations apply as discussed in the ExoMars design.

6.11 Top deck mechanisms

In addition to the locomotion and the arm and gripper subsystems, two other large mechanisms are present on SFR: the SOLar Array Subsystem (SOLAS) and the DEployable MAST Subsystem (DEMAS). They are both located on the top deck of the rover and each of them contains electrical actuators and HDRMs that are controlled by the ACE. A view of these mechanisms in their stowed and deployed configurations is provided in Figure 6-10 with the rover body shown in transparency.

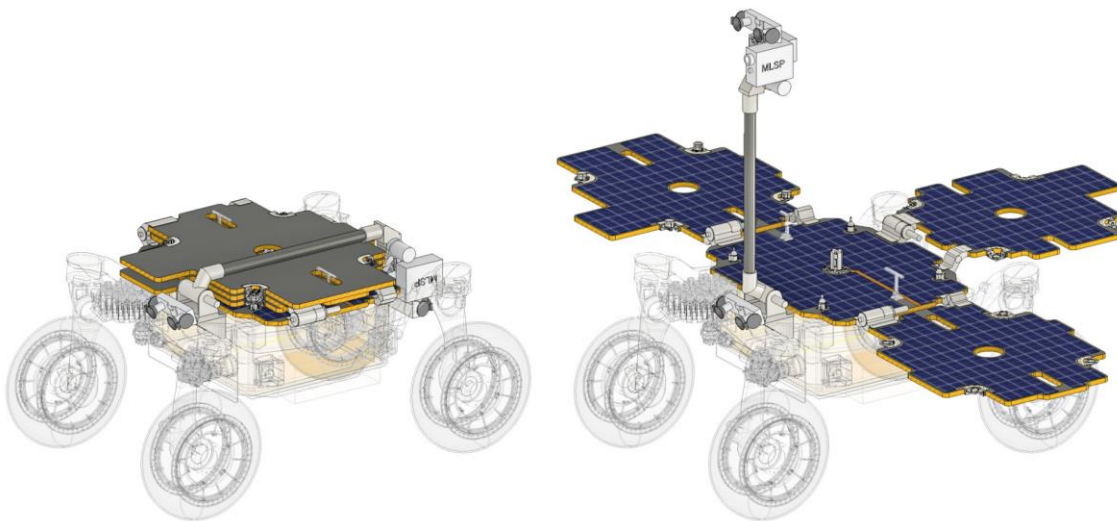


Figure 6-10 – SFR top deck mechanisms stowed (left) and deployed (right)

SOLAS contains the solar panels that generate electrical power for SFR, whose specifications are described in Section 6.13. The mechanism provides four attachment points on the corners of the panels, where they are secured together and to the rover body to withstand launch vibration. During the egress of the rover from the lander, four HDRMs separate these interfaces so that the three deployable panels can rotate. Hinges powered by brushed DC motors rotate them one at a time by 180° and then lock them in place with a passive latch.

The hinge and HDRM designs are strongly based on ExoMars, which uses a very similar mechanism to deploy its solar arrays.

In Figure 6-10 it is evident how the SFR solar panels do not have any exposed solar cells when stowed, hence the rover is not power-independent until they are deployed. The deployment is performed while the rover is still receiving power from the lander through its umbilical cable, which is disconnected only after SFR has become power-positive. The deployment sequence of the panels is closely coupled with egress operations and the design of the egress arm, which is still evolving, as mentioned in Section 6.1.1.

Observing Figure 6-10 it can also be seen how DEMAS is stowed over the solar arrays, so it must be deployed first. The mast boom extends from a hinge on the front, over the stack of solar panels, to the back of the vehicle, where the head is secured by an HDRM on the rear face. The primary function of the mast is to hold the NavCam approximately two meters above the ground and orientate it to map the terrain for the rover's GNC. The mast head also provides interfaces for an additional imaging payload, dedicated to recording the MAV launch, which has only been preliminarily studied at this stage. On the base structure of the mast is mounted the LocCam, which is fixed to the vehicle's reference frame and does not require active pointing.

DEMAS contains three electric hinges powered by brushed DC motors: a deployment hinge at the base, pan and tilt axes on the mast head. The deployment hinge is used only at the beginning of the mission and then latches into position like the solar panels, while the pan and tilt actuators operate throughout the mission. All of them use technology similar to the ExoMars mast, at exception of the position sensors. The SFR GNC needs accurate pointing of the cameras to build high-quality maps of the surface and position the rover with relation to them. Since the accuracy requirements could not be met with typical potentiometers (widely used on ExoMars), it was decided to use resolvers for the DEMAS actuators. These are identical to the ones in the AGS, which are discussed in Section 8.4.1.

6.12 Thermal control

The thermal architecture of the Sample Fetch Rover has elements in common with the ExoMars one, described in Section 4.4.10: an insulated and thermally-controlled enclosure, formed by the rover body, contains the most sensitive components, while the external hardware is let to cool down overnight and is warmed up by electric heaters in the morning. However, the SFR thermal control departs from the heritage design in some fundamental areas. Firstly, SFR, differently ExoMars and any other Mars rover before, does not contain Radioisotope Heater Units (RHU). While RHUs are generally advantageous in cold environments like Mars, this decision was made to avoid the complexity and cost associated with handling nuclear material and to prevent potential delays caused by its procurement. Without RHUs, the only source of night-time survival heat are electric heaters powered by the battery, making energy management even more critical, demanding efficiency and good insulation.

The answer to these challenges is a relatively novel solution for Mars, but not unknown for other spacecraft: Phase Change Material Capacitors (PCMC), a thermal energy storage solution that relies on the latent heat of a chosen substance. SFR is a rather powerful machine and can generate significant waste heat during diurnal operations, while at night, without RHUs, the rover gets cold and requires electric power to control its temperature. PCMCs

mitigate this imbalance, as they absorb the excess heat during the day, melting and stabilising the temperature inside the rover, and they release it in the evening, solidifying and contributing to keeping the rover warm. They are implemented on SFR as two containers, filled with 2 kg of hexadecane⁵⁷ each and able to store almost 1 MJ of thermal energy in total. They are bolted to an internal conductive panel called service module, onto which all the internal equipment is mounted. Figure 6-11 shows a transparent PCMC under test, where it is possible to see the solid phase transforming into liquid in presence of a heated vertical wall. Differently from SFR, the PCMC in this test used a more common paraffinic wax with a melting point around 28°C.

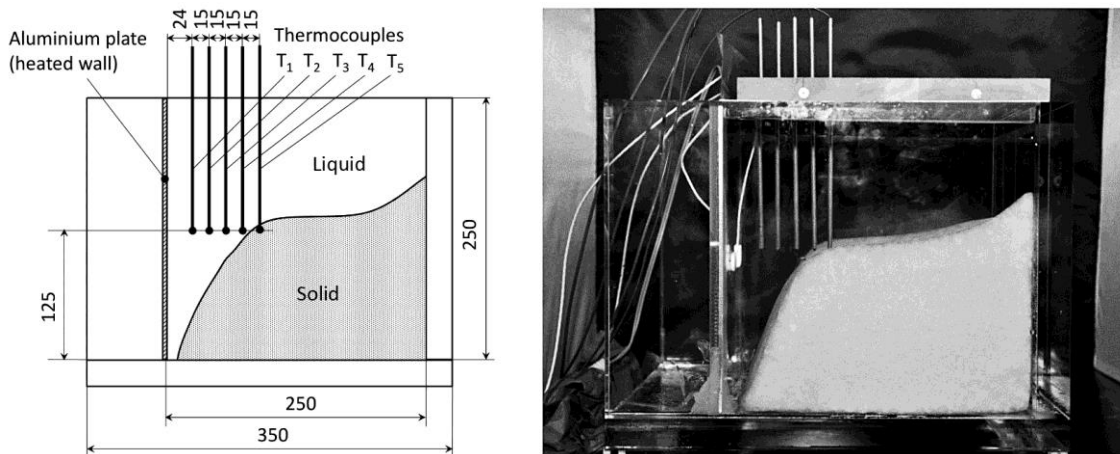


Figure 6-11 – Example of PCMC under test in a thermal chamber (credit: J. Stetina)

To extract the excess heat from the spacecraft, SFR uses the same ExoMars technology: propylene loop heat pipes fitted with thermostatic valves and connected to external radiators. However, the presence of the PCMCs allows to operate these devices in a slightly different way and improve the energy efficiency of the system. The heat pipes and radiators are not very effective at rejecting heat during the day when the external environment is warm. Instead of sizing the system to reject heat continuously, it is accepted that the heat pipes will have little contribution during this time and the PCMCs will absorb the extra energy. In the evening, as the environment becomes colder, the heat pipes' efficiency will increase and they will gradually offload the energy accumulated during the day, solidifying whatever fraction of hexadecane had melted. The heat pipes automatically turn off when the temperature goes below the PCMC transition temperature. This implies that the PCMCs will be able to help internal heating only during the first part of the night, leaving SFR on electrical power for the coldest hours. It is, however, a necessary measure, as failure to ensure that the PCMCs are fully solidified could mean overheating the following day.

One last difference with the ExoMars approach to thermal control is that SFR, whilst having electric heaters on all external hardware, aims to exploit as much as possible passive warm-up by the environment, in an effort to preserve energy. This means that SFR would typically spend the first half of each sol warming up and charging the battery, then would wake up only around local noon or even later. Evidently, this limits the time available for operations and is, in fact, one of the factors that require SFR to drive much faster than other rovers.

⁵⁷ Hexadecane, or cetane, is an alkane hydrocarbon with the chemical formula $C_{16}H_{34}$. Its melting temperature is approximately 18°C.

Nonetheless, it is an overall more efficient way of operating, not only because it saves warm-up energy, but also because when the spacecraft is awake it uses a baseline of “housekeeping” power that is independent from other activities, such as, for example, traversing. By traversing faster, even if the traverse energy was the same, the housekeeping energy would be reduced. It remains possible, if needed, to invest more energy into an early warm-up, allowing to tune the activity profile to mission scenarios that are more energy-constrained or more time-constrained.

6.13 Electrical power system

The power architecture of the Sample Fetch Rover is very similar to that of ExoMars, with the exception of the PCDE, which is not implemented as a separate unit, but part of the IABS, described in Section 6.7. SFR uses a built-to-print copy of the ExoMars battery, taking advantage of the already consolidated technology. This is a package of 56 SAFT MP 76065 XTD Li-ion cells, for a total nominal capacity of 1140 Wh and an operational voltage range between 21.0 V and 29.4 V. The unit is identical to that shown in Figure 4-22.

On the top deck is a solar array with a different layout from the ExoMars one, as it is formed by one fixed panel and three primary deployable ones, while ExoMars has one fixed panel, two primary deployable ones and two secondary deployable ones. This is largely driven by the different packaging constraints of the vehicles on their respective landers. Because of these limitations, the SFR solar array is slightly smaller and contains 36 strings of 18 cells each, for a total of 748 elements. The cell technology is the same Azur Space 3G30, providing a beginning-of-life power generation efficiency of 30%. The SFR solar array is sized to produce approximately 120 W on Mars at noon at the end of life (considering dust coverage and radiation aging), but can output more than 210 W at the beginning of life.

Another notable difference with ExoMars is the concept of operations for the daily activities, which affects the power profile. As noted in the previous section, SFR tends to wake up late to minimise warm up energy and also to save on “housekeeping” energy required to keep all the systems operational. In fact, when the avionics are active and the ACE is powered, there is a considerable baseline power consumption even if the rover is not moving. The design response to this issue is to drive faster and concentrate operations only in a small interval of time. Furthermore, SFR features a very efficient sleep mode, as described in Section 6.7.

This approach has the downside that operations concentrated in a smaller time tend to be more power-intensive. Traversing is a clear example of this: at the low speeds typical of planetary rovers, it is reasonable to assume that driving over a certain combination of terrain features roughly takes a fixed amount of mechanical energy. It derives that, being SFR much faster than ExoMars, its traverse power consumption will be significantly higher. It should be noted that this applies to the energy discharged outside of the vehicle, but the mechanical losses in the drive actuators depend on the transmission design, and higher speeds often allow simpler, more efficient gear trains. This latter contribution is dominant on ExoMars, but not on SFR, due to the more efficient actuator design (see Chapter 7), meaning that the considerations above hold true. The result is that the power consumption of the SFR locomotion actuators is typically around 100 W, but can spike to over 500 W when climbing difficult obstacles. This translates into a current draw in excess of 20 A, which sizes the power distribution circuits on the rover.

6.14 Planetary protection

As discussed in Section 5.2.4, the Mars Sample Return campaign is included in the category V restricted of the COSPAR classification, meaning that the most stringent planetary protection requirements apply, with maximum confinement of the returned material and break-the-chain events to prevent contamination. However, while these considerations are relevant for the campaign as a whole, SFR is not meant to provide any additional confinement or break-the-chain functions and is destined to remain on Mars. Therefore, from its point of view, the planetary protection aspects are not particularly different from those of the ExoMars Rover. SFR is, in fact, subject to the same requirements of any category IV mission.

The same cleanliness and contamination control methods apply as described in Section 4.4.12 for the ExoMars Rover. Likewise, the SFR hardware is designed to be compatible with the techniques used to remove or kill biological contaminants. This means compatibility with surface cleaning methods (typically wiping with a solution of isopropyl alcohol and distilled water) and sterilization methods (typically DHMR treatment at 125°C). Such constraints have an impact in the selection of materials for the rover, which need to withstand contamination control procedures. These also include assay of the biological contamination, or bioburden, which usually requires compatibility with distilled water. Some exceptions are allowed for areas sensitive to corrosion, bi-metallic interfaces or absorbent materials, as long as neighbouring areas can be assayed.

The design drivers associated with planetary protection are not limited to materials selection, but also include the definition of the geometry of components. This should minimise the presence pockets and narrow features that are difficult for a human operator to clean. When confined cavities are vented, this must be done through a labyrinth that impedes the migration of particles that might have been left inside the cavity. If the cavity contains organic substances, like lubricants, then it must be vented through a HEPA filter that prevents the egress of such substances. Any other potential non-filtered passages must hermetically sealed.

Moreover, assembly and integration of the hardware must follow strict protocols to preserve its cleanliness. Since SFR is planned to be built in the same Airbus facility as the ExoMars rover, it can take advantage of the same Bio-Clean Facility, described in Section 4.4.12. Any tools and ground support equipment that comes in proximity to the flight hardware must meet the same level of cleanliness. Any transportation of hardware from and to the facility must use packaging that preserve its cleanliness. This also applied to the finished rover, which will use a specialised bio-clean transport container

An additional set of unique requirements is placed onto SFR by one aspect of its mission that is not strictly planetary protection but closely related: safeguarding integrity of the samples. This is one of the highest priorities for the rover, as there would be little value in returning samples that have been compromised. The associated requirements include mechanical integrity, in particular for the area of the seal, which is sensitive to mechanical loads. This drives the design of the systems that handle the tubes to ensure that the applicable load limits are respected at all times.

Thermal protection of the tube is also required, as the sample material could be chemically altered if its temperature rose substantially above its natural range. This means that the hardware in the vicinity of the tubes must not trap significant heat under any sunlight conditions. Lastly, the tubes cannot be exposed to strong magnetic fields to avoid changing their

potential magnetic properties. In practice, this means that no electric motors can come in close proximity of the tubes at any point of their handling. These requirements ensure that the samples will remain well contained inside the tubes and will retain their full scientific potential all the way back to Earth.

7 DEVELOPMENT OF THE SFR SYSTEMS: LOCOMOTION

Unlike any other planetary rover before, the Sample Fetch Rover does not venture into unknown territory. Robots will have explored the area years before its arrival and collected large amounts of data on the terrain. In particular, the path travelled by Perseverance will be known in detail through the numerous navigation images that are regularly downloaded by mission controllers. This route is known as the “highway” and, even though SRL might not land exactly on it, the first thing that SFR will do after deployment is find the highway and follow it to the depot⁵⁸. It might not be the absolute best path, but the fact that there is previous knowledge on it greatly reduces risks and uncertainties, making it the most desirable approach.

This aspect is of great significance for the SFR locomotion subsystem because it means that the vehicle can be designed to tackle well-defined terrain features. Even though the specific path is not known yet, but rather there is a network of possible paths, and even though complete in-situ imagery will not be available until late in Perseverance’s mission, orbital imagery and geological assessment of the terrain allow to delineate quite well the traverse requirements. From the large-scale morphology, terrain slopes are known, surface materials can be inferred, rock distribution can be measured for large size obstacles and extrapolated to smaller ones. With this information, once the route and the time available are set, the required locomotion performance is defined. Naturally, this process is not straightforward and is the result of an intricate multi-layer analysis, as will be discussed in this chapter.

The following pages give an account of the SFR locomotion subsystem design and the process that led to it. One clarification is due as to the terminology used herein, in particular the designations “locomotion” and “mobility”. In this work, and often in the discussion of European planetary rovers in general, the term “locomotion” identifies the low-level mechanical and electrical functions to drive the vehicle through the terrain, in other words, the

⁵⁸ From the discussion in Section 5.2.1, it derives that there will always be a known highway between the landing site and the depot, because Perseverance will lay down the depot and subsequently scout the landing site.

mechanisms and their drive electronics. The term “mobility” usually includes these as well as the higher-level control and decision making to reach safely a destination, i.e. the GNC software and hardware. This is not an official or particularly strict distinction and, for example, in the American nomenclature “mobility” and “locomotion” are synonyms and they do not include GNC. It is however useful to highlight that the topics here discussed focus mostly on the locomotion mechanism and its electro-mechanical design, with occasional remarks as to the higher-level systems. For an overview of the control electronics and GNC design, Sections 6.5 and 6.6 can be consulted, respectively.

7.1 Trade-offs and early developments

The first challenge in defining the locomotion subsystem of a planetary vehicle is to firm up its architecture, which is typically defined by parameters such as the number of wheels, the suspension mechanism, the type and location of actuators, etc. In the early phases of mission analysis, some key factors are often qualitative and only partially understood, so a common approach is to start with known architectures from heritage or literature review and use a trade-off process to evaluate their performance and choose the best candidate. Once completed this step, critical technologies can be identified and prioritised for development, in particular, those characterised by a low Technology Readiness Level (TRL).

7.1.1 Number of wheels

For SFR, one of the first assessments focused on the number of wheels. As it can be seen in Figure 6-2, the first rover concept was a six-wheeled platform with a triple bogie suspension. This simply represents the heritage starting point based on the ExoMars experience, but it was soon put through a trade-off process that evaluated its merits relative to a four-wheeled configuration, which is summarised by Table 7-1.

Feature	Weight	4 wheels		6 wheels	
		Score	Justification	Score	Justification
Mass	0.19	8	Close to mass target	5	Over mass target
Stowed volume	0.23	10	Compliant to volume allocation on the lander	5	Non-compliant to volume allocation on the lander
Traverse performance	0.16	5	Reduced obstacle climbing ability, sensitive to wheel design	8	High slope and obstacle performance
Efficiency	0.23	10	Small number of actuators leads to low friction losses	7	Up to 30% greater consumption than 4 wheels
Redundancy	0.07	2	Failure likely results into immobilisation	7	Failed wheel can be dragged to some extent
Heritage	0.12	4	Apollo LRV (crewed), terrestrial applications	9	Multiple Mars and Moon robotic missions
Overall weighted scores		7.6		6.6	

Table 7-1 – Trade-off on the number of wheels

In this approach, a weight is associated to each feature on the basis of its significance for the mission and for the system’s design. A score is then given through a quantitative or, where not possible, a qualitative assessment of the performance of each configuration with respect to that feature. The total weighted score provides an indication on which configuration is

overall the most desirable. The individual scores also help identify what are the weak points of each candidate and the issues that should be tackled first if it were to be chosen. Table 7-1 shows how the four-wheeled configuration became the preferred option for SFR (although both a four and a six-wheeled design were progressed in parallel for a period of time). It also shows how redundancy, heritage and obstacle climbing ability emerged as the weak points of that architecture.

The first weakness is quite elementary: if one wheel, or its drive system, failed, a six-wheeled vehicle could use the other five to drag it along and still be able to move, albeit with degraded performance. On the other hand, a four-wheeled vehicle would remain with only three wheels to provide traction and the resistive force of the blocked one would likely make it ungovernable. The response to this issue is provided by the nature of the SFR mission: the key objective of the rover is to acquire and deliver a payload in time. While on a scientific mission it is desirable to have a degraded mobility mode as a backup, in a logistical mission with a binary success criterion, this would likely bring a time penalty too high to achieve the target. It derives that this type of redundancy is not particularly useful for the SFR mission and therefore a low weight is assigned to this feature. On SFR, fault tolerance will be provided by redundant electronics, redundant harness, robust wheel design, consolidated motor and gear train technology, but not by the number of wheels.

The limited heritage available on four-wheeled planetary locomotion can only be addressed by an accelerated development programme, using early prototypes to characterise and mature this technology. This approach led to the construction of a full-scale model of the rover quite early in the project timeline to test the vehicle's behaviour on representative terrain, the results of which are discussed in Section 7.4.

Lastly, rough terrain traversal, and in particular obstacle climbing ability, is a well-known limitation of four-wheeled vehicles. Little can be done about its fundamental cause, which is that vehicles with more wheels have more ground contact points to produce traction and less weight on wheels encountering obstacles. However, this shortcoming can be mitigated by the careful choice of wheels and suspension mechanism. In particular, the more compliance these two elements provide to asperities in the terrain, the easier it will be to overcome obstacles. The size and tractive performance of the wheels are also essential in facilitating obstacle climb.

These considerations eventually led to the architecture for which the rover is known today: a rocker arm suspension with four large compliant wheels. A trade-off exercise similar to the previous one was performed on the suspension mechanism, with other candidates such as fixed wheels axles (no compliance to the ground), sprung suspension designs and a combination of fixed front axle and a rear bogie. The rocker arm emerged as the evident favourite due to its relatively simple design, pitch-averaging behaviour on the rover body, good stability, ability to distribute evenly the load and guarantee ground contact on all four wheels.

The wheel size, on the other hand, has been constantly receiving upward pressure from the challenging terrain requirements, which called for the largest wheels that could be reasonably accommodated. This eventually hit a limitation in the lander volume, converging onto the size that is used today. The process is well summarised by Figure 6-2, where the rover is seen to start with very small wheels that then gradually grow and shrink back down in the last design iteration. The wheel technology offered by NASA's Glenn Research Center (GRC) immediately proved attractive in view of the limitations of a four-wheeled platform,

thanks to their high compliance, efficiency, traction performance as well as durability and technology maturity.

7.1.2 Actuator technology

The actuators that power the joints of the locomotion subsystem and enable movement of the craft are another defining factor of the traverse performance. Hence, the technologies that characterise them have been also subject of early trade-offs. In particular, Table 7-2 analyses the choice of motor type between Brushed Direct Current (BDC) and BrushLess Direct Current (BLDC) and the type of output gear stage between Planetary Gearbox (PG) and Harmonic Drive (HD). The table is split in two blocks to improve readability.

Feature	Weight	BDC motor + PG output		BLDC motor + PG output	
		Score	Justification	Score	Justification
Mass	0.16	7	25% heavier than BDC + HD	8	20% heavier than BDC + HD
Efficiency	0.23	10	Overall actuator efficiency at cold predicted as 60%	10	Overall actuator efficiency at cold predicted as 60%
Temperature tolerance	0.14	9	Tolerant to temperature, small variation in efficiency	9	Tolerant to temperature, small variation in efficiency
Thermal performance	0.09	8	Easy to place heaters on the gearbox and extract heat from the motor	8	Easy to place heaters on the gearbox and extract heat from the motor
Lifetime	0.16	7	Analysis shows sufficient but limited flight data	7	Analysis shows sufficient but limited flight data
Heritage	0.09	7	MSL, Perseverance	6	MSL, Perseverance, limited heritage on BLDC in Europe
Drive electronics	0.14	10	Simplest drive electronics and harness	7	Complexity in electronics and harness to drive BLDC

Overall weighted scores	8.5		8.1	
--------------------------------	------------	--	------------	--

Feature	Weight	BDC motor + HD output		BLDC motor + HD output	
		Score	Justification	Score	Justification
Mass	0.16	10	Lowest mass option	9	5% heavier than BDC + HD
Efficiency	0.23	5	Overall actuator efficiency at cold predicted as 32%	5	Overall actuator efficiency at cold predicted as 32%
Temperature tolerance	0.14	6	Sensitive to temperature, large variation in efficiency	6	Sensitive to temperature, large variation in efficiency
Thermal performance	0.09	5	Difficult to warm up HD and extract waste heat	5	Difficult to warm up HD and extract waste heat
Lifetime	0.16	8	Demonstrated by MER on Mars	8	Demonstrated by MER on Mars
Heritage	0.09	10	MER, MSL, Perseverance, ExoMars	6	MSL, Perseverance, limited heritage on BLDC in Europe
Drive electronics	0.14	10	Simplest drive electronics and harness	7	Complexity in electronics and harness to drive BLDC

Overall weighted scores	7.5		6.6	
--------------------------------	------------	--	------------	--

Table 7-2 – Trade-off on actuator technology

It should be noted that this assessment was carried out with particular attention to the driving actuators, but it was already known that the steering actuators would have used the same components. This trade-off indicated that the most promising technology was a combination of brushed motors with planetary gearboxes, although the equivalent brushless option is not very far behind and only has the disadvantage of requiring more sophisticated control electronics, which would be riskier to implement in a cold environment.

The actuator architecture used on the ExoMars Rover is a brushed DC motor with a Harmonic Drive output, which does not score particularly high in this chart. However, if this same trade-off was done for ExoMars, efficiency, temperature tolerance and thermal performance would probably have less weight, since the energy spent driving is not the highest priority for a science mission. Mass would have greater importance to maximise the instrument payload allowance and so would heritage to minimise risk. It follows that this same approach is actually consistent the ExoMars actuator choice, given the different constraints of the mission.

Having established the actuator type, another point worth discussing is the positioning of such actuators on the rover. For the driving actuators the decision is fairly straightforward, since they are typically accommodated inside the wheel hubs and a four-wheeled vehicle needs to maximise traction, requiring one drive actuator in each wheel. For steering, there is a wider design space to explore, as summarised by Table 7-3.

Feature	Weight	All wheels steering		Front wheels steering		Skid steering	
		Score	Justification	Score	Justification	Score	Justification
Mass	0.19	6	4 steering actuators required	8	2 steering actuators required	10	No steering actuators required
Power	0.22	9	Minimum drive power + 4 steering actuators	10	Minimum drive power + 2 steering actuators	4	Drive power increases up to 100% for sharp turns
Manoeuvrability	0.28	10	Maximum manoeuvrability including crabbing	8	Medium manoeuvrability, typical terrestrial vehicle	4	Reduced manoeuvrability, high slippage, low accuracy
Complexity	0.14	7	High mechanical complexity, medium control complexity	8	Medium mechanical complexity, medium control complexity	10	Low mechanical complexity, low control complexity
Heritage	0.17	10	Several planetary rovers, already compatible with ExoMars GNC	6	Apollo LRV, terrestrial applications	5	Lunokhod, terrestrial applications
Overall weighted scores		8.6		8.1		6.2	

Table 7-3 – Trade-off on the steering architecture

The solution with steering actuators on all four corners of the vehicle emerges as the most advantageous, largely because of the need for accurate manoeuvring around the tubes in the depot and the importance of energy efficiency when turning. This architecture is also directly compatible with the GNC algorithms already developed for the ExoMars Rover, which has the same manoeuvring ability.

The option with only front wheels steering follows shortly behind. This would be very similar to the architecture typical of cars and many other terrestrial vehicles. It is characterised

by good energy efficiency if the driving actuators are commanded varying speeds to match their curved trajectories, essentially implementing an electrical differential. However, it lacks the crabbing functionality that allows the rover to move in a straight line in any direction, which is desirable when positioning close to the sample tubes.

The skid steering solution would use the same steering principle of tanks and other compact industrial machinery: wheels (or tracks) on different sides are commanded to different speeds to achieve a heading change. Despite being very simple, it is characterised by considerable energy losses for sharp turns. It also requires the wheels to slip considerably on the ground, causing poor control accuracy and high sinkage in loose soil.

7.1.3 Other critical technologies

As part of the initial architecture definition process, new technologies with low readiness level are identified and proposed for early development activities to reduce the risk associated to them. It has already been mentioned how the general approach to four wheeled locomotion for a robotic rover, while well understood from terrestrial applications, is still relatively unproven in the context of a real mission. From this stemmed an advanced locomotion and GNC breadboard plan, where “breadboard” is a term borrowed from electronic engineering⁵⁹ to identify an early prototype that is representative only of certain aspects of the design. The locomotion breadboard test programme is summarised in Section 7.4.

Other critical technologies requiring advanced development were identified in the high-torque actuators with full planetary gear trains, the rear differential linkage and the compliant wheels. For the latter, the initial research led to NASA proposing their spring tyre technology for use on SFR, as mentioned in Section 7.1.1. This design had already been in development for several years at NASA’s Glenn Research Center (GRC) and so provided a significant reduction in risk. Nonetheless, an accelerated development plan was established to adapt it to the SFR needs.

In section 6.1 is discussed a trade-off study that is clearly not at the level of the locomotion subsystem but rather at campaign level: the SRL architecture study and its impacts on landing and mobility performance. However, while being at much higher level, the implications of this trade on the SFR locomotion are significant and need to be assessed to inform the decision at campaign level. The fact that the paths and the terrain are known allowed to set up an analysis to evaluate how variations of the SFR locomotion subsystem would perform over these paths. The ability to trade locomotion sizing for traverse performance eventually led to the rover baseline that is known today, but different concepts were explored along that path. It is worth noting one in particular, which remained the SFR baseline for considerable time, until SRL ran into serious accommodation issues, and is associated with the maximum traverse performance for the rover. Its design and the thought process behind it are described hereafter.

⁵⁹ An electronic breadboard is a solder-free platform to build semi-permanent circuits prototypes.

7.1.4 The Gullwing design: peak locomotion performance

The most demanding mission scenario ever studied for SFR was one in which the rover could be deployed anywhere up to 15 km away from the sample tube depot. This meant no guarantee of having a “highway” nearby with relatively easy terrain. In other words, SFR would have to be capable of traversing any terrain feature that Perseverance can traverse and possibly more, but in a considerably shorter time. Keeping in mind that Perseverance is a one-tonne, six-wheeled nuclear vehicle, this led to a markedly oversized locomotion subsystem and some peculiar solutions to maximise the traverse performance.

7.1.4.1 Mechanism design

The locomotion design produced in response to these challenges was nicknamed “Gullwing” for its characteristic deployment mechanism. Figure 7-1 offers stowed and deployed views of this design, while Figure 7-2 shows in more detail the kinematics of the deployment mechanism. It is noted that deployment in this configuration happened with the rover still upside down on the lander’s top deck, hence the space of motion is constrained to avoid collisions.

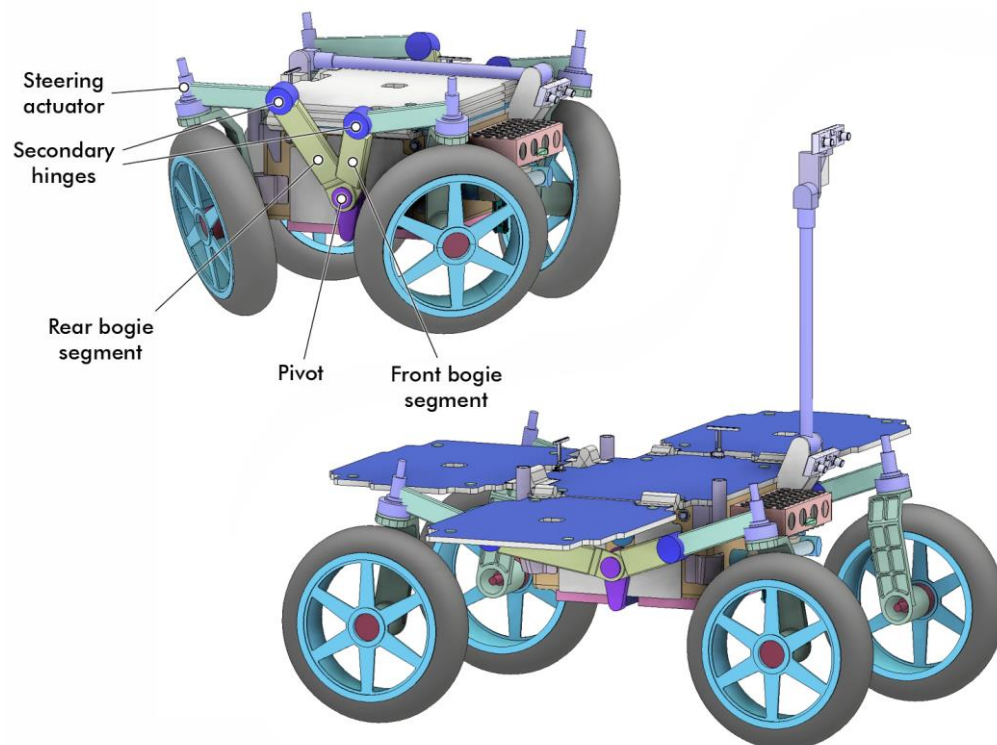


Figure 7-1 – Stowed (top left) and deployed (bottom right) SFR Gullwing design

The Gullwing design already used NASA spring tyres, but of a significantly larger size compared to the final SFR design. The wheels had an outer diameter of 700 mm, larger than that of most common cars. The deployed footprint was 1.6 m in length and 1.2 in width, with a ground clearance of approximately 400 mm. The first, obvious challenge for this concept was to package wheels of that size, arranged over a large rectangular footprint, into a small cylindrical volume. This was achieved through a folding layout that allowed the front and rear segments of each bogie to rotate independently around the central pivot and also pre-

sented a secondary hinge halfway through each segment. In this way, if the wheels are configured to an appropriate steering angle, they can be gathered towards the rover body and secured onto its corners, obtaining a rather compact package (see Figure 7-1).

During deployment, the front and rear bogie segments would rotate in opposite directions around the pivot axis, both disconnected from the differential, which, at this stage, is still restrained by a dedicated differential lock. The rotations around the secondary hinges can be coupled to the main one through tie rods, thus creating a four-bar linkage on each bogie as shown in Figure 7-2. This mechanisation would make the complete deployment achievable with only one actuator per side.

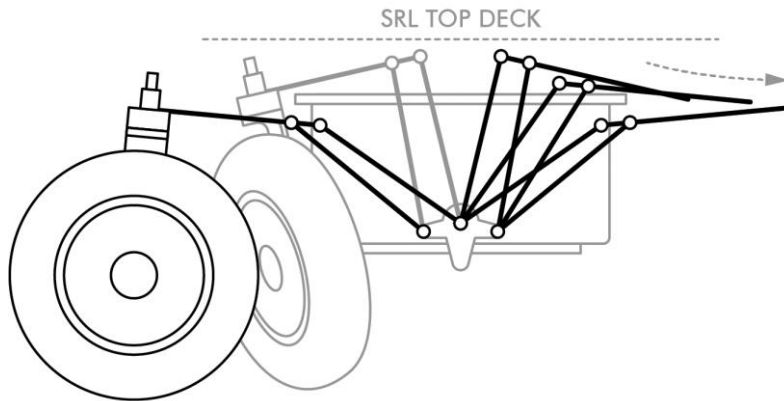


Figure 7-2 – Gullwing deployment kinematics with four-bar linkages

Once reached the deployed position, latching mechanisms on the pivot would secure together the two bogie halves and the connection to differential linkage, creating one single solid body that can oscillate freely once the differential is unlocked. The design of a pivot assembly to achieve this kind of functionality is not trivial. A preliminary solution is shown in Figure 7-3, while Figure 7-4 provides a detailed cross-section view of the assembly.

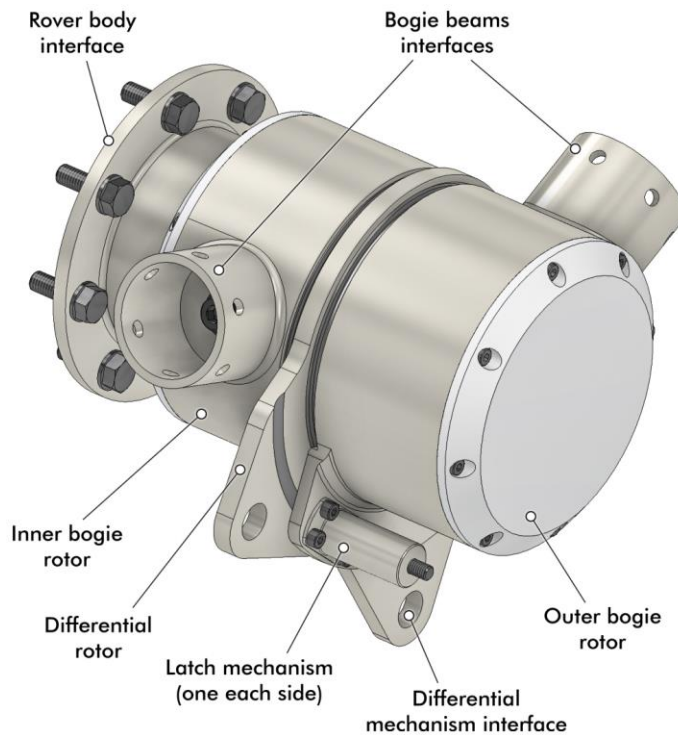


Figure 7-3 – Gullwing pivot assembly

The assembly can be subdivided into four main bodies:

- **Pivot shaft.** Stationary and mounted on the rover body, it supports the other rotating elements and carries mobility loads once on the surface.
- **Inner bogie rotor.** Attached to one end of the inner torsion spring, it rotates independently from the other components during deployment, then latches with the differential and outer bogie rotors. It provides the mechanical interface to one bogie segment.
- **Outer bogie rotor.** Attached to the other end of the inner torsion spring, it rotates independently from the other components during deployment, then latches with the differential and outer bogie rotors. It provides the mechanical interface to the other bogie segment and carries the latching mechanisms.
- **Differential rotor.** Stationary during deployment, then latches with the bogie rotors to move as a single body once a central differential lock is released. It connects to the differential mechanism located under the vehicle.

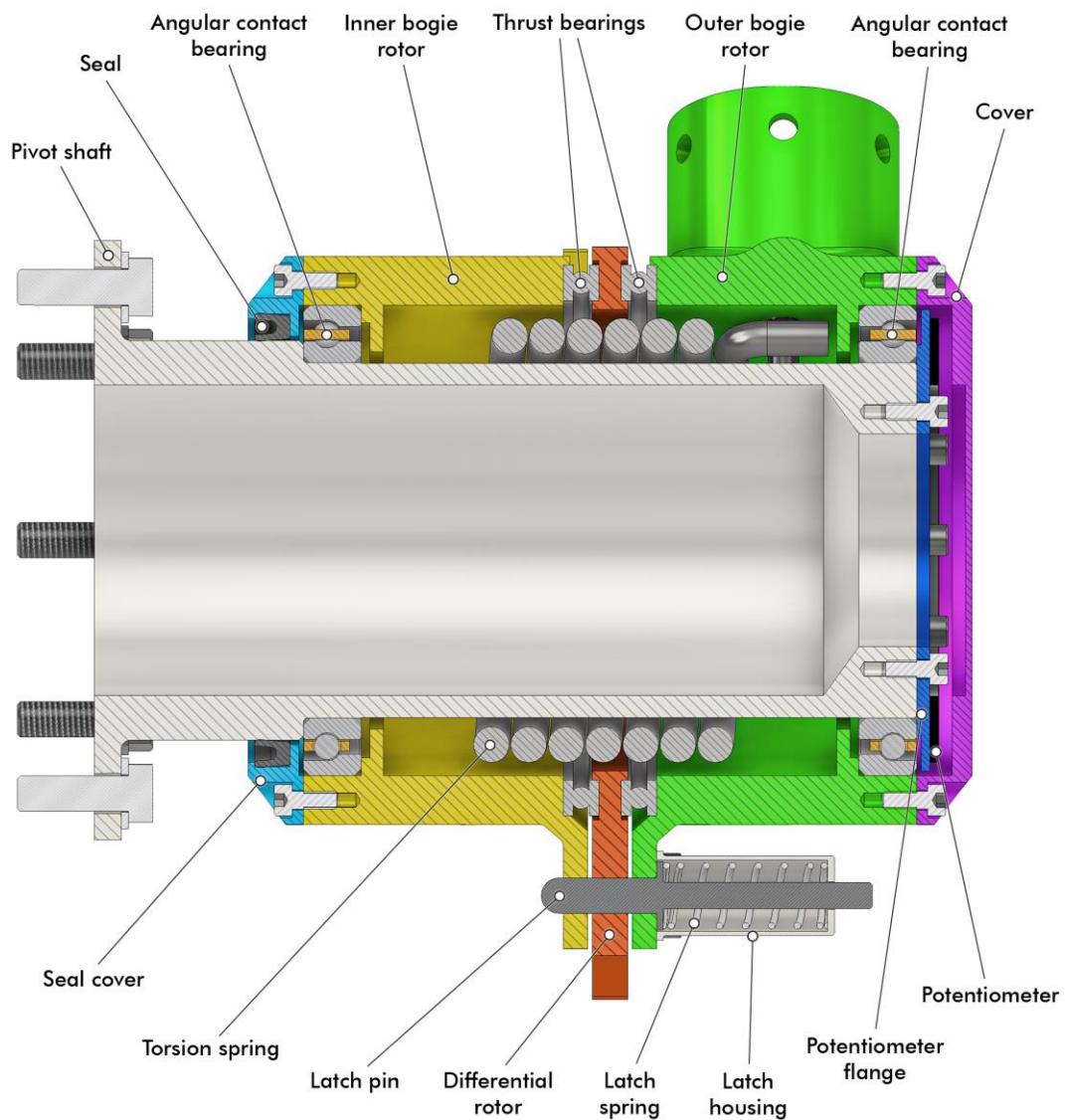


Figure 7-4 – Cross section of the Gullwing pivot

It can be seen in the cross section in Figure 7-4 above how a large torsion spring is accommodated inside the assembly, between the pivot shaft and the rotating elements. This spring

provides the only deployment actuation necessary to push the bogie rotors in opposite directions and unfold the Gullwing mechanism. The spring drives the two rotors by pushing pins located at the interface points with the bogie beams. The differential rotor is not connected to the spring and interfaces with the bogie rotors through thrust bearings that allow relative motion. These bearings are used only for the deployment motion and do not move again once the latches have engaged. The oscillation of the pivot during roving is enabled by the angular contact bearings between the bogie rotors and the pivot shaft.

Latching is provided by two assemblies mounted onto the outer bogie rotor. Each of them contains a pin preloaded by a spring. The pin runs against a solid-lubricated groove on the differential rotor until the outer bogie rotor reaches the deployed position, where the pin encounters a corresponding hole and is pushed through it by the spring. The same process is repeated for the inner bogie rotor. Once the pins are fully engaged, the three rotors will behave as a rigid assembly, able to transfer torques between the two bogie segments and the differential. This assembly forms the pivot rotor of the rocker arm suspension. A potentiometer is placed between the pivot shaft (stator) and the outer bogie rotor to measure the angular position of the suspension during traverse. Lastly, a Teflon seal protects the only rotary interface remaining exposed after latching to prevent ingress dust in the mechanism.

It should be noted that this early design does not yet include end stop features and means to regulate or absorb the energy during deployment. It has also not been subject to any mass optimisation process, so the metal work does not reflect an optimised flight design. The choice of actuator is strongly driven by the torque required to overcome the friction in the rotary joints in the deployable mechanism, which has been only preliminarily investigated at this stage of the design. If this torque becomes too large, it might be impractical to provide it with a spring. In that case, an electric actuator would have to be fitted into the assembly so that its rotor and stator can drive the two bogie rotors in opposite directions.

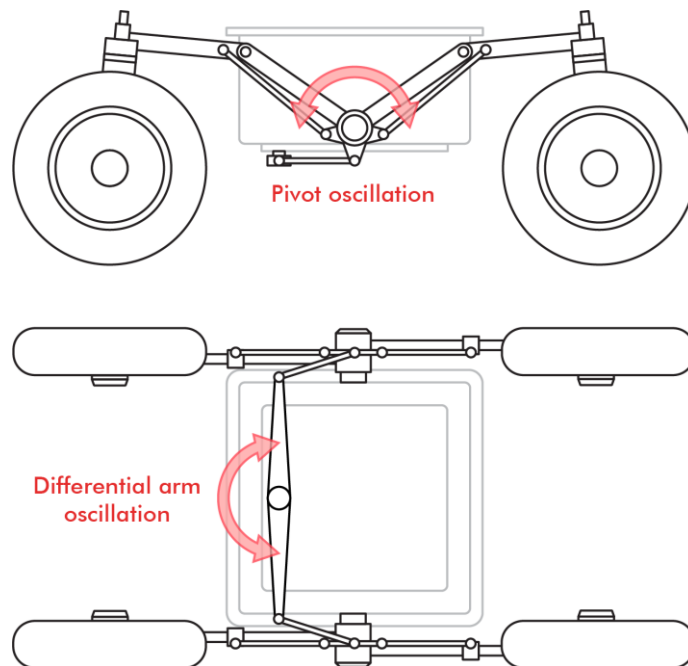


Figure 7-5 – Possible differential layout on the rover underbelly

In this deployment scheme, the differential mechanism cannot be connected directly to the bogie segments, as that would impede their free motion during deployment. The differential

must therefore pick up the motion from its dedicated rotor. A proposed mechanical implementation is based on a differential arm driven by tie-rods mounted to the vehicle's underbelly. Figure 7-5 provides a scheme of this layout. The purpose of this linkage is to constrain the rotation of the two bogies to be equal and opposite, thus providing the pitch-averaging behaviour that is characteristic of this suspension. Its working principle is presented in detail in Section 7.2.1, where is described a differential mechanism that operates in a different plane but provides the exact same functionality: the rotation of a bogie causes the rotation of the differential arm, which causes the opposite rotation of the other bogie. The Gullwing differential arm oscillates in a plane that is parallel to the rover's underbelly, while the differential arm in Section 7.2.1 rotates in a plane that is parallel to the rover's rear face.

7.1.4.2 Terrain scenario

It is of particular interest to discuss the terrain features and the analysis process that led to this configuration, as they offer a striking example of how the design of a rover platform can respond to well-defined terrain challenges. The sizing scenario for the Gullwing SFR was identified as a 250-mm-tall step obstacle wider than the rover that would have to be climbed with left and right wheels at the same time, while going upslope on a 10° incline. This situation is a geometric interpretation of a geologic environment called "fractured terrain", which indicates an area where plates of bedrock (typically in the order of metres in size) have been broken and dislocated over time, giving rise to a rugged rocky ground with uneven blocks of bedrock, cracks and crevasses. Figure 7-6 shows an example of this type of terrain in a rock formation named "Kimberley" and imaged by NASA's Curiosity rover at the base of Mount Sharp. The height of the step features in the foreground is comparable to those considered for SFR.



Figure 7-6 – Example of fractured terrain imaged by NASA's Curiosity rover (credit: NASA / JPL-Caltech)

To climb these challenging obstacles, the wheel diameter was maximised to the largest size that could be realistically accommodated inside the stowed volume. This is because larger wheels engage with obstacles on a lower portion of their circumference, reducing the tangential traction force that is required to lift the vehicle’s weight and surmount the obstacle. This tangential force between tyre and obstacle is identified as R_T in Figure 7-7. The illustration helps to visualise the problem by depicting wheels of different sizes at the moment in which they lose contact with the ground and begin to climb the obstacle. Each of these instances can be considered a view of one of the two wheels that are encountering the step feature described above.

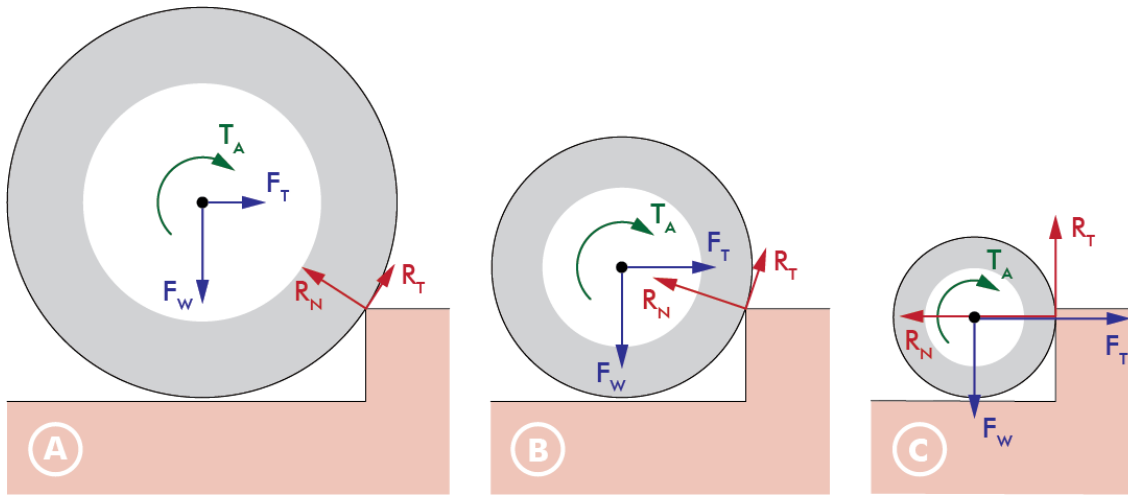


Figure 7-7 – Obstacle climbing forces on wheels of different sizes

The vectors in the figure represent the loads applied to the wheel at the actuator interface and the obstacle contact point (there are no other loads in this plane since the wheel has already left the ground in this illustration). T_A is the torque being provided by the driving actuator, F_W is the force due to the weight of the vehicle (which can be considered fixed), F_T is the force due to the thrust of the other wheels, R_N is the reaction force of the obstacle normal to the wheel surface and R_T is the reaction force of the obstacle tangential to the wheel surface. The magnitude of this latter vector is tied to that of R_N by a correlation similar to that of static friction:

$$R_T = \mu_{eq} R_N$$

Here μ_{eq} is an equivalent coefficient of friction to represent the interaction between wheel and obstacle, which in reality is much more complex and influenced by local deformation, geometric engagement and dynamic effects. This coefficient varies significantly depending on obstacle engagement by the wheel. Testing of SFR prototypes (discussed in Section 7.4) suggests that a typical value can be taken as $\mu_{eq} = 0.8$.

To succeed in climbing, the vertical components of R_T and R_N must counteract the weight force. As shown in Figure 7-7, for a wheel radius much larger than the obstacle height (A), both vectors have significant vertical components and the climb can be achieved more easily than with a smaller wheel radius. A limit case is found if the wheel radius is smaller than the obstacle height (C): in this situation R_T is vertical and must be equal to the weight force to surmount the obstacle. Since R_T is tied to R_N as noted above, R_N must be increased to produce sufficient vertical force. However, R_N is simply driven by the thrust produced by the other wheels of the vehicle, and in this case, $R_N = F_T$. For a four-wheeled vehicle, it is unlikely that

the wheels remaining on the ground can produce sufficient thrust to overcome this situation, especially if there are only two, therefore the wheel would fail to climb. Incidentally, six-wheeled vehicles can succeed in this situation and climb obstacles well above the wheel radius, as discussed in Section 4.4.3 for the ExoMars rover.

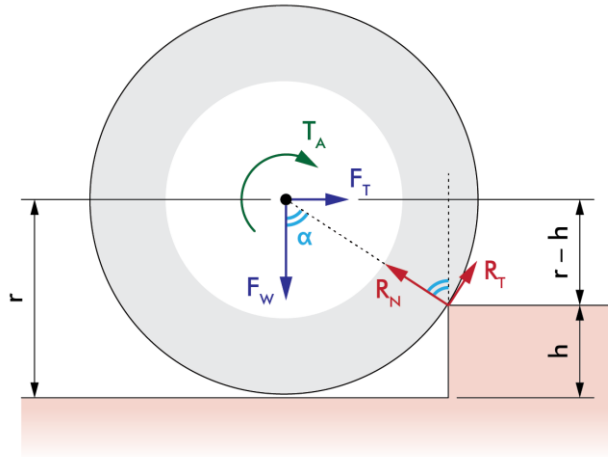


Figure 7-8 – Obstacle climbing forces with annotated geometry

Taking reference from Figure 7-8, it is straightforward to write the equilibrium equations for a generic obstacle climbing scenario as follows:

$$\begin{cases} R_N \cos(\alpha) + R_T \cos\left(\frac{\pi}{2} - \alpha\right) = F_W \\ R_N \sin(\alpha) - R_T \sin\left(\frac{\pi}{2} - \alpha\right) = F_T \end{cases}$$

The first equation represents the vertical equilibrium of the wheel and the second one the horizontal equilibrium. Remembering that $R_T = \mu_{eq} R_N$, these can be rewritten as:

$$\begin{cases} R_N [\cos(\alpha) + \mu_{eq} \sin(\alpha)] = F_W \\ R_N [\sin(\alpha) - \mu_{eq} \cos(\alpha)] = F_T \end{cases}$$

which provide an expression of the required thrust to push the wheel up the obstacle and overcome the weight force F_W :

$$F_T = \frac{\sin(\alpha) - \mu_{eq} \cos(\alpha)}{\cos(\alpha) + \mu_{eq} \sin(\alpha)} F_W$$

For a given vehicle and attitude, the weight force of the wheel is constant. The equivalent coefficient of friction between wheel and obstacle μ_{eq} is a characteristic of the system, so the required thrust force is a function of the angle α :

$$F_T = f(\alpha) F_W$$

The values of α that are meaningful for this analysis are those in the interval between 0 and $\pi/2$, where the function follows the profile shown in Figure 7-9. It can be clearly noted how this is a monotonically increasing function of α , confirming that, as described earlier, when the wheel becomes smaller (or the obstacle larger) the required thrust increases. For $\alpha = \pi/2$, the height of the obstacle is equal to the radius of the wheel (or greater, in fact, because the force distribution does not change anymore). At that point the required thrust is maximum and equal to F_W/μ_{eq} , which is the normal load necessary to produce a tangential force, R_T , of equal magnitude to the weight force, F_T .

As α decreases (i.e., the obstacle becomes smaller, or the wheel larger), the required thrust becomes negative. This means that the wheel is able to climb the obstacle thanks to its own traction alone, without additional push from the other wheels. The modulus of F_T is then the amount of drag force that the wheel can overcome whilst climbing the obstacle. In the limit case where $\alpha = 0$, the wheel, which is simply rolling on flat ground, can produce a horizontal force equal to $\mu_{eq} F_W$.

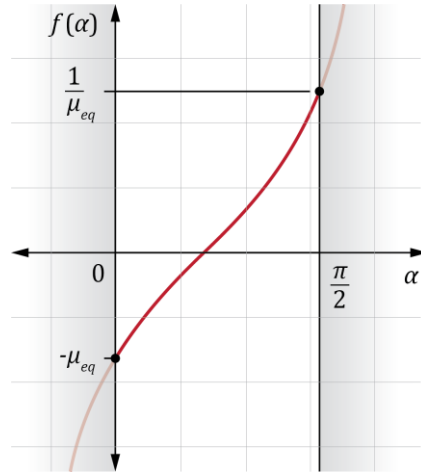


Figure 7-9 – Plot of the function $f(\alpha)$

Lastly, the angle α can be expressed as a function of the ratio h/r as follows:

$$\alpha = \cos^{-1}\left(\frac{r-h}{r}\right) = \cos^{-1}\left(1 - \frac{h}{r}\right)$$

This provides a generic method of obtaining a first-order approximation of the thrust required to climb a certain obstacle with a certain wheel size, given the friction properties and the weight of the vehicle. Vice versa, it allows to establish the wheel size required to surmount the obstacle if the thrust available can be estimated by other means (e.g., through characterisation or simulation of the wheel traction on the substrate soil).

From the considerations above, it is clear how it became necessary to maximise the wheel size for this high-performance version of SFR. Nevertheless, multibody analysis of this configuration (using the model described in Section 7.3.1) showed that, while the 700 mm diameter was more than sufficient to bring the front wheels above the step feature, the rear ones would consistently struggle to climb, especially in an upslope case. Closer inspection of the load distribution identified two primary causes for this behaviour:

1. The slope and the step under the front wheels cause the rover body to pitch upwards, transferring weight from the front to the rear wheels. Using again Figure 7-7 as a reference, this means that the rear wheels will need a greater vertical component in the obstacle reaction forces to climb and, at the same time, the front wheels will have less normal force to produce the traction required to increase those rear reaction forces.
2. A less obvious contribution comes from the wheel driving torques, whose reaction tends to rotate the bogie in favour of the climb for the front wheels, while it opposes the climb for the rear ones, giving rise to another load to overcome. For a difficult obstacle climb, the driving torques can be significant. Figure 7-10 provides a qualitative understanding of this behaviour.

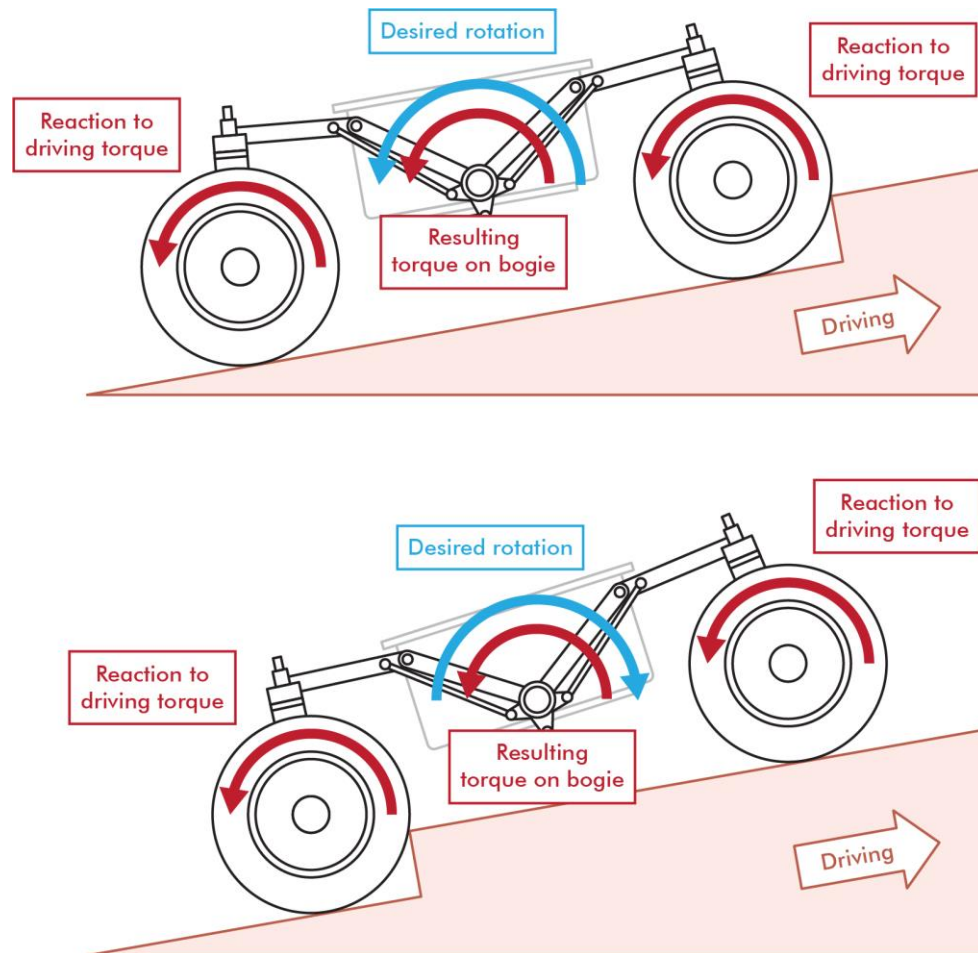


Figure 7-10 – Torques on a bogie for front and rear wheel climbing

These considerations hold true in general, not only for this particular step obstacle, and they represent an intrinsic property of the rocker arm suspension: the rear wheels will be, in most cases, the limiting factor for obstacle climbing performance. To address this limitation and equilibrate the climbing performance between front and rear wheels, it was decided to adopt a slightly unusual solution for planetary rovers: offset the Centre Of Gravity (COG) towards the front of the vehicle. This puts more weight on the front wheels, increasing traction, and relieves the rear wheels, reducing the resistance to climbing.

By observing closely Figure 7-1, it can be seen how the rear segments of the bogies are longer than the front ones. The COG achieved in this way is biased forward to 57% of the wheelbase (whereas normally it would be around 50%). This is an unusual configuration because it is typically desirable for planetary rovers to have approximately symmetric mobility layouts, so that the performance in every direction is similar and the vehicle can always reverse out of a dead end. For SFR, it was accepted that the vehicle would spend the vast majority of its time driving forward and that a point turn might be necessary to back out of some extreme situations.

The considerations made so far implicitly assume that the loads and motions occur predominantly in a plane, in particular, a vertical plane parallel to the vehicle's velocity vector. This is true in first approximation for an ideal case where left and right wheels encounter the step exactly at the same time, but it becomes less relevant for more realistic situations

where the obstacle is attacked at an angle or is not present at all on one side. In these situations, the lateral behaviour of the system becomes greatly important and it usually requires more sophisticated analysis than what is described here. More advanced traverse modelling was developed to cover these needs and is discussed in Section 7.3.

While multibody dynamic analysis is very accurate in predicting the behaviour of the vehicle, several unknowns remain in the interaction between wheel and terrain, also referred to as “terramechanics”. This area relies significantly on empirical knowledge and is very sensitive to the wheel design and terrain properties. To improve the understanding of these phenomena, it is essential to carry out tests as early as possible. In a fortunate coincidence, a test vehicle with the right geometry and wheel size was available at NASA GRC from a previous project: the Scarab rover, shown in Figure 7-11 (pictured while performing other tests, not related to SFR). This platform can be reconfigured to achieve different footprints and COG locations, and has a pitch-averaging suspension similar to that of SFR. Scarab is much heavier than SFR, but its tyres were modified to produce a similar response to the intended SFR design, so that the results would be reasonably scalable for the design under consideration.



Figure 7-11 – Scarab rover undergoing testing at NASA’s Glenn Research Center (credit: NASA / GRC / N. S. Kilkenny)

A testbed representing the rocky step feature was assembled at GRC with materials readily available and numerous climbing attempts were performed with Scarab in subsequent iterations. The availability of this platform has been instrumental in defining the SFR architecture and understanding its interaction with the terrain early in the development. Without this contribution, the vehicle’s design would have remained undefined for much longer, the spring mesh tyre technology would have been considered a major risk, and possibly the Sample Fetch Rover would not have converged onto the distinctive architecture that characterises it today.

The use of Scarab enabled a rapid design iteration process, where a new rover architecture would be defined and evaluated in a simulation environment, then the geometry and weight distribution of Scarab would be modified to reproduce the same conditions and tests carried out to demonstrate the performance in the real world. This approach also improved the model's fidelity to a great extent, providing an incremental validation at each iteration.

Eventually, the high-performance Gullwing design had to give way to a more compact version of SFR due to a reduction in the volume available on the lander. Orbital imagery was reassessed and it was possible to identify a set of routes that did not include areas of fractured terrain. These are the so-called "green pathways" in Figure 5-7, which are expected to avoid large step obstacles. The SRL landing accuracy was improved to ensure that SFR would be delivered in close proximity to one of these pathways.

Nevertheless, the new SFR baseline has its foundation in the knowledge acquired during this intense period of testing and redesigning. Furthermore, if it was possible to justify the reduction in traverse performance for the campaign trade-offs described in Section 6.1, it was mostly thanks to the remarkable improvements in the simulations enabled by testing with Scarab.

7.2 Design of the locomotion mechanisms

The following paragraphs describe the design of the SFR locomotion mechanisms as they are today, after all the trade-offs and preliminary studies. The prominent electromechanical system in this area is the Fetch Actuator System for Traverse (FAST). FAST comprises the rocker arm suspension, actuators, HDRMs and associated mechanisms. The wheels are not included in its perimeter since they are customer-furnished items built by NASA. Nevertheless, from an engineering point of view, they form an integral part of the locomotion subsystem and therefore are discussed in these pages. FAST is developed by MDA in Canada, which has been supporting the SFR project since its early phases. The detailed FAST design, the locomotion analysis and testing have been carried out by MDA as part of the FAST study contract. Table 7-4 provides a summary of the organisations involved in the development of the SFR locomotion and their role. Figure 7-12 offers a general view of the assembly with its key elements identified and a semi-transparent rover body for context.

Organisation	Role
ESA	End customer, partner with NASA as part of MSR
Airbus	Prime contractor for SFR, including GNC and high-level mobility performance
MDA	Contractor for FAST
NASA GRC	Provider of superelastic wheels in partnership with ESA
Maxon	Supplier of actuators for FAST

Table 7-4 – Main organisations and their roles in the development of the SFR locomotion

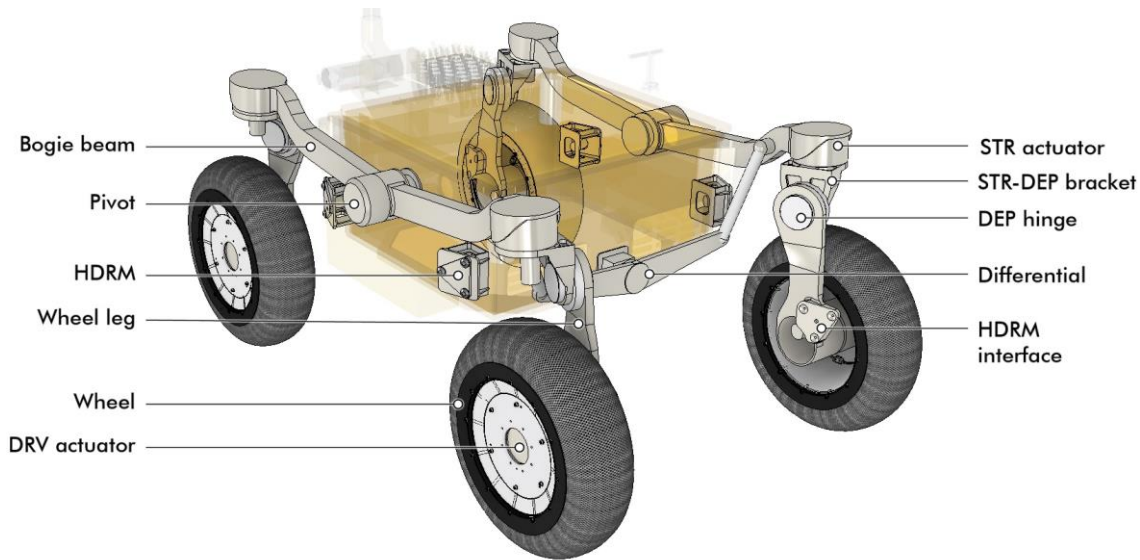


Figure 7-12 – FAST overview (rear left wheel in the foreground)

These sections will aim at providing an overview of FAST, rarely descending into the detailed engineering, which, on the threshold of its Preliminary Design Review (PDR), already extends over thousands of pages. The focus will be on the system architecture, the key technologies and the areas that were co-engineered with Airbus as prime contractor and, therefore, are of greater relevance to this PhD.

The current SFR baseline, for what concerns locomotion, corresponds to last iteration discussed in Section 6.1: four spring tyres, 550 mm in diameter, arranged over a ground contact footprint 1.3 m long and 1 m wide. This layout is more compact than that of the Gullwing design, discussed in Section 7.1.4, and it does not necessitate folding of the bogie beam to fit in the launch envelope. This enabled simplification of the deployment mechanism, which only relies on four sprung hinges (identified as “DEP hinges” in Figure 7-12), further discussed in Section 7.2.3.

The suspension is sized to climb one-sided obstacles up to 295 mm and slopes up to 20°, whilst maintaining a vehicle speed of 67 mm/s, or 0.24 km/h. FAST is the electro-mechanical system responsible for providing this capability and is one of the largest assemblies of the rover. Its mass is 45 kg without wheels and it takes considerable volume around the spacecraft, contributing to its unique appearance. The design of its major components is discussed hereafter.

7.2.1 Rocker arm suspension

The primary functions of the rover’s suspension are to provide compliance to asperities in the terrain and to distribute the load on the four wheels as evenly as possible. Any vehicle with more than three ground contact points requires additional degrees of freedom to ensure that all wheels are contacting the surface. On a four-wheeled rover one additional degree of freedom is sufficient to achieve this, so the SFR suspension does exactly that.

As anticipated in Section 4.2.1, two oscillating beams are connected to the sides of the rover body through freely-rotating pivots. These beams are called “rockers” or “bogies”. The for-

mer term is the more academically precise, especially in relation to other similar suspensions⁶⁰, however, the latter is the more common and used throughout the SFR project. If the two bogies were free to rotate independently from each other, it would imply the addition of two degrees of freedom, i.e., one more than required. In practical terms, that would leave the rover body free to pitch around the pivots, leading to capsizing if the centre of gravity was higher than the pivots axis and undesirable oscillations if it was lower. To remove this degree of freedom, it would be sufficient to leave one bogie free and fix the other two wheels onto the rover, but that would create an unbalanced locomotion layout where the side without articulation would struggle to climb obstacles. To address this issue, the differential linkage is added to combine the rotations of the two bogies in such a manner that, if one rotates in one direction with respect to the rover body, the other one is imposed an equal rotation in the opposite direction, thus keeping the rover body at an average pitch angle between the two.

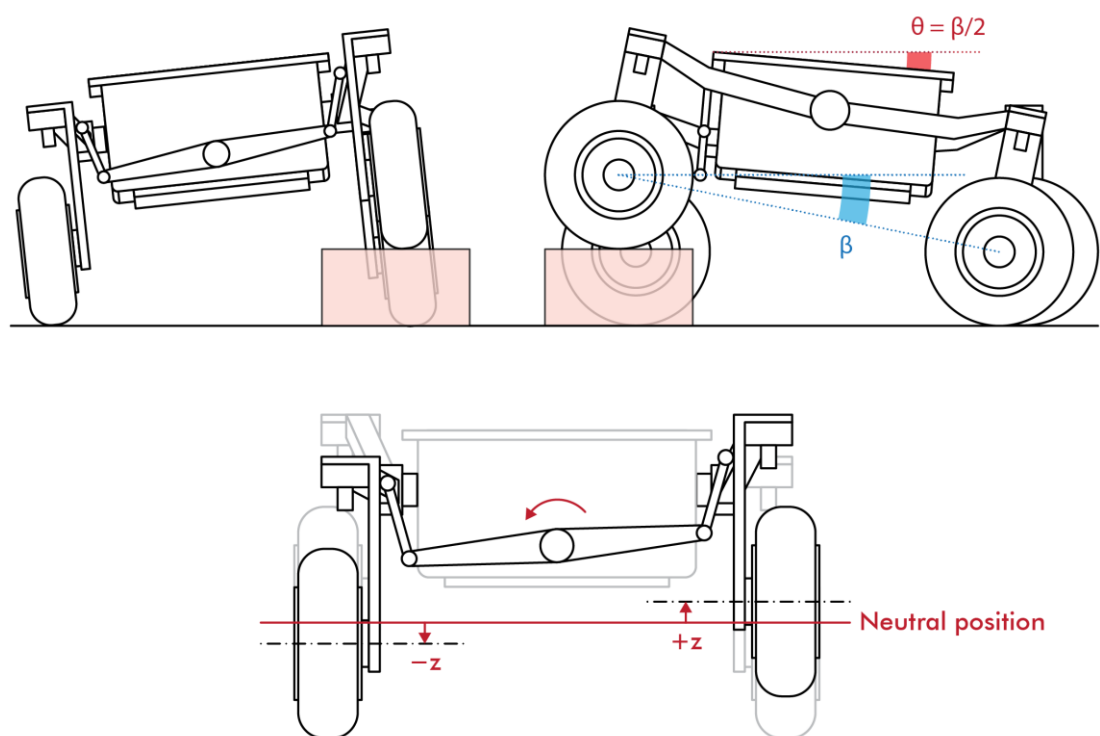


Figure 7-13 – Kinematics of the FAST differential in presence of an obstacle: rear view (top left), right view (top right), orthogonal view of the rear face (bottom)

Figure 7-13 offers a kinematic scheme of how the differential produces the pitch-averaging behaviour that makes this suspension particularly effective. It can be observed how, in this example, an obstacle lifts the rear right wheel by a certain amount. This pulls up the corresponding end of the differential arm through a tie-rod, causing the other end to lower. Such action forces the wheel on the other side to descend by the same amount. The system settles on an equilibrium configuration where all wheels are in contact with the surface and the rover body pitch angle is half of that of the bogie on the obstacle (the pitch of the other bogie

⁶⁰ The rocker bogie suspension makes a distinction between the two terms, where the rocker is the member hinging on the rover body and the bogie is the one connected to rocker and carrying two wheels on its ends. For the rocker arm suspension, this distinction is no longer relevant as there is only one oscillating element per side.

is zero since it is on flat ground). It should be noted that there are simplifications in this description, in particular, three-dimensional contributions outside the main planes of motion are neglected and so are elastic deflection and change of contact patch geometry. These constitute, however, contributions an order of magnitude smaller than the displacements due to the differential action.

7.2.1.1 Sizing the suspension for the terrain

It is natural to think about obstacle climbing as the key sizing factor for the FAST suspension. While that is certainly a major design driver, it is not the only defining parameter of the system. The major design drivers coming from the traverse terrain are the following:

- **Obstacle size.** Strong driver for wheel diameter and traction (both on the ground and on the obstacle edge). Also defines suspension travel and ground clearance to avoid collision between the obstacle and the rover body.
- **Slope angle.** It defines the minimum angle⁶¹ at which the rover must remain stable without tipping over. This drives the footprint and the maximum height of the centre of gravity. Also contributes to determine the traction required for steep slopes.
- **Substrate material.** In combination with the slopes and obstacles above, it defines the traction required to succeed in the climb and the wheel contact patch to avoid sinking in loose soil.
- **Impacts and blocked wheel loads.** The impacts when slipping off rocks and other mobility load cases where wheels are trapped by various terrain features contribute to sizing the strength and stiffness of all the mechanical elements. In some cases, these are already enveloped by launch loads.

Since SFR moved away from the Gullwing design and the fractured terrain described in Section 7.1.4, the sizing obstacle is not a step feature anymore, but rather a single-sided obstacle. This represents one of the typical scattered rocks present almost everywhere on Mars to a varying degree, produced by meteoritic impacts and weathering (see Figure 3-2, for example). These rocks usually follow statistical distributions where the frequency of rocks decreases with their size. Such rock coverage can be inferred from orbital imagery and comparison with in-situ data from previous missions. A well-known method to approximate rock distributions on Mars is Golombek's model [61]. The model defines the Cumulative Fractional Area (CFA) covered by rocks of diameter D or larger as a function of D :

$$CFA_k(D) = k e^{-q(k) D}$$

where k is the fraction of the total area covered by all rocks (a characteristic of local terrain morphology) and the parameter $q(k)$, which governs how rapidly the fraction of the total area covered by rocks decreases with increasing diameter, is approximated by:

$$q(k) = 1.79 + \frac{0.152}{k}$$

⁶¹ The minimum stability angle is usually higher than the slope angle to take into account local roughness, wheel sinkage and deflection, dynamic oscillations and margin. As a rough order of magnitude, the minimum stability angle is typically 10° greater than the maximum slope that the vehicle can encounter.

These equations produce the graphs shown in Figure 7-14 for different values of k , superimposed with in-situ measurements from various Mars missions [62].

As mentioned, the parameter k is a characteristic of the terrain and can be inferred from orbit. This allows to produce maps of the mission site where random rock distributions generated from Golombek's model are superimposed to the terrain. Once the obstacle climbing ability of the vehicle is set, a statistical analysis can be performed on these maps, where the rover follows multiple paths, driving around the rocks that it cannot climb. This calculates what percentage of paths are successful and what is the distance (or time) penalty associated with avoiding obstacles. This process was used to decide an appropriate obstacle climbing ability for SFR. Following some iterations, the analysis showed that, if the rover could overcome obstacles up to 275 mm high (a wheel radius), it would always be able to find a path on the maps and the obstacle avoidance penalty would be generally satisfactory.

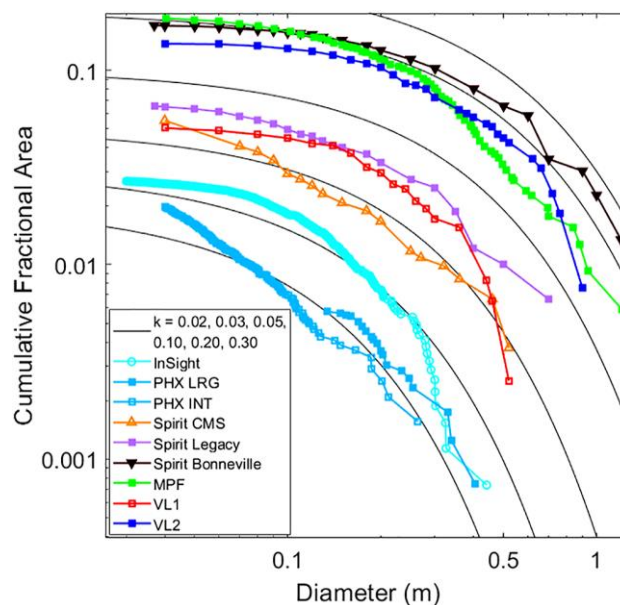


Figure 7-14 – Golombek's CFA curves and in-situ measurements (credit: M. Golombek)

It is reminded, once again, that these are compact rocks that encounter only one wheel at a time (the statistical distribution makes an encounter with two large rocks at the same time extremely unlikely). Such obstacles are more benign than the wide steps described previously and are the reason why it was possible to reduce the size of the SFR locomotion subsystem. FAST remains capable of traversing step features and crevasses, although of smaller size.

It must also be clarified that the obstacle performance of a vehicle cannot be effectively summarised by one rock size: while on flat, compact ground the rover would climb obstacles 275 mm high with ease, on slopes or soft soils its climbing power would decrease. The result of this reasoning is a mapping of obstacle size to slopes and substrates, whose analysis is further discussed in Section 7.3.1.

Once the obstacle size is known, it can be used to size the mechanical capability of the suspension and the ground clearance that it must provide, however, some further steps need to be considered for these. The rover's GNC system is responsible of autonomously identifying and classifying obstacles based on NavCam stereo imagery. If, on flat ground, an obstacle is measured as higher than 275 mm, it would be marked as non-negotiable and the

vehicle would steer clear of it. This process is unavoidably affected by errors (due to image quality, illumination, DEM reconstruction, etc.), amounting to a total of 20 mm in the worst case. It derives that an obstacle could be up to 20 mm higher or lower than the measured value, so a rock estimated as 275 mm high – and therefore traversable – by GNC could be up to 295 mm high. For this reason, the sizing obstacle for FAST is always 20 mm higher than the targeted obstacle for that particular terrain configuration.

When sizing the ground clearance, other contributions need to be taken into account in addition to the GNC error: the possible sinkage of wheels in the soil, the deflection of the whole system and appropriate margin. The result is that, to clear a rock that is up to 295 mm high with GNC error included, the unloaded system must have a ground clearance of 375 mm⁶². This approach is summarised by Figure 7-15.

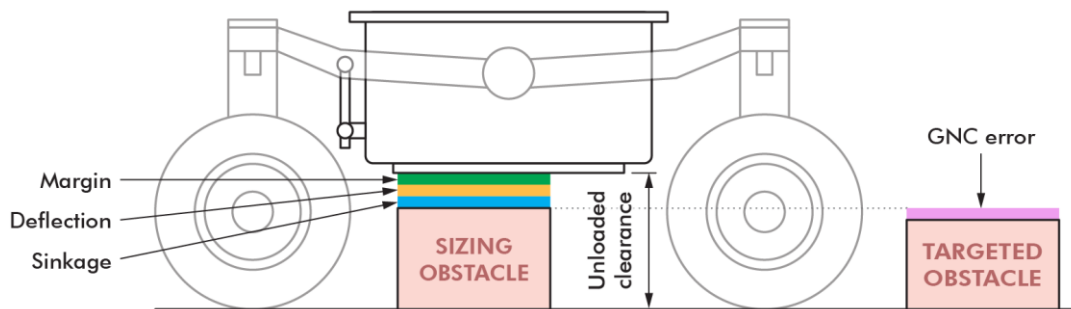


Figure 7-15 – Process to size obstacle climbing ability and ground clearance

One last terrain aspect worth dwelling upon for the sizing of the FAST suspension is the slope capability. From the geography of Jezero Crater, it is known that SFR will have to climb inclines up to 20°. As always, the actual climbing performance is also dependent on the terrain, which, if composed of dune sand, might lose cohesion well before that angle and cause the rover to slip without climbing.

Considering the 20° requirement, adding potential roughness and dynamic effects, it is evident how slope negotiation is another major driver for the suspension design. SFR must have a rather high stability angle to navigate this terrain, which means a large footprint and a low centre of gravity. However, the footprint is constrained by the stowed volume and the COG position is in direct conflict with the ground clearance requirement, which demands a higher rover body. To support the careful balancing act between these two requirements, a static stability analysis was carried out with a simplified version of the multibody model of the rover described in Section 7.3.1, which led to some notable observations.

The first finding was that the rocker arm suspension can have a minimum in stability when tilting along its diagonal direction. This appeared counterintuitive, since it would be reasonable to expect that an object with a rectangular footprint could tolerate a greater tilt along its diagonals than along the directions of its sides. Nonetheless, the analysis for SFR was showing that the rover would tip over at a smaller inclination when the local gradient of the ground⁶³ was aligned with the diagonal direction of its footprint.

⁶² This is the CAD-measured vertical distance between the rover belly pan and the lowest point of the tyre.

⁶³ Here the gradient of the ground indicates the vector of the partial derivatives of the function of the plane that describes the height of the ground. Geometrically, it is simply the vector that points in the direction of greater change of height, i.e. directly upslope.

Further study of the load distribution identified the cause of this behaviour in the fact that an articulated suspension is not a rigid rectangular surface, but it allows the wheels to move in such a way that one can lose contact with the ground. If, for example, the front right wheel was located downslope, it would be loaded with a greater portion of the vehicle's weight than the other ones. The reaction force would tend to raise such wheel with respect to the rover body.

Considering the behaviour of the differential described by Figure 7-13, to a rotation of a bogie corresponds a counter-rotation of the other one, so, if the front right wheel (downslope wheel) is pushed upwards with respect to the rover body, then the rear left wheel (upslope wheel) also tends to move upwards in the same reference frame. This motion is opposed by the ground reaction forces on the front left and rear right wheels. However, as the slope angle increases, these two wheels become less loaded and the wheel downslope becomes more loaded. This eventually initiates a rotation of the bogie that lifts the wheel located upslope and causes the vehicle to lose stability. Such phenomenon is illustrated by Figure 7-16.

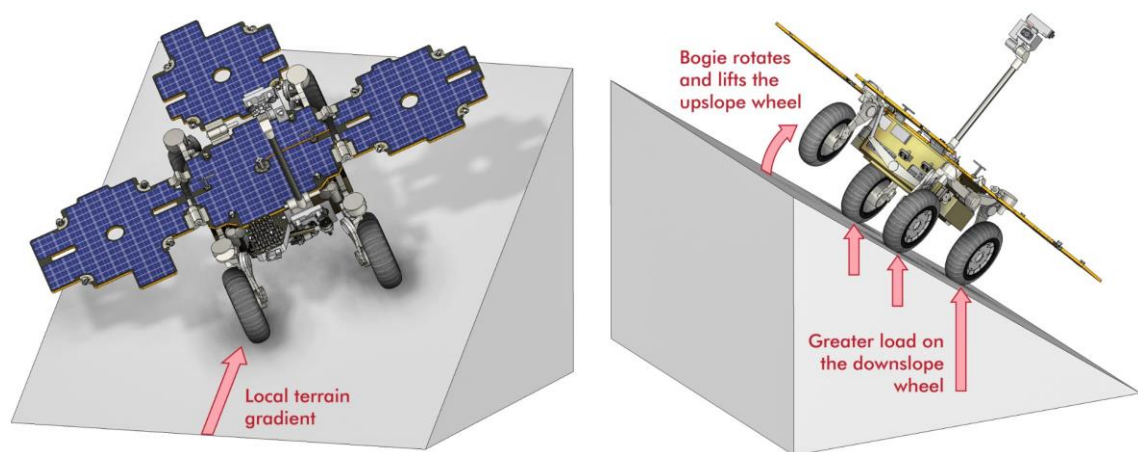


Figure 7-16 - CAD visualisation of a diagonal slope case

Another remarkable observation made through this analysis was that the position of the pivots has a noticeable influence on the behaviour just described. In particular, if the pivots are located above the centre of gravity of the rover body, its weight will produce a stabilising torque around the pivot that opposes the tipping over motion. If the pivots are high enough, this action becomes sufficient to neutralise the diagonal weakness of the rocker arm suspension, which is why SFR has its pivots located high up, close to the top deck.

If it was possible to identify this solution it was only thanks to the simulation of the complete suspension mechanics for various slope heading directions. The approach used in this analysis is essentially to take a scenario similar to that depicted in Figure 7-16 and rotate the vehicle around its vertical axis, so that the heading direction with regards to the gradient of the ground changes in discrete steps. At each rotation step, the static equilibrium of the suspension is solved for increasing inclination until loss of contact with the ground is detected, indicating tip-over.

The outcome of this analysis for the final SFR architecture (with raised pivots) is shown in Figure 7-17. An uncertainty is added to account for unknowns in the COG location (contributing approximately $\pm 1^\circ$ to the stability angle) and tyre deflection (contributing approximately -2° to the stability angle) at the time of the analysis. This leads to a minimum stability

angle of 35° in the lateral direction (corresponding to pure rolling of the vehicle) and 44° in the longitudinal direction (corresponding to pure pitching of the vehicle).

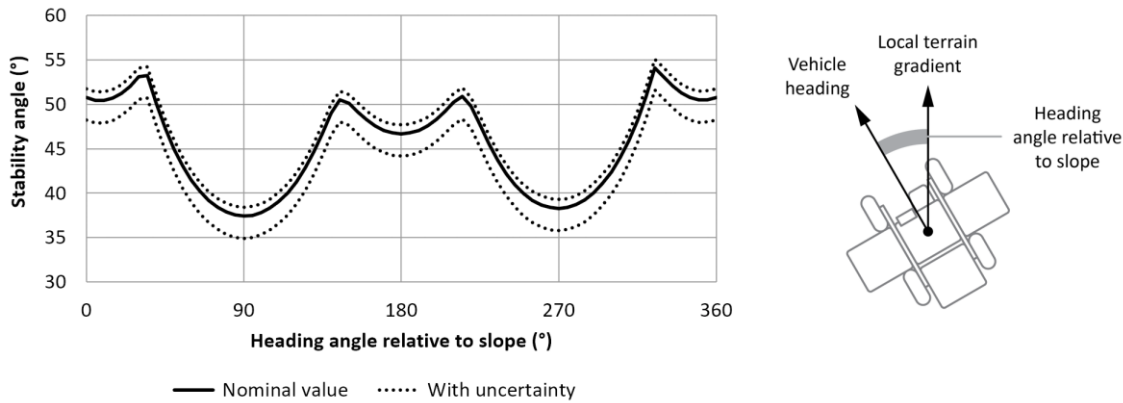


Figure 7-17 – SFR critical stability angle as a function of heading angle.

7.2.1.2 Mechanisation of the suspension

Once the kinematics required to comply with terrain features are understood, a mechanisation can be outlined for the suspension system. Using Figure 7-12 as a visual reference, the main mechanical elements forming this assembly, wheels excluded, can be identified as follows:

- Pivot
- Bogie beam
- Steering actuator
- STR-DEP transition bracket
- Deployment hinge
- Wheel leg
- HDRM
- Driving actuator
- Differential tie rod
- Differential arm
- Differential pivot

The pivot is one of the key interfaces between FAST and the rover body and its purpose is to transfer the vehicle’s weight to the suspension whilst providing the rotary degree of freedom required to comply with uneven ground. The pivot is a simple rotary joint, with a central shaft bolted to the rover and an outer housing that forms part of the bogie beam. Between the two are large diameter journal bearings to withstand mobility loads and guarantee a low resistance to the rotation, which is desirable to equalise the load on the wheels and to maintain the ride as efficient as possible. The oscillation range of the pivot is estimated to be less than $\pm 7^\circ$ for the worst-case obstacles. Its position is always known to the rover’s GNC system thanks to a potentiometer placed in its housing. A rotary seal protects the assembly from the ingress of dust.

The bogie beam is a single solid body rotating around the pivot. A trade-off is still open on whether it is built as a machined piece or round tubular sections with end fittings. The outcome will depend on detailed assessment of the mass, stiffness and ease of manufacturing of the two options. The bogie’s stiffness and strength are driven by mobility and launch loads, since it is a rather large appendage offset from the main structural frame. The other

mechanical interfaces of the bogie are the connections with the differential tie rods and the steering actuators located on each end of the beam. The bogies also carry the harness for the electrical components further out in the FAST assembly.

The rotor of each steering actuator is bolted to its interface in the bogie beam. This means that the stator, where the harness enters the actuator, is located underneath, towards the wheel. Such arrangement adds moving harness but has the benefit of placing the smaller end of the actuator (the motor side) in the lower portion, where volume is needed by the deployment hinge. The range of the steering actuators is over $\pm 90^\circ$, providing the rover with the ability to follow trajectories of any curvature and crab in any direction. The internal design of the steering actuators is further discussed in Section 7.2.2.

The steering actuator is connected to the deployment hinge by an intermediate STR-DEP bracket, which is simply an angular machined piece interfacing with the two joints. The deployment hinge is the element that allows the wheel leg to fold up at the sides of the rover body for accommodation on the lander. This is the only deployment joint that is required to stow FAST, since the bogie is short enough to fit into the allowable volume without further mechanisation. The deployment hinge is a sprung rotary joint with a latch and a binary sensor to confirm deployment. Its functioning is further discussed in Section 7.2.3.

The wheel leg is a structural piece that connects the deployment hinge to the drive actuator, providing the rover with the desired ground clearance once deployed. Each wheel leg also carries an HDRM interface, which holds it attached to the rover when stowed. These separable interfaces are the holding points used to increase the structural stability of the FAST assembly during highly dynamic events. Their purpose is to limit the response to the vibration environment and so the loads induced onto the system. The wheel leg is therefore an important load path during launch and EDL, when the large offset mass of the wheel is excited by vibrations and quasi-static accelerations.

Four HDRMs are attached to the rover body, one for each wheel leg. The mechanism is based on a non-explosive actuator that separates the two mating parts. The device was preliminarily selected as a TiNi Frangibolt, using a Shape-Memory Alloy (SMA) element in nickel-titanium (also known as Nitinol) that expands when heated and fractures a notched bolt. Its operating principle is shown in Figure 7-18. Around the Frangibolt are arranged the mating interfaces of the HDRM. These are cup / cone couplings that, once preloaded by the bolt, allow to transfer the launch loads from the wheel leg to the rover body structure.

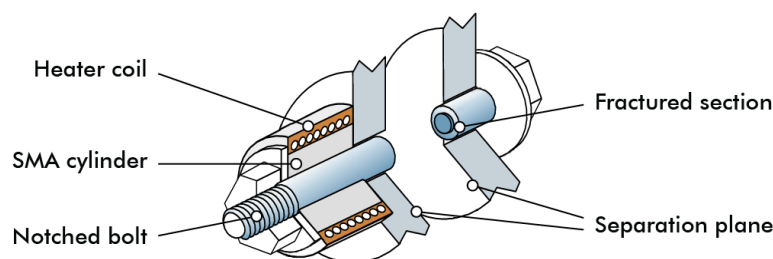


Figure 7-18 – Operating principle of a Frangibolt SMA actuator (credit: EBAD)

At the end of each wheel leg is located a driving actuator. Differently from the steering actuator, it has an unlimited range of rotation, but presents an otherwise very similar construction. Its design is discussed in Section 7.2.2.

Moving on to the rear of the vehicle, it can be observed in Figure 7-19 how each bogie beam is connected to a tie rod. These tie rods have the purpose of linking the rotation of each bogie to the differential arm, so that it can perform its function of constraining the two rotations to be opposite and equal in magnitude, as described in the previous section. The tie rods in this illustration are only notional volumes to define the correct kinematics, but are not representative of their mechanical design. A more realistic representation is provided by Figure 7-20, showing some common tie rods used in automotive steering. Since the rotation of the differential arm and the bogies occur in orthogonal planes, the tie rods have spherical bearings on their ends, which will be encapsulated in a sleeve of textile material for operation in dusty environments.

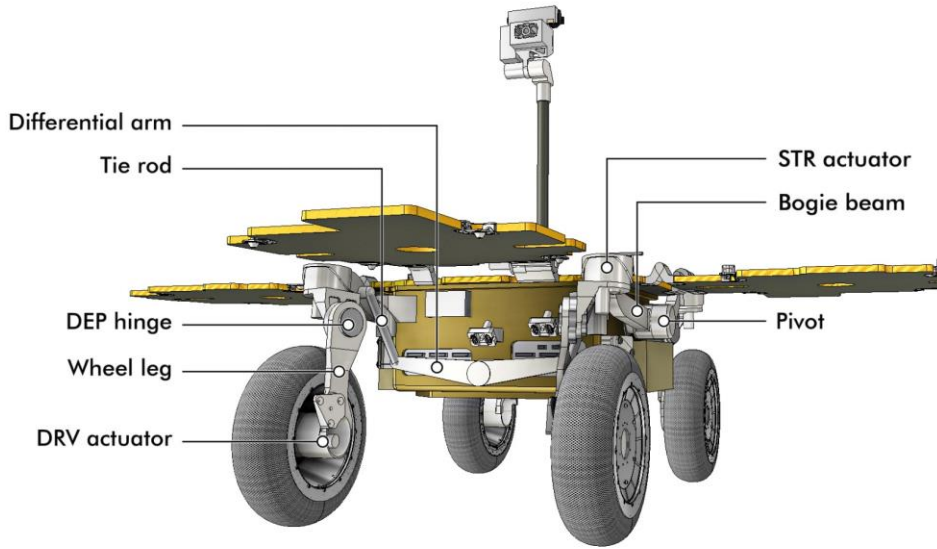


Figure 7-19 – Rear view of SFR with main locomotion components



Figure 7-20 – Automotive tie rods, similar to the FAST differential

The differential arm is a freely rotating element, similar to a bogie, but smaller and much simpler in geometry. Its mechanical loads are benign compared to those of a bogie beam, making it possible to adopt a more lightweight construction. The differential arm rotates around a pivot which is, again, similar but smaller than the side pivots and carries less load.

7.2.2 Actuators

The actuators are a central element in the vehicle’s traverse performance. They must provide torque to overcome large obstacles, a relatively high speed and accurate position control for steering. They also have to be efficient while doing so across a wide temperature

range. It is useful to take the ExoMars locomotion actuators as a comparison, where similar issues have already been solved for less demanding performance requirements. For what concerns the torque / speed characteristic of the actuators, the sizing points are reported in Table 7-5, along with the holding torque requirements [63].

Requirement	SFR FAST	ExoMars BEMA
Max. torque point	87.6 Nm at 14.6°/s	87.0 Nm at 7.0°/s
Max. speed point	5.4 Nm at 24.7°/s	7.5 Nm at 7.6°/s
Holding torque	28 Nm	35 Nm

Table 7-5 – Sizing torque and speed requirements for FAST and BEMA actuators

It can be noted how the maximum torques are very similar, which is reasonable because the SFR and ExoMars wheels have a similar normal load and the sizing scenario corresponds lifting that load over an obstacle. However, the speed values are quite different, with the SFR ones reaching more than three times the ExoMars ones.

Figure 7-21 provides a chart with all the torque / speed points for the SFR and ExoMars actuator. Analysing this distribution, it was established that one common design for driving and steering actuators would have been sufficient to satisfy all the requirements, as it was done on ExoMars. This approach would greatly simplify development and manufacturing activities. The SFR driving and steering actuators share all the parts of the transmission, bearings and housings, but present one prominent difference: the steering actuators include a position sensor (a potentiometer) that is not present on the driving ones. In Figure 7-21 are also reported the torque / speed curves of the FAST and BEMA actuators at their minimum operational temperature of -60°C.

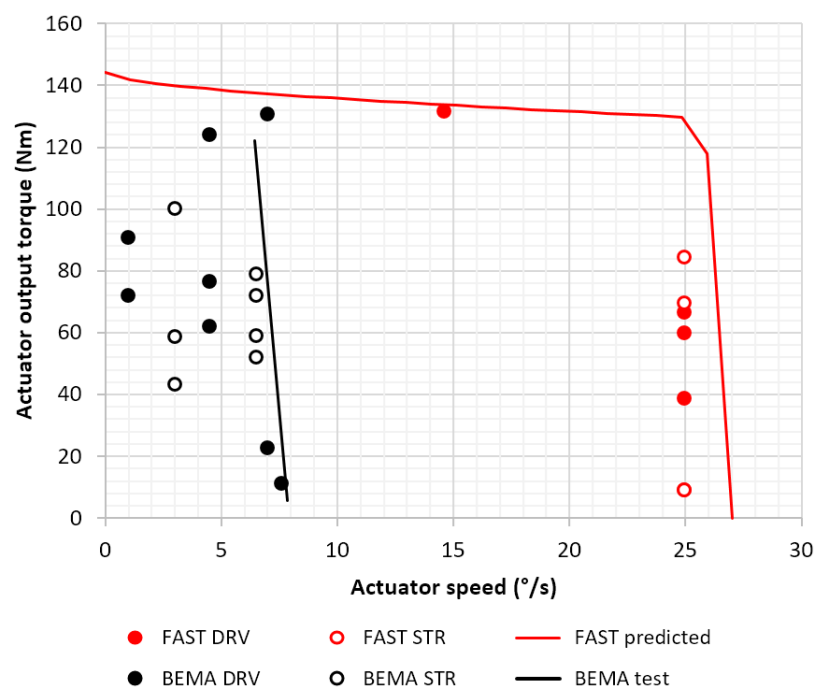


Figure 7-21 – Torque / speed requirements and performance curves at -60°C for FAST and BEMA actuators

The actuator architecture defined in response to these requirements is based on a DC brushed motor and a four-stage planetary gearbox, as already justified by the trade-offs in Section 7.1.2. On the front end of the motor (where it connects to the gearbox) is placed an electrically-actuated friction brake that engages automatically when the actuator is not powered. On the other side is a magneto-resistive motor encoder. The stator and rotor housings are made of machined titanium alloy and supported by a single cross-roller bearing, which constitutes the main load path for the actuator. Aluminium covers close off the assembly, while a two-stage rotating seal protects the rotating interface from any soil ingress. A HEPA filter is added for venting and, on steering actuators, also a custom potentiometer to provide absolute position knowledge. Some of these elements, like the rotary seal and the potentiometer are a direct reuse of BEMA parts, while others are fairly new technology. Table 7-6 provides a detailed comparison between the main components of the two actuators.

It can be observed how the SFR actuators are not too dissimilar from the ExoMars ones, but the technology had to be upgraded in various areas to adapt to the more challenging mobility requirements. The motor is still a brushed Maxon DCX model, but quite larger in size to provide more power. The transmission is perhaps the most evident difference in the actuators' architecture. ExoMars had a small planetary gearbox feeding into a Harmonic Drive, which is a quite common choice in high-torque applications for spacecraft, because Harmonic Drives package very large reduction ratios into lightweight units and can deliver remarkably high torques for their size.

Feature	SFR FAST	ExoMars BEMA
Motor	Maxon DCX 32L brushed motor	Maxon DCX 22L brushed motor
Gearbox	4-stage planetary	3-stage planetary + Harmonic Drive
Total gear ratio	1738:1	5280:1
Motor encoder	7-bit magneto-resistive, redundant	3-bit hall-effect, redundant
Brake	Electromagnetic active friction brake	Magnetic passive detent brake
Main bearings	Single cross roller	Double angular contact
Seal	Spring-energized Teflon seal	Spring-energized Teflon seal
Position sensor (STR only)	Resistive potentiometer	Resistive potentiometer
Mass	2.70 kg	1.89 kg
Volume	Ø 125 mm, length 160 mm	Ø 125 mm, length 126 mm

Table 7-6 – Comparison between FAST and BEMA actuator architecture

However, while the Harmonic Drive's torque density is unrivalled, its working principle relies on the elastic deformation of a flexible spline⁶⁴. This deformation takes energy and requires good lubrication. Unfortunately, all the fluid lubricants that have a low enough vapour pressure to operate in space without boiling also have a relatively high freezing point, meaning that at typical Martian temperatures they are rather viscous and inefficient. The result is that the overall efficiency of a gear train like that of ExoMars can drop to around 30% at the coldest operational temperature of -60°C. The need for high energy efficiency made this solution unsuitable for SFR, as predicted by the trade-offs in Section 7.1.2.

The FAST actuators adopted a custom-built four-stage planetary gear train with a smaller reduction ratio than the ExoMars BEMA ones (also thanks to the higher speed and the more capable motor) that maintains an efficiency well above 50% across the temperature range. Due to the number of actuators, the simpler suspension and the more efficient spring tyres, the difference between FAST and BEMA is particularly pronounced for overall traverse energy: driving in a straight line over a benchmark terrain BEMA would consume 6.9 kJ/m while FAST less than 1.2 kJ/m.

Despite the excellent average performance, the FAST actuators still have large motors, which can become rather power-hungry in certain situations. On particularly difficult configurations of obstacles and slopes, the overall FAST power demand can peak to over 500 W⁶⁵, which is a sizable amount for a Mars rover. Considering the low voltage at which the system operates (28 V nominally, but down to 24.5 V on low battery), this translates into a current draw in excess of 20 A. Such high currents put non-insignificant strain on the power system, but they are a necessary toll for navigating harsh terrain at relatively high speed. This actuator design is what enables SFR to drive faster and in a more efficient way, responding to two of the key challenges of the mission: time and energy.

Regarding the other elements of the actuator, it can be noticed how the encoder was upgraded to one with a greater resolution. This is due to the desire for a finer speed control and to obsolescence of the BEMA encoder parts. The brake is another novel feature of the SFR actuators. Typically, motor brakes are used to provide holding torque when the system is off. On BEMA, a magnetic toothed wheel on the motor shaft is coupled with corresponding teeth on the stator: when stationary, the magnetic flux provides holding torque, but, once overcome by the motor, the torque becomes pulsating and quickly disappears as the motor picks up speed. This is a simple, passive design, but it has no stopping power: it only engages when the motor is already stationary.

On FAST, the high efficiency of the gear trains makes them easier to backdrive, to the point that, if power was removed on a downward slope (e.g., in reaction to an anomaly on board), the rover would continue to roll downhill uncontrolledly. To prevent this behaviour, the rover needs brakes that automatically engage when the actuators are not powered and are able to dissipate the energy of the moving rover. Similar types of "fail-safe" electromagnetic brakes are common in industrial applications, where friction surfaces are clamped against a rotating disk by springs. Only when current is fed through an actuating coil the friction blocks overcome the spring force and release the disk, leaving it free to rotate. However, the

⁶⁴ A flexible spline, or Flex Spline, is a cup-shaped gear with external teeth that is deformed by an elliptical piece rotating inside it.

⁶⁵ For comparison, the expected maximum power draw of the ExoMars Rover's locomotion is less than 300 W.

ability to fail engaged that makes these brakes so desirable in the industry poses a major issue for this application: if a brake failed closed, the rover would be immobilised and the mission lost. Therefore, the FAST brake is a custom design, inspired to the industrial equivalent, but provided with redundant release coils and fully integrated into the transmission assembly.

While the rest of the actuator design is fairly close to ExoMars heritage, all the items just described are novel technologies to some degree, which are brought together for the first time in this assembly. It is therefore highly desirable to test these items as early as possible to reduce risk on the actuator development. An accelerated breadboard test programme was established to do exactly that and the actuator shown in Figure 7-22 was built according to the preliminary FAST design. This assembly includes the DCX 32L motor, the magneto-resistive encoder (not redundant), the friction brake, the planetary gear train, the output bearing and the main structural housing. Potentiometer, seal, heaters and covers are not included in this prototype. For comparison, in Figure 7-23 is shown a fully assembled BEMA flight actuator. It is evident how the two actuators present different aspect ratios, mostly due to BEMA's more compact Harmonic Drive. It is also true that the FAST breadboard actuator is missing some components, like the potentiometer and the seal, which would add some volume towards the front end.

The testing of this breadboard actuator covered launch vibration, shock, functional and performance demonstration in ambient environment as well as at Mars-representative pressure and temperatures. The tests showed that the critical components of the FAST actuator work successfully together to deliver the performance required by the SFR mission and allowed to collect valuable data on the behaviour of some novel items like the integrated friction brake, which was built for the first time for this actuator. The information gathered provides confidence that the development is on the right path and can be used to fine-tune the design for optimal performance.

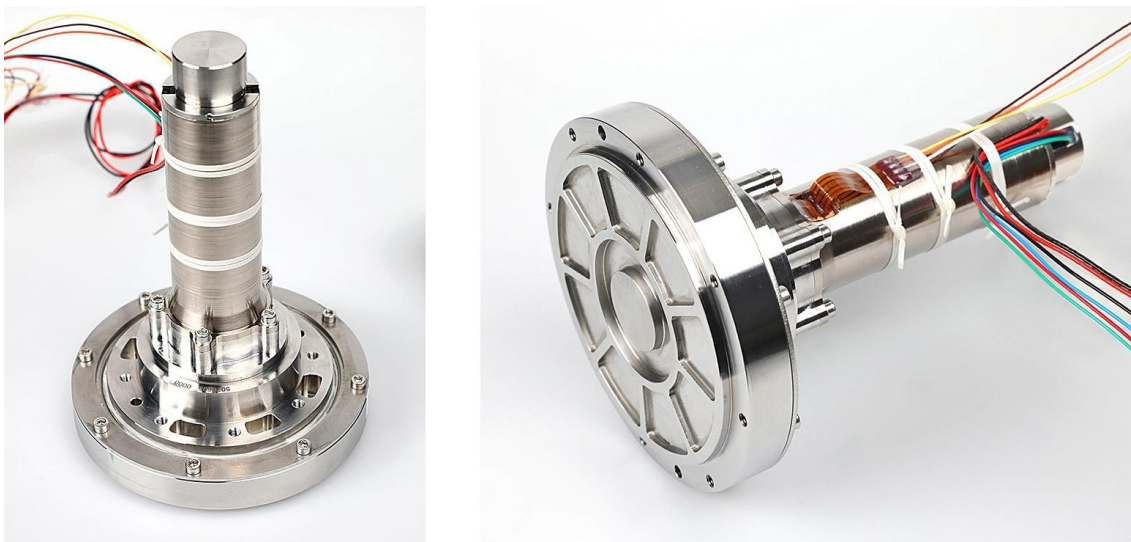


Figure 7-22 – FAST breadboard actuator (credit: Maxon Motors)



Figure 7-23 – ExoMars BEMA flight actuator (credit: MDA)

During the tests it was also possible to carry out a preliminary thermal characterisation of the actuator, which gathered data on its capability to warm up in a cold environment and reject heat in a hot environment. The thermal performance is, in fact, another important characteristic of the actuator, because it defines the amount of energy needed to warm up in the morning and the amount of time that it can operate under heavy load before overheating, which both link back to the key challenges in the SFR mission.

Like most of the external hardware on the rover, locomotion actuators have to withstand the minimum Martian night temperature of -125°C and the DHMR treatment temperature of $+125^{\circ}\text{C}$, however it is uncommon for active components to operate across such a wide range. On the cold end of the spectrum, the grease inside the gearbox freezes into a solid block not far below -60°C , so this is usually taken as a minimum operational temperature. On the hot side, the maximum temperature is set by the tolerance of the motor to overheating of the windings, which can cause permanent demagnetisation of the magnets nearby. This depends on the detailed motor design, but it is typically not much higher than $+125^{\circ}\text{C}$.

The ability to retain heat during warm-up and to reject it during high-power operations define how easy it is to maintain the actuator inside its operational range, leading to apparently contradictory requirements. The thermal characterisation demonstrated that this conflict can be resolved using the topology of the heat sources inside the actuator. Warm-up performance was optimised by placing heaters on the housing of the faster planetary stages, where good lubrication is most needed. Heat rejection was improved by connecting the outer housing to the motor, where most of the waste heat is generated.

7.2.3 Deployment

It has been discussed extensively in the early sections of Chapter 6 and 7 how the stowage of the locomotion subsystem on the lander has always been a major challenge for SFR. The layout and mechanisation of the FAST deployment has been carefully co-engineered with the SRL design authority. When the complex mechanisation of the Gullwing deployment in Section 7.1.4 was abandoned, it was replaced by four simple hinges located just below the steering actuators. Such deployment hinges allow the wheel legs to be stowed by rotating upwards and connecting to HDRM interfaces on the rover body. This achieves a rather compact package, as shown in Figure 7-24.

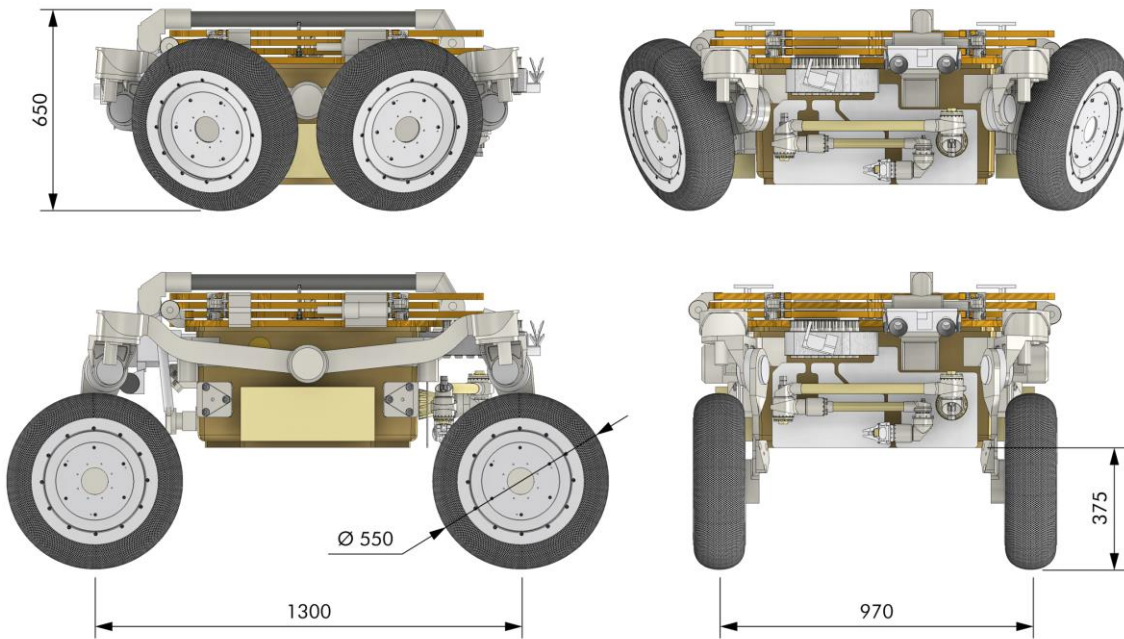


Figure 7-24 – FAST stowed and deployed, side views (left) and front views (right) with salient dimensions in mm

An important feature of this configuration is that the deployment happens with the rover in an upright orientation, i.e., after it has been rotated by the egress arm and is suspended above the terrain. In this orientation, the deployment can be mostly gravity-driven, as the heavy wheel and actuator will tend to rotate downwards. Springs are added to the deployment hinges to ensure that friction is overcome and that the end of travel is reached even in case the rover is not perfectly aligned with the gravity vector, so that the last part of the motion is actually going upwards.

A latch is present on the same deployment hinge, where spring-loaded pins or similar features engage with corresponding slots as soon as the rotation reaches the correct position, permanently coupling⁶⁶ the wheel leg and the STR-DEP transition bracket as one solid body. The deployment latch would rely on a similar solution to that described in Section 7.1.4.1, although smaller in size.

The wheel weight and the action of the spring can provide significant acceleration to the assembly, which, in a worst case, could reach the end of travel with a dangerous amount of kinetic energy. To avoid this, methods of controlling the deployment speed will be adopted, although the specific device has not been selected yet. Some candidates are: crushable materials, viscous dampers and mechanical speed regulators.

⁶⁶ This connection is not physically irreversible: on ground, the latch can always be released with a dedicated resetting tool. In mission, however, there are no means to release the latch once engaged.

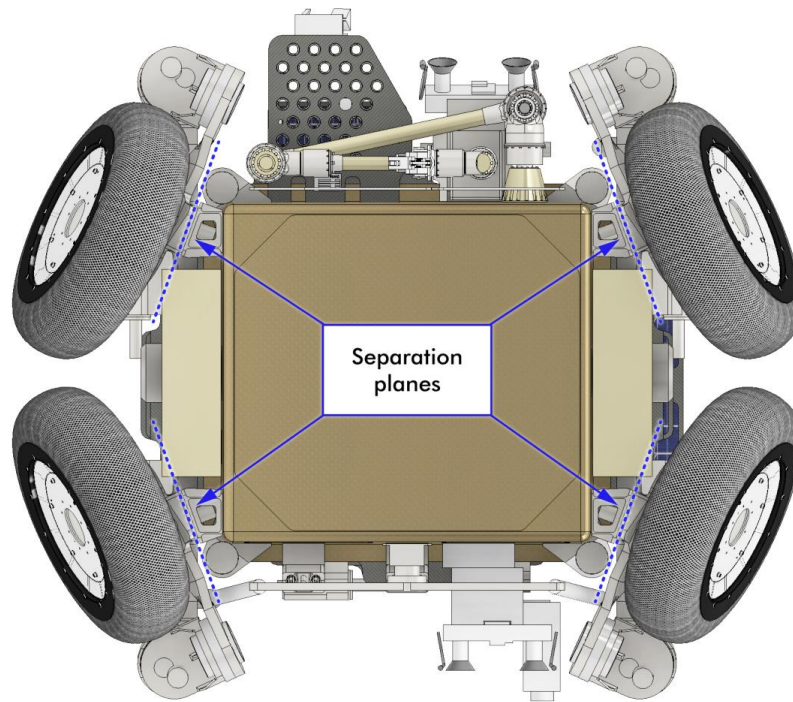


Figure 7-25 – FAST separation planes

By observing Figure 7-25, it can be noticed that the separation plane of each HDRM is vertical, slightly angled with respect to the side of the rover. Therefore, the first motion to clear the fractured bolt and the cup / cone interfaces should be normal to that plane, i.e., sideways, away from the rover body. However, the deployment motion just described is a rotation that begins by moving the wheel leg downwards.

The solution to this discrepancy lies in a cam that inhibits deployment of the wheel leg until it has been steered away from the HDRM interface. This means that the first motion after separation is actually a steering motion, commanded by the rover. Only after a few degrees of rotation the cam is free and the wheel leg springs downwards. This concept can be visualised with the help of Figure 7-26, which describes three steps in the deployment sequence.

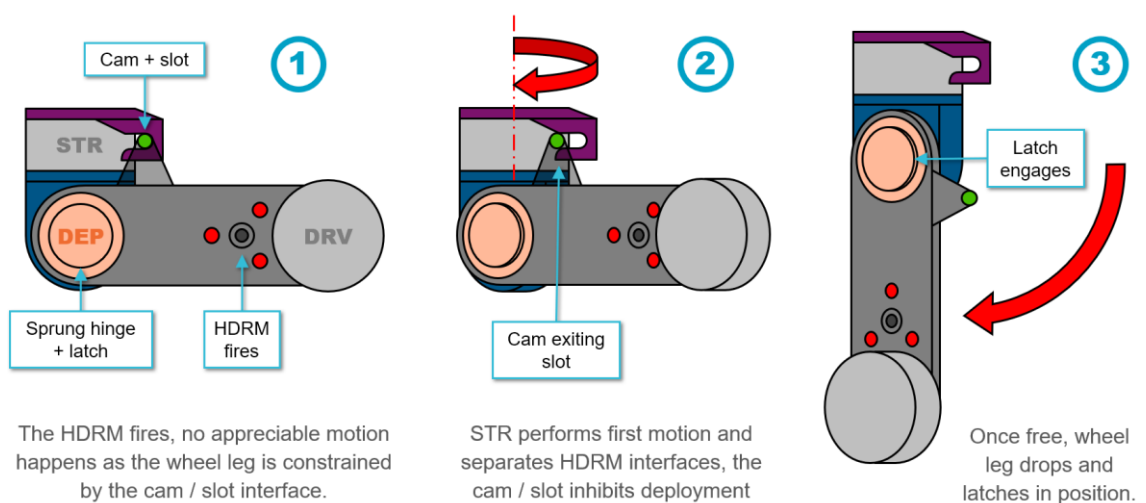


Figure 7-26 – Visualisation of the FAST first motion and deployment

While Figure 7-26 still illustrates correctly the principle, it was decided to incorporate the cam and slot directly into the HDRM in a future iteration of the design, where their mechanical implementation would be more straightforward. In fact, in this area, the metal work of the wheel leg and the HDRM bracket are in close proximity to each other and well-suited to carry the cam interface loads. A cam feature can be machined in the wheel leg, interfacing with a slot in the HDRM structure that constrains its initial motion after separation.

One last important aspect of the FAST deployment sequence is that, even if the hinge is sprung, an electric signal is required to confirm successful deployment and latching of each leg. To provide it, micro switch sensors are included in the hinge. The rationale for this requirement is due to the fact that the deployment happens in mid-air, while SFR is still supported by the lander's egress arm. Most of the sequence is automated to avoid waiting for ground commands, so the lander needs to receive positive confirmation of FAST deployment before lowering the rover onto the ground.

7.2.4 Wheels

As discussed in Section 7.1.1, the choice of a four-wheeled architecture, while having several advantages for the system, tends to be more reliant on the performance of the individual wheel, especially if there is a desire to navigate difficult terrain and overcome large obstacles. The simple fact that there are fewer contact points available to support the vehicle and produce traction, makes them more critical for the traverse performance. This was immediately identified as a source of risk for the SFR development and contributed to the interest for the spring tyre technology under development at NASA GRC.

The superelastic spring tyre offered good traction and load bearing capability on loose soil, but also – particularly relevant to SFR – ability to envelope obstacles, high energy efficiency, and extended durability. These latter aspects are probably the areas where the spring tyre design stands out the most from other candidate solutions.

Firstly, some clarification of the terminology is due. The spring tyre was invented in 2009 by NASA Glenn Research Center and Goodyear Tire & Rubber Company [64]. A spring tyre consists of a flexible toroidal structure constructed by several inter-coiled helical springs, also called tyre mesh, which has the ability to deform under load and contour to the terrain surface. The mesh is secured by a rim onto a hub using a clamp system with features that interlock with the springs. The assembly of tyre mesh, rim and hub is referred to as a Wheel and Tyre Assembly (WTA) or, more directly, a wheel. An example of this assembly is provided in Figure 7-27, which depicts a recent prototype of an SFR wheel.

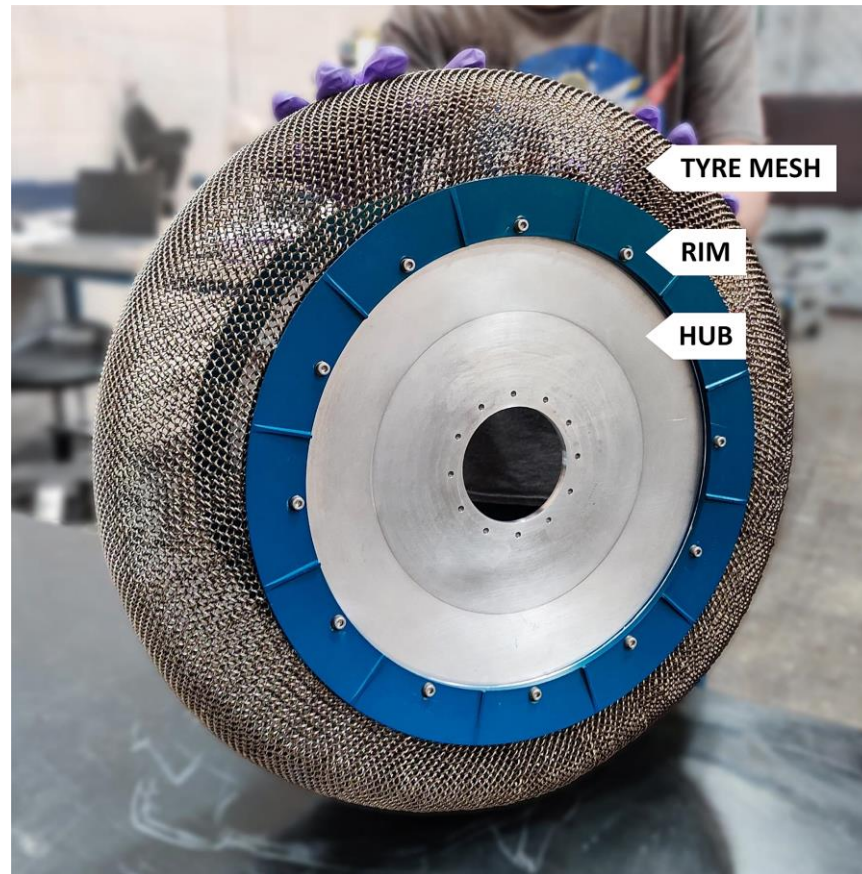


Figure 7-27 – SFR wheel and its constituent parts (credit: NASA / GRC)

While the springs used in this first design were made of steel alloy, a second patent was submitted in 2016 for a superelastic spring tyre composed by nickel-titanium alloy (Nitinol) springs [65]. The term “superelastic” refers to the fact that this alloy can withstand strain values more than 10 times higher than steel before undergoing permanent deformation. The phenomenon is due to a peculiar phase transition in its crystal structure. Nitinol, already mentioned in Section 7.2.1.2, is a shape-memory alloy, which can produce significant deformation when subjected to temperature variations. In particular, it does so by transitioning from a martensitic phase to an austenitic one under the application of heat, which corresponds to its traditional use as shape-memory alloy actuator. However, the austenitic phase, within a certain temperature range, exhibits another interesting property: if subject to high strain, it transitions to a particular type of stress-induced martensitic crystal. This rearrangement of the crystalline lattice can absorb a considerable amount of deformation, but is not stable, so it returns to the original austenitic phase when the load is removed, restoring the original shape of the component and producing the superelastic behaviour.

Figure 7-28 helps visualise the principles of Nitinol phase transition, with some important clarifications: firstly, superelasticity only emerges inside a certain temperature range, which can be tuned by careful control of the alloy’s composition and manufacturing process. If the temperature is too high, austenite is not able to turn into martensite and simply yields. If the temperature is too low⁶⁷, martensite is stable and does not turn back into austenite,

⁶⁷ This lower limit corresponds to the starting point of a temperature-induced martensitic transition (i.e., with no load applied).

causing some permanent deformation to remain. Luckily, a solution exists that enables this behaviour at typical Mars surface temperatures.

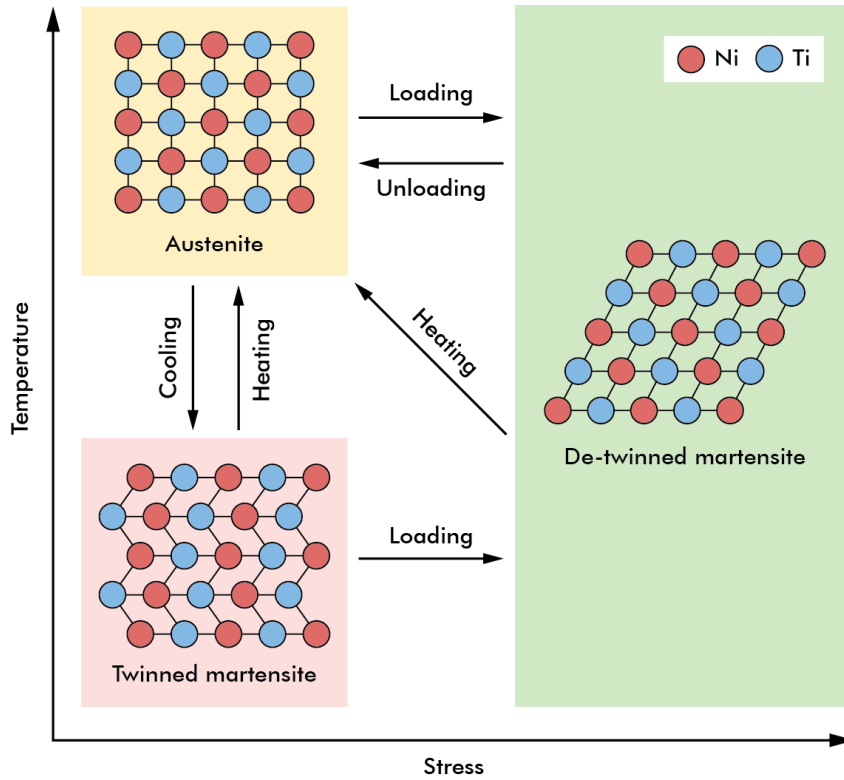


Figure 7-28 – Phase transitions of nickel-titanium alloy

The second point to note is that superelasticity does not mean strength. In fact, austenitic Nitinol is not as strong as aerospace-grade steel or titanium alloys and its martensitic phase is even less strong. This means that, after all the useful material has transitioned to stress-induced martensite, that martensite eventually yields quite easily. However, this is not particularly critical for the superelastic tyre: thanks to its geometry, when the load and the deformation increase, the number of springs involved also increases, distributing the load on more material. The result is a variable stiffness profile not dissimilar from that of off-road pneumatic tyres.

These spring tyre technologies are remote descendants of one eminent wheel in space exploration: the Apollo Lunar Roving Vehicle’s wire mesh tyre. Already reported in Figure 4-1, its similarity with the SFR wheel is evident. The detailed construction of the two tyres differs in the fact that the Apollo tyre mesh was woven with steel wires in an over / under pattern [66], much like a textile, while the SFR tyre mesh is composed by inter-coiled springs. The weave pattern tended to create stress concentrations at the wire intersections, which limited the scalability and durability of the design, while the inter-coiled springs have more freedom of movement and flexibility to reorganize and conform to irregular surfaces.

Figure 7-29 offers a schematic of the key steps involved in manufacturing a wire mesh tyre, while Figure 7-30 shows a detail of the spring interlacing process to produce a spring tyre. In the latter, each spring is inter-coiled with the next one with a screw-like motion, gradually building a rectangular mesh. The last spring is coupled with the springs at both ends of the rectangle, turning it into a cylinder, very similar to that in the third step of the wire mesh

construction in Figure 7-29. For the spring tyre, the final shape is achieved simply by pushing the two edges of the cylinder together through clamping at the wheel rim. This makes the springs arch outward and produces the toroidal shape of the tyre.

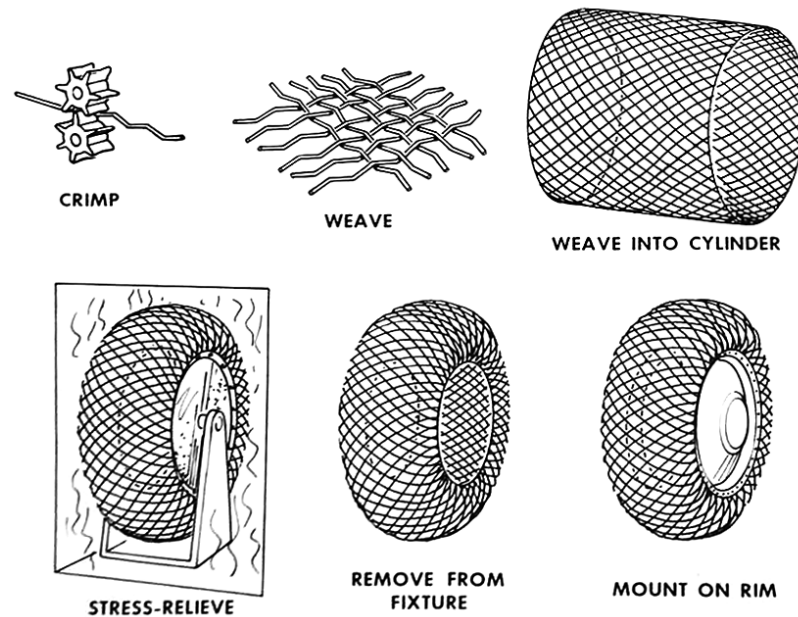


Figure 7-29 – Main steps in the construction of the Apollo wire mesh tyre (credit: D. Freidman)

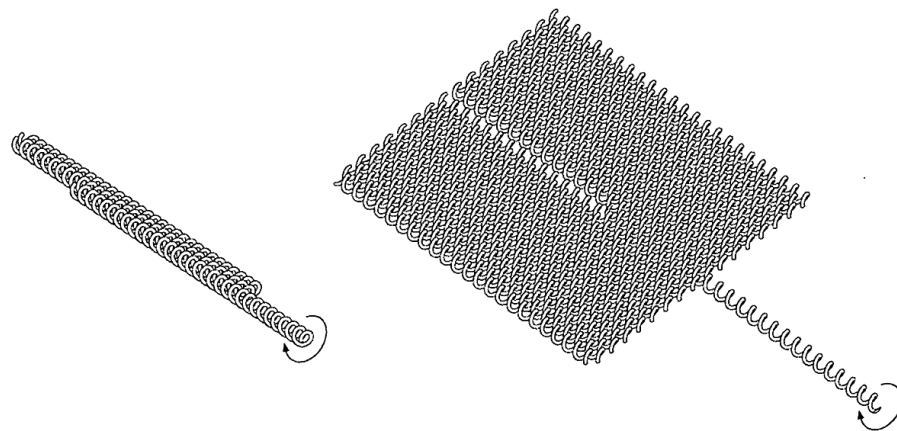


Figure 7-30 – Process of interlacing springs to create a spring tyre (credit: NASA / Good-year)

The availability of a wheel design that had already been under development for years was a great benefit for the SFR project and allowed to retire several risks associated to this critical component. As it happens in automotive, tyre specifications are tuned to the type of vehicle and the required driving performance, so significant work still had to be done to adapt this design to be suitable for SFR. This was possible only through a direct and open collaboration among all parties involved in the rover's design, its locomotion subsystem and the development of the spring tyres.

A co-engineering group composed by experts from every organisation involved was established to guide the wheel design. The group was dedicated to rapid iteration through a multi-layer approach that would run through mission analysis at rover level to establish the

required traverse performance, terramechanical simulation at locomotion level to identify the required wheel performance and wheel design assessment in response to these requirements. If a design issue or a need for change of requirements arose from the wheel or other intermediate level, the same chain would be followed in reverse to estimate the impacts on the mission.

Some specific challenges of the SFR wheel development were associated to achieving the required traction (including in loose soil) and obstacle climbing ability. This implies a sufficiently large contact patch with the ground and enough enveloping ability on the obstacle edge⁶⁸, generally demanding more deformation and a softer wheel. On the other hand, these requirements are in conflict with durability, which for the SFR mission is not insignificant and generally needs deformation to be minimised. As discussed in Section 7.1.4, the interaction between wheel and terrain is very difficult to predict based on theory alone and the simulations are generally as good as is the empirical data used to validate them. Hence, GRC initiated an aggressive build-and-test approach with incrementally representative prototypes. This effort has been vital to advance the wheel design well before the rover had a consolidated baseline. Figure 7-31 shows an early prototype of a 700-mm-diameter tyre undergoing life testing on simulated terrain inside a thermal chamber.

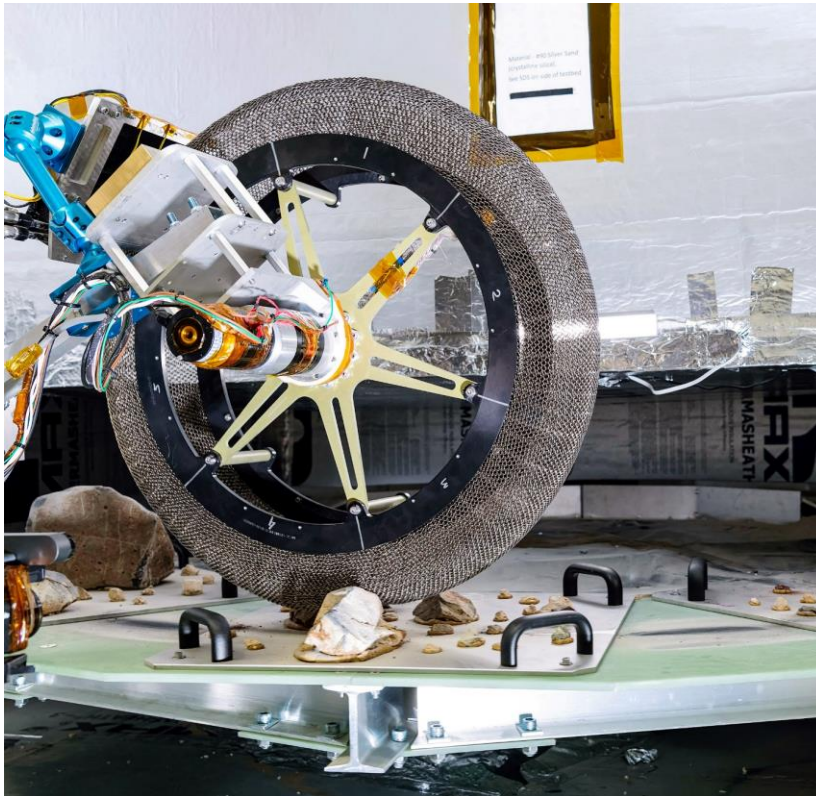


Figure 7-31 – Wheel prototype during life testing (credit: NASA / JPL-Caltech / GRC)

Life testing on early prototypes revealed that the primary failure mode was fatigue breakage of the spring elements. Analysis of the results showed that the tyre was being displaced

⁶⁸ These aspects are also heavily affected by the friction coefficient between the wheel mesh and the terrain material, however, that was found to be a parameter on which there is very little design control, since the wheel material and small-scale geometry are defined by its construction and the terrain material varies greatly.

laterally off its centreline by large rocks and pinched at the rim, creating stress concentrations. To address the issue, the tyre material processing was changed to have lower residual stress, springs with thinner wires were used to reduce bending stress, and the spring geometry was modified to reduce deflection and prevent pinching. Repeat testing demonstrated that the changes had mitigated the failure, and the item survived 4 times the maximum expected traverse life for SFR without detrimental damage.

Testing also allowed to characterise the traction performance on loose sand, which requires a sufficiently large contact patch to be achieved by deformation of the tyre. This is evaluated for the hottest operational temperature, where the alloy is stiffest. In contrast, establishing sufficient traverse life means limiting deformation and associated material stress. This is evaluated for the coldest operational temperature, where the alloy is softest. It was observed that the spring geometry allowed the fine sand to seep excessively through the mesh, thus, the pitch and diameter of the springs were adjusted to achieve a denser mesh. Further details on wheel testing are provided in Section 7.4.

Launch vibration testing was also performed on wheel prototypes to ensure that the flexible mesh would not undergo excessive displacement or encounter resonance issues. This is another area where simulations typically fall short of capturing the complex behaviour of the mesh geometry, which contains tens of thousands of contact points, so testing is a preferable way to characterise the system. The results were rather promising and showed that the displacement was limited to a few millimetres and the first natural frequency was in excess of 100 Hz⁶⁹.

7.3 Traverse analysis

Some examples have been presented in the previous chapters of how traverse analysis at various levels has supported the development of the SFR locomotion subsystem and wheels. It is worth dwelling on a few of these analyses to explain their nature and how they can support the mission.

7.3.1 Terramechanical simulations

Early in the SFR development, MDA developed a simulation environment based on a terramechanical model coupled with a dynamic model of the SFR locomotion. The simulation was gradually augmented as the design of the rover and the locomotion became more detailed and as more information was gathered from wheel testing. Ultimately, this model became the primary tool to predict the vehicle performance on all the combinations of soils, slopes and obstacles that could be found on its path. This model was instrumental in supporting the campaign-level trade-offs that shaped the SRL and SFR designs. Figure 7-32 reports an example of the model's graphic interface processing an obstacle climbing case with visualisation of the contact forces and coefficients of friction.

⁶⁹ This high frequency is desirable for the wheels because it would ensure that their first vibrational mode is not excessively excited by the vibration of the suspension or the structure (which have lower natural frequencies).

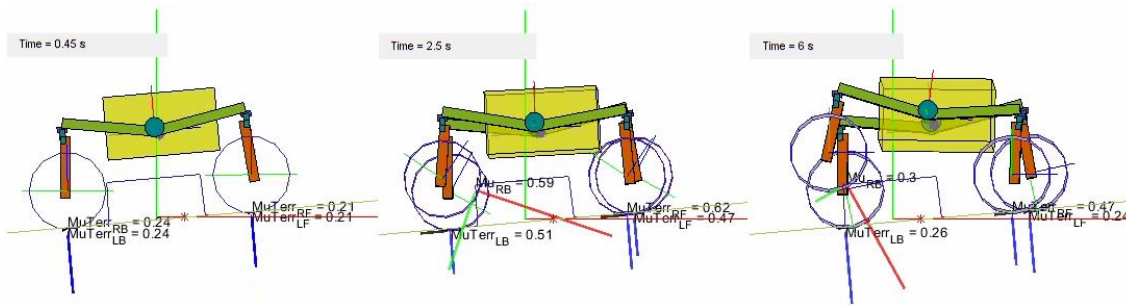


Figure 7-32 – Visualisation of the terramechanical simulation solving an obstacle climbing case (credit: MDA)

The tool is implemented in MATLAB environment and is composed by two major elements: a multibody dynamic model to represent the rover motion and a terramechanical model to represent the interaction with the terrain. The implementation of both was adapted for SFR from previous work by Ghotbi B. [37]. The multibody model uses a custom MATLAB library that solves numerically the dynamic equations of a three-dimensional system of flexible bodies. The analysis captures in detail the mechanical behaviour of the locomotion mechanism, with representative mechanical joints and stiffness properties assigned to the main contributing elements (e.g., bogie beams and tyres). The rover body and its appendages are modelled as a rigid body with assigned mass properties.

The terramechanical model provides loads in input to the multibody model coming from the interaction with the ground. It estimates traction, sinkage, slippage and rolling resistance for each wheel through terramechanical equations that represent the characteristics of the terrain material and the wheel behaviour on it. The whole simulation is solved numerically at each time step, for intervals as small as desired. In general, a small time increment is desirable to capture the dynamic phenomena involved in terrain interaction, which have characteristic times shorter than a second. It derives that a model like this typically runs slower than real time. This is not an issue when producing local, high-fidelity locomotion simulation, but it needs to be taken into account if the analysis has to be extended to an entire mission, as will be discussed in Section 7.3.2.

The multibody dynamic part of the simulation is relatively well-understood and validated. The accuracy of its results is essentially driven by how well defined are the stiffness properties and mass distributions of the various elements. The terramechanical model, on the other hand, is where most of the unknowns reside, partly because of the empirical nature of wheel / soil interaction, partly because of the limited information available on the actual mechanical properties of the Martian soil. Significant efforts went into filling gaps in these areas, with early wheel testing for the former and geological assessments for the latter.

Orbital imagery allowed geologists to categorise the mission area into a variety of terrain classes with different origins and characteristics. For the purpose of traverse performance simulation, they were narrowed down to a list of the most widespread and the most challenging for locomotion design. The substrates associated with these terrains (i.e., the underlying material forming the driving surface, separate from obstacles, which are usually made of rocky material) can be compared with Martian simulants available on Earth to provide an approximation of their mechanical properties. In particular, the terrain classes were mapped to corresponding ES simulants, described in Section 3.3.4. The main three substrates on which most of the analysis and test was performed are the following:

1. **Compacted regolith.** Also called the “highway” soil. Varying in granulometry but generally dense and cohesive, capable of providing good bearing capacity and traction with negligible sinkage. Most of the mission paths are purposely on this soil. The equivalent simulant is ES-4.
2. **Aeolian drift or dune sand.** Fine material that is deposited by the wind, usually in ripples or dunes. It offers little cohesion and flows easily, causing slippage and sinkage. Traction on this soil is very limited and is therefore used as a worst-case scenario. The equivalent simulant is ES-2.
3. **Bedrock.** An exposed layer of solid rock emerging above the regolith. It can exhibit cracks, gaps and roughness to a varying degree, but can also be rather smooth if shaped mostly by wind erosion. Since the ES simulants were developed to represent regolith, there is no equivalent for bedrock, however, the material can be reproduced using certain types of sandstone.

The advantage of identifying equivalent simulants is that they are well characterised, so their parameters can be used in the analysis and the results can be validated by testing on the actual simulant. Figure 7-33 and Figure 7-34 provide examples of the occurrence of these soils on Mars: the first one shows Perseverance next to a rock nicknamed “Rochette”, from which two core samples were acquired for return to Earth. In front of the rover are some small patches of exposed bedrock, while Perseverance was sitting on compacted regolith at the time of the image.



Figure 7-33 – Perseverance at “Rochette” sampling site (credit: NASA / JPL-Caltech)

The second image shows Curiosity next to a sand accumulation called “Namib Dune”, which it is testing with its wheels. This dune is composed of aeolian drift sand that flows easily when disturbed. It is worth noting how the left wheels of the rover were intentionally kept on bedrock to avoid any risk of becoming trapped in a situation similar to that of Figure 3-13.

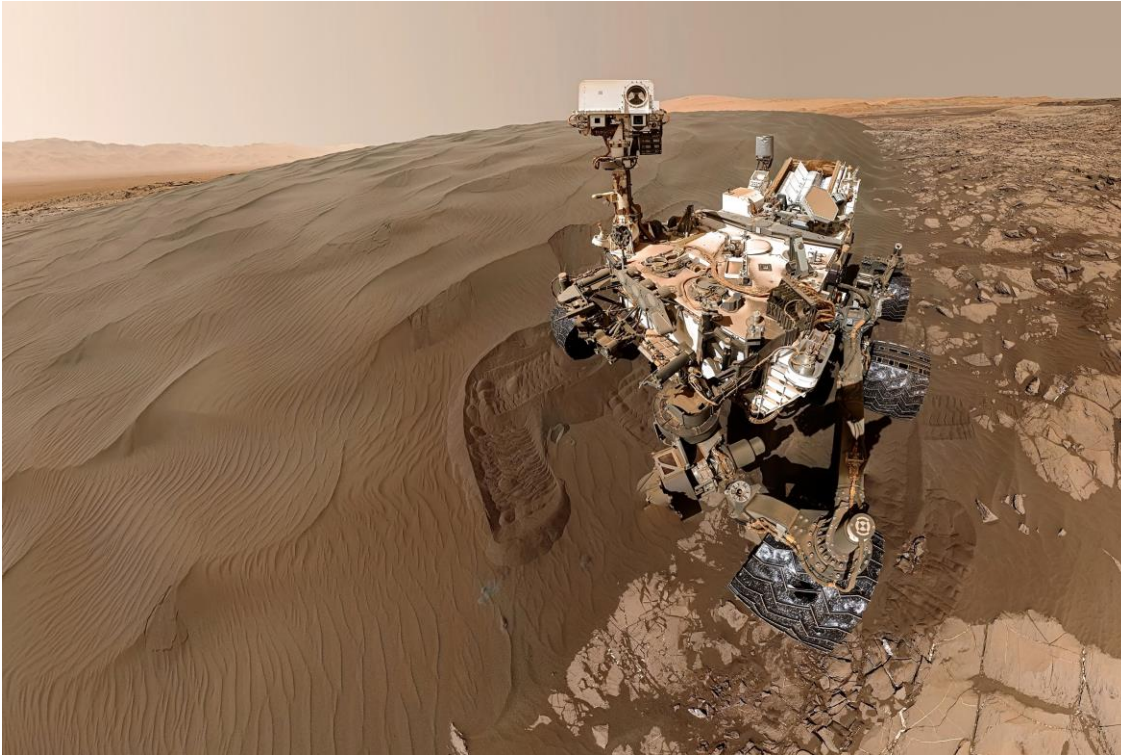


Figure 7-34 – Curiosity at “Namib dune” (credit: NASA / JPL-Caltech)

Once complete with soil properties, wheel – soil interaction parameters and validated through test data, the terramechanical model becomes a powerful tool to estimate the locomotion performance of the vehicle. The simulation can predict what obstacles and slopes the rover can climb on each substrate and evaluate the success of any manoeuvre on the terrain. As it does that, it also computes mechanical loads on the system, actuator torques and powers.

The analysis was run regularly during the SFR development on a spectrum of soil types, slopes and obstacle heights. The outcome would provide data points to update the overall performance of the rover on the mission paths. Some results are provided in Table 7-7, reporting the predicted obstacle climbing ability of the SFR baseline considered in this work. As mentioned in Section 7.2.1.1, there is a 2 cm difference between the mechanical capability and the height of the maximum targeted obstacle, which is reported in brackets.

Slope angle	Max. obstacle on compact soil (cm)	Max. obstacle on drift soil (cm)	Max. obstacle on bedrock (cm)
0°	29.5 (27.5)	29.5 (27.5)	29.5 (27.5)
5°	29.5 (27.5)	20 (18)	25 (23)
10°	24 (22)	10 (8)	16 (14)
15°	13 (11)	-	9 (7)
20°	5 (3)	-	-

Table 7-7 – Obstacle performance on different substrates predicted by the terramechanical model

7.3.2 Surface Operations Engineering Tool

While terramechanical simulations can assess the rover’s performance locally, another layer of analysis is required to extend these results to the overall mission. A Surface Operations Engineering Tool (SOET) was set up by Airbus in the early phases of the project as an end-to-end simulator for SFR. Since the SFR mission is not fully defined, but constrained to a limited number of paths, a statistical approach is suitable for this analysis. SOET is also implemented in MATLAB, but, differently from the terramechanical model, it must run much faster than real time to cover many mission scenarios in a useful time.

The tool processes all combinations of start and end points for traverse, changing other inputs in discrete steps, such environmental conditions and possible timelines of activities on the surface. The outcome is an array of several hundreds of possible missions, showing which combinations would lead to mission success and which ones would not. Detailed reports can be generated to assess what caused the failures, which is typically running out of time or energy to complete the assigned tasks. The review of the SFR mission analysis typically follows a “3-sigma rule”, i.e., it aims at a success rate of 99.7% across the spectrum of possible mission scenarios.

The terramechanical simulations described in the previous section are one of the many inputs to SOET, providing the capability and performance indicators for traversing different terrains encountered on the paths. It would be unfeasible for SOET to solve the detailed terramechanical model on hundreds of paths, so it simply interpolates its results based on local terrain classes. The local terrain is defined for each traverse segment by processing maps of the surface, which provide the substrate, slope and rock distribution at that location. From these parameters, the traverse capability, energy and time required to drive on that terrain can be extracted from the results of the terramechanical model.

Figure 7-35 provides an overview of the information flow into SOET and around it. It can be observed how the locomotion branch does not only provide performance parameters for SOET, but also supports a number of locomotion-specific tasks (such as actuator, suspension and wheel design) and non-locomotion-specific tasks (such as computing power losses for the thermal model).

Before being used into SOET, the locomotion inputs are processed by GNC analysis. Knowing the obstacle capability of the locomotion subsystem the GNC system will steer the vehicle to avoid obstacles that are above that threshold, driving a slightly longer distance each time

it does so. Such distance penalty can be calculated statistically for various levels of rock coverage. The rock coverage (CFA, as described in Section 7.2.1.1) is estimated from orbit for each area of the map, so the associated path penalty can be computed. The energy and time predictions of the terramechanical model are augmented with these penalties when they are processed in SOET to obtain the global traverse performance of the rover.

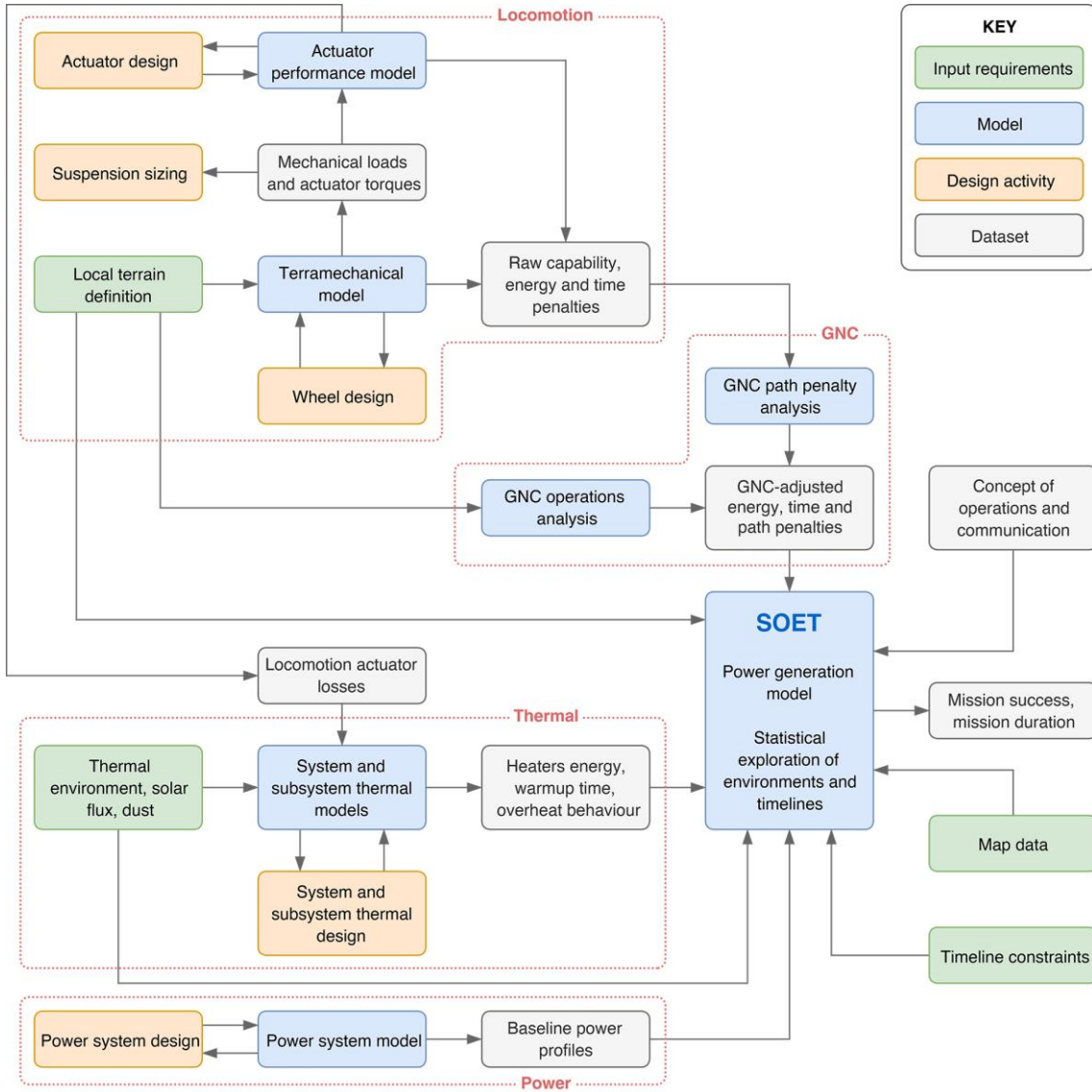


Figure 7-35 – Information flow in SOET and associated analyses

The algorithm in SOET follows each path and accumulates energy and time penalties as it progresses along the route. This runs on the backdrop of the Martian diurnal cycle with its solar illumination and temperature profiles. The tool simulates the behaviour of the rover’s thermal control and electrical power system, so each day the rover warms up before commencing traverse operations and it continues for as long as there is sufficient power. Communication passes and ground planning cycles are also coded in the simulation, including allowances for less predictable events such as faults and planning mistakes. The mission success for each simulation run is defined by managing to complete the outbound and return traverse within the allowable time and energy.

7.3.3 Other analyses

Other analysis tools that are worth mentioning, since they are rather specific to the rover's mobility, include the calculation of the vehicle's stability angles, which is already described in Section 7.2.1.1. This analysis has a central role in defining the architecture of the vehicle, especially in sizing its footprint. It was also observed how, in this case, it determined the mounting point of the pivot joints, constraining the mechanical interfaces of the rover's structural frame. The stability calculation is purely static, simply solving a multibody model of the rover to determine the slope angle at which one wheel loses contact with the ground. Since it does not account of dynamic effects, robust margins must be placed on its results, so, in operation, the rover would automatically stop well before its attitude reaches the critical angle.

To augment the calculation of stability angles, detailed non-linear dynamic simulations are also carried out for some corner cases. These are more resource-intensive and can cover only specific scenarios, however, they capture far more accurately the behaviour of the vehicle when interacting with terrain features. One area where such approach is particularly effective is the determination of impact loads. They emerge when driving or sliding off a large rock and they are the sizing factor for most of the locomotion subsystem's structure and other deployable appendages like the mast and the solar arrays. The non-linear dynamic model allows to simulate these particularly energetic events, including the response of the highly compliant tyres.

Another relevant piece of analysis is the motorisation assessment, which focuses on verifying that motors have sufficient torque to overcome all worst-case losses and resistive loads whilst still producing the desired output. This analysis is actually common to any spacecraft and is performed in accordance to the European Cooperation for Space Standardisation (ECSS) rules. Nonetheless, the application to planetary locomotion of regulations developed with microgravity in mind can be challenging and potentially lead to overdesign. According to the standard ECSS-E-ST-33-01C Rev.2, Space Engineering: Mechanisms [67], the minimum design torque for a rotary actuator, T_{min} , is given by the following equation:

$$T_{min} = MF (U_I I + U_S S + U_M H_M + U_R F_R + U_Y H_Y + U_A H_A + U_D H_D) + U_C T_C + T_L$$

In this expression, MF is the motorisation factor and is always equal to 2 according to the regulation. The terms that follow represent resistive torques internal to the actuator and are clarified by Table 7-8. With reference to the uncertainty factors, the values to use in the equation above are chosen from the table on the basis of how the associated resistive torque contributor has been quantified: if it is computed by analysis, then the uncertainty for the theoretical value is used, if it is determined through test on representative hardware, then the uncertainty for the measured value is used. Lastly, T_L is the required output torque, which, in the case of locomotion actuators, is given by:

$$T_L = MF K_L T'_L$$

where K_L is an uncertainty factor on the estimation of the required load (established on the basis of the fidelity of the model, typically ranging from 1.2 to 1.5 in this case) and T'_L is the raw prediction of the resistive torque to overcome during traverse.

Resistive torque contributor	Symbols	Uncertainty for theoretical value	Uncertainty for measured value
Inertial loads due to external acceleration	I	$U_I = 1.1$	$U_I = 1.1$
Spring	S	$U_S = 1.2$	$U_S = 1.1$
Magnetic effects	H_M	$U_M = 1.5$	$U_M = 1.1$
Friction	F_R	$U_R = 3$	$U_R = 1.5$
Hysteresis	H_Y	$U_Y = 3$	$U_Y = 1.5$
Others (e.g., harness)	H_A	$U_A = 3$	$U_A = 1.5$
Adhesion	H_D	$U_D = 3$	$U_D = 1.5$
Inertial loads due to actuator acceleration	T_D	$U_D = 1.25$	$U_D = 1.25$

Table 7-8 – Resistive torque contributors and uncertainty factors

The application of this approach to planetary locomotion faces two peculiar aspects: firstly, the output torque T'_L and the resistive contributions are unusually large and, with uncertainty and motorisation factors, they would need actuators that are prohibitively powerful and heavy. Secondly, multiple actuators can be involved in providing the same function (e.g., driving), meaning that the contributions of their motorisation factors add up in overcoming the external load.

In light of these considerations, a tailored approach was established to replace the typical motorisation factor of 2 with an array of factors varying from 1 to 2, depending on the scenario. The sizing cases were categorised according to their probability of occurrence and their severity, then a motorisation factor was associated to them based on the combination of the two. For example, a large obstacle at the limit of the rover capability (275 mm) is expected to occur in the order of 100 times in the overall mission, so the associated probability is medium. The failure to overcome such obstacle would cause a GNC error that stops the vehicle and calls for ground intervention, which is undesirable but not mission-threatening, so its criticality is also medium. The corresponding motorisation factor is 1.5, requiring the motor to provide 1.5 times the torque required by this scenario instead of 2, thus avoiding excessive oversizing of the mechanism.

Lastly, the locomotion subsystem is involved in a variety of standard spacecraft analyses that contribute to shaping its design, such as Finite Element Method (FEM) modelling of launch vibration, thermal analysis for warm-up and overheating, thermo-elastic distortion, etc. However, all of these are common processes of spacecraft engineering and not particularly specific to planetary mobility, so they will not be discussed here.

7.4 Traverse testing

To augment the fidelity of the terramechanical model described in Section 7.3.1 and validate the novel design of the superelastic spring tyre, a testing campaign was devised with the aim to characterise the traction performance of wheel prototypes on representative soil simulants. These are single-wheel tests, where a wheel is driven on a testbed filled with soil by a rig that simulates the vehicle's weight by applying a normal load onto the wheel. One

of the most important performance indicators to characterise is the drawbar pull, i.e., the net thrust produced by the wheel, as a function of slip ratio. The results obtained are shown in Figure 7-36 for ES-4 simulant (compacted regolith) and Figure 7-37 for ES-2 simulant (dune sand). The wheel prototypes used in this test would be then be mounted on a 1:1 scale breadboard model of SFR for full vehicle testing.

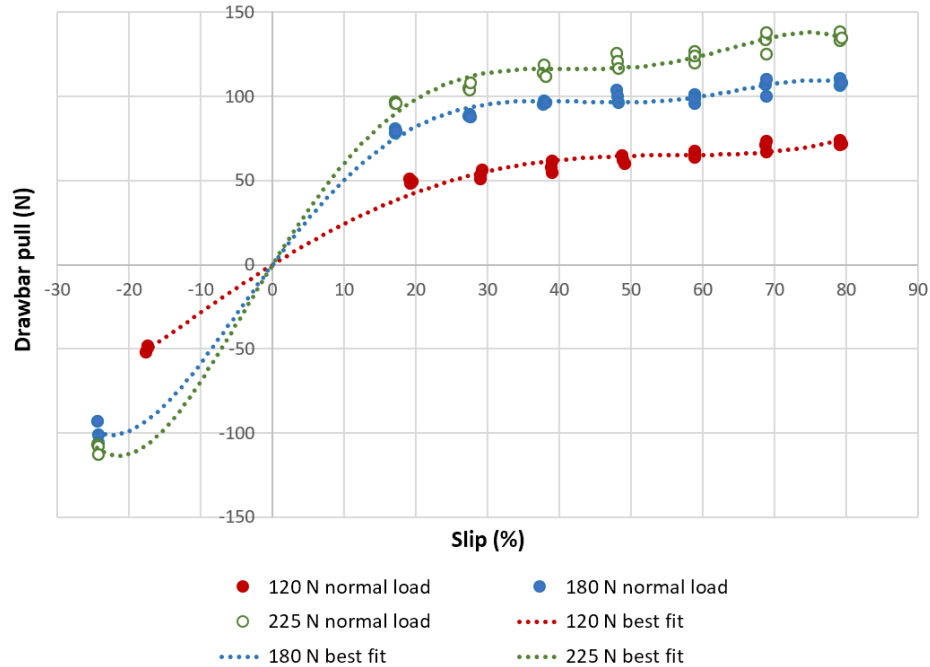


Figure 7-36 – Drawbar pull as a function of slip ratio on ES-4 for a prototype SFR wheel

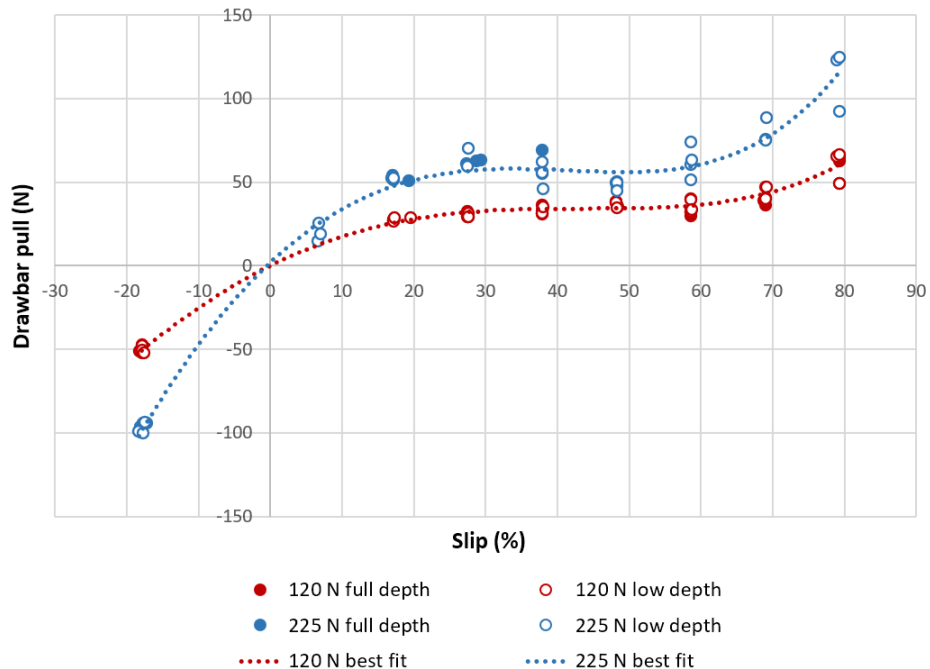


Figure 7-37 – Drawbar pull as a function of slip ratio on ES-2 for a prototype SFR wheel

The slip ratio used in these tests is defined as:

$$s = \frac{v - \omega r_e}{v}$$

where v is the velocity of the vehicle, ω the angular velocity of the wheel and r_e the effective rolling radius (accounting for tyre deflection). When the slip ratio is negative, it means that the vehicle is moving faster than the velocity commanded to the wheels, for example, when skidding downslope.

In Section 7.1.1 it was noted how a full-scale locomotion breadboard would be highly advantageous in addressing risks associated to four-wheeled planetary mobility and unknowns around the usage of superelastic spring tyres. The platform shown in Figure 7-38 was developed by MDA for such purpose and tested on a variety of representative terrains.

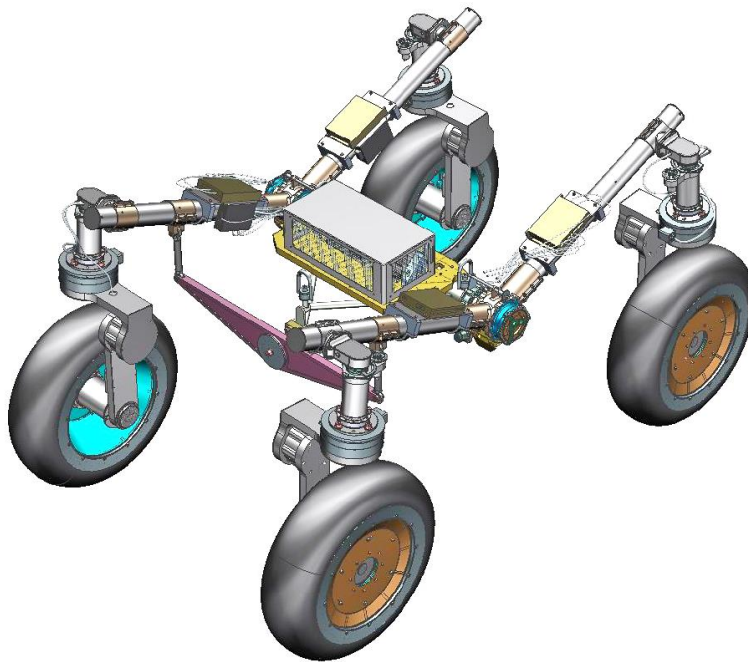


Figure 7-38 – Design of the SFR locomotion breadboard (credit: MDA)

One of the challenges associated to full-vehicle locomotion testing is that it has to produce loads on the wheels that are representative of Martian gravity, which is only 38% of Earth's. While for a single-wheel test the desired load can be applied through adjustment of the test rig, on a mobile platform this constrains the total mass to be 38% of the flight system's mass. The only alternatives are complex offloading systems using cables that are undesirable and can affect the locomotion behaviour, reducing its fidelity.

On SFR, the locomotion subsystem accounts for an unusually large mass fraction of the vehicle: around 30% of its total mass. This means that, if FAST was built according to the flight design, there would be very little mass left for the rover frame, control electronics and sensors. Furthermore, the centre of gravity would be far too low compared to the flight configuration. To address these issues, the breadboard rover uses a very lightweight version of the SFR locomotion, with fully-representative kinematics, but stripped down to the minimum structure necessary. The resulting platform is able to closely reproduce the weight and COG of the flight rover.

A test campaign was outlined for this platform, with the overall objectives of validating the SFR locomotion design, measuring its traverse performance, characterising wheel behaviour, quantifying the mechanical loads generated during mobility, augmenting the fidelity of the simulation and identifying areas of improvement in the rover's mobility [68]. A specialised rover test centre was selected, located at Beyond Gravity's (former RUAG Space)

site in Zurich. The facility uses a 6 m by 6 m testbed that can be filled with ES simulants or bedrock and populated with obstacles. The testbed is mounted on a tilting platform that can be configured to any slope up to 26°. Several force and torque sensors are incorporated in the system and also placed on the terrain when needed. The facility is equipped with a 3D tracking system to measure the motion of the vehicle and cameras positioned at multiple viewing angles.

The test programme focused on characterising the rover's ability to climb slopes and obstacles, but also included lateral slope cases, static stability tests, impact loads and traversal of randomly-structured terrain. An initial investigation was carried out to determine the most difficult obstacle shape to climb. The survey included rocks shaped like rectangular blocks, hemispheres or pyramids and demonstrated that the rectangular block clearly produced greater torques and slippage, thus becoming the reference sizing shape for all obstacle analyses. This initial investigation also demonstrated how the limiting factor is always the rear wheel climb, as predicted by the analysis in Section 7.1.4.

The slope and obstacle characterisation produced the results reported in Table 7-9, which, compared to the predictions in Table 7-7, shows better performance than expected for all combinations. The values reported here reflect the raw locomotion capability, so should be compared with the prediction without the 2 cm margin. The maximum slopes that the rover can climb without obstacles were found to be 12° on ES-2 and more than 25° on ES-4 and bedrock.

Slope angle	Max. obstacle on compact soil, ES-4 (cm)	Max. obstacle on drift soil, ES-2 (cm)	Max. obstacle on bedrock (cm)
0°	32.5 ⁷⁰	32.5	31 ⁷¹
5°	29.5	29.5	31
10°	25	25	31
15°	18	Not tested	27
20°	10	Not tested	15

Table 7-9 – Obstacle performance of the SFR locomotion breadboard on different substrates and slopes

The critical stability angle was measured as 35.8° in the lateral direction, in good accordance with the analysis in Section 7.2.1.1. Impact loads were measured through force impact plates positioned where the wheel would land descending an obstacle. These loads will be used to size the mechanical elements of the suspension and the wheels. Lastly, test runs on randomly distributed rocks were performed to reproduce certain CFA levels. These produced very good results in terms of energy consumption, measured at 250 J/m on CFA 5%

⁷⁰ On this breadboard the ground clearance is greater than on the flight configuration, allowing to test obstacles taller than 29.5. The limit of the purely wheel-driven capability (i.e., neglecting ground clearance) was not found for the low slope angles, but is expected to be well above 32.5 cm.

⁷¹ The tallest obstacle on bedrock is only 31 cm due to the bedrock substrate taking up some height, however, the capability is expected to be even greater than that on other soils.

and 300 J/m on CFA 10% (both on 0° slope). One of the tests included a “torture track” configuration with a great number of sharp rocks – many more than any CFA level that SFR would encounter – to test the robustness of the wheels. Figure 7-39 shows some snapshots of the testing: slope climbing on ES-2 (A), static stability (B), torture track (C), obstacle climbing on bedrock (D).

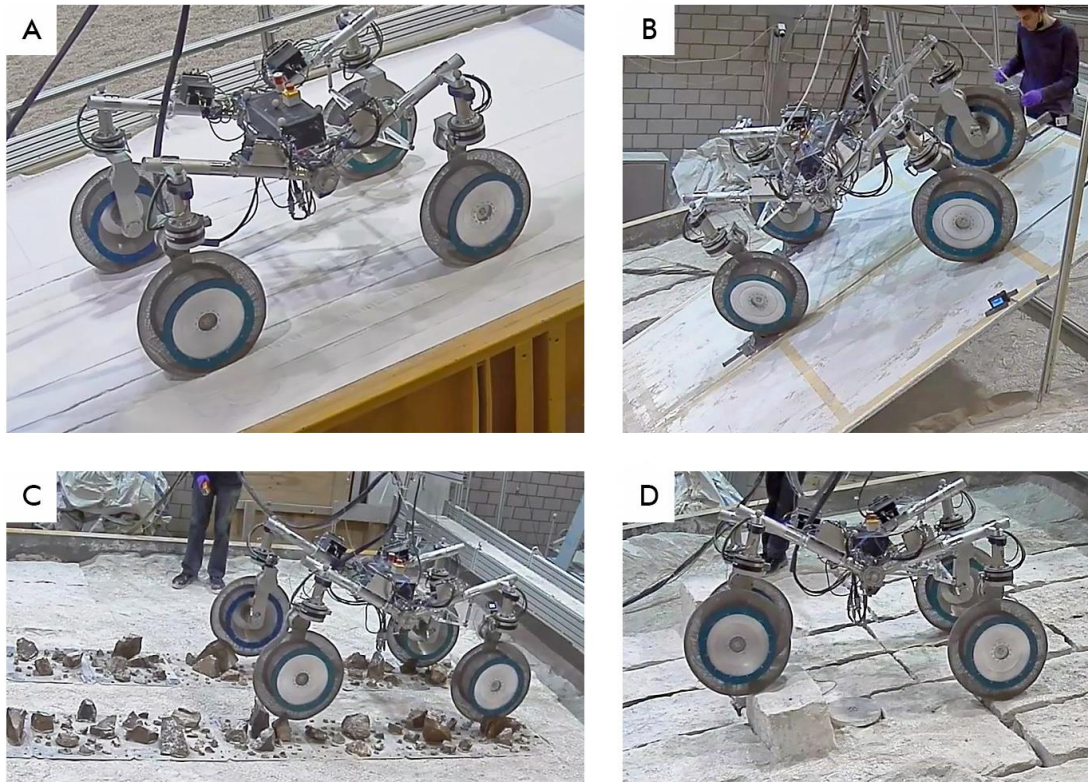


Figure 7-39 – Snapshots of the breadboard locomotion testing (credit: MDA / Beyond Gravity)

The results of this test campaign have been extremely valuable in demonstrating that the design of the SFR locomotion subsystem is on the right path and in retiring risk on its development. The superelastic spring tyres have consistently performed above expectations, proving that they are an appropriate choice for a four-wheeled platform. The information gathered has been used to calibrate the simulations described in Section 7.3.1, leading to a higher-fidelity estimation of the vehicle’s capability, the energy and time penalties associated with each terrain configuration. This allowed to tune the GNC system to account for this performance and provided confidence that SFR can complete its mission within the time and energy available.

8 DEVELOPMENT OF THE SFR SYSTEMS: SAMPLE ACQUISITION

The essence of the SFR mission can be crudely summarised as traversing to the depot, acquiring tubes and traversing back to the lander to deliver those tubes. In this view, the two most prominent high-level functions of the spacecraft are locomotion and tube acquisition. While the former has been described in the previous chapter, the latter will be covered in the present one, which is dedicated to the system responsible for acquiring up to 30 Returnable Sample Tube Assemblies (RSTAs) from the surface of Mars: the RSTA Acquisition System (RAS).

The elements that form the RAS are spread across the perimeters of multiple subsystems, sometimes shared with other functions (e.g., cameras used also by GNC during traverse), so the aim of this chapter is to summarise how they come together to enable autonomous retrieval of the sample tubes. The following pages will firstly outline the architecture of the system and its operations, then describe the chosen technical solutions and discuss how their implementation is justified by analysis.

Before entering the detailed discussion, one clarification should be made as to the terminology associated with the sample tube. In this document so far, the item to be retrieved from the surface of Mars is described as an RSTA (or, more simply, “tube”), corresponding to the assembly shown in Figure 5-6. However, late in the SFR development, a choice was made to leave another piece of hardware attached to the tube, called “glove”⁷². The glove is a titanium part connected to the wider portion of the tube, whose function is to facilitate its handling inside the Perseverance rover. The reason for leaving this component on the tube is to aid subsequent handling by the robotic systems on board the lander. The thereby obtained item is called an “RSTA and Glove Assembly” or RGA and the RAS was requested to be compatible with it. However, this was only preliminarily assessed at the time of writing and therefore will not be included in this summary. Most of the considerations discussed here

⁷² This decision can be made while Perseverance is already on Mars because it has the functionality to separate the glove from the tube or not before dropping it in the depot.

remain valid also for the acquisition of RGAs, even though they are larger than RSTAs and have different mechanical interfaces, so they would affect the detailed mechanical design of some components.

8.1 RAS architecture

The RSTA Acquisition System performs the high-level functions of identification, acquisition, manipulation and stowage of the sample tubes. To achieve these functions, the system is composed of a suite of hardware items and software applications, as follows:

- **Vision system**, containing:
 - Navigation Camera (NavCam), shared with the rover’s GNC (see Section 6.6). The same stereo camera that maps the rover’s surroundings for traverse is used by the RAS to image the terrain in search of the tube.
 - RSTA Detection Camera (RDC), a small “eye-in-hand” camera on the manipulator’s wrist, dedicated to close-up imaging of the tube.
 - Vision-Based Detection Software (VBDS), the algorithm that analyses images and returns the estimated position of the tube in space.
- **Arm and Gripper Subsystem (AGS)**, containing:
 - Robotic arm, a 6-DOF manipulator to reach and handle the tube.
 - Gripper, the arm’s end effector that captures the tube and carries it to its storage location.
 - RSTA Re-grip Bracket (RRB), a temporary resting feature for the tube to allow to switch the grasping point.
 - AGS control software, the program that transforms high-level commands into arm motion profiles and monitors their execution.
- **RSTA Storage Assembly (RSA)**, a structure containing 30 slots to secure the sample tubes acquired by the RAS.
- **Acquisition Management Software (AMS)**, the software in charge of the end-to-end acquisition sequence, from the moment the rover arrives at the tube location to when it is ready to depart.

The RAS also uses other elements on board the rover that are part of other systems, in particular the Actuator Control Electronics (ACE), which control all mechanisms on board including the AGS, the Integrated Avionics Box Subsystem (IABS), which runs all the software required by the RAS, and the Mission Management Software (MMS), the central software of the Sample Fetch Rover that orchestrates every phase of the mission and issues commands to the AMS. Some of the hardware elements mentioned above can also be seen in Figure 6-6. Table 8-1 provides a summary of the main organisations involved in the RAS and their roles in its development.

Organisation	Role
ESA	End customer, partner with NASA as part of MSR
Airbus	Prime contractor for SFR, technical authority for the RAS and developer of the AMS
Leonardo	Contractor for the AGS, including control software, RDC and RRB
Sener	Contractor for the gripper
GMV	Developer for the VBDS
Beyond Gravity	Contractor for the RSA
Maxon	Supplier of actuators for the AGS

Table 8-1 – Main organisations and their roles in the development of the RAS

8.1.1 Design drivers

The main design drivers that have influenced the RAS implementation are the tube pickup timeline, the topology of the depot terrain and the physical configuration of the rover. With regard to the timeline, it might not appear particularly demanding upon first assessment, since SFR has a period in the order of 100 sols to pick up 30 tubes during a typical mission. However, it is easy to underestimate the time required to carry out complex robotic operations on a deep space mission.

If, for example, the rover was primarily teleoperated by ground, the sequence would take an enormous amount of time. It can be imagined how a command (e.g., move the arm to a certain location) would be scripted, checked and issued by ground, beamed to Mars through a Deep Space Network (DSN) antenna and received by an orbiter of the Mars Relay Network (MRN) a few minutes later. Following that, the orbiter would have to store the data until a usable pass over the rover's location, which might be hours away. Once the instructions are downlinked to the rover, they would be executed over a timespan of minutes to hours for typical robotic operations like in this example. At the end of the activity, the rover would collect telemetry and any useful information on the outcome, then wait for an orbiter link and transmit the data. A few minutes later, ground would have feedback on the execution of their instruction. At that point, even if everything went perfectly and mission controllers already had the next batch of instructions ready for upload, the rover would have most likely transitioned to sleep, so any other activities would be carried out the next day.

The heavy time penalties that come with telecommunications across the Solar System can be avoided only through a high degree of operational autonomy, so that the spacecraft is able to continue its mission for prolonged periods without ground intervention. Even Perseverance, which has excellent autonomy and direct-to-Earth communication capability (i.e., it does not need to wait for an orbiter pass) takes days, sometimes weeks, to collect a sample. If the RAS took the same time to retrieve it, the SFR mission would be completely unfeasible.

As a result, SFR is able to carry out its tube acquisition operations in full autonomy. Not only can it approach, identify, pick-up and stow a tube by itself, but it can also handle various failures and anomalies and decide whether to re-try with alternative strategies or stop the sequence. Furthermore, once operations on a tube are terminated, it can automatically drive to the next one marked for pickup. If operations are interrupted in the evening, the rover would be able to resume from that point the following day. The most frequent termination condition for RAS operations is due to the sun producing shadows too long to allow reliable visual recognition.

The morphology of the terrain on which the tubes are deposited drives the design of the vision algorithms and of the manipulation systems, in particular the gripper. Naturally, this terrain cannot be known until Perseverance has prepared the depot, but a series of guidelines, established in cooperation between the SFR and the Perseverance teams, allow to bound its characteristics. Tubes cannot be deposited on loose sand, because they would get covered by the action of the wind and become unrecoverable. They cannot be deposited on any type of terrain that is too featureless, as there would be no reference points for positioning the rover. On the other hand, the presence of large rock formations can impede access to the tubes.



Figure 8-1 – Tubes lying on terrain with rocks and crevasses (credit: NASA / JPL-Caltech)

The ideal depot location is an area of flat bedrock or compacted regolith with a degree of general roughness and small rocks. This implies that there will be features that can produce various shadows and shapes that the vision system must be robust to. It also means that there will be situations where the tube is lying in proximity of an obstacle or in a depression, so the arm and gripper need to be able to access narrow spaces. Figure 8-1 provides some examples of such situations. It should be noted that this figure contains several tubes in close proximity, which are arranged in this way to exercise the vision system but do not represent a real depot layout.

The last key design driver for the RAS is the physical configuration of the rover, in particular the forward-facing area, where most of the RAS elements are located. The mechanical architecture of the rover is heavily constrained by its accommodation on the lander and the stowage of the locomotion subsystem, described in Chapters 6 and 7. As a consequence, the ground footprint and the size of the rover body cannot go beyond certain limits. These constraints define, respectively, the workspace on the ground between the wheels from where the tube can be picked up and the area on the vehicle's front face where the RAS hardware can be mounted.

The SFR GNC controls the vehicle by monitoring terrain features, so it is generally unaware of the presence of tubes. However, the location of each tube with respect to the terrain is known a priori, so can be inferred during navigation. In the depot area there will be DEM data available at medium to high resolution, enabling SFR to position itself with respect to the tube before attempting visual detection. This operation is affected mainly by two types of error: on position knowledge and on position control. The error on position knowledge is based on the quality of the DEMs (the one produced by Perseverance and the one generated on board SFR) and the feature matching process. The error on position control is mostly due to interactions with the terrain (such as areas with different traction, slip, sinkage, resistance caused by obstacles), plus a small contribution from the locomotion actuators' accuracy. A conservative estimate places the total error at approximately ± 310 mm, with a contribution of 100 mm from position knowledge and 210 mm from position control.

It derives from the above that, as the rover attempts to position itself for picking up a tube, it will have a maximum error of ± 310 mm in any direction. Expressing it from the rover's point of view, it means that the centroid of tube can end up in any location within a 620-mm-diameter circle on the surface. Adding the tube length, this leads to a circle of 765 mm in diameter containing the entire tube.

The circular region just described is of great importance for the physical architecture of the RAS and of SFR. It defines the area that must be visible by the cameras for tube recognition, it sizes the robotic arm's workspace and it constitutes a keep-out zone where the wheels cannot drive to avoid the risk of damaging the tube. As the pickup area is located between the front wheels, this circle also sets a minimum value to the width of the rover. The tube pickup area just described is reported in Figure 8-2, while Figure 8-3 provides the projection of this area in the field of view of the NavCam tilted downwards.

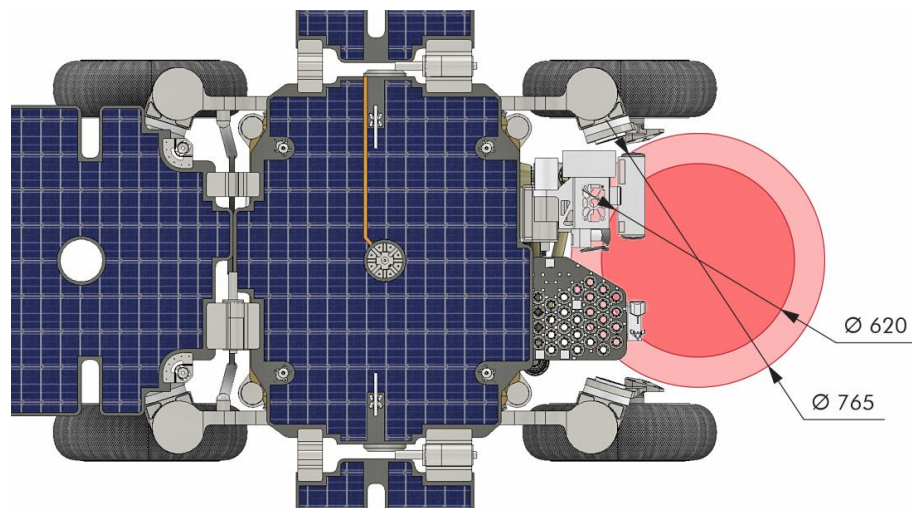


Figure 8-2 – Tube pickup area in front of the rover (red circles)

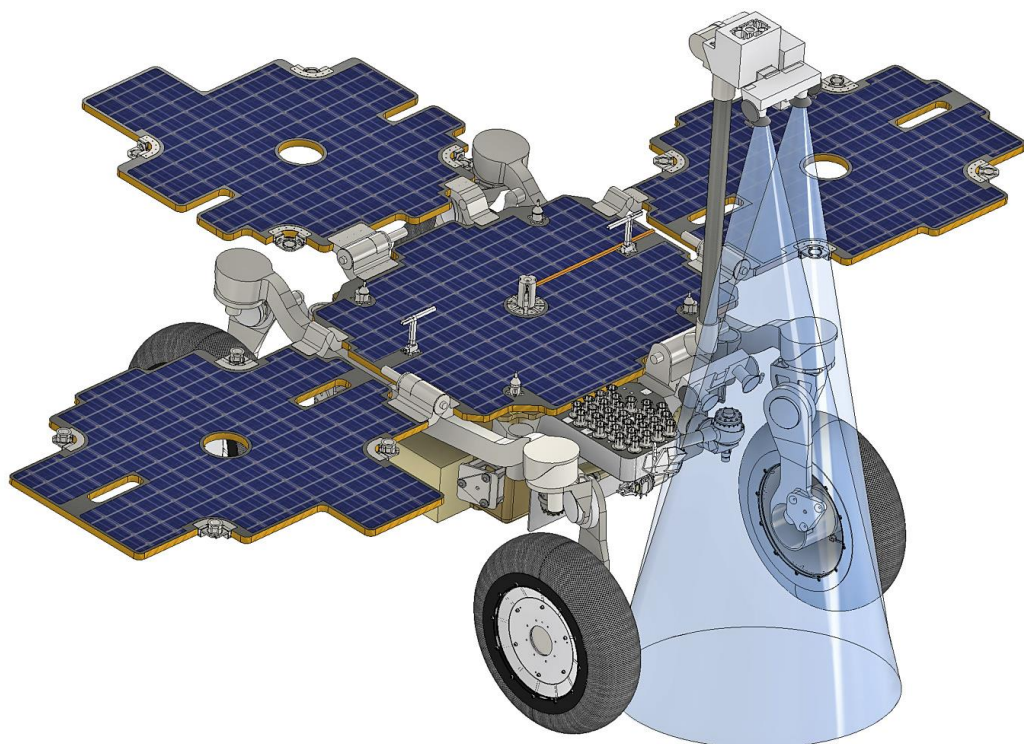


Figure 8-3 – Tube pickup area with viewing cones from the NavCam

One last driving requirement worth noting on the physical layout comes from the interface with the lander for tube transfer. All tubes must be provided with their “heads” (i.e., the larger portion of the tube) pointing upwards. In addition, their spacing and the hardware around them must guarantee access corridors for the large Sample Transfer Arm (STA). This drives the size and location of the tube storage assembly, contributing to the constraints on the front face of the rover.

8.2 Tube fetching operations

In response to the challenging timeline described in the previous section, the tube fetching operations are highly automated, so that the rover can carry out most of them without the intervention of mission controllers. SFR can handle several error conditions and failures by itself and would call for ground only for critical faults or if tube safety is threatened. This implies the definition of a robust failure management strategy for all those situations that are not planned but have a non-insignificant probability of occurring. Once again, the approach is statistic: only the most credible events are covered to avoid excessive complexity in the software. The following pages describe the typical operational sequence of the RAS and the management of some of these exceptions as they occur.

8.2.1 Tube approach

The Sample Fetch Rover orientates itself primarily by observing terrain features. This is true also when driving up to a tube in the depot. As described in Section 6.6, the SFR GNC provides a novel function, never implemented on board a planetary rover before: Absolute Global Localisation (AGL). This feature allows the rover to compare DEMs or images of its surroundings with maps stored on board and estimate its position with relation to them [69]. AGL is available in two variants: AGL-T for traverse operations and AGL-D for depot operations.

AGL-T is activated regularly while driving and it compares the local topology with maps from the High-Resolution Imaging Science Experiment (HiRISE) payload on board Mars Reconnaissance Orbiter. HiRISE data has a resolution of approximately 0.3 m and the AGL-T process is expected to achieve a positioning accuracy better than 10 m (varying on the basis of the quality of the HiRISE data at that particular location).

The rover transitions to AGL-D upon arrival in the depot area. This location will have been mapped by Perseverance with a resolution varying from a few cm for the overall coverage to 1 mm in close proximity of the tube. The AGL-D process is expected to achieve a position knowledge accuracy better than 10 cm, in line with the assumptions in Section 8.1.1. A simulation was run using a dataset from a previous rover field trial where both NavCam images and ground truth information are available. The ground truth map was scaled down to the worst-case resolution from Perseverance and was provided to the AGL-D algorithm as reference. The algorithm was then fed with NavCam images that were combined into DEMs and compared to the reference. The results are shown in Figure 8-4, which plots the 2D position error (obtained by comparison with ground truth) and the 2D uncertainty (estimated by the AGL-D feature-matching algorithm) for 1000 test runs on this dataset.

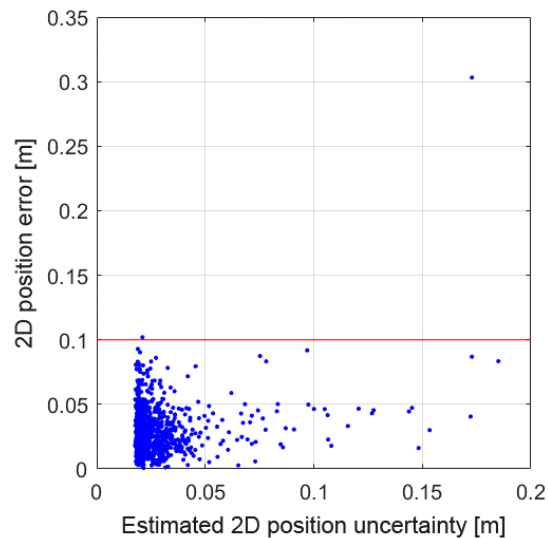


Figure 8-4 – Results of AGL-D performance simulation (credit: M. Dinsdale)

Once the rover has completed the approach and is parked in proximity of the tube, one final command tilts the mast head down so that the cameras' line of sight is orthogonal to the ground. The locomotion and mast actuators are then powered off and the control is handed over to the Acquisition Management Software. This marks the beginning of the RAS operations.

8.2.2 Tube detection

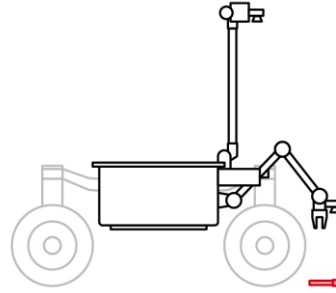
The first part of the RAS operational sequence is dedicated to the identification of the tube and estimation of its position with respect to the rover. The detailed sequence of activities is presented in Table 8-2.

Activity	Illustration
<p>1. NavCam-based detection</p> <ol style="list-style-type: none"> a. AMS requests NavCam stereo image acquisition b. NavCam images are sent to VBDS for processing c. VBDS returns 5-DOF tube pose⁷³ and point cloud of the terrain around the tube d. AMS verifies that the tube is reachable by the arm without collisions and computes preliminary approach trajectory 	

⁷³ The roll angle around the tube's major axis is neglected as it is not required for the operations.

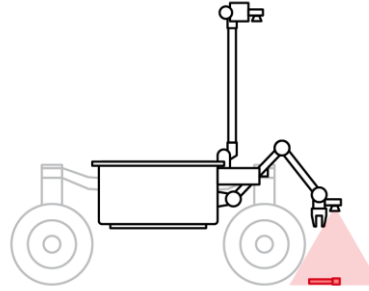
2. AGS deployment

- a. AMS requests a deployment trajectory to a pre-defined idle pose to AGS software
- b. AMS sends motion profiles to ACE
- c. ACE commands AGS actuators to achieve the desired trajectory



3. RDC-based detection

- a. AMS generates two arm poses for stereo imaging of the tube with RDC
- b. AMS requests trajectory to first RDC pose to AGS software
- c. AMS sends motion profiles to ACE
- d. ACE commands AGS actuators to achieve the desired trajectory
- e. AMS requests RDC image acquisition
- f. Steps b. to e. are repeated for second RDC pose
- g. RDC images are sent to VBDS for processing
- h. VBDS returns updated 5-DOF tube pose



4. Generation of pickup trajectory

- a. AMS generates set of waypoints to the tube location
- b. AMS sends waypoints to AGS software to generate pickup trajectory
- c. AGS software returns pickup trajectory
- d. AMS confirms successful completion of tube detection sequence to MMS

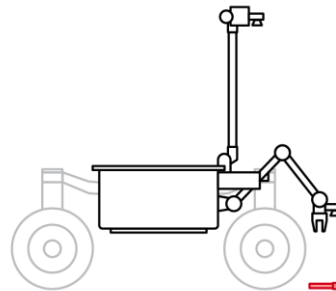


Table 8-2 – Operational sequence for tube detection

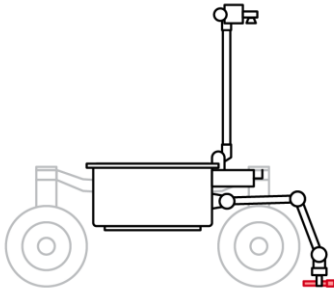
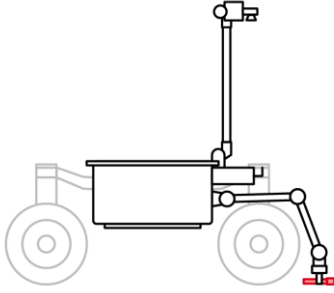
It can be noticed in the sequence how the visual detection process is performed in two iterations: a first one using the NavCam on the mast and a second one using the RDC on the robotic arm’s wrist. This is due to the fact that the NavCam provides a wide view of the terrain that certainly includes the tube, while the RDC allows more targeted close-up imaging that increases the accuracy of the pose estimation on the tube. For tubes that are clearly visible and not placed in challenging terrain (i.e., there are no features around them that require accurate position knowledge to be avoided), the NavCam-based detection alone can be sufficient. When approaching those tubes, step 3 can be inhibited in the sequence to save time. Knowledge of the terrain from Perseverance’s data allows to configure this a priori in certain cases.

It was discussed in Section 8.1.1 how a high degree of autonomy is necessary to meet the pickup timeline and particularly how the resolution of certain types of failure must be attempted on board before calling for ground intervention. The activities in Table 8-1 constitute the nominal sequence, but a significant number of alternative approaches are coded into the AMS logic to deal with exceptions. For example, the NavCam-based visual detection is an activity that cannot be guaranteed to always succeed due to lighting conditions and terrain features around the tube.

If the first detection attempt failed, the AMS would request more images with different exposures to try to mitigate shadowing issues. In case this also failed, the rover would exit from its RAS operation mode and re-engage the locomotion subsystem to drive around the tube location and obtain another viewing angle, which might be more favourable to detection. If even this last attempt was unsuccessful, the system would request ground intervention. However, it would not do so in a way that interrupts the fetching sequence: it would simply save all the images acquired for transmission to ground control and move on to the next tube. In this way, mission operators can address the issue offline, with minimum impact on the operational schedule of the rover, and return to that tube at a later time. Similar strategies are coded in multiple areas of the RAS operations to maximise the rover's ability to autonomously manage anomalies.

8.2.3 Tube grasping

The sequence of operations for the tube grasping phase is reported in Table 8-3 (the numbering is continued from Table 8-2).

Activity	Illustration
<p>5. Arm motion to pickup point</p> <ul style="list-style-type: none"> a. AMS sends motion profiles for pickup trajectory to ACE b. ACE commands AGS actuators to achieve the desired trajectory c. AGS motion is stopped by detection of contact with the tube or the ground by sensors on the gripper⁷⁴ 	
<p>6. Tube grasping</p> <ul style="list-style-type: none"> a. AMS commands (via ACE) to close the gripper b. AMS sends motion profiles to follow the pickup trajectory in reverse to ACE c. ACE commands AGS actuators to achieve the desired trajectory d. AMS commands (via ACE) to close the gripper again to guarantee preload⁷⁵ e. AMS sends motion profiles for idle pose to ACE f. ACE commands AGS actuators to achieve the desired trajectory g. AMS verifies that AGS telemetry⁷⁶ indicates presence of the tube between the gripper's fingers 	

⁷⁴ These sensors and the detailed gripper design are further discussed in Section 8.4.2.

⁷⁵ Once the tube has been lifted above the ground, a second closing motion is commanded. Its purpose is to restore the preload in case sand was present between the tube and the fingers and had fallen out during pickup, loosening the grip.

⁷⁶ The fingers strain gauges and position sensors are read to confirm that the position at which the preload is detected is consistent with a tube being present between the fingers.

7. Grasp check

- a. AMS requests trajectory to a predefined grasp-check pose⁷⁷ to AGS software
- b. AMS sends motion profiles to ACE
- c. ACE commands AGS actuators to achieve the desired trajectory
- d. AMS requests NavCam stereo image acquisition
- e. NavCam images are sent to VBDS for processing
- f. VBDS returns confirmation of tube presence and position of the gripping point on the tube's shaft

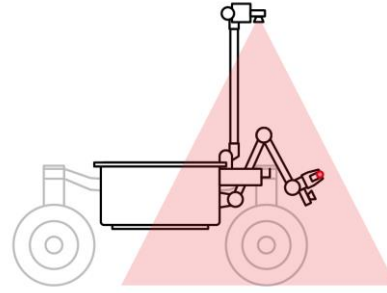


Table 8-3 – Operational sequence for tube grasping

These operations contain the first contact between SFR and a sample tube: that would be the first time two human-made objects, launched at different times, meet on another planet. It has been mentioned in Section 8.1.1 how the safety of the tube and its content are a major design driver. In the case of direct mechanical manipulation of the tube this becomes even more critical. Mars Sample Return aims to provide humankind with pristine samples from the Martian surface, so there is little value in returning damaged tubes that would expose their content to contamination from the Earth's atmosphere. The point that is particularly sensitive to mechanical damage is the area of the seal, where thin metal parts are plastically deformed to form an airtight connection.

The operational sequence takes this aspect into account and aims to ensure that no hardware on the rover ever makes contact with the tube seal. As a result, some types of faults cannot be corrected on board. In particular, if the grasping activity is not successful and the tube is not detected in the gripper after a pickup attempt, the AMS would return to point 1 in the sequence and trigger another detection of the tube. If that shows that the tube is still in the workspace and can be picked up, then the activity would restart. On the other hand, if the tube is not detectable anymore, it might mean that it has rolled away or it has been dropped⁷⁸ at some point in the sequence. In that case, the rover would acquire various images and call for ground. It would not even try to drive away as the tube might be in proximity of a wheel. It is a prerequisite of the autonomous RAS operations that the tube remains in full control at all times.

One last aspect worth noting in this sequence is the role of the grasp check operation. This is not only to confirm that there is a tube in the gripper, but also to estimate the position of the gripping point along the tube shaft, which is affected by errors during grasping. Knowing this position is useful for aligning the tube during insertion into the RRB, part of the next set of activities.

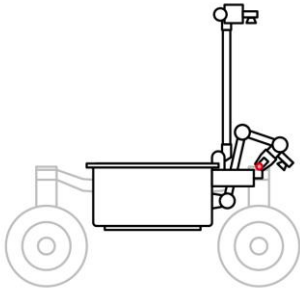
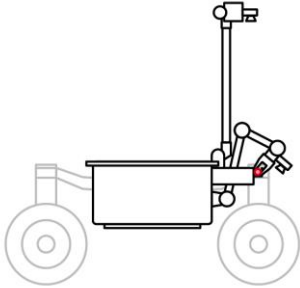
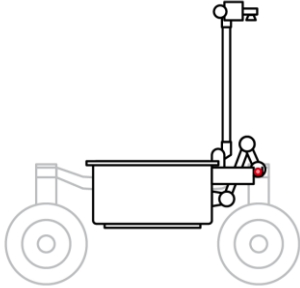
8.2.4 Tube stowing

Table 8-4 provides a summary of the tube storage operations (the numbering is continued from Table 8-3).

⁷⁷ The grasp-check pose brings the sample tube up towards the NavCam to facilitate imaging.

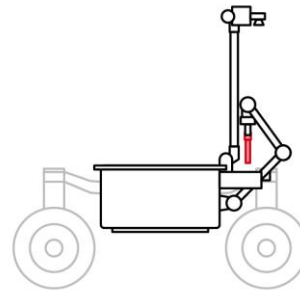
⁷⁸ Dropping to the ground from this height is not harmful for the sample tube. That is, in fact, how the tubes are released by Perseverance.

Steps 9 and 10 in this sequence are dedicated to insertion and extraction in the RSTA Re-grip Bracket (RRB). The role of this device is simply to provide a temporary station to switch the grasp of the tube from a “body grip” (approximately located in the middle portion of the tube shaft) to a “head grip” (holding the head of the tube with the shaft pointing away from the gripper). The head grip is necessary to secure the tube into the storage, where the shaft is inserted into the storage slot and would not be accessible. The tube storage assembly and the insertion motion are further discussed in Section

Activity	Illustration
<p>8. RRB approach</p> <ol style="list-style-type: none"> AMS requests trajectory to a predefined RRB approach pose to AGS software AMS sends motion profiles to ACE ACE commands AGS actuators to achieve the desired trajectory 	
<p>9. RRB insertion</p> <ol style="list-style-type: none"> AMS requests trajectory to first RRB alignment point to AGS software AMS sends motion profiles to ACE ACE commands AGS actuators to achieve the desired trajectory AGS motion is stopped by contact with the first RRB alignment sensor Steps a. to d. are repeated for second RRB alignment point AMS commands (via ACE) to open the gripper 	
<p>10. RRB extraction</p> <ol style="list-style-type: none"> AMS requests trajectory to a predefined RRB pickup pose to AGS software AMS sends motion profiles to ACE ACE commands AGS actuators to achieve the desired trajectory AGS motion is stopped by detection of contact with the tube by sensors on the gripper AMS commands (via ACE) to close the gripper AMS requests trajectory to a predefined RRB extraction pose to AGS software AMS sends motion profiles to ACE ACE commands AGS actuators to achieve the desired trajectory 	

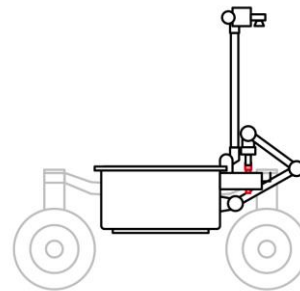
11. RSA approach

- a. AMS requests trajectory to a predefined RSA approach pose to AGS software
- b. AMS sends motion profiles to ACE
- c. ACE commands AGS actuators to achieve the desired trajectory
- d. AMS allocates a slot in the RSA to the tube and retrieves the approach pose for that slot
- e. AMS requests trajectory to RSA slot approach pose to AGS software
- f. AMS sends motion profiles to ACE
- g. ACE commands AGS actuators to achieve the desired trajectory



12. RSA insertion

- a. AMS requests trajectory to RSA slot insertion pose to AGS software
- b. AMS sends motion profiles to ACE
- c. ACE commands AGS actuators to achieve the desired trajectory
- d. AGS motion is stopped by reaching the end of travel on the RSA slot
- e. AMS commands (via ACE) to open the gripper



13. Arm stowage

- a. AMS requests trajectory to a predefined idle pose to AGS software
- b. AMS sends motion profiles to ACE
- c. ACE commands AGS actuators to achieve the desired trajectory
- d. AMS sends motion profiles to ACE for predefined arm stowage sequence
- e. ACE commands AGS actuators to achieve the desired trajectory
- f. Once stowage is confirmed by AGS sensors, AMS flags sequence as completed and hands over to MMS

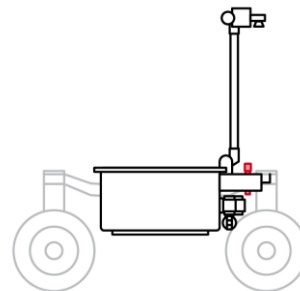


Table 8-4 – Operational sequence for tube stowing

The set of activities in Table 8-4 concludes the RAS operations. The entire sequence, from step 1 to 13, is repeated for each tube, with deviations, as mentioned above, in case of failure or if ground control chose different activity plans for some specific tubes. As a matter of fact, in the SFR mission there is one last sequence involving the RAS, although this happens with the system completely inactive: the tube transfer operation. This constitutes the handover of the tubes to the Sample Retrieval Lander (SRL), for which SFR has to park in a specific location within the workspace of the Sample Transfer Arm (STA). The vehicle is then switched off and the STA autonomously offloads all the tubes from the storage and secures them into the canister that will be launched into orbit.

8.3 Vision system

The components used for visual detection of the sample tube are spread across the perimeter of multiple subsystems. They consist in the Navigation Camera (NavCam, part of the

rover's GNC), the RSTA Detection Camera (RDC, part of the AGS perimeter) and the Vision-Based Detection Software (VBDS, coded on the rover's computer in the IABS). A brief summary of their design is provided below.

8.3.1 Cameras

As described in Section 8.2.1, the first attempt to detect a sample tube is always made using the NavCam on top of the rover's mast. This camera offers a wide view that can be assumed to always contain the tube, so it does not require any specific pointing beyond being tilted downwards. However, the accuracy on tube pose estimation from the NavCam is limited by the width of the stereo bench, which is only 0.15 m, while the tube is more than 1.7 m away. Triangulation errors are significant when dealing with such a small stereo base, so for the tubes that require precise positioning of the gripper to avoid terrain features, the NavCam is not sufficient.

The RSTA Detection Camera (RDC) is a single-lens camera, it is close to the ground and requires pointing towards the tube's location (previously estimated using the NavCam). Through movement of the arm, the camera can acquire a stereo pair of images from two positions that have a spacing of the same magnitude of the tube distance from the camera, thus achieving a much tighter pose estimation error. Furthermore, RDC images can be requested at any moment during the tube grasping sequence, allowing ground to command the arm more accurately for difficult pickup situations. Figure 8-5 shows CAD models of the NavCam and the RDC mounted on the robotic arm, while Table 8-5 reports some key specifications of the two cameras.

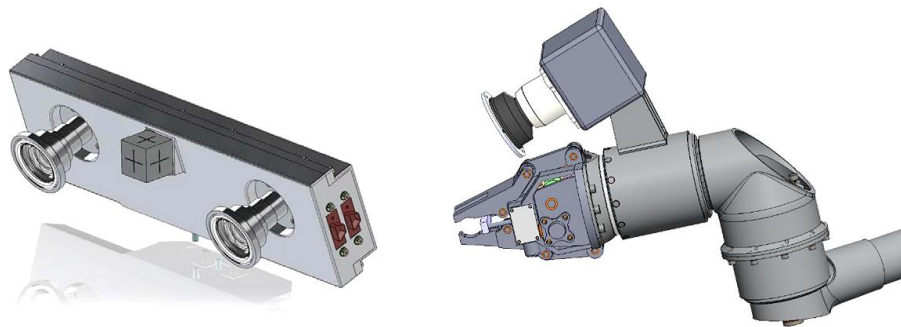


Figure 8-5 – NavCam (left) and RDC on the arm's wrist (right) (credit: Neptec / Leonardo)

Feature	NavCam	RDC
Field of view	65° x 65°	65° x 65°
Resolution	2048 x 2048 px	1024 x 1024 px
Colour mode	Monochrome	Monochrome
Focusing distance	1.7 m – ∞	150 mm – 350 mm
Stereo base	150 mm	Single lens
Mass	0.95 kg	0.30 kg

Table 8-5 – Key features of the NavCam and RDC

8.3.2 Vision-Based Detection Software

It has been discussed on multiple occasions how SFR takes advantage of the availability of imagery and data from Perseverance to simplify both traverse and RAS operations. Bringing this reasoning further, it could be envisaged to implement a tube detection strategy that attempts to recreate the very same images acquired by Perseverance. If the two pictures correspond, the presence of the tube in them is certain and its location can be estimated accurately through an image-to-image feature-matching process.

However, this approach encounters fundamental issues. Firstly, the control of a rover on rough terrain is not sufficiently accurate to replicate so closely another vehicle's position. Secondly, the camera properties and viewing angles would be different, as would the lighting conditions unless the pictures are taken at the same time of the day, during the same season and with similar weather. Lastly, SFR could arrive at the tubes years after the images have been taken, so the constant deposition of dust by the wind could have changed the appearance of the tubes and the scenery.

The SFR Vision-Based Detection Software (VBDS) is used to provide identification and pose estimation of a tube in different steps of the acquisition sequence: during tube detection from the NavCam, from the RDC or during the grasp check (see Section 8.2). The software must meet its performance under varying conditions of illumination and dust coverage. Furthermore, it must be executable within the limits of the computational resources on board and within the time available in the pickup sequence (the time for tube detection is in the order of 10 minutes, depending on the images used).

The working principle of the VBDS is a semantic segmentation performed using convolutional neural networks. The segmentation approach consists in pixel-level labelling and grouping of pixels that are recognised as belonging to the same object. In this specific case, the pixels can be labelled only as belonging to the tube or the terrain. The neural network used for the segmentation is ESPNetv2, pre-trained with a tube template. Once a group of pixels has been effectively identified as a tube, the 3D point cloud formed by those pixels is processed to estimate its position and orientation in space. The algorithm does not attempt to establish the rotation along the major axis of the tube (roll) because it is not necessary for the handling and the features to be detected for that would be too small for the resolution available.

8.4 Arm and Gripper Subsystem

The Arm and Gripper Subsystem (AGS) is developed by Leonardo for the Sample Fetch Rover project. It consists in a 6-DOF robotic arm with its control software, an end effector, an RSTA Re-grip Bracket (RRB) and supporting hardware. The RDC is also formally within this perimeter, although it has been already discussed as part of the vision system Section 8.3. These components can be seen in Figure 8-6. The primary function of the subsystem is to provide the manipulation capability required to bring the tube from the ground to its designated storage on SFR.

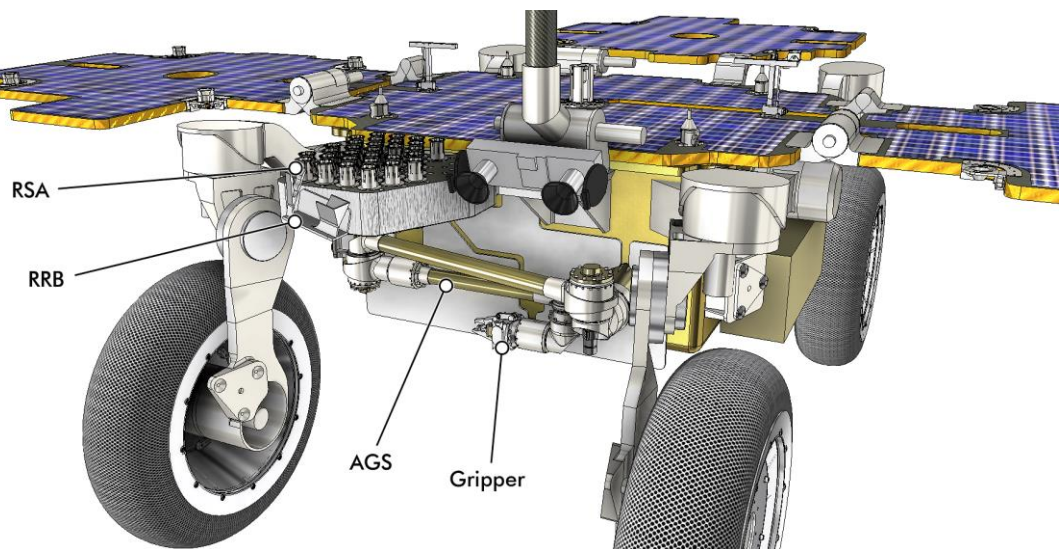


Figure 8-6 – Front face of the rover with RAS hardware annotated

8.4.1 Arm design

The robotic arm can be easily identified on the front face of SFR in Figure 8-6. It is stowed onto the rover body, under the tube storage, and its workspace extends between the wheels and at the front of the vehicle. Figure 8-7 depicts the arm extended to a typical tube pickup location.

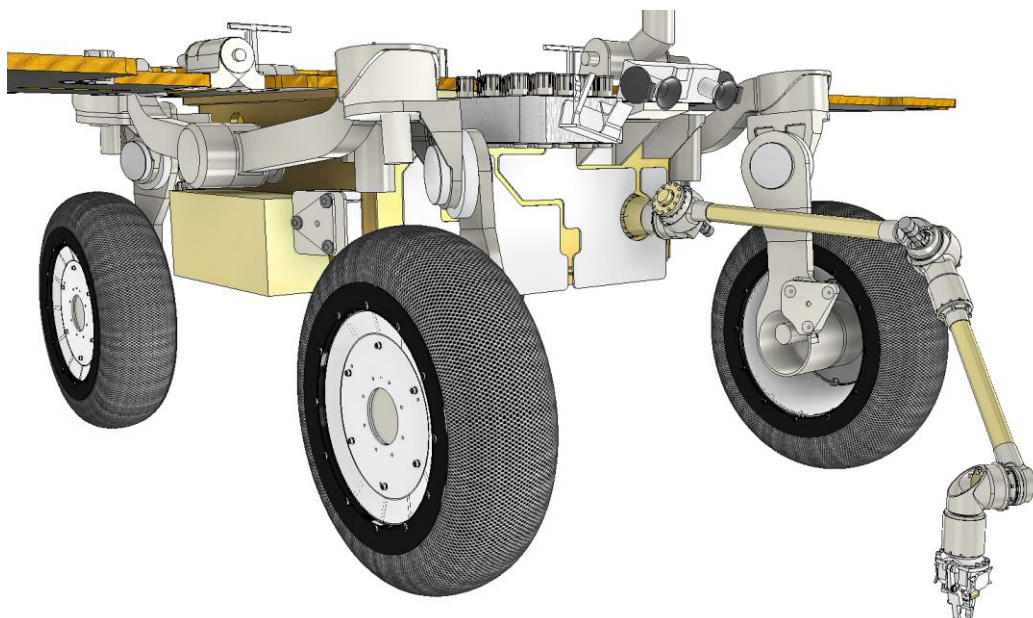


Figure 8-7 – AGS in a tube pickup pose

The stowed volume and the arm's reach are strongly conflicting requirements. The former is essentially limited by the rover's width and the latter is driven by the size of the tube pickup area described in Section 8.1.1. To satisfy both design drivers, the arm must be folded onto itself into a compact package and the pickup area must be situated as close as possible to the rover (where a hard constraint is placed by the visibility from the NavCam). The arm

is also mounted close to the ground to facilitate reaching the tube, however, it must be considered that also delivering the tubes into the storage is a driver for vertical reach.

The arrangement of the six joints along the arm is designated as R-P-P-R-P-R, where R indicates roll and P pitch, starting from the base of the manipulator. Two principal limbs define the length of the arm, with clusters of actuators located at their extremities. This layout is depicted in Figure 8-8. The arm's limbs are composed by aluminium tubes, while the housings of the joints and their mounting brackets mostly use machined titanium for their construction. The entire assembly has a mass of less than 10 kg.

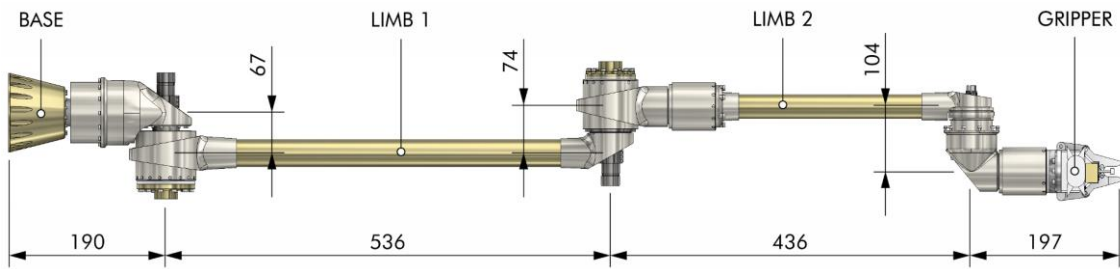


Figure 8-8 – Extended robotic arm with key dimensions in mm

The robotic arm uses two sizes of actuators in its joints, identified as light and heavy. The first three joints from the base have to support long limbs with offset masses at their ends, therefore they use the heavy actuator. The last three joints only support the mass of the wrist and gripper, so they use the light design. Like all the actuators on board SFR, the AGS joints use brushed DC motors. The two sizes differ in gear ratio, but they implement the same geartrain architecture: a three-stage planetary gearbox feeding into an output Harmonic Drive. This is different from the FAST actuator design described in Section 7.2.2, but more similar to a classical design for high-torque space applications. The robotic arm does not consume significant power, but its design is highly sensitive to the suspended mass. Therefore, lightness is far more desirable than efficiency, leading to the choice of a Harmonic Drive for the output gear. These and other key features of the AGS joints are summarised in Table 8-6.

Braking is required only for the heavy joints, whereas for the light ones the internal losses are sufficient to counteract the worst-case loads. The same type of motor brake described in Section 7.2.2 is used on the AGS. One peculiar feature of the AGS actuators is the position sensing solution, which differs from the typical resistive potentiometer (ExoMars heritage technology and widely used in extreme environments like Mars). Both light and heavy joints use redundant, single-speed pancake resolvers for position sensing. The light joints mount two General Dynamics resolvers size RP019 and the heavy joints use size RP022.

The choice of different position sensors is driven by the accuracy requirements of the arm, especially for pickup of the tube and insertion into the storage. While a typical value for a potentiometer's position knowledge accuracy is around 1° (occasionally 0.5° for high-spec flight units), resolvers offer an improvement of one order of magnitude, often producing an error as small as a few arcminutes⁷⁹. The major downside of resolvers is the complexity of

⁷⁹ These values are the theoretical position knowledge performance of the sensor and they do not include the contributions of the reading electronics, harness or mechanical errors.

their reading electronics. A potentiometer can be fed with a DC voltage and the measurement of the resulting voltage drop simply provides the position of the rotor. A resolver, on the other hand, requires excitation with a sinusoidal alternating current at a specific frequency and a resolver-to-digital converter to transform the signal into a binary reading representing the position of the rotor.

Feature	AGS light joint	AGS heavy joint
Motor	Maxon DCX 14L brushed motor	Maxon DCX 22L brushed motor
Gearbox	3-stage planetary + Harmonic Drive	3-stage planetary + Harmonic Drive
Total gear ratio	55146:1	37191:1
Motor encoder	7-bit magneto-resistive, redundant	7-bit magneto-resistive, redundant
Brake	None	Electromagnetic friction brake
Main bearings	Double angular contact	Double angular contact
Position sensor	Single-speed resolver	Single-speed resolver
Required output torque	8 Nm	81 Nm
Required holding torque	3 Nm	47 Nm
Mass (excluding interface flanges)	0.6 kg	1.2 kg

Table 8-6 – AGS actuators specifications

Like many other critical components on board SFR, the robotic arm takes advantage of existing technology and early prototype testing. In this particular case, a lightweight robotic arm of similar size and capability was already available at Leonardo. The prototype is called DELIAN and is already built to operate in Martian environment [70]. The possibility to use this arm since the start of the project allowed early testing on the RAS that provided valuable insight on the operation of the system.

In the first instance, the arm was mounted onto pre-existing ExoMars rover test platforms, which provided mobility functions and cameras similar to those on SFR, enabling a rudimentary end-to-end testing of the system. One of these breadboard tests in the Airbus Mars Yard is shown in Figure 8-9. These test campaigns then grew in fidelity as more hardware was produced from the preliminary SFR designs. The results provided early validation of the system's architecture and the flight design of the AGS remained strongly based on the DELIAN arm.

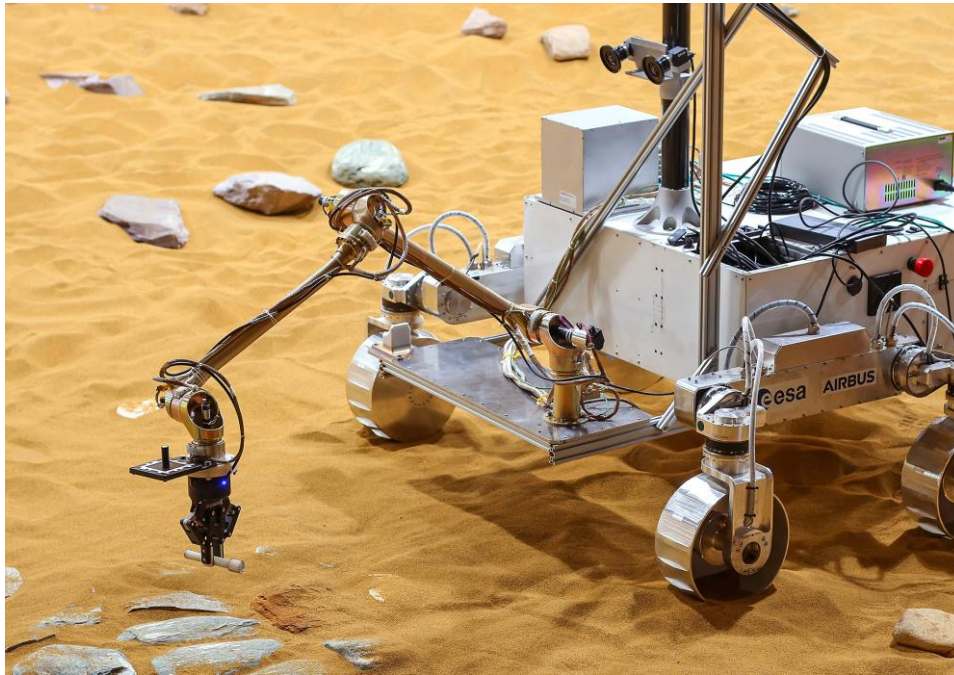


Figure 8-9 – Breadboard testing with the DELIAN arm in the Mars Yard

The AGS interfaces with an unstructured environment during pickup of the tube and with a more deterministic one during re-grip and stowage. The first one can be considered essentially unknown until the VBDS returns an estimation of the tube pose and a point cloud of the terrain around it. The capture of the tube can be successful even in presence of errors in the order of several millimetres (unless it is a particularly difficult geometry), however, the difficulty in estimating the tube's location with relation to the rover or the arm makes this case none the less challenging. On the other hand, the hardware on the rover like the RRB and the RSA is much better characterised and does not change during mission, although it typically requires more precise manipulation to correctly engage the features on the tube.

The currently specified arm position control performance can be summarised as follows:

- Absolute positioning accuracy: ± 5 mm and $\pm 1^\circ$
- Relative positioning accuracy: ± 2 mm and $\pm 0.5^\circ$
- Positioning repeatability: ± 2 mm and $\pm 0.5^\circ$

Here absolute positioning refers to the placement of a reference frame on the end effector with respect to a reference frame fixed to the robotic arm's base. Relative positioning refers to the positioning of a reference frame on the end effector with respect to a previous position of the same reference frame. The latter is more accurate because it is less affected by systematic errors (like gravity and thermal distortion in the arm, which don't change significantly during the motion), leaving mostly random errors.

These numbers are typical values, but in reality, they vary as a function of the arm configuration, so the arm has different performance in different areas of the workspace. It must be noted that these include only errors internal to the arm's perimeter, so other errors, for example, thermal distortion in the external interfacing hardware (RRB and RSA) or vision errors must be added to these. The errors associated with visual estimation of the tube pose are particularly significant as they can be an order of magnitude greater than the arm's positioning accuracy, as analysed in Section 8.6.

It would be ideal to operate the arm in all the scenarios above with a “fly by numbers” approach, where the manipulator is commanded to the target pose and any errors are accommodated by mechanical compliance or clearance around the target. However, this is not always possible and, in particular for contact operations, could lead to collisions and overloading of the hardware, so specialised sensors have been introduced in the AGS to assist these operations. In particular, the gripper is equipped with a detection plate that senses the presence of the tube in its capture zone and with strain gauges on the fingers that measure the gripping force (further discussed in the next section). The RRB is also equipped with two sensors that stop the motion of the arm when the tube is correctly aligned in the lateral and axial direction.

Protecting the integrity of the tubes is the highest priority for any element of the RAS, since it directly affects the campaign-level objective of returning pristine material from the surface of Mars. By design, the arm’s torque capability is more than sufficient to damage a tube if handled improperly. When the tube is in close proximity of other features, for example during difficult pickup or insertion into the storage, the positioning error of the arm could bring it into contact with its surroundings and exceed its load limits. Mechanical analysis of these scenarios showed how the inherent flexibility of the arm would be insufficient to prevent overloading of the tube in some cases. Since the accuracy of the arm is already at the limit of the position sensing technology available, the possible responses to this issue could be to increase the mechanical compliance or add further sensors to detect dangerous loads.

The choice was made to introduce a 6-axis force torque sensor on the manipulator’s wrist, which provides more operational flexibility and ability to control any load on the tube within configurable ranges. This new component was only preliminary investigated at the time of writing, so it is not described in detail in this document. A redundant sensor was chosen from ATI, the same manufacturer of the force torque sensors on board the Perseverance rover, depicted in Figure 8-10.



Figure 8-10 – Force torque sensor on board NASA’s Perseverance rover (credit: ATI)

The accommodation of this item is not straightforward, since it adds considerable mass and volume at the end of the manipulator and requires a large amount of harness lines to be routed on the arm. Considering additional heaters and HDRM lines for the sensor, approximately 50 additional lines are estimated. This will unavoidably lead to a mass increase on the arm and a more complex harness routing system. Moreover, an impact on the electronics design is also expected since the sensor will require dedicated signal-processing boards.

From this preliminary study, it is clear that accommodating a 6-axis force torque sensor on a 10-kg-class robotic arm is extremely challenging and would likely push the AGS well outside this mass envelope.

One last aspect worth discussing about the arm's design is its launch restraint system. The manipulator is a long, slim appendage and therefore requires structural support to withstand the severe mechanical environment. Launch load paths are provided by clamps that wrap around the elbow and wrist joints, so that the main structural beams forming the arm are supported at both ends. The clamps are released on Mars by Frangibolt actuators like those described in Section 7.2.3, allowing the arm to deploy. The base structure of the clamps is used throughout the mission as resting features for the arm during traverse operations, which ensure that high mobility loads, such as those associated with descending large obstacles, would not affect the joints' gear trains.

8.4.2 Gripper design

The SFR gripper is part of the AGS and is developed by AVS for the Sample Fetch Rover project. It has two primary functions: to capture the tube from the ground using the body grip and to insert it into a slot in the storage assembly using the head grip. The need for two different gripping geometries arises from the fact that the wider end of the tube – the “head” – must remain accessible once inserted into the storage. This area will be used for subsequent manipulation and is populated with mechanical features that can be exploited for precise handling. The head is also the main load path for maintaining the tube secured inside the tube in the Orbiting Sample, from launch from Mars up to crash-landing on Earth.

On the other hand, the middle portion of the tube shaft, corresponding to the body grip area, is easier to access when the tube is lying horizontally on the ground and has a simpler geometry that allows for larger errors during grasping. Due to these considerations, the tubes are picked up using a body grip and stowed using a head grip, requiring the gripper to be compatible with both and necessitating an intermediate re-grip bracket to switch from one to the other. The two possible gripping geometries are visualised in Figure 8-11.

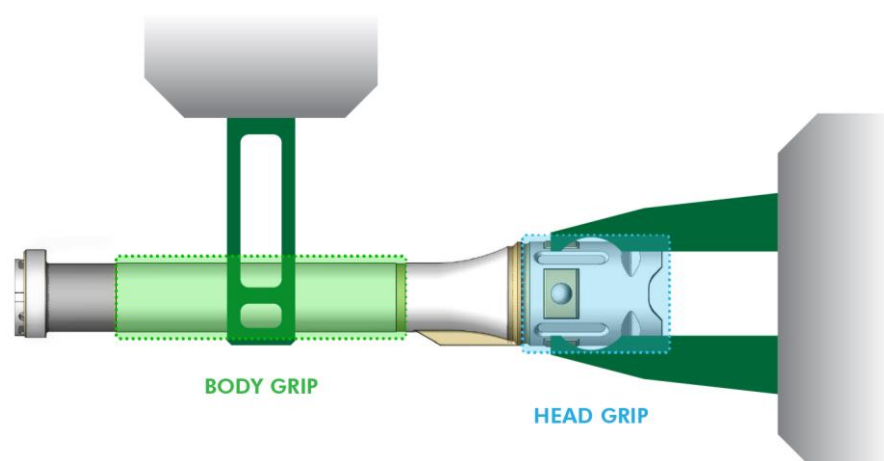


Figure 8-11 – Body grip and head grip areas on the tube (credit for tube image: NASA / JPL-Caltech)

The two different interfaces define the profile of the surfaces on the gripper's fingers that need to engage with them. Another defining factor for the gripper design is certainly associated with the terrain. While every effort will be made to select a depot area that presents

minimum challenges for pickup, it is likely that there will be a certain degree of roughness and the tubes might end up in proximity of features that obstruct access to them. Furthermore, due their cylindrical shape, they will have the tendency to roll into local depressions and cracks.

To overcome these challenges, the gripper needs to be slender and nimble, thus, while the tube interface shapes the internal geometry of the fingers, the terrain shapes the external geometry and the overall footprint. One last aspect to consider is the presence of sand that, although will not be abundant in the depot terrain, can be transported by wind over the years and deposited in small amounts around the tube. The finger's profile must be able to penetrate through the sand and reach the tube's body without scooping up a significant amount of material, since that would compromise the stability of the grip.

As for any other novel technology, a breadboard plan was established to produce early prototypes of the gripper. Their testing allowed to evaluate the performance of different configurations and inform the gripper development. The breadboard gripper design included a number of interchangeable parts, for example the finger tips and the RSTA detection plate, in order to experiment with different geometries. The resulting design is shown in Figure 8-12. In this image, the gripper is shown with short finger tips, which ended up not being selected for the flight design.

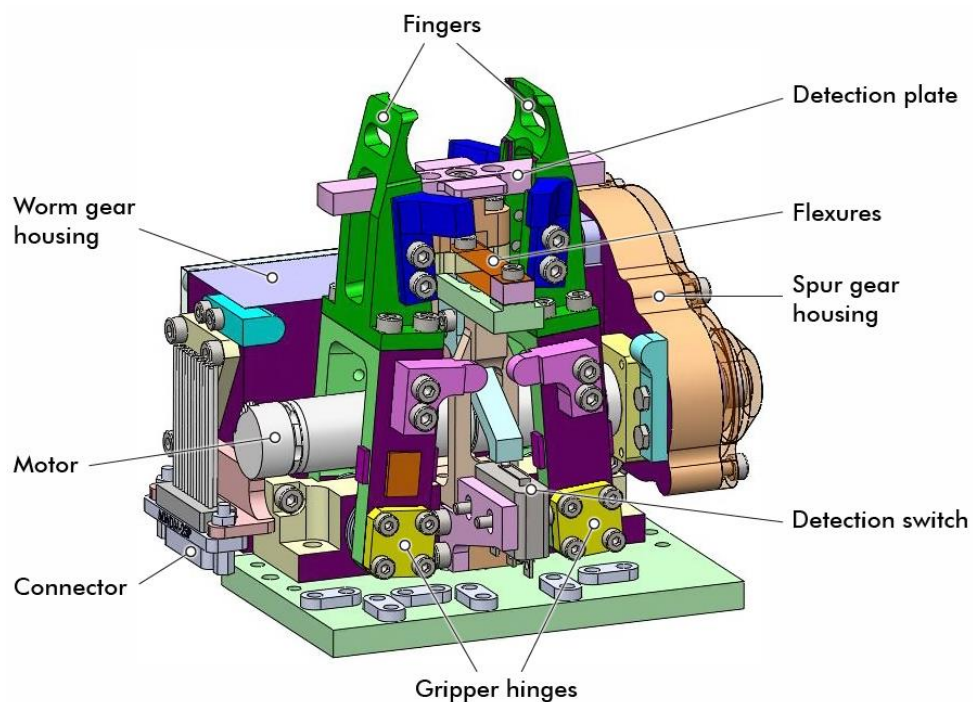


Figure 8-12 – Design of the SFR breadboard gripper (credit: AVS)

The breadboard gripper was tested with different terrain geometries and dust, its ability to comply with errors and misalignment was characterised, as well as the stability and accuracy of its grasp [71]. Various sensors on the assembly monitored the loads on the tube throughout the test campaign. Figure 8-13 shows the fully assembled breadboard gripper, in this case mounting long finger tips, which proved necessary to comply with narrow terrain geometries.

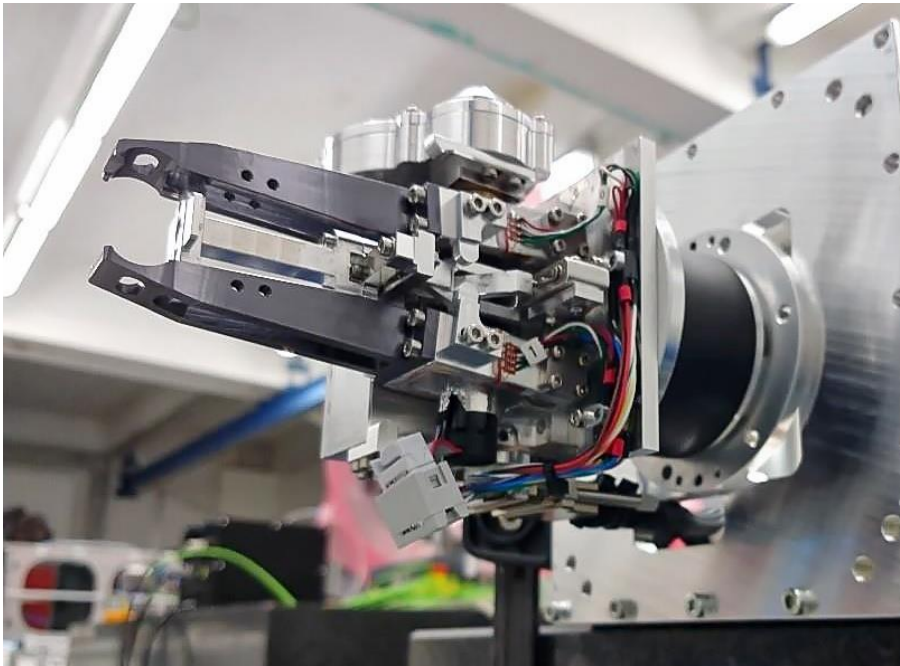


Figure 8-13 – SFR breadboard gripper during testing (credit: AVS)

The gripper is a 1-DOF system, actuated by a Maxon DCX 14L motor driving a 3-stage planetary gearbox, both already used on the arm's light joint. The gearbox feeds into a spur gear that drives a worm gear to open and close the gripper. Each finger is connected to a worm wheel driven by a worm on the same shaft: one with a left-handed thread and the other one right-handed, so that their motion is always symmetrical and synchronised. This transmission is not reversible, so the grasp can be maintained even without power.

Strain gauges are placed at the base of the fingers to estimate the closing force exerted onto the tube by measuring the bending of the finger's structure. These sensors were initially meant only for the breadboard tests, but proved so useful in controlling the grasping process that they have been passed over to the flight design. A typical set point for the closing force is in the order of 20 N. When the measurement on one of the strain gauges reaches this value, the closing motion is halted.

Between the two fingers is a detection plate to sense the presence of the tube in the grasping area. The plate is guided by flexures that allow an approximately linear motion: when pushed by the tube, this triggers a micro switch at the base of the gripper that stops the tube approach motion of the arm. The gripper is robust against contact with the terrain, even with the full force of the arm. The strain gauges could be used to detect contact with the ground, but they are optimised to detect bending in the fingers, so their signal is not particularly reliable for this purpose. Since the addition of a force torque sensor on the arm's wrist is being considered, this would be a more effective way of detecting contact with the ground.

Another peculiar aspect of the gripper design – and, to a lesser extent, of the whole arm – is that it must preserve not only the mechanical integrity of the sample tube, but also the magnetic one. This implies strict limits on the magnetic fields that can be experienced by the sample material, since it could contain information on Mars' geomagnetism that can be easily altered. Such limitations translate into a ban on ferromagnetic materials in close proximity of the tube. The gripper fingers and its structure are mostly made of titanium and aluminium, which do not pose any issues, however, its brushed DC motor is, by necessity, ferromagnetic and generates magnetic fields during operation.

This is appeared of particular concern considering the construction of the DCX Maxon motors, which are defined as “permanent magnet motors with coreless windings”, where the windings are formed into a cup structure that rotates around a permanent magnet. Such arrangement is depicted on the left in Figure 8-14. In a motor with this layout there are coils moving at high speed immediately under the motor housing, with potential magnetic fields induced into the surrounding space. FEM magnetic analysis at Maxon suggested that the magnetic circuits should close mostly inside the housing, as shown on the right in Figure 8-14. However, these models usually focus on the inside of the motor, where the electromotive force is generated, rather than on the leakage outside.

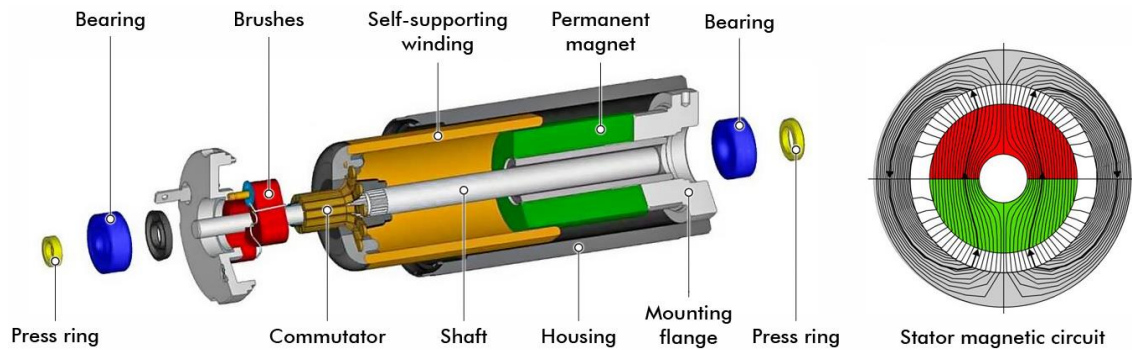


Figure 8-14 – Maxon DC motor cross section (left) and stator magnetic circuit (right)
(credit: Maxon Motors)

Given that all the SFR motors are derived from industrial models, the most immediate way of retiring this risk was to take measurements in the proximity of commercially-available Maxon motors with a magnetic probe. The test yielded reassuring results, demonstrating that the magnetic flux is indeed well-contained inside the housing and there is little difference between an active or inactive motor. The magnetic field intensity was characterised as a function of distance from the housing, leading to the conclusion that approximately 50 mm would be sufficient to protect the sample from magnetic fields. In the SFR gripper, the motor is located close to the base to ensure that the magnetic requirements are never breached on the tube.

As previously mentioned, the need for a re-grip station arose from the fact that the tubes are picked up using one type of grip but stowed using another. The RSTA Re-grip Bracket (RRB) is part of the AGS perimeter, even though it is actually mounted on the front end of the storage assembly for ease of access. The overall design of the RRB is based on a V-shaped sprung mechanism that engages with the tube to provide an accurate centring. This is needed to ensure that the head grip is engaged successfully and with enough precision to carry out the subsequent insertion into the storage. The RRB is equipped with two sensors to stop the motion of the arm once the tube is axially and laterally aligned in its seat. A prototype of the RRB is shown in Figure 8-15.

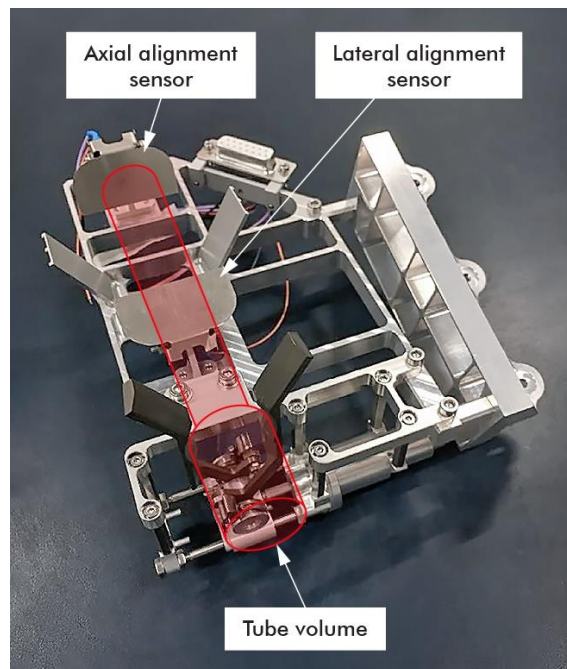


Figure 8-15 – RRB prototype with superimposed tube volume (credit: Leonardo)

8.5 Tube storage

The RSTA Storage Assembly (RSA) is developed by Beyond Gravity for the Sample Fetch Rover project. Its main purpose is to accommodate up to 30 sample tubes and store them securely during the return traverse. The RSA is also required to support tube transfer operations by providing accurate tube positioning, visual markers and access corridors for the lander’s Sample Transfer Arm (STA). The access requirements also mean that the tubes must be held so that their heads are accessible, as they constitute their main mechanical interface for further handling.

The size of the RSA is limited by the volume available on the lander and also by visibility considerations since its footprint must not occlude the view of the pickup zone from the NavCam (refer to Figure 8-3). On the other hand, the tubes cannot be arranged too densely or too close to the surrounding hardware, otherwise the access corridor for STA would be compromised. The assembly must also be shaped so that it is entirely accessible by the rover’s robotic arm without collisions. These design drivers led to the configuration shown in Figure 8-16, which is based on a shelf-like structure composed by a thick sandwich panel with aluminium honeycomb core and carbon fibre skins. This provides a lightweight construction that is populated with storage slots in the form of titanium tubes with sprung clips on their upper ends.

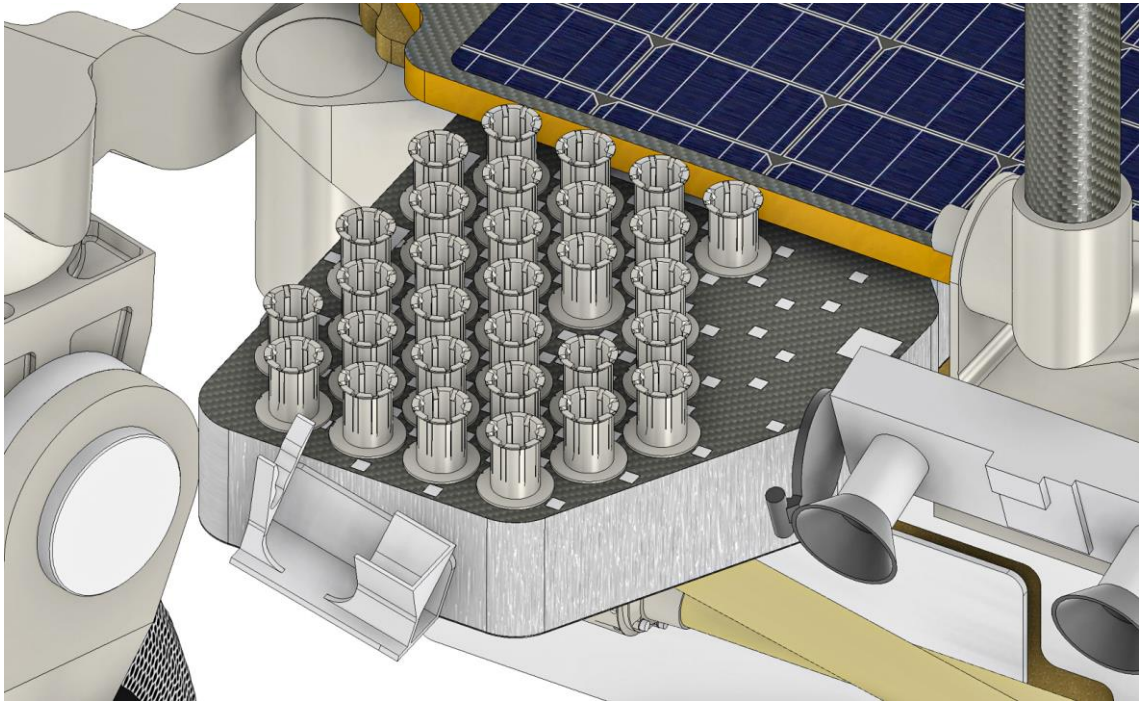


Figure 8-16 – RSTA Storage Assembly

The choice of the interface mechanism is mostly driven by the accuracy with which the tubes must be held. Due to time constraints, the tube transfer operations are fully automated, so STA relies on visual recognition of the RSA and proceeds to unload the tubes one at a time. Grasping the tube's head requires rather precise placement of the end effector, so the position of the tube with relation to the storage must be well-controlled. This led to a storage design that engages tightly with the tube through metallic clips. Each storage unit is a turned titanium piece with flexures machined in its body to capture a groove at the base of the tube's head, as depicted in Figure 8-17. At the lower end of the slot is placed a ring that acts as end stop, ensuring an accurate axial positioning.

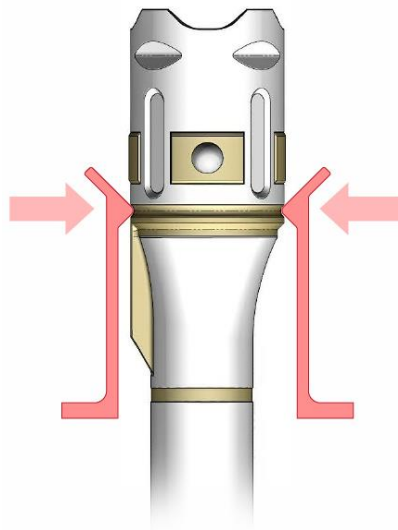


Figure 8-17 – Representation of the tube engagement geometry (credit for tube image: NASA / JPL-Caltech)

The interface mechanism described above must be tight around the tube head and rather stiff to guarantee a robust engagement under mobility loads. This means that the clearance

around the tube during insertion is very limited, leading to the positioning accuracy issues anticipated in Section 8.4.1. Since it was decided to implement force torque sensing rather than passive compliance, this capability can be used to aid tube insertion.

The SFR flight electronics are not powerful enough to perform real-time force torque control, so the operation is based on load thresholds. The arm is commanded to perform the insertion trajectory and, if any of the loads detected by the force torque sensor rises above a preconfigured threshold, the motion is halted immediately. A short-range motion to relieve the load is computed offline from the arm control, then sent to the arm. Once the load is successfully removed, the insertion motion is resumed. This approach is followed until the tube reaches the end of travel and engages with the retain mechanism. The end of travel produces a distinctive spike in the vertical force⁸⁰ in the expected position range, which is detected by the sensor as indication of successful storage.

It has been discussed above how SFR must ensure that the sample tubes are protected against mechanical damage and magnetic contamination. One last aspect of safeguarding the scientific value of the samples is related to temperature. The material must be maintained at temperatures that are not too far from the natural range experienced on the surface of Mars, otherwise it might become chemically altered if exposed to excessive heat. This constraint becomes relevant in particular for the storage because the sample tube is designed to maintain the right temperatures while lying on the surface of Mars. However, once placed into the storage, its radiative and convective environments change, so the hardware around it must be designed to guarantee a suitable temperature range. In particular, the RSA is required to avoid geometries that trap solar irradiation and direct it towards the tube or that prevent it from discharging heat towards the environment.

8.6 Fetching analysis

Among the analysis work encompassing the typical fields of spacecraft engineering, three pieces in particular are worth discussing in further detail since they are highly specific to the RAS: the RSTA Acquisition and Fetching Timeline (RAFT) analysis, the grasping error budget and the mechanical modelling of the robotic arm.

8.6.1 RSTA Acquisition and Fetching Timeline

A highly-autonomous decision-making process was coded into the AMS to operate in the unstructured and – to some extent – unknown environment of the depot terrain. This opens up a wide spectrum of alternative approaches that the RAS might follow during operations. Considering the uncertainty on depot terrain, which cannot be observed yet, but only inferred by comparison with other Martian terrain, this leads to a great number of possible mission scenarios, similar to the situation described in Section 7.3.2 for traverse operations. As in the previous case, such variation lends itself well to a statistical approach to mission analysis. The RSTA Acquisition and Fetching Timeline (RAFT) analysis uses a similar strategy to SOET, but instead of focusing on traverse operations, it models fetching operations.

⁸⁰ It should be noted that, in this configuration, the tube can tolerate well axial forces and the corresponding load limit can be set higher than in other operations.

Like SOET, RAFT is coded in MATLAB and reuses some of the modules already present in SOET, for example, the simulation of the environment, communication passes and lost sols for general anomalies. Unlike SOET, which achieves statistical significance by exploring hundreds of combinations that are established in a deterministic way, RAFT implements true randomness. Operational steps have a probability of success associated to them and, at each execution of the model, they fail or succeed randomly according to that probability. In a typical simulation campaign, the model is run 10 000 times to sufficiently explore the possible combinations of events and achieve statistical significance.

A RAFT simulation run starts at point 1 of the concept of operations illustrated by Table 8-2. Each sub-activity is assigned a probability of success: in some cases, it is predefined and, in some others, it is calculated by the simulation (e.g., activities whose success is influenced by the environment being encountered at that particular moment). Some steps have a probability of success of 100%, such as exchanges of data and arm motions in free space. The reason is that failure of these activities is extremely rare and associated with major malfunctions, which are covered by other layers of margin added to the analysis results, like the allocation lost sols for on-board faults.

Assigning success rates to each function is a challenging task on its own, and it is usually done through statistical analysis of error distributions, specific simulation of the task under consideration and, as more prototypes are built, input from test data. The vision-based detection (step 1.c. in Table 8-2) is a good example of this process. The VBDS software development started with a certain specification that could be used as a starting point to define the success rate. During the coding of a preliminary algorithm, virtual scenarios were used to test it, in the form of images of computer-generated landscapes with tubes deposited on them. Software like Blender or PANGU⁸¹ can be used for this purpose. Thousands of these images were fed to the prototype VBDS software, producing a first update to the success rate and accuracy.

Nonetheless, the synthetic reproduction of a highly complex natural environment is rarely satisfactory, so “sandbox” testbeds were built with visually representative terrain and cameras similar to the SFR ones. Several images were acquired with different lighting conditions, tube locations and sand coverage. The results of vision-based detection on these images were used to update the success rate for tube identification in RAFT.

The logic coded in RAFT replicates the on-board decision-making process, so, when a failure is encountered, a new branch of the decision tree is followed. In the case of vision-based detection, the retry sequence described in Section 8.2.2 would be enacted, triggering different exposures and movement of the rover before abandoning the task and moving on to the next tube. It is important to remember that each of these activities costs time and energy, which will ultimately be the defining factors of mission success. The RAFT simulation runs on the backdrop of the evolving environment, with a daily energy profile and the arrival of the evening that can interrupt operations due to low power or low illumination of the scene. After simulating the collection of tubes in the depot thousands of times, the tool produces a report of how many missions have been successful and what is the distribution of mission

⁸¹ Blender is an open-source 3d rendering software, while PANGU, Planet and Asteroid Natural Scene Generation Utility, is a software developed by the University of Dundee in collaboration with ESA to generate photorealistic views of the surface of several Solar System bodies.

duration. As in SOET, multiple analytics tools are available to extract any desired parameters and indicators from the simulation, usually of particular interest in the investigation the failure cases.

In some situations, the probability of success is a strong function of the local environment, i.e., the conditions specific to that individual tube, such as the terrain on which it is located. To cover these scenarios, depot terrain models were developed by NASA using DEMs produced by the Curiosity rover and populating them with tubes. While the placement of tubes is somewhat arbitrary and the terrain only reflects an expectation of how the depot might be, these models are useful to analyse the performance of the system against more or less challenging terrain geometries. The simulation processes each tube placed on the DEM by measuring the distance between points belonging to the tube and points belonging to the terrain around the tube shaft. This allows to define the maximum opening that the gripper can have to avoid hitting the terrain before grasping the tube.

Ideally, the gripper should have an opening that is as wide as the error⁸² on the visual estimation of the tube's pose in order to have confidence that the tube will be found between the fingers during approach (further discussion on this error budget can be found in Section 8.6.2). However, in some cases, the terrain might make it necessary to command a smaller opening, thus creating the possibility that the tube might not be in the capture range and reducing the probability of success of the operation. Figure 8-18 provides a visual summary of this reasoning.

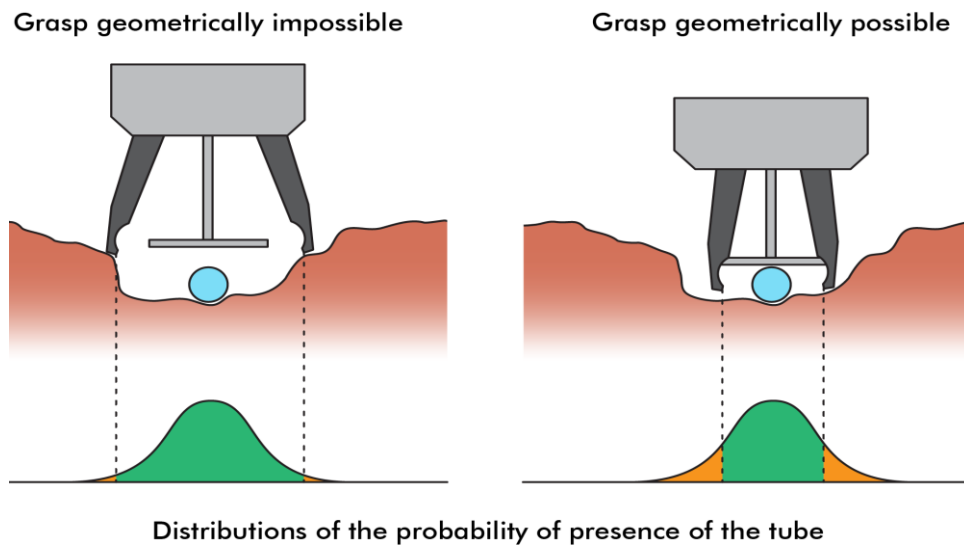


Figure 8-18 – Grasping a tube in a depression using a wide opening (left) and a narrow opening (right)

It can be assumed that the vision error produces a spatial distribution of probability of presence of the tube profile similar to a normal distribution. It derives that, if the opening of the

⁸² Usually, the 3σ error is used for these calculations, i.e., a value that envelops 97% of the cases, assuming that the error is a normally-distributed random variable.

gripper is reduced, then some of that distribution is left outside of the capture range⁸³. The probability of success of the operation is simply the integral of the portion of the curve contained within the capture range.

A tool like this can also be used in mission, once the tubes are deposited on the Martian surface and the geometry around them is known. The analysis would estimate the grasping probability of each tube, flagging which are the difficult ones. For some of them, the probability might be judged too low to attempt a fully autonomous pickup and the rover might be pre-programmed to switch to a step-by-step approach driven by ground control. This costs precious time but can be significantly more effective in tight geometries.

8.6.2 Grasping error budget

It has been discussed above how the errors in locating the tube with respect to the gripper play a key role in the grasping success. The overall accuracy is dominated by the vision-based pose estimation, although that is not the only contribution. An error budget analysis is performed to control the error both in the lateral and axial directions of the tube. The former defines the required opening of the gripper and the success of grasping as a function of the terrain, while the latter determines if the tube can be safely grasped within the specified body grip area on the shaft (see Figure 8-11).

The required gripper opening is given by the sum of the following contributions to the lateral error budget:

- **Tube radius**, equal to 7.5 mm. This is not an error but rather a fixed quantity that needs to be accommodated on each side of the tube's axis to succeed in grasping.
- **Vision error**, currently estimated at ± 7.6 mm for NavCam-based detection and formed by the following contributions:
 - Equivalent resolution of the cameras on the ground plane (pixel/mm).
 - Pose estimation error, defined by the performance of the detection software.
 - Camera aberrations that cannot be fully neutralised by calibration.
- **Arm positioning error**, currently estimated at ± 7.4 mm in a worst-case configuration and given by the sum of the following contributions for all arm joints and limbs:
 - Position sensing error, given by the performance of the resolvers in the arm's joints and their reading circuits.
 - Position control error, driven by how accurate the control electronics are at achieving the target position.
 - Geartrain error, caused by backlash and deformation in the joint's geartrains.
 - Structural deflection in the arm's limbs or other structural components due to gravity, external loads or thermoelastic effects.
- **Margin**, which can be specified a priori or computed against a desired total value for the error budget. The latter approach is used in the RAS.

The composition of this error budget is illustrated in Figure 8-19.

⁸³ By observing Figure 8-18, it can be imagined how the fingers of a gripper that is not fully opened might also contact the tube, risking to damage it. In this case, a sensor is needed to protect the tube from overloading, such as the force torque sensor being considered for the arm's wrist.

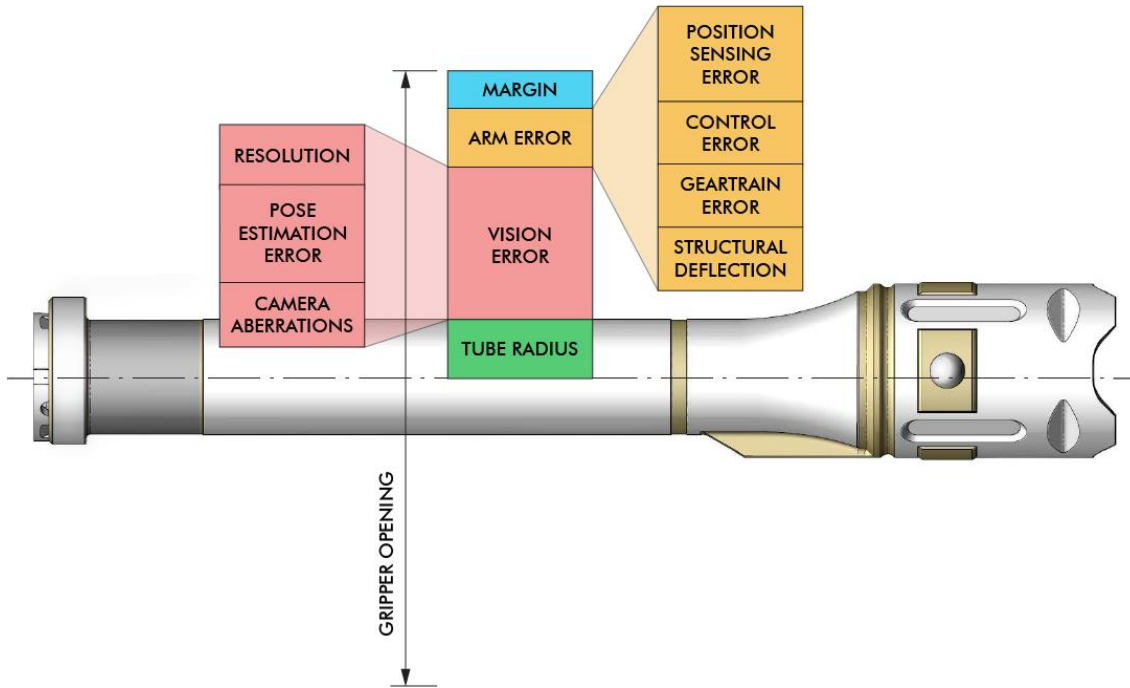


Figure 8-19 – Lateral error budget for tube grasping (credit for tube image: NASA / JPL-Caltech)

The vision and arm errors are considered random⁸⁴ and not correlated to each other, so their contributions can be summed with a Root Sum Squared (RSS) method, which follows the generic formula below:

$$e_{RSS} = \sqrt{\sum_{i=1}^n e_i^2}$$

where e_{RSS} is the total error and e_i the i^{th} error contribution out of a total of n . This calculation leads to a minimum opening requirement of 36.2 mm. Preliminary testing with the gripper on various geometries showed that an opening of 43 mm is generally successful and hence was taken as a target value, leading to a margin of 3.4 mm on each side.

The same process is repeated for the longitudinal error, along the tube’s axis. In this case, there is a hard constraint on the overall budget since the body grip area along the tube shaft is only 58 mm long. Similarly to the calculation above, the error budget includes 7.5 mm on each side for the finger’s width (which is 15 mm in total), ± 26.6 mm for the NavCam vision error and ± 7.4 mm for the arm positioning. This leads to a total of 70.2 mm, which exceeds the allocated length of 58 mm. Figure 8-20 shows how the contributions stack up along the tube’s shaft.

⁸⁴ It should be noted that the vision error follows a random distribution when multiple images of multiple tubes are analysed, but it does not vary randomly if multiple images of the same tube are processed without changing the rover’s position. In other words, if the same scene is offered multiple times to the vision algorithm, the error on the estimated tube pose will remain fairly constant. This means that taking multiple images of the same tube does not improve the accuracy of the vision algorithm.

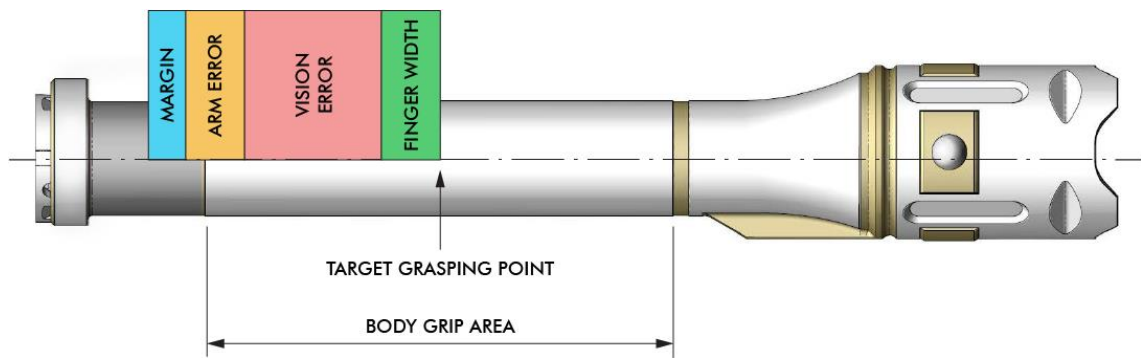


Figure 8-20 – Longitudinal error budget for tube grasping (credit for tube image: NASA / JPL-Caltech)

Multiple strategies can be adopted to improve this budget, such as biasing the target grasping point towards the tube's head, which would avoid contact with the sealing area but risk disturbance from the key feature on the tube. The major contribution is obviously from the vision-based detection, so another strategy would be to improve the precision of the algorithm (currently preliminary) in the longitudinal direction. Alternatively, the most straightforward approach is simply to use the RDC instead of the NavCam, which would immediately bring the required length to 55.2 mm, providing positive margin. Since the error calculation is based on a series of worst-case assumptions on the detection conditions, these conditions can be used as a discriminator between those tubes that need RDC detection (with associated extra time) and those that can be acquired using only the NavCam.

8.6.3 Mechanical models of the arm

Another piece of analysis where some specific considerations for the RAS should be discussed is related to the mechanical modelling of the robotic arm. This model is developed by Leonardo with the typical approach of structural analysis for a spacecraft appendage. It is a FEM model built using Patran⁸⁵ as pre-processing software and solved in Nastran⁸⁶. The model is used in the common analyses of spacecraft engineering, such as verification against launch loads and investigation of modal frequencies in the stowed configuration, which are not dissimilar from any other spacecraft hardware and so are not discussed here. The same elements can be rearranged to analyse the arm in a deployed configuration, which is more interesting in this case.

The flexible model of the deployed arm allows to calculate its deflection under load and particularly under gravity. The arm is a rather slim structure and its deformation due to gravity alone is a significant contributor to the error budget at the end effector. Being able to predict this displacement allows to correct it when operating the arm, thus reducing its impact on the positioning accuracy. Since the model of the arm will always be imperfect and some elements are especially difficult to model with high fidelity, such as backlash in the gear trains, the error due to gravity cannot be fully neutralised. The correction implemented

⁸⁵ Patran is a pre- and post-processing software for finite element analysis, distributed by Hexagon.

⁸⁶ Nastran is a finite element solver tool for structural analysis developed by MacNeal-Schwendler Corporation for NASA and now distributed by Hexagon.

in mission is expected to correct approximately 60% of the gravity-induced displacement⁸⁷. Figure 8-21 shows a snapshot of a gravity deflection analysis on this model.

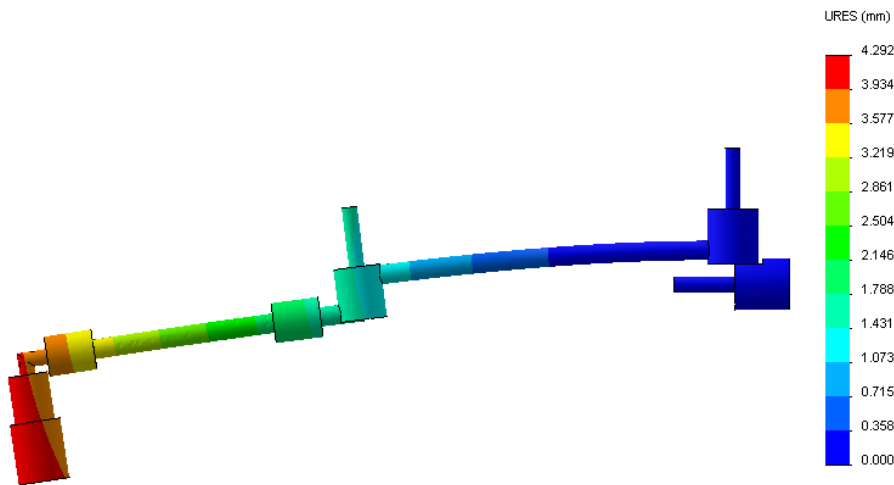


Figure 8-21 – FEM analysis of arm deflection under Martian gravity (credit: Leonardo)

The SFR flight computer is far from powerful enough to solve a detailed FEM model, so what is coded in the on-board gravity compensation algorithm is simply a function that approximates the expected displacement at the tip depending on the configuration of the joints. The expected displacement is then provided as an input to the AGS trajectory generation algorithm, which corrects the target pose by this quantity when generating the arm's motion profiles.

A challenging feature of the robotic arm design is that it must be able to complete all its operations in the Martian gravity field as well as in the Terrestrial one during ground testing, since using offloading devices would be impractical with its range of motion. This is generally feasible in terms of mechanical sizing because the motorisation margins are large enough to approach Earth gravity loads, so the arm can be operated with reduced motorisation margins. However, the gravity-induced error would most likely impede interaction with the surrounding hardware. The gravity compensation model becomes useful also in this case, reducing the error and enabling ground testing of the arm⁸⁸.

Lastly, a flexible model of the deployed arm is also useful for modal analysis. This is performed in the same way as for the launch package: by searching modal shapes and frequencies with Nastran. In this case, the results are not used to demonstrate robustness against the launch vibration but rather to improve the control of the arm. By knowing the resonant frequencies of the assembly, the motion laws can be adjusted to minimise excitation of those frequencies.

⁸⁷ The efficacy of the gravity compensation model is currently estimated based on previous experience of similar applications at Leonardo.

⁸⁸ The gravity compensation remains imperfect, so the error under Earth gravity will still be greater than in mission, but generally small enough not to cause frequent stops due to incorrect positioning.

9 CONCLUSION

The research work presented in these pages reached its conclusion with the SFR Preliminary Design Review (PDR), a milestone at which the European Space Agency evaluates if the development of the spacecraft is ready for proceeding into the implementation phase, thereby authorising the detailed design and build process. This decision point is often associated with the mission adoption, i.e., the final commitment to fund and fly the mission under consideration. In the case of SFR, while the review was passed successfully, demonstrating that the design is fit to fly, it was already clear that the mission adoption would not be straightforward. Then, in the political aftermath of the Russian invasion of Ukraine, the cancellation of the project was eventually confirmed.

Nonetheless, over the three years of this PhD, the development of the rover was advanced from initial concept to preliminary design, leading to a solution that responds appropriately to the demanding requirements of the Mars Sample Return Campaign. The spacecraft architecture was consolidated and robust solutions were presented in the key areas of this research. Furthermore, critical technologies for the mission were identified and matured during this period. Despite the cancellation, the knowledge acquired through this project will remain available for future applications. An effort was made to condense as much as possible of that knowledge into this dissertation.

This volume provides an overview of the context, the motivations, the design and analysis processes that led to such achievements. In Chapter 5 is presented the 2019 architecture for Mars Sample Return, which shapes and is shaped in return by the SFR design. Chapter 6 describes the rover's architecture in response to the needs of this campaign. It offers a broad view of how SFR can use the technologies described in Chapter 4, in particular the heritage of the ExoMars Rover, to operate in the Martian environment and carry out its mission.

A deeper dive into the core topics of this research is carried out in Chapters 7 and 8, discussing the rover's mobility and robotic systems, which are also particularly critical to its role in MSR. A carefully balanced mix of heritage technology and new solutions was necessary in these areas to meet the mission objectives. These would eventually define the most distinctive features of the vehicle and establish its remarkable capability. The major design choices regarding these systems are presented and justified herein. Where possible, preliminary analysis or even test results are discussed.

It must be mentioned that, while the cancellation has brought most of the design work to a halt, some testing activities are still proceeding and will carry on for the near future. In particular, a rover-level, integrated breadboard test campaign has only just started. A full-scale SFR prototype was built around the locomotion breadboard described in Section 7.4. It was fitted with a complete vision system, an on-board computer running flight-representative GNC software, off-the-shelf rechargeable batteries and Wi-Fi communication ability to allow standalone operation. This breadboard rover is shown in Figure 9-1 during a field test in the UK.



Figure 9-1 – SFR integrated breadboard field tests

The initial tests were remarkably successful and demonstrated that the vehicle can drive autonomously over long distances, traversing more than 300 metres in a single day without human intervention. They also showed that the on-board Absolute Global Localisation (see Section 6.6) is very effective in estimating the rover's position on the map. Thanks to this feature, there are no theoretical limits, with the exception of failures, to the distance that the rover can drive autonomously. The locomotion hardware is only a prototype, but it has already exceeded the mission lifetime of 5 km without noticeable degradation in performance. This rover is currently in the process of being fitted with a robotic arm to also enable tube acquisition, after which further testing will follow.

These results are a testament to the validity of the rover's design and the effectiveness of the technologies on which it is founded. It is also thanks to these achievements that SFR will not quietly fade into oblivion. As part of future work following this project, studies are already under way to investigate the application of these technologies to other missions.

Advanced mobility, autonomous navigation, robotic manipulation, recognition and acquisition of payloads are all attractive technologies for future planetary expeditions other than Mars Sample Return. An assessment is under way with the objective of transferring these

technologies to a lunar rover inspired to the SFR design. Earth's moon is becoming the most reasonable near-term application for planetary rovers due to the returning interest in human and robotic exploration.

It is possible that the robotic descendants of SFR will one day roam on the Moon, Mars or other worlds, supporting humankind's next steps into the Solar System. Wherever they will be, these machines will find similar challenges to those encountered in this project. This document contains some of the knowledge of how these hurdles were overcome for the Sample Fetch Rover; the rest lies with the exceptional team that made it.

10 REFERENCES

- [1] Williams, D. R. (2020) *Chronology of Lunar and Planetary Exploration* [Online]. Available at <https://nssdc.gsfc.nasa.gov/planetary/chronology.html>
- [2] J. N. Nielsen (2019) 'Bound in Shallows: Space Exploration and Institutional Drift', *Centauri Dreams* [Online]. Available at <https://www.centauri-dreams.org/2019/12/27/bound-in-shallows-space-exploration-and-institutional-drift>
- [3] Phillips, K. J. H. (1995) *Guide to the Sun*, Cambridge University Press.
- [4] Müller, D. et al. (2020) 'Europe's next mission to the Sun', *Nature Astronomy*, Vol. 4, February 2020, p. 205.
- [5] Vaughan, R. et al. (2013) 'Avoiding the burn: Maintaining a Sun-safe attitude for the Solar Probe Plus spacecraft', *AIAA Guidance, Navigation, and Control (GNC) Conference*.
- [6] Potter, A. E. et al. (2002) 'The sodium tail of Mercury', *Meteoritic & Planetary Science*, Vol. 3, p. 1165.
- [7] Denton, A. (2018) 'The Venus controversy', *The Planetary Society* [Online]. Available at <https://www.planetary.org/articles/the-venus-controversy>
- [8] Greaves, J. S. et al. (2020) 'Phosphine gas in the cloud decks of Venus', *Nature Astronomy*, Vol. 5, July 2021, p. 655.
- [9] Nakamura, M. et al. (2016) 'AKATSUKI returns to Venus', *Earth, Planets and Space*, Vol. 68, 6, May 2016, p. 68.
- [10] Williams, J. P. et al. (2017) 'The global surface temperatures of the Moon as measured by the Diviner Lunar Radiometer Experiment', *Icarus*, Vol. 283, February 2017, p. 300.
- [11] Wright E. et al. (2019) 'Apollo Landing Sites with Moon Phases', *NASA Scientific Visualization Studio* [Online]. Available at <https://svs.gsfc.nasa.gov/4731>
- [12] Stubbs T. J. et al. (2005) 'Impact of dust on Lunar exploration', *NASA Solar System Exploration Division*.
- [13] Ulivi P. (2004) *Lunar Exploration: Human Pioneers and Robotic Surveyors*, Springer London.
- [14] Bagenal F. (2007) 'The magnetosphere of Jupiter: Coupling the equator to the poles', *Journal of Atmospheric and Solar-Terrestrial Physics*, Vol. 69, p. 387.
- [15] Helled R. (2018) 'The Interiors of Jupiter and Saturn', *Oxford Research Encyclopedia of Planetary Science*, Oxford University Press.

- [16] Debras F. et al. (2019) 'New Models of Jupiter in the Context of Juno and Galileo', *The Astrophysical Journal*, Vol. 872, February 2019, p. 22.
- [17] Iess L. et al. (2017) 'Measurement and implications of Saturn's gravity field and ring mass', *Science*, Vol. 364, January 2017, p. 1046.
- [18] Postberg F. et al. (2018) 'Macromolecular organic compounds from the depths of Enceladus', *Nature*, Vol. 558, June 2018, p. 564.
- [19] Roe H. G. (2012) 'Titan's Methane Weather', *Annual Review of Earth and Planetary Sciences*, Vol. 40, p. 355.
- [20] Podolak M. et al. (1995) 'Comparative models of Uranus and Neptune', *Planetary and Space Science*, Vol. 43, December 1995, p. 1517.
- [21] Ness N. F. et al. (1986) 'Magnetic Fields at Uranus', *Science*, Vol. 233, July 1986, p. 85.
- [22] Suomi V. E. et al. (1991) 'High Winds of Neptune: A Possible Mechanism', *Science*, Vol. 251, February 1991, p. 929.
- [23] Agnor C. B., et al. (2006) 'Neptune's capture of its moon Triton in a binary-planet gravitational encounter', *Nature*, Vol. 441, May 2006, p. 192
- [24] West J. L. et al. (2018) 'Space Mission Hibernation Mode Design: Lessons learned from Rosetta and other pathfinding missions using hibernation, *2018 IEEE Aerospace Conference*.
- [25] Stern A. et al. (2018) *Chasing New Horizons: Inside the Epic First Mission to Pluto*, Macmillan Publishers.
- [26] McComas D. et al. (2012) 'The Heliosphere's Interstellar Interaction: No Bow Shock', *Science*, Vol. 336, May 2012, p. 1291.
- [27] Soffen G. A. (1976) 'Scientific Results of the Viking Missions', *Science*, Vol. 194, December 1976, p. 1274.
- [28] Sagan C. (1994) *Pale Blue Dot: A Vision of the Human Future in Space*, Random House.
- [29] Goswami, N. et al. (2021) Human physiology adaptation to altered gravity environments', *Acta Astronautica*, Vol. 189, August 2021, p. 216.
- [30] Franz H. B. et al. (2017) 'Initial SAM calibration gas experiments on Mars: Quadrupole mass spectrometer results and implications', *Planetary and Space Science*, Vol. 138, April 2017, p. 44.
- [31] Leighton, R. B. et al. (1966) 'Behavior of Carbon Dioxide and Other Volatiles on Mars', *Science*, Vol. 153, July 1966, p. 136.
- [32] Poulakis P. et al. (2015) 'Overview and Development Status of the ExoMars Rover Mobility Subsystem', *Astra 2015 - 13th Symposium on Advanced Space Technologies for Robotics and Automation*.
- [33] Leovy C. E. et al. (1973) 'Mechanisms for Mars Dust Storms', *Journal of the Atmospheric Sciences*, Vol. 30, July 1973, p. 749.
- [34] Matthiä D. et al. (2017) 'The radiation environment on the surface of Mars - Summary of model calculations and comparison to RAD data', *Life Sciences in Space Research*, Vol. 14, August 2017, p. 18.
- [35] Wadsworth J. et al. (2017) 'Perchlorates on Mars enhance the bacteriocidal effects of UV light', *Scientific Reports*, Vol. 7, July 2017.
- [36] Genta G. (2012) *Introduction to the Mechanics of Space Robots*, Springer.
- [37] Ghotbi B. (2015) *Performance evaluation and dynamics of rovers for planetary exploration*.
- [38] Patel N. et al. (2010) 'The ExoMars Rover locomotion subsystem', *Journal of Terramechanics*, Vol. 47, March 2010, p. 227.

- [39] Grandy D. et al. (2019) 'Development and qualification of the ExoMars Bogie Electro-Mechanical Assembly (BEMA) rotary actuators', *ESMATS 2019 – 18th European Space Mechanisms and Tribology Symposium*.
- [40] Azkarate M. et al. (2015) 'First experimental investigations on wheel-walking for improving triple-bogie rover locomotion performances', *Astra 2015 – 13th Symposium on Advanced Space Technologies for Robotics and Automation*.
- [41] Winter M. et al. (2015) 'ExoMars Rover Vehicle: Detailed Description of the GNC System', *Astra 2015 – 13th Symposium on Advanced Space Technologies for Robotics and Automation*.
- [42] Hult T. et al. (2010) 'The ExoMars Rover Vehicle OBC', *Proceedings of DASIA 2010 Data Systems In Aerospace*.
- [43] Wenkert D. D. et al. (2016) 'Enabling International Data Relay at Mars', *SpaceOps 2016 Conference*.
- [44] Vago J. L. (2017) 'Habitability on Early Mars and the Search for Biosignatures with the ExoMars Rover', *Encyclopaedia of Astrobiology*, Springer.
- [45] Prado-Montes P. et al. (2017) 'ExoMars 2020 LHPs: from the concept to the flight models', *47th International Conference on Environmental Systems*.
- [46] Ferrando E. et al. (2016) 'Photovoltaic Assemblies for the Power Generation of the ExoMars Missions', *11th European Space Power Conference*.
- [47] Amos S. et al. (2016) 'Battery for Extended Temperature Range, ExoMars Rover Mission', *11th European Space Power Conference*.
- [48] COSPAR (2005) *COSPAR Planetary Protection Policy*.
- [49] Martin Marietta Corp. (1974) *A feasibility study of unmanned rendezvous and docking in mars orbit*.
- [50] Price H. et al. (2000) 'Mars Sample Return spacecraft systems architecture', *2000 IEEE Aerospace Conference*.
- [51] Klein E. et al. (2014) 'The Mobile MAV Concept for Mars Sample Return', *2014 IEEE Aerospace Conference*.
- [52] Mattingly R. et al. (2011) 'Mars Sample Return as a Campaign', *2011 IEEE Aerospace Conference*.
- [53] Andrews, R. G. (2020) 'Rocks, Rockets and Robots: The Plan to Bring Mars Down to Earth', *Scientific American* [Online]. Available at <https://www.scientificamerican.com/article/rocks-rockets-and-robots-the-plan-to-bring-mars-down-to-earth1>
- [54] Muirhead B. K. et al. (2021) 'Mars Sample Return Campaign Concept Architecture', *Planetary Science and Astrobiology Decadal Survey 2023-2032*.
- [55] Moeller R. C. et al. (2020) 'The Sampling and Caching Subsystem (SCS) for the Scientific Exploration of Jezero Crater by the Mars 2020 Perseverance Rover', *Space Science Reviews*, Vol. 217, December 2020.
- [56] Kminek G. et al. (2021) 'MSR Caching Strategy Workshop', *Mars Exploration Program Analysis Group (MEPAG) Meeting*, January 2021.
- [57] Zurbuchen T. H. (2022) 'Explore Science', *Space Science Week 2022*.
- [58] Farley K. (2018) 'Mars 2020 Mission', *Mars Exploration Program Analysis Group (MEPAG) Meeting*, April 2018.
- [59] Yaghoubi D. et al. (2022) 'Integrated Design Results for the MSR SRC Mars Ascent Vehicle', *2022 IEEE Aerospace Conference*.
- [60] Dillman R. et al. (2008) 'Overview of the Mars Sample Return Earth Entry Vehicle', *Sixth International Planetary Probe Workshop*.

- [61] Golombek M. et al. (1997) 'Size-frequency distributions of rocks on Mars and Earth analog sites: implications for future landed missions', *Journal of Geophysical Research*, Vol. 102, February 1997, p. 4117.
- [62] Golombek M. et al. (2021) 'Rock size-frequency distributions at the InSight landing site, Mars', *Earth and Space Science*, Vol. 8, December 2021.
- [63] Ridolfi P. et al. (2021) 'Development of the Sample Fetch Rover Locomotion Subsystem', *72nd International Astronautical Congress*, October 2021.
- [64] Benzing J. A. et al. (2009) 'Tire', Patent no. US 8,141,606 B2.
- [65] Padula S. A. et al. (2016) 'Superelastic Tire', Patent no. US 10,449,804 B1.
- [66] Asnani V. et al. (2009) 'The development of wheels for the Lunar Roving Vehicle', *Journal of Terramechanics*, Vol. 46, April 2009, p. 89.
- [67] ECSS Secretariat (2019) *ECSS-E-ST-33-01C Rev.2, Space Engineering: Mechanisms*.
- [68] Ghotbi B. et al. (2022) 'CHABLIS – A mobility breadboard vehicle for the ESA's Mars Sample Return Sample Fetch Rover', *Astra 2022 – 16th Symposium on Advanced Space Technologies for Robotics and Automation*.
- [69] Dinsdale M. et al. (2022) 'Absolute Localisation by Map Matching for Sample Fetch Rover', *Astra 2022 – 16th Symposium on Advanced Space Technologies for Robotics and Automation*.
- [70] Rusconi A. et al. (2015) 'DExtrous Lightweigh Arm for exploration (DELIAN)', *Astra 2015 – 13th Symposium on Advanced Space Technologies for Robotics and Automation*.
- [71] Pilati A. et al. (2022) 'Breadboard testing activities of the Arm and Gripper Subsystem for Mars sample retrieval', *Astra 2022 – 16th Symposium on Advanced Space Technologies for Robotics and Automation*.